

University of Warwick institutional repository: <http://go.warwick.ac.uk/wrap>

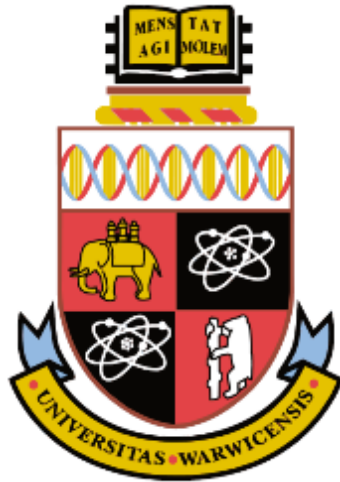
A Thesis Submitted for the Degree of PhD at the University of Warwick

<http://go.warwick.ac.uk/wrap/66553>

This thesis is made available online and is protected by original copyright.

Please scroll down to view the document itself.

Please refer to the repository record for this item for information to help you to cite it. Our policy information is available from the repository home page.



**Anti-stress gene response in cell and tissue
ageing: role of transcription factor NF-E2-
related factor-2 and effect of dietary
activators**

July 2014

Florence A.G. Hariton

A thesis submitted in partial fulfilment of the requirements
for the degree of

Doctor of Philosophy in Medical Sciences

University of Warwick, Warwick Medical School

July 2014

Contents

List of Figures and Tables.....	vi
Acknowledgements	xiv
Dedication	xv
Declaration	xvi
Abstract	xvii
Abbreviations and Symbols	xviii
1. Introduction - Ageing, senescence and the Nrf2 system.....	1
1.1 Ageing.....	1
1.1.1 Theories of ageing.....	2
1.1.2 Experimental models of ageing.....	4
1.2 Cell senescence as a model of ageing	10
1.2.1 The Hayflick Limit.....	12
1.2.2 Markers of cell senescence.....	13
1.2.3 Replicative senescence in <i>vivo</i>	19
1.2.4 Mechanism of cell senescence	20
1.2.5 Theories of ageing as applied to cell senescence – accumulation of macromolecular damage	24
1.3 The Nrf2 system.....	33
1.3.1 Antioxidant response element.....	37
1.3.2 The Nrf2 system in ageing and senescence.....	38
2. Project-specific background.....	40
2.1 The human fibroblast model in cellular senescence research	40
2.1.1 Human fetal lung MRC-5 fibroblasts.....	41
2.1.2 Human foreskin BJ fibroblasts.....	42
2.2 Interventions for healthy ageing.....	43
2.3 Experimental interventions: caloric restriction mimetic for increased lifespan and decreased senescence.....	45
2.3.1 Caloric restriction and delay of ageing	45
2.3.2 Caloric restriction mimetic compounds	47
2.3.3 Nrf2 activation by dietary activators.....	53

2.4 Dietary bioactive compounds: Sulforaphane (SFN) and Hesperetin (HESP)	57
2.4.1 Sulforaphane (SFN)	57
2.4.2 Hesperetin (HESP)	59
2.5 Nutrient sensing via the ChREBP/MondoA–Mlx complex	60
2.6 Aim and objectives	63
2.6.1 Aim	63
2.6.2 Objectives	63
3. Materials and Methods	66
3.1 Materials	66
3.1.1 Human fibroblasts	66
3.1.2 Human leukaemia 60 cells	67
3.1.3 Cell viability	67
3.1.4 Enzymes, substrates, co-factors, antibodies, primers, other biochemical and miscellaneous reagents	67
3.1.5 Immunocytochemistry, electrophoresis and Western blotting reagents	69
3.1.6 Analytical standards for stable isotopic analysis of metabolites	70
3.1.7 Equipment, instrumentation and software	72
3.2 Cell culture	73
3.2.1 Effect of sulforaphane treatment on growth of MRC-5 cells <i>in vitro</i> .	73
3.2.2 Effect of hesperetin on growth of MRC-5 cells <i>in vitro</i> .	74
3.2.3 Effect of chronic treatment with sulforaphane on the development of MRC-5 cell senescence <i>in vitro</i>	74
3.2.4 Effect of chronic treatment with hesperetin on the development of MRC-5 cell senescence <i>in vitro</i> .	74
3.3 Analytical methods	75
3.3.1 Senescence-associated beta-galactosidase staining	75
3.3.2 Bradford Assay	76
3.3.3 Real-time polymerase chain reaction analysis of mRNA	76
3.3.4 Custom mRNA array analysis by the Nanostring method	79
3.3.5 Glycation, oxidation and nitration of cellular protein	87
3.3.6 Analysis of N _ε -(γ -L-glutamyl)-L-lysine (GEEK)	97
3.3.7 Nucleotide oxidation and glycation	99
3.3.8 Dicarbonyls analysis	101
3.3.9 Assay of D-glucose	102
3.3.10 D-Lactate assay	103
3.3.11 L-Lactate assay	105

3.3.12 Assay of cellular reduced and oxidised glutathione and glyoxalase pathway intermediate S-D-lactoylglutathione	105
3.3.13 Immunocytochemistry	107
3.3.14 Western Blotting	109
3.3.15 Assay of glycolytic intermediates in MRC-5 fibroblasts treated with SFN and/or high glucose	110
3.3.16 Microarray analysis	112
3.3.17 Statistical analysis	116
4. Results	117
4.1 Effects of sulforaphane and hesperetin on MRC-5 fibroblast senescence <i>in vitro</i>	117
4.1.1 Growth curve of MRC-5 fibroblasts <i>in vitro</i>	117
4.1.2 Dose-response of MRC-5 fibroblasts treated with sulforaphane	118
4.1.3 Dose-response of MRC-5 fibroblasts treated with hesperetin	119
4.1.4 Effect of sulforaphane treatment on MRC-5 fibroblasts growth	119
4.1.5 Effect of hesperetin treatment on MRC-5 fibroblasts growth.....	126
4.1.6 Senescence-associated beta-galactosidase staining of MRC-5 fibroblasts treated with SFN	129
4.1.7 Cell senescence marker beta-galactosidase – assessment of beta-galactosidase protein	130
4.1.8 Changes in gene expression induced by sulforaphane in early passage, non-senescent MRC-5 cells <i>in vitro</i>	132
4.2 Characterization of gene expression and cell metabolism in cells escaping senescence by treatment with sulforaphane and hesperetin.	143
4.3 Characterisation of gene expression in MRC-5 fibroblasts escaping senescence by treatment with sulforaphane using genome-wide microarray analysis	160
4.4 Expression of fructose-2,6-bisphosphate 6-phosphofructo-2-kinase/fructose-2,6-biphosphatase 2 protein PFKFB2	168
4.5 Change in gene expression of MRC-5 fibroblasts <i>in vitro</i> during the approach to senescence	169
4.6 Effect of progression towards senescence and sulforaphane on protein glycation, oxidation and nitration markers in MRC-5 fibroblasts <i>in vitro</i>	174
4.6.1 Protein glycation	177
4.7 Effect of progression towards senescence and sulforaphane on nucleotide glycation and oxidation in MRC-5 fibroblast cultures.....	184
4.8 Effect of progression towards senescence and sulforaphane on formation of Nε(γ-glutamyl)lysine (GEEK) in MRC-5 fibroblast cultures.....	187
4.9 Effect of sulforaphane on dicarbonyl precursors of protein and nucleotide glycation in cultures of MRC-5 fibroblasts <i>in vitro</i>	190

4.10 Effect of treatments at the approach to senescence on the consumption of glucose by MRC-5 and BJ fibroblasts <i>in vitro</i>	196
4.10.1 Effect on the approach to senescence and treatment with sulforaphane on the consumption of glucose by MRC-5 fibroblasts <i>in vitro</i>	196
4.10.2 Effect on the approach to senescence and treatment with sulforaphane on the consumption of glucose by BJ fibroblasts <i>in vitro</i>	197
4.10.3 Effect on the approach to senescence and treatment with hesperetin on the consumption of glucose by MRC-5 fibroblasts <i>in vitro</i>	198
4.11 Effect of approach to senescence and sulforaphane on reduced glutathione concentration in MRC-5 fibroblasts cell pellets	199
4.12 Characterization of the mechanism of decrease glucose metabolism by SFN and HESP action linked to delay of fibroblast senescence.....	200
4.12.1 Effect of approach to senescence and sulforaphane on the concentration of L-lactate in cultures of MRC-5 fibroblasts <i>in vitro</i>	200
4.12.2 Effect of the approach to senescence, sulforaphane and hesperetin on D-lactate production in MRC-5 fibroblasts <i>in vitro</i>	201
4.13 Effect of sulforaphane on the cellular content of glycolytic intermediates	202
4.14 Immunostaining for Mondo A in MRC-5 fibroblasts <i>in vitro</i>	205
5. Discussion	209
5.1 Effects of SFN and HESP on MRC-5 and BJ senescence <i>in vitro</i>	210
5.1.1 Effect of sulforaphane treatment on MRC-5 fibroblasts growth	210
5.1.2 Effect of hesperetin treatment on MRC-5 fibroblasts growth.....	212
5.1.3 Effect of sulforaphane on staining and expression of senescence-associated beta-galactosidase in MRC-5 fibroblasts.....	213
5.2 Characterization of gene expression and cell metabolism in cells escaping senescence by treatment with SFN and HESP <i>in vitro</i>	215
5.2.1 Changes in gene expression induced by sulforaphane in early passage, non-senescent MRC-5 cells <i>in vitro</i>	215
5.2.2 Characterization of gene expression and cell metabolism in cells escaping senescence by treatment with sulforaphane and hesperetin.	218
5.2.3 Characterisation of gene expression in MRC-5 fibroblasts escaping senescence by treatment with sulforaphane using genome-wide microarray analysis.....	220
5.2.4 Characterisation of gene expression in MRC-5 fibroblasts <i>in vitro</i> during the approach to senescence.....	222
5.2.5 Effect of progression towards senescence and sulforaphane on protein glycation, oxidation and nitration markers in MRC-5 fibroblasts <i>in vitro</i> ..	223
5.2.6 Effect of progression towards senescence and sulforaphane on nucleotide glycation and oxidation in MRC-5 fibroblasts <i>in vitro</i>	226
5.2.7 Effect of sulforaphane on dicarbonyl precursors of protein and nucleotide glycation in cultures of MRC-5 fibroblasts <i>in vitro</i>	226

5.2.8 Effect of progression towards senescence and sulforaphane on formation of Nε(γ-glutamyl)lysine (GEEK) in MRC-5 fibroblast cultures.	228
5.3 Characterization of the mechanism of decrease glucose metabolism by SFN and HESP action linked to delay of fibroblast senescence	230
5.3.1 Effect of the approach to senescence and treatment with sulforaphane and hesperetin on the consumption of glucose by MRC-5 and BJ fibroblasts <i>in vitro</i>	230
5.3.2 Characterization of the mechanism of decrease glucose metabolism by SFN and HESP action linked to delay of fibroblast senescence.....	232
5.3.3 Effect of sulforaphane on the cellular content of glycolytic intermediates	233
5.3.4. Characterization of glucose sensing by ChREBP/MondoA-Mlx transcription factors in response to SFN treatment in MRC-5 fibroblasts..	234
6. Conclusion and Further work.....	237
6.1 Conclusion	237
6.2 Further Work.....	239
Appendix A. Isoforms Codeset design of genes of interest for Nanostring analysis: sulforaphane treatment in young MRC-5 fibroblasts <i>in vitro</i>	240
Appendix B. Targets Codeset design of genes of interest for Nanostring analysis: sulforaphane treatment in young MRC-5 fibroblasts <i>in vitro</i>	242
Appendix C. Isoforms Codeset design of genes of interest for Nanostring analysis: early and late passage expression analysis in response to sulforaphane and hesperetin	246
Appendix D. Targets Codeset design of genes of interest for Nanostring analysis: early and late passage expression analysis in response to sulforaphane and hesperetin	249
Appendix E. Significant changes in microarray gene expression between controls at passage 3 and controls at passage 11 after Bonferroni factor of 20773 was applied (P<0.05).....	253
Appendix F. Significant changes in microarray gene expression between SFN treatment at passage 11 and control at passage 3 after Bonferroni factor of 20773 was applied (P<0.05).....	257
Bibliography.....	264

List of Figures and Tables

Figure 1. <i>Saccharomyces cerevisiae</i>	5
Figure 2. Effect of age on <i>Saccharomyces cerevisiae</i>	5
Figure 3. Morphological signs of ageing in <i>Caenorhabditis elegans</i>	7
Figure 4. Implications of the <i>daf-2</i> gene in the lifespan of <i>C. elegans</i>	7
Figure 5. Mechanism of life extension by caloric restriction in the <i>Drosophila melanogaster</i>	9
Figure 6. Survival rate of mice as a function of caloric intake.	10
Figure 7. The 3 phases of cell culture as described by Hayflick and Moorhead. .	12
Figure 8. Morphological changes observed in WI-38 fibroblast.	15
Figure 9. The β -Galactosidase reaction with chromogenic substrate.	16
Figure 10. Senescence detected by beta-galactosidase activity staining in replicative senescent and non-senescent WI-38 human foetal lung fibroblasts....	16
Figure 11. The structural organisation of the tumour suppressor protein p53.	18
Figure 12. The structural organisation of the tumour suppressor protein pRb.	19
Figure 13. The telomere shortening process.	21
Figure 14. Activating pathways of senescence.	22
Figure 15. Schematic model of senescence and its biological functions.	23
Figure 16. Formation of oxidised amino acid residues from oxidative damage to proteins.....	26
Figure 17. Mechanisms of oxidative damage involved in the ageing process.....	27
Figure 18. Mechanisms of formation of AGEs from glucose, glycolytic intermediates and lipid peroxidation.....	30
Figure 19. Molecular structure of the physiologically reactive glycating dicarbonyls 3-deoxyglucosone (3-DG), glyoxal and methylglyoxal.	30
Figure 20. Reactive glycating species function in the ageing process.	31
Figure 21. Mechanism of formation of major protein glycation adducts, N ϵ -fructosyl-lysine and hydroimidazolone N δ -(5-hydro-5-methyl-4-imidazolone-2-yl)ornithine (MG-H1).....	32
Figure 22. Protein glycation adduct residues in physiological systems.....	32
Figure 23. Examples of the battery of protective genes regulated by the Nrf2 system and their role in the anti-stress gene response.....	34

Figure 24. Current understanding of transcriptional control of ARE-linked gene expression by the Nrf2/Keap1 system.	36
Figure 25. Cell signalling sustaining Nrf2 translocational oscillations for control of ARE-linked gene expression.	37
Figure 26. Topographic differentiation of fibroblasts.....	41
Figure 27. Chemical structure of resveratrol.....	48
Figure 28. Resveratrol mimics caloric restriction by inhibiting cAMP phosphodiesterases (PDEs).	50
Figure 29. Molecular structure of rapamycin.....	51
Figure 30. Summary of the main signalling pathways responsible for the delay of ageing by diverse dietary activators.	52
Figure 31. Dose-response of natural compounds against risk of chronic disease.	57
Figure 32. Glucosinolates and myrosinase are stored in separate cell compartments.	58
Figure 33. Chemical structure of the bioflavanoid Hesperetin (Mw = 302 g/mol).	59
Figure 34. Regulation of ChREBP/MondoA–Mlx activity.....	61
Figure 35. Domain structure of ChREBP/MondoA and Mlx.	62
Figure 36. Oxidation of glutathione by diamide.	71
Figure 37. Representative dissociation plot for primers.	77
Figure 38. Typical calibration curve for RT-PCR.	79
Figure 39. Overview of NanoString nCounter gene expression system.	82
Figure 40. Protein glycation, oxidation and nitration adduct residues in physiological systems.	88
Figure 41. Formation of Nε(γ-glutamyl)lysine (GEEK).....	89
Figure 42. Typical calibration curves for glycation adducts – AGEs.	96
Figure 43. A typical calibration curve for glutamyl lysine.	98
Figure 44. The conversion of GdG into dG and MGdG.	100
Figure 45. Coupled enzymatic assay for glucose – hexokinase method.....	102
Figure 46. Typical calibration curve for D-glucose.	103
Figure 47. The formation of pyruvate from D-lactate via the enzymatic reaction with D-lactic dehydrogenase.....	104
Figure 48. Typical calibration curve for D-lactate.....	104
Figure 49. Typical calibration curve for L-lactate.	105

Figure 50. Fragmentation of glutathione in multiple reaction monitoring mass transitions.	107
Figure 51. Layout of semi-dry transfer for Western blotting.....	109
Figure 52. Growth curve for MRC-5 fibroblasts <i>in vitro</i>	117
Figure 53. Dose-response curve for the effect of sulforaphane on growth of MRC-5 fibroblasts <i>in vitro</i>	118
Figure 54. Dose-response curve for the effect of hesperetin on growth of MRC-5 fibroblasts <i>in vitro</i>	119
Figure 55. MRC-5 fibroblasts PDL as a function of passage number – Study 1.	121
Figure 56. MRC-5 fibroblasts cPDL as a function of passage number – Study 1.	121
Figure 57. MRC-5 fibroblasts cPDL as a function of passage number. Replicate study 2.	123
Figure 58. MRC-5 fibroblasts cPDL as a function of passage number. Replicate study 3.	124
Figure 59. MRC-5 fibroblasts cPDL as a function of passage number. Replicate study 4 – effect of early and late treatment.	125
Figure 60. MRC-5 fibroblasts PDL as a function of passage number - HESP study.	127
Figure 61. MRC-5 fibroblasts cPDL as a function of passage number - HESP study.	128
Figure 62. Characteristic blue staining indicating β -galactosidase expression in senescent MRC-5 fibroblasts.	129
Figure 63. Percentage of senescent MRC-5 fibroblasts as a function of passage.	130
Figure 64. Western blotting of young and senescent MRC-5 fibroblasts for beta-galactosidase.	131
Figure 65. Quantitation of Western blotting of young and senescent MRC-5 fibroblasts for beta-galactosidase.	131
Figure 66. Gene expression of MRC-5 fibroblasts induced by sulforaphane. Nanostring study. Antioxidant genes.	134
Figure 67. Gene expression of MRC-5 fibroblasts induced by sulforaphane. Nanostring study. Antiglycation genes.	136

Figure 68. Gene expression of MRC-5 fibroblasts induced by sulforaphane. Nanostring study. Phase II conjugation genes.	136
Figure 69. Gene expression of MRC-5 fibroblasts induced by sulforaphane. Nanostring study. Pentophosphate pathway genes.	137
Figure 70. Gene expression of MRC-5 fibroblasts induced by sulforaphane. Nanostring study. Lipogenic and glycolytic regulation genes.	137
Figure 71. Gene expression of MRC-5 fibroblasts induced by sulforaphane. Nanostring study. Nrf2 regulation genes.	138
Figure 72. Gene expression of MRC-5 fibroblasts induced by sulforaphane. Nanostring study. Proteolysis related genes.....	139
Figure 73. Gene expression of MRC-5 fibroblasts induced by sulforaphane. Nanostring study. Inflammatory/immune response genes.	139
Figure 74. Gene expression of MRC-5 fibroblasts induced by sulforaphane. Nanostring study. Extracellular matrix regulating genes.	141
Figure 75. Gene expression of MRC-5 fibroblasts induced by sulforaphane. Nanostring study. Serpines.....	141
Figure 76. Gene expression of MRC-5 fibroblasts induced by sulforaphane. Nanostring study Senescence-associated genes.	142
Figure 77. Gene expression of MRC-5 fibroblasts induced by sulforaphane. Nanostring study Reference genes.	142
Figure 78. Relative mRNA copy number in young (Passage 3) and senescent (Passage 11) MRC-5 fibroblasts with or without treatment with 1 μ M SFN after Bonferroni correction of 49.....	149
Figure 79. Relative mRNA copy number in young (Passage 3) and senescent (Passage 9) MRC-5 fibroblasts with or without treatment with 5 μ M HESP after Bonferroni correction of 49.....	157
Figure 80. Western blotting of young and senescent MRC-5 fibroblasts for 6- phosphofructo-2-kinase/fructose-2,6-bisphosphatase-2.	168
Figure 81. Quantitation of Western blotting of young and senescent MRC-5 fibroblasts for 6-phosphofructo-2-kinase/fructose-2,6-bisphosphatase-2.....	168
Figure 82. Gene expression of MRC-5 fibroblasts at the approach to senescence. RT-PCR study. Anti-glycation related genes.....	170
Figure 83. Gene expression of MRC-5 fibroblasts at the approach to senescence. RT-PCR study. Anti-oxidant related genes.....	171

Figure 84. Gene expression of MRC-5 fibroblasts at the approach to senescence. RT-PCR study. Pentosephosphate pathway genes.....	172
Figure 85. Gene expression of MRC-5 fibroblasts at the approach to senescence. RT-PCR study. Nrf2 regulation related genes.	172
Figure 86. Gene expression of MRC-5 fibroblasts at the approach to senescence. RT-PCR study. NADPH-dependent oxidoreductase genes carbonyl reductase 1 (CBR1).....	172
Figure 87. FL residue content of MRC-5 cell protein and flux of formation of FL free adducts.	178
Figure 88. MG-H1 residue content of MRC-5 cell protein and flux of formation of MG-H1 free adducts.....	179
Figure 89. 3DG-H1 residue content of MRC-5 cell protein and flux of formation of 3-DG-H free adducts.....	180
Figure 90. CMA residue content of MRC-5 cell protein and flux of formation of CMA free adducts.	181
Figure 91. GSA residue content of MRC-5 cell protein and flux of formation of GSA free adducts.	182
Figure 92. 3-NT residue content of MRC-5 cell protein and flux of formation of 3-NT free adducts.	183
Figure 93. Detection and quantitation of 8-oxodG in culture medium of MRC-5 cell in culture.....	185
Figure 94. Concentration of 8-oxodG in medium of cultures of MRC-5 cells and 8-oxodG efflux from cells.....	186
Figure 95. Detection and quantitation of N ϵ (γ -glutamyl)lysine (GEEK) in cellular protein of MRC-5 cell in culture.....	188
Figure 96. Concentration of N ϵ (γ -glutamyl)lysine (GEEK) in medium of cultures of MRC-5 cells and GEEK efflux from cells.....	189
Figure 97. Cellular protein concentration of N ϵ (γ -glutamyl)lysine (GEEK) in MRC-5 cells at passage 4 and 8 with and without 1 μ M SFN.....	190
Figure 98. Concentration of glyoxal in medium of cultures of MRC-5 cells and glyoxal efflux from cells.	193
Figure 99. Concentration of methylglyoxal in medium of cultures of MRC-5 cells and methylglyoxal efflux from cells.	194

Figure 100. Concentration of 3-deoxyglucosone in medium of cultures of MRC-5 cells and 3-deoxyglucosone efflux from cells.....	195
Figure 101. Effect of approach to senescence and sulforaphane on the consumption of D-glucose by MRC-5 fibroblasts <i>in vitro</i>	196
Figure 102. Effect of approach to senescence and sulforaphane on the consumption of D-glucose by BJ fibroblasts <i>in vitro</i>	197
Figure 103. Effect of approach to senescence and hesperetine on the consumption of D-glucose by MRC-5 fibroblasts <i>in vitro</i>	198
Figure 104. Effect of approach to senescence and sulforaphane on the reduced glutathione content of MRC-5 fibroblasts <i>in vitro</i>	199
Figure 105. Effect of approach to senescence and sulforaphane on the apparent flux of L-lactate production by MRC-5 cells <i>in vitro</i>	200
Figure 106. Effect of approach to senescence and sulforaphane on the flux of formation of D-lactate by MRC-5 cells <i>in vitro</i>	201
Figure 107. Effect of approach to senescence and hesperetin on the flux of formation of D-lactate by MRC-5 cells <i>in vitro</i>	202
Figure 108. Glycolytic intermediates for entry of glucose into glycolysis and the pentose phosphate pathway.....	203
Figure 109. Detection of glucose-6-phosphate and fructose 6-phosphate by liquid chromatography-tandem mass spectrometry. MRM chromatograms.....	204
Figure 110. Immunostaining for localization of Mondo A in MRC-5 cells <i>in vitro</i>	206
Figure 111. Immunostaining for localization of Mondo A in MRC-5 cells <i>in vitro</i>	207
Figure 112. Immunostaining for localization of Mondo A in MRC-5 cells <i>in vitro</i>	208
Figure 113. Summary of mechanism of activation of Nrf2 system and delay of senescence by SFN in MRC-5 fibroblasts.	236
Table 1. Phenotypic and molecular markers of cellular senescence.....	14
Table 2. Dietary activators of nrf2.	38
Table 3. Comparison of proliferative senescence and the ageing of non-dividing BJ fibroblasts.....	43

Table 4. Effects of CR on selected parameters of morphology, physiology, ageing, and disease in rhesus monkeys.....	46
Table 5. Examples of divergent effects of dietary bioactive and other compounds on human cellular senescence in vitro.	54
Table 6. Genes of interest for Nanostring analysis in MRC-5 fibroblasts treated with or without SFN at passage 4.	83
Table 7. Genes of interest for Nanostring analysis analysis in MRC-5 fibroblasts treated with or without SFN or HESP at passage 3 and 11.....	85
Table 8. Gradient table for protein damage analytes detection on LC-MS/MS....	91
Table 9. Column switching programme for protein damage analytes detection on LC-MS/MS.....	92
Table 10. Mass spectrometric multiple reaction monitoring detection of protein oxidation and glycation adducts.....	93
Table 11. Calibration standard-cocktail of stock solution for GEEK analysis.	97
Table 12. Gradient table for Nε-(γ-L-glutamyl)-L-lysine detection on LC-MS/MS.	98
Table 13. Mass-spectrometric multiple reaction monitoring detection of Nε-(γ-L-glutamyl)-L-lysine.....	99
Table 14. Detection of imidazopurinones and related deoxyguanosine-derived adducts by liquid chromatography-tandem mass spectrometry multiple reaction monitoring.	100
Table 15. Gradients for the dicarbonyl assay using LC-MS/MS.	101
Table 16. Mass-spectrometric multiple reaction for detection of dicarbonyls....	102
Table 17. UPLC Elution profile for glutathione analysis.	106
Table 18. Optimised MRMs for glutathione analysis.	106
Table 19. Immunocytochemistry conditions.....	108
Table 20. Composition of 10% SDS-PAGE gel for western blotting.....	109
Table 21. UPLC Elution profile for glycolytic intermediates analysis.....	111
Table 22. Optimised MRMs for glycolytic intermediates analysis.....	112
Table 23. Transcription Master Mix components.....	114
Table 24. Seeding density of MRC-5 cells in passages for the sulforaphane treatment study.....	120
Table 25. Seeding density of MRC-5 cells in passages for the sulforaphane treatment study. Replicate study 2.	123

Table 26. Seeding density of MRC-5 cells in passages for the sulforaphane treatment study. Replicate study 3.	124
Table 27. Seeding density of MRC-5 cells in passages for the sulforaphane treatment study. Replicate study 4.	126
Table 28. Seeding density of MRC-5 cells in passages for the hesperetin treatment study.	127
Table 29. Relative mRNA copy number in young (Passage 3) and senescent (Passage 11) MRC-5 fibroblasts with or without treatment with 1µM SFN.	145
Table 30. Relative mRNA copy number in young (Passage 3) and senescent (Passage 9) MRC-5 fibroblasts with or without treatment with 5µM HESP.	153
Table 31. Comparison of significant changes in gene expression in MRC-5 fibroblasts controls at passage 3 and passage 11 using a Bonferroni correction factor of 20773.	162
Table 32. Comparison of significant changes in gene expression in MRC-5 fibroblasts SFN treatments at passage 3 and passage 11 using a Bonferroni correction factor of 20773.	163
Table 33. Comparison of significant changes in gene expression in MRC-5 fibroblasts control at passage 3 and treatment at passage 11 using a Bonferroni correction factor of 20773.	164
Table 34. Comparison of significance in gene expression using Microarray and Nanostring methods in MRC-5 fibroblasts treated with SFN at passage 3 and 11.	165
Table 35 Correlation analysis of gene expression in ageing MRC-5 fibroblasts.	173
Table 36. Protein damage adduct residues of cell cytosolic protein in MRC-5 fibroblasts treated with or without 1µM SFN at passage 4 and 8.	175
Table 37. Protein damage adduct residues and flux of free adducts in culture medium in MRC-5 fibroblasts treated with or without 1µM SFN at passage 4 and 8.	176
Table 38. Effect of sulforaphane on early-stage glycolytic intermediates in MRC-5 cells <i>in vitro</i>	205

Acknowledgements

I am sincerely grateful to my supervisor Professor Paul J. Thornalley for his support and guidance throughout my PhD. This thesis would not have been possible without your supervision. I would also like to thank Dr. Naila Rabbani for her encouragements and feedback.

I wish to thank Dr. Tony Shmygol for his kind help and patience during my confocal microscopy training. I thank Unilever for the joined sponsorship of this project, especially Dr. Linda Wainwright for her initial guidance and Dr. Mark Fowler for following me until completion of this thesis. I am very grateful to Della Hyliands for her help and cheerful nature during my placement at Unilever laboratories for the transcriptomic analysis. I thank Dr. Jay Moore for his guidance in the statistical analysis of transcriptomic data. Special thanks go to Dr. Ming Zhan Xue for answering all my technical questions and training on western blotting and RT-PCR. I am also forever grateful to Dr. Attia Anwar for her technical support on LC-MS/MS and friendship. I also thank the BBSRC for their joint funding of this project.

I would like to thank all the past and present members of the Protein Damage and Systems Biology Research Group for their kindness, support and friendship throughout my PhD. It was a great honor to work with all of you in such a friendly and inspiring atmosphere.

Finally, I would like to thank my parents, Denise and Claude Hariton, and my little brother William for motivating me every day. William, thank you for your calming influence and unconditional love for me. Throughout my education you have always stood by my side and have protected me like a big brother. Maman, you have always been the person I look up to when I am facing obstacles because when you set your heart on accomplishing something you always give yourself the best chances of succeeding. You are my inspiration for doing this PhD. Because you always believed I could do it. Papa, you have made yourself available every single time I needed you. You are my mentor, my confident and my friend. I am thankful for your sense of humor, outlook on life and care. These four last years have brought us closer than ever and you have been amazing parents, as always. I can only hope that one day I will inspire and support my children as much as you have done for myself and William.

Dedication

To my beloved grand-parents who have always been the greatest teachers in my life. I remember the day Papé taught me how to read and the day Papi taught me about the importance of hard work. I know that you would have been proud of me today. I thank my Mamie for teaching me courage in the most difficult situations and my Mamé for teaching me kindness and love towards others.

Cette these est dediée a mes grand-parents qui m'ont donnés la plus belle et heureuse enfance. Votre amour me fait vivre, et sans vous je ne serais qu'une fraction de ce que je suis maintenant. Je vous aime.

I dedicate every single day spent working on this project to my loving husband Damian Michael Gannon. You have supported and loved me throughout this PhD in every possible way, and marrying you was my greatest and happiest achievement. I am truly blessed to have you in my life.

Declaration

I am aware of the University regulations governing plagiarism and I declare that all the work presented in this thesis, unless otherwise specifically stated, was original research performed by myself under the supervision of Professor Paul J. Thornalley. None of this work has been previously submitted to any other degree. All sources of information have been acknowledged by means of reference.

Florence A. G. Hariton

Abstract

The concept of cellular senescence is based on the notion that proliferation of normal diploid cells can only occur for a limited period of time after which cells slowly cease to divide and die. This limitation of lifespan for *in vitro* cell cultures was first described by Leonard Hayflick in 1961, going against the theory formulated by Alexis Carrel claiming that cells kept in culture have an unlimited potential for division (Carrel and Ebeling, 1921).

Evidence from cell senescence studies have been used to explain the basis of healthy ageing as well as develop food supplements promoting the delay of ageing. Since these discoveries, there has been marked expansion of anti-stress gene response research with relation to the role of the transcription factor NF-E2-related factor-2 as well as healthy ageing with regards to dietary activators intake.

This study examined the effects of sulforaphane (SFN) and hesperetin (HESP) on MRC-5 cell senescence *in vitro* as well as characterized gene expression and cell metabolism in cells escaping senescence by treatment with SFN and HESP and the mechanism of decrease glucose metabolism by SFN and HESP action linked to delay of fibroblast senescence. The effects of treatment of MRC-5 with the dietary bioactivators SFN and HESP was studied and shown to delay cellular senescence in these cells *in vitro*. Similar findings for SFN treatment of BJ cells were found previously by studies of the host team. Caloric restriction mimetic mechanisms by treatment with 1 μ M SFN and 5 μ M HESP was shown due to the decrease in culture glucose consumption increase with senescence in these treatment groups and this CR restriction mimetic effect and decrease in the flux of formation of D- and L-lactate in the SFN-treated group was consistent with previous studies done in CR and ageing in mice models (Hargopan, Ramsey and Weindruch, 2003). Moreover, in this study, SFN was shown to act as a CRM dietary bioactive through cellular contents of glycolytic intermediates with SFN-treatment (Bensaad et al., 2006).

Finally, the mechanism by which SFN induces delay of senescence through CR was shown to be due to the extraction of Mondo A from the cell nucleus to the cytoplasm.

Abbreviations and Symbols

µg	Microgram
µl	Microliter
2-DG	Glucose analog 2-deoxyglucose
2-DG6P	2-deoxyglucose-6-phosphate
3 DG-H	Hydroimidazolone of 3-dexyglucosone
3-DG	3-deoxyglucosone
3-NT	3-nitro tyrosine
53BP1	Tumor suppressor p53-binding protein 1
8-OxodG	8-oxo-7,8-dihydro-2'-deoxyguanosine
A1 UDP	Glucuronosyltransferase 1
AASA	α-aminoadipic semialdehyde
ACTB	Beta Actin
AESF	4-(2-aminoethyl) benzenesulfonyl fluoride hydrochloride
AGEs	Advanced glycation endproducts
AKR1C1	Aldoketo reductase 1C1
AKRB1	Aldoketo-reductase B1
AKRB2	Aldoketo-reductase B2
AKRd	Aldoketo reductase
AldDH	Aldehyde dehydrogenase
AMP	Adenosine monophosphate
AMPK	AMP-activated kinase
AREs	Anti-oxidant response elements
ATF-2	Activating transcription factor 2
ATM	Ataxia telangiectasia mutated kinase
ATR	Rad3-related protein
BEH	Bridged Ethane Hybrid column
bHLHZ	Basic helix-loop-helix-leucine zipper
BSA	Bovine serum albumin
C/EBPb	CCAAT/enhancer-binding proteins
cAMP	3'-5'-cyclic adenosine monophosphate
CAT	Catalase
CBR1	Carbonyl reductase-1

CCL2	Monocyte chemoattractant protein-1/Chemokine (C-C motif) ligand 2
CDKIs	Cyclin-dependent kinase inhibitors
CDKN1A	Cyclin-dependent kinase inhibitor 1/p21
CDKN2A	Cyclin-dependent kinase inhibitor 2A/P16INK4a
cDNA	Complementary DNA
CEL	N_{ϵ} -(1-carboxyethyl)lysine
CFD	Chromosome Frequency Distribution
CHK1	Checkpoint kinase 1
CHK2	Checkpoint kinase 2
ChoREs	Carbohydrate response elements
ChREBP	Carbohydrate-responsive element-binding protein
CK2	Casein kinase-2
ClO^-	Hypochlorite
CLS	Chronological Life Span
CLTC	Clathrin, heavy chain
CMA	N_{ω} -carboxymethyl-arginine
CML	N_{ϵ} -carboxymethyl-lysine
$\text{CO}_3^{\bullet -}$	Carbonate radical anion
COL1A1	Collagen 1-alpha
cPDL	Cumulative PDL
CR	Caloric restriction
CRM	Caloric restriction mimetic
CRM1	Chromosome region maintenance 1
CSCs	Cancer stem cells
CTP	Cytidine triphosphate
CTSO	Cathepsin O
Cu^{2+}	Cupric ion
Cul3	Cullin-3
CXCL1	GRO-alpha oncogene/Chemokine (C-X-C motif) ligand 1
d_3 -AAA	2,5,5-[$^2\text{H}_3$]DL- α -amino adipic acid
DAF-2	insulin-like growth factor 1 (IGF-1) receptor in <i>C. elegans</i>
DALYs	Disability-adjusted life years
DAPI	4',6-diamidino-2-phenylindole
DCD	Dimerization and cytoplasmic localization domain

DCR2	Decoy receptor 2
DDR	DNA damage response
DETAPAC	Diethylenetriamine penta-acetic acid
DILPs	Insulin-like peptides
DMSO	Dimethyl sulfoxide
DNA	Deoxyribonucleic acid
DNA-SCARS	DNA segments with chromatin alterations reinforcing senescence
dNTPs	Deoxynucleotide triphosphates
DTT	Dithiothreitol
EC	Endothelial cells
ECACC	European Collection of Animal Cell Cultures
ECL	Enhanced chemiluminescence
EDTA	Ethylenediaminetetraacetic acid
ELN	Elastin
EmC	Embryonic cells
ER	Endoplasmic reticulum
F3PK	Fructosamine-3-phosphokinase
FASN	Fatty acid synthase
FBS	Fetal bovine serum
Fe ³⁺	Ferric ion
FL	N _ε -fructosyl-lysine
FTH1	Ferritin
FYN	Fyn kinase
G6P	Glucose-6-phosphate
G6PDH	Glucose-6-phosphate dehydrogenase
GADD153	Growth-arrest and DNA-damage inducible protein 153
Gas1	Growth-arrest-specific protein 1
GC ₅₀	Median growth inhibitory concentration value
GCLC	γ-glutamylcysteine ligase – catalytic subunit
GCLM	γ-glutamylcysteine ligase – modulatory subunit
GdG	3-(2'-deoxyribosyl)-6,7-dihydro-6,7-dihydroxyimidazo-[2,3-b]purine-9(8)one
GE	Gene expression
GEEK	N _ε (γ-glutamyl)lysine

G-H1	Hydroimidazolone of glyoxal
g-H2AX	Histone variant H2AX
GLB1	Senescence-associated beta-galactosidase
Glo1	Glyoxalase 1
GPx	Glutathione peroxidase
GPX1	Glutathione peroxidase-1
GRACE	Glucose-response activation conserved element
GSA	Glutamic semialdehyde
GSH	Reduced glutathione
GSM	Glucose-sensing module
GSM	Glucose-sensing module
GSR	Glutathione reductase
GSSG	Glutathione oxidised form
GSTD1	Glutathione-S-transferase D1
GSTP1	Glutathione transferase P1
GSTs	Glutathione S-transferases
GTP	Guanosine-5'-triphosphate
GUSB	Beta-glucuronidase
H ₂ O ₂	Hydrogen peroxide
HCl	Hydrochloric acid
HDFs	Human diploid fibroblasts
HEPES	4-(2-hydroxyethyl) piperazine-1-ethanesulfonic acid
HepG2	Human hepatocellular liver carcinoma cell line
HESP	Hesperetin
HIF-1	Hypoxia-inducible factor 1
HIF1- α	Hypoxia-inducible factor 1 alpha
HIRA	Histone repressor A
HK	Hexokinase
HK1	Hexokinase-1
HL60	Human leukaemia 60 cells
HMGA	high mobility group A proteins
HMOX1	Haem oxygenase-1
HO \cdot	Hydroxyl radical
HOMA	Homeostatic model assessment

HP-1b	Heterochromatin protein 1b
HPLC	High performance liquid chromatography
HSA	Human serum albumin
hTERT	Catalytic subunit of human telomerase
ICAM-1	Toll-4 receptor and intercellular adhesion molecule-1
IGF	Insulin-like growth factor
IGF-1	Insulin-like growth factor 1
IGF-BP2	Insulin-like growth factor binding proteins 2
IGF-BP5	Insulin-like growth factor binding proteins 5
IgG	Immunoglobulin G
IL1	Interleukin-1
IL15	Interleukin-15
IL1B	Interleukin 1-beta
IL3	Interleukin-3
IL6	Interleukin-6
IL8	Interleukin-8
INR	Insulin receptor
INS-1	Insulin type 1 protein
KCl	Potassium chloride
kDa	KiloDalton
KEAP1	Kelch-like ECH-associated protein 1
KH ₂ PO ₄	Potassium dihydrogen phosphate
L	Liter
LC-MS/MS	Tandem mass spectrometric detection
LDL	Low density lipoprotein
LF	Lipofuscin
LID	Low-glucose inhibitory domain
MAFG	Maf protein-G
MCP-1	Monocyte chemoattractant protein-1
MCR	Mondo conserved regions
MDC1	DNA damage checkpoint protein 1
MDM2	Double minute 2 homolog protein
ME1	Metallothionein 1
MeCN	Acetonitrile

MEM	Eagle's Minimum Essential Medium
MetSO	Methionine sulfoxide
MG	Methylglyoxal
MGdG	MG-derived imidazopurinone, 3-(2'-deoxyribosyl)-6,7-dihydro-6,7-dihydroxy-6/7-methylimidazo-[2,3-b]purine-9(8)one isomers
MG-H1	Methylglyoxal derived hydroimidazolone N _δ -(5-hydro-5-methyl-4-imidazolone-2-yl)ornithine
ml	Milliliter
MLX	Max-Like BHLHZip Protein2
MLXIP	MondoA (MLX interacting protein)
mM	Millimolar
MMLV-RT	Moloney Murine Leukemia Virus Reverse Transcriptase
MMP1	Fibroblast collagenase/matrix metalloproteinase-1
MMP13	Collagenase-3/matrix metalloproteinase-13
MMP3	Stromelysin-1/matrix metalloproteinase-3
MMPs	Matrix metalloproteinases
MMTV	Mouse mammary tumor virus
MOLD	Methylglyoxal-derived lysine dimer
MondoA	Anti-MLX-interacting protein
MRM	Multiple reaction monitoring
mRNA	Messenger ribonucleic acid
Mrp2	Multidrug resistance-associated protein 2
MSC	Mesenchymal stem cells
mTOR	Rapamycin kinase
mTORC1	mTOR complex 1
mTORC2	mTOR complex 2
Na ₂ HPO ₄	Disodium hydrogen phosphate
NaCl	Sodium chloride
NAD	Nicotinamide adenine dinucleotide-oxidised form
NADH	Nicotinamide adenine dinucleotide, reduced form
NADPH	Nicotinamide adenine dinucleotide phosphate, reduced form
NBS1	Nijmegen breakage syndrome protein
NEAA	Non-essential amino acids

NFE2L2	Nuclear factor (erythroid-derived 2)-like 2
NFK	N-formylkynurenine
NF-kB	Nuclear factor kappa light chain enhancer of activated B cells
NFKB1	Nuclear factor NF-kappa-B p105 subunit/p50
NFKB3	Transcription factor p65
nM	Nanomolar
nmol	Nanomol
NOS	Nitric-oxide synthase
NQO1	Quinone reductase
Nrf2	Nuclear factor erythroid 2-related factor 2
NT	Nitrotyrosine
O ₂ ⁻	Superoxide
OMM	Outer mitochondrial membrane
p21	Cyclin-dependent kinase inhibitor 1
PAI-1	Plasminogen activator inhibitor type-1
PAM	Peptidyl- α amidating monooxygenase
PBS	Phosphate buffered saline
PCA	Perchloric acid
PDEs	Phosphodiesterases
PDL	Population Doubling Limit
PEG	Polyethylene glycol
PFKFB2	6-Phosphofructo-2-kinase/fructose-2,6-bisphosphatase-2
PFKFB4	6-Phosphofructo-2-kinase/fructose-2,6-bisphosphatase-4
PGAM5	Protein threonine phosphatase
PGC-1 α	Peroxisome proliferator-activated receptor-gamma coactivator 1 α
PML	Promyelotic Leukemia
pmol	Picomol
PRDX1	Peroxiredoxin-1
PRDXs	Peroxiredosins
PSMA1	Proteasome subunit A1
PSMB5	Proteasome subunit B5
PVDF	Polyvinyl difluoride
QTN	Quercetin
RB1	Retinoblastoma gene

RES	Resveratrol, 3, 4',5-trihydroxy- <i>trans</i> -stilbene
RHEB	Ras homolog protein enriched in brain
RLS	Replicative Life Span
ROOH	Hydroperoxides
ROS	Reactive oxygen species
RPMI	Roswell Park Memorial Institute 1640 medium
RS	Replicative senescence
RT-PCR	Reverse Transcription polymerase chain reaction
SA-B-GAL	Senescence-associated beta-galactosidase
SAHF	Senescence-associated heterochromatic foci
SASP	Senescence-associated secretory phenotype
SAX SPE	Anion-exchange solid-phase extraction
SDS-PAGE	Sodium dodecyl sulphate polyacrylamide gel electrophoresis
SERPINB2	Plasminogen activator inhibitor-2
SERPINE1	Plasminogen activator inhibitor-1
SFN	R-sulforaphane
SIPS	Stress induced premature senescence
SIR2	Silent information regulator 2
SIT1	Signaling threshold regulating transmembrane adaptor 1
SOD	Superoxide dismutase
SOD1	Superoxide dismutase-1
SOD2	Mitochondrial superoxide dismutase
SPSS	Statistical Package for the Social Sciences
SQSTM1	Sequestosome 1
SQSTM1	Sequestosome-1/p62
SREBF1	Sterol response element binding protein-1
T3	Triiodothyronine
T4	Thyroxin
TAF	Telomere-associated foci
TALDO	Transaldolase
TALDO1	Transaldolase-1
TBST	Tris-buffered saline with Tween 20
TCA	Trichloroacetic acid
TEMED	N,N,N',N'-tetramethylethylene-1,2-diamine

TFA	Trifluoroacetic acid
TFs	Transcription factors
THF	Tetrahydrofuran
TIF	Telomere dysfunction-induced foci
TKT	Transketolase
TLR4	Toll-like receptor 4
TNFRSF10D	Tumor necrosis factor receptor superfamily, member 10d, decoy with truncated death domain
TOR	Target of Rapamycin
TSH	Thyroid stimulating hormone
Tween-20	Polysorbate 20
TXN	Thioredoxin
TXNIP	Thioredoxin interacting protein
TXNRD1	Thioredoxin reductase-1
UDP	Glucuronyl transferase
UGT1A1	Uridine diphosphate glucuronyltransferase A1
UPLC	Ultra high performance liquid chromatography
UV	Ultraviolet
X-Gal	5-bromo-4-chloro-3-indolyl-beta-D-galactopyranoside

1. Introduction - Ageing, senescence and the Nrf2 system

1.1 Ageing

Ageing is a multi-factorial and near universal process of multi-cellular organisms (Huges and Reynolds, 2005). This complex process was originally described by Benjamin Gompertz in 1825 as an exponential chance of death as age increases (Gompertz, 1825). Ageing has been defined at the population level as a “process of intrinsic deterioration that is reflected as an increase in the likelihood of death and a decline in the production of offspring” (Partridge and Gems, 2002) and at the organism level “decrease in physiological reserves which cannot adapt to any additional and even physiological stress, whilst still supporting acceptable functioning in the steady state” (Fulop et al., 2010). It is the primary risk factor for disease of major social impact: cancer, diabetes, cardiovascular disorders, and neurodegenerative diseases (Lopez-Otin et al., 2013). In Western countries, the decline in mortality combined with the decrease in birth rates is leading to a stable increase in the ageing population number (Martin and Sheaff, 2007). Another aspect in determining life expectancy is the concept of genetic predispositions. Studies conducted on twins have demonstrated that only around 25% of variations on life expectancy can be associated with genetic predisposition (Skytthe et al., 2003), implying that environmental factors, which could be controlled, are mainly responsible for healthy ageing (Abbott, 2004). Species-associated lifespan and association of genetic polymorphism within species in genome-wide association with longevity studies have demonstrated a genetic link to ageing (Kenyon, 2010). However, diversity in the lifespan of different populations based on their diet and geographic location can be observed. For example, the Okinawa prefecture in Japan shows an unusual extended life span of its population. The average life span for Americans and Okinawans is 79 and 84 years respectively, and the maximum lifespan is 101 years in Americans compared to 105 years in the Okinawan population (Willcox et al., 2007). This increase in the lifespan of the Okinawans is thought to be due to their large intake of green vegetables, soy and sweet potatoes, as well as lower caloric intake and higher Vitamin E intake as a result of their diet (Suzuki et al.,

2010). This reflects a complex interaction of genes, environment and nutrition in the ageing process – compounded in longevity studies by infection, inflammation and access to medicines (Harman, 2010).

In studies of ageing and longevity it is instructive to also consider major causes of death – particularly when employing experimental models of ageing for comparison with human ageing where causes of mortality may be different. For experimental studies of longevity with laboratory animals - rats and mice, the major causes of death in ageing is tumourigenesis (Suzuki et al., 2010). This contrasts with ageing in the human population where the major cause of death is cardiovascular disease, followed by cancer, cerebrovascular disease and complications of diabetes (Fullop et al., 2010). Indeed ageing is a risk factor for a large number of health impairments and disease in the human population such as dementia, osteoporosis and frailty, which contribute to the major causes of death resulting from this condition. Given the large environmental influence on human longevity it is likely that appropriate lifestyle and dietary interventions may help provide for healthy ageing and decrease morbidity and improve lifespan. Dietary supplements for healthy ageing are likely to achieve high compliance; *cf.* high intake of vitamin supplements for putative improvement of health (Fusco et al., 2007). Currently it is unclear and often controversial which dietary supplements are likely to be effective.

1.1.1 Theories of ageing

Several theories of ageing have been formulated. The most well-established being the evolutionary theory, the rate-of living (“burn out”) theory, the aberrant gene regulation theory and the accumulation of cell damage theory.

1.1.1.1 Evolutionary theory of ageing

The evolutionary theory of ageing is based on the principle that ageing is a phenomenon that is seen universally in all animals (Partridge and Gems, 2002). However, each organism ages differently which leads to the assumption that evolution is the key element leading to ageing rather than wear and tear. The evolutionary theory was further approved after Haldane studies on Huntington’s disease (Haldane, 1941). This lethal genetic disease is only symptomatic once the

adult life of the patient is reached, by which time he may already have had progeny which could be affected by the disease. From these observations, ageing has been defined as an evolutionary genetic disease which strikes later on in life (Partridge and Gems, 2002). The contribution of genetics to diversity of human ageing was assessed in twin studies – see above. There are also many genes known to be influential on lifespan of animals in experimental studies of ageing – so-called “vitagenes”. Epigenetic influences on ageing may be explained, at least in part, by changes in expression of vitagenes induced by dietary factors (De Magalhaes and Church, 2005).

1.1.1.2 Rate-of-living theory of ageing

The rate-of-living theory of ageing was first suggested in 1928 by Pearl, and states that animals with a smaller energy expenditure or metabolic rate should, in theory, live longer (Pearl, 1928). Indeed, the rate at which calories are burned in the body is closely related to oxygen consumption and respiration (Walker et al., 2005). This later observation, along with the fact that damaging reactive metabolites are produced at increased rates as energy expenditure increases – reactive oxygen species (superoxide, hydrogen peroxide, hydroxyl radical; ROS), reactive nitrogen species (peroxynitrite and others; NOS) and dicarbonyls (glyoxal, methylglyoxal and others), lead to the theory that ageing occurs as a result of increased macromolecular damage. Initial theories focussed on oxidative damage (Harman, 1956). Others have highlighted possible roles of NOS (Lam et al., 2009) and reactive dicarbonyls in the contribution of glycation to ageing (Sejersen and Rattan, 2009).

1.1.1.3 Gene regulation theory of ageing

The gene regulation theory of ageing is based on the principle that, although expression of specific genes seems to be modified as age progresses (Weindruch et al., 2002), ageing occurs as a result of impaired expression of genes promoting longevity (Weinert and Timiras, 2003). The main observations made on this theory have been done in *C. elegans* and later on confirmed in *Drosophila melanogaster* (Tatar et al., 2003). Indeed, extension of life span has been shown to be regulated by expression of genes inhibiting insulin-like

signalling, hence demonstrating the role of gene regulation in ageing (Weinert and Timiras, 2003). This theory finds contemporary evidence and discussion on the effects of vitagenes – particularly in functional genomics studies utilising mutant gene deletion (knockout) and gene overexpressing transgenic organisms.

1.1.1.4 Accumulation of cell damage theory of ageing

The concept of accumulation of cell damage as a theory of ageing was originally formed from the disposable soma theory formulated by Kirkwood in 1977, stating that energy must be used wisely to be able to perform cellular maintenance aimed at conserving longevity (Kirkwood, 1977). Accumulation of cell damage from extrinsic and intrinsic sources affect DNA repair, protein repair and the antioxidant response as well as other protective mechanisms responsible for maintenance of the aging status. Indeed, somatic mutations and damage to the DNA impair cell division (Kim et al., 2002), as well as protein damage in the form of damage to the proteasome and chaperone proteins (Soti and Csermely, 2003) and increased steady-state concentrations of reactive oxygen species (ROS) due to impairment of the antioxidant cellular response (Huges and Reynolds, 2005). These are all factors contributing to the accumulation of cell damage theory of ageing.

Perspectives of theories of ageing tend towards a unified theory that embrace aspects of all of the above theories and reveal new features and emphasis of the contributory factors underlying the above theories (Partridge and Gems, 2005).

1.1.2 Experimental models of ageing

Models used experimentally to gain insight on the mechanisms of ageing range from yeast *Saccharomyces cerevisiae*, nematode *Caenorhabditis elegans*, fruit flies *Drosophila melanogaster*, laboratory rodents (mice, rats and others) to human subjects.

1.1.2.1 Yeast: *Saccharomyces cerevisiae*

The single-cell yeast, such as *Saccharomyces cerevisiae* (Figure 1), is a very good candidate in order to establish genes involved in the ageing process (Fontana et al., 2010).

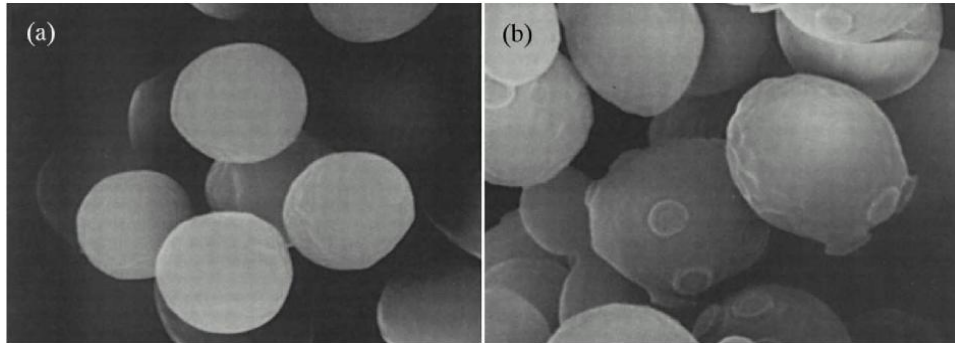


Figure 1. *Saccharomyces cerevisiae*.

(a) after 8 divisions and (b) showing morphological signs of ageing after 25 divisions. Source: Barker and Smart, 1998.

Indeed, yeast cells undergo characteristic changes as they age, such as: an increase in cell surface, a decrease in the ability to reproduce, accumulation of non-chromosomal DNA and dark stains on their surface (Powell et al., 2000) - Figure 2.

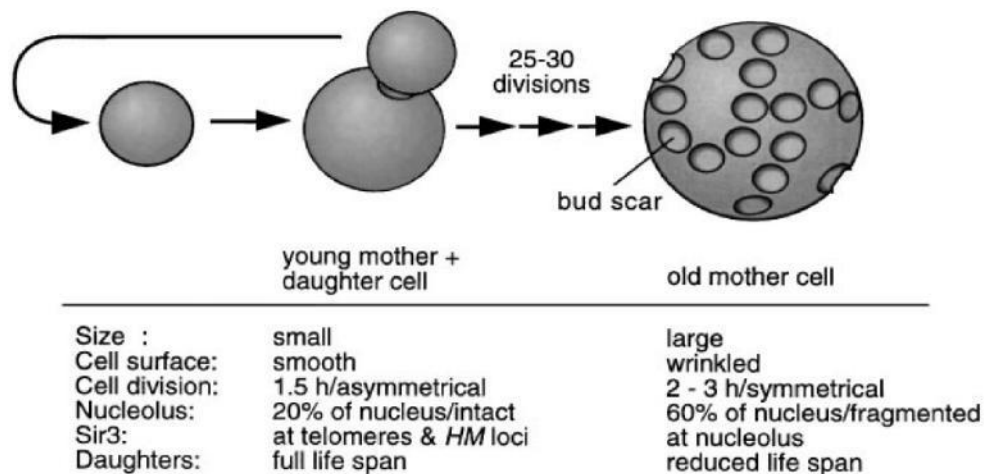


Figure 2. Effect of age on *Saccharomyces cerevisiae*.

As age progresses, mother cells produce smaller daughter cells which leads to formation of budding scars on the mother cell, as well as production of smaller daughter cells. Source: Sinclair et al., 1998.

Yeast cells are also useful in the understanding of the ageing process as the daughter cells produced from old mother cells inherit all the characteristics associated with ageing. Moreover, yeast has been extensively used for the study of Replicative Life Span (RLS) in the ageing process (Kennedy et al., 1994). Indeed, yeast replicative senescence studies have led to the identification of a battery of genes such as SIR2, a homologue of the mammalian sirtuin 2, which are thought to be involved in the regulation of life span (Steinkraus et al., 2008). The use of yeast to study the role of SIR2 in ageing has shown that SIR2 expression leads to an increase in RLS which then leads to a decrease in acetylation at the histone H4 lysine 16, which in turn is responsible for induction of silencing at the telomere and sub-telomere regions (Dang et al., 2009). Moreover, yeast models have been used for the monitoring of Chronological Life Span (CLS) which allows for observing of survival of non-dividing cells (Fabrizio and Longo, 2003) as well as the effects of caloric restriction on life span. Indeed, studies have shown that yeast lifespan is modified depending not only on the total caloric intake but also the nature of the glucose content to which they are exposed (Wu et al., 2013).

1.1.2.2 Nematode Caenorhabditis elegans

Caenorhabditis elegans is a small soil nematode of around 1 mm in length which is found in compost and gardens. These small organisms have a short life span of 2 - 3 weeks as well as rapid reproductive cycle which makes them ideal candidates for the study of ageing (Kaletsky and Murphy, 2010). As well as displaying morphological signs of ageing seen in humans (Figure 3) such as a loss of motility and reproductive capacity (Hughes et al., 2007), gene mutations in this organism can change the *C. elegans* into the dauer worm. The dauer worms are thin and can move but they do not eat. Dauers can remain viable for 3 months and go through a dormant stage with limited ageing.

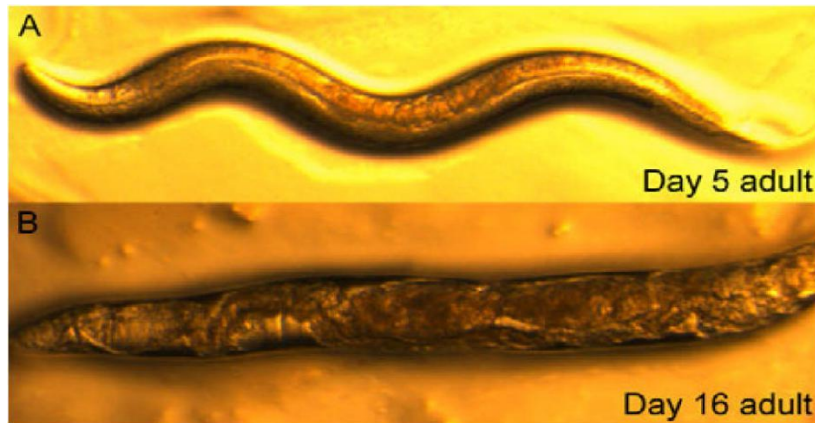


Figure 3. Morphological signs of ageing in *Caenorhabditis elegans*. (A) A 5 days old adult with good mobility and (B) a 16 days old adults with a wrinkly appearance and decreased mobility. Source: Partridge and Gems, 2002.

Indeed, as seen in Figure 4, mutations in the *daf-2* gene involved in the insulin/IGF signalling pathway has been shown to be responsible for the formation of dauer worms from *C. elegans* (Partridge and Gems, 2002).

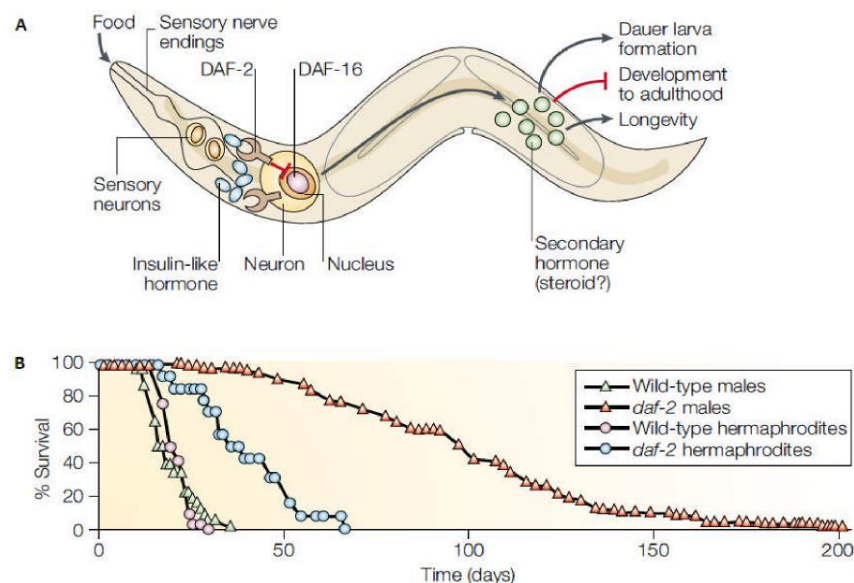


Figure 4. Implications of the *daf-2* gene in the lifespan of *C. elegans*. *daf-2* is involved in development to adulthood via the insulin/IGF signalling pathway. (B) Mutations of the *daf-2* gene leads to the formation of dauer larva from *C. elegans* which have a considerably longer lifespan. Source: Partridge and Gems, 2002.

Moreover, in the 1980s, Johnson and Wood discovered that life span in *C. elegans* has the particularity of being strongly influenced by gene polymorphism (Johnson and Wood, 1982). Indeed, this short-lived multicellular organism has been used in order to study insulin/IGF signalling in ageing (Friedman and

Johnson, 1988; Kenyon et al., 1993; Kimura et al., 1997). This expression of IGF-1 has been linked with life extension by sometimes three fold the normal lifespan as observed in wild type *C. elegans* (Partridge and Gems, 2002). Moreover, the study of *C. elegans* has provided insight on the involvement of the neuroendocrine system in the modulation of ageing. Indeed, insulin/IGF mutants also carry a mutation in the age-1 gene which in turns encodes for the lipid kinase enzyme (phosphatidylinositol-3 kinase) which is responsible for the transmission of information to trigger the Dauer-2 state in *C. elegans* (Kenyon et al., 1993). Another interesting observation is that the *C. elegans* genome contains 37 genes that encode insulin-like proteins, one of which INS-1, is very closely related to human insulin (Pierce et al., 2001). Indeed, INS-1 modulates the action of Daf-2 by antagonising it rather than activating it.

1.1.2.3 Fruit fly: Drosophila melanogaster

The fruit fly *Drosophila melanogaster* is a very useful organism in the study of ageing as it can give indication on mechanisms of ageing in different tissues and sexes (Fontana et al., 2010). Depending on the strain, *Drosophila* can live up to 70 days and show an increase in lifespan with caloric restriction (CR). Indeed, when female *Drosophila* consume 60% and male consume 40% of their normal caloric intake, a 60% and 40% life extension, respectively, can be observed (Murphy and Partridge, 2008). As seen in Figure 5, this mechanism is thought to be regulated by insulin-like peptides (DILPs) which have a direct action on the ovaries and the isoprenoid hormone responsible for male fertility (Brogiolo et al., 2001).

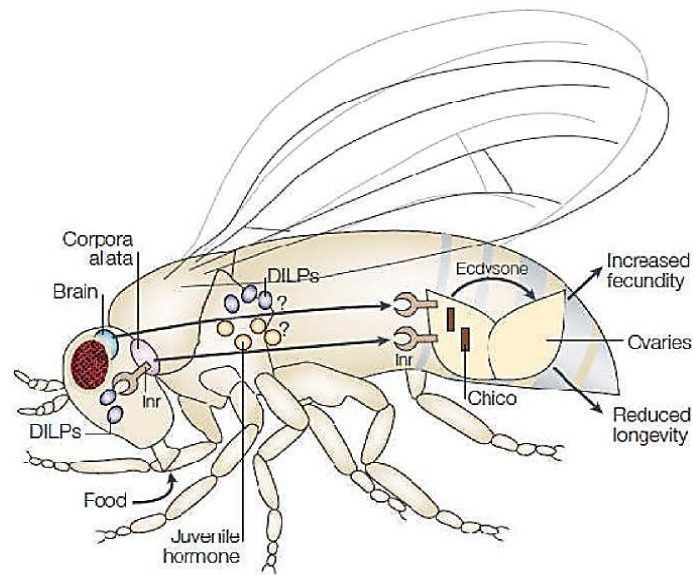


Figure 5. Mechanism of life extension by caloric restriction in the *Drosophila melanogaster*.

Upon binding of DILPs from food, the insulin receptor (Inr) is coupled with the insulin receptor substrate (chico) which leads to regulation of male juvenile sex hormones production and female ovaries development. Upon mutation of Inr and chico, an increase of lifespan of up to 85% and 52% respectively can be seen. Caloric restriction also increases lifespan of up to 3 folds in wild type *Drosophila*. Source: Partridge and Gems, 2002.

As described earlier in the *C. elegans* ageing models, the *Drosophila* equivalents of Daf-2 and age-1 (Inr-insulin-like receptor and Dp110 respectively) are responsible for determining organ and body size in these fruit flies (Weinkove and Leivers, 2000). Indeed, this mechanism is thought to be controlled by the neuroendocrine system as characterised in *C. elegans* models. Moreover, this phenomenon is somewhat faulty as only specific mutations in the insulin/IGF signalling pathway increases lifespan in the *Drosophila* and mainly had an effect on females (Partridge and Gems, 2002).

1.1.2.4 Mice

Studies of invertebrate experimental models of ageing give insight on the genes and mechanisms involved in longevity but mice are the closest model to human, which is important for the initiation of clinical trials (Fontana et al., 2010). The effect of caloric restriction in mice on their lifespan was first observed in 1986 by Weindruch and colleagues. Their observations are shown in

Figure 6, where survival is increased as CR is increased (Weindruch et al., 1986).

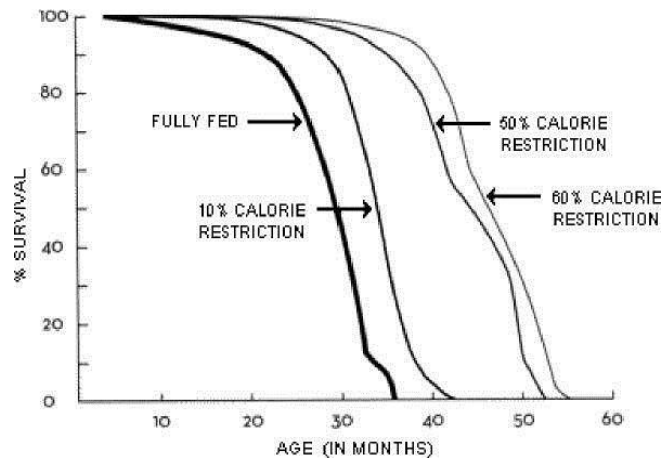


Figure 6. Survival rate of mice as a function of caloric intake.

Mice show a 20 months life extension and an extended survival rate after a 60% caloric restriction compared to an *ad libitum* feeding regime. Source: Weindruch et al., 1986.

Moreover, genetic manipulation of mice is very useful in the study of the ageing process – with expectation that where beneficial effects are found it may provide insight into critical mechanisms of ageing and where to focus efforts into development of pharmacological agents for healthy ageing. Indeed, transgenic mice genetically modified to overexpress catalase have been shown to have an extension of lifespan of up to 30 months which raises the implications of this enzyme in the ageing process (Schriner et al., 2005). However, overexpression of plasminogen activators Plau genes in mice has been shown to lead to decrease in their development, accompanied by a self-imposed caloric restriction with a 20% increase in lifespan (Miskin and Masos, 1997).

1.2 Cell senescence as a model of ageing

The above experimental models of ageing have the fundamental weakness for application to human ageing that they do not involve human cells. To develop a model of aging based on human cells the phenomenon of human cell senescence *in vitro* has been explored. Ageing is studied experimentally as proliferative senescence. The term proliferative senescence or replicative senescence (RS) refers to the inability of cells to divide further after they have gone through several replicative cycles. Therefore, as most cells in the body are post-mitotic,

meaning that they are non-dividing, RS is only a “model” of ageing as opposed to an exact representation of the ageing process.

Senescence as a model of ageing has raised controversy since its introduction by Leonard Hayflick (Hayflick, 1965). For example, the *in vivo* ageing mechanism is seen as a whole, whereas cell senescence differs in time course of events in different primary cell cultures where multiple mechanisms are involved, raising the issue of fidelity of the senescence model to the ageing process (Cristofalo and Pignolo, 1993). Moreover, it has been suggested that senescence is a process that can only occur *in vitro*. However, this argument was refuted by a study done on skin fibroblasts of older baboons where increased RS was seen as age increased (Jeyapalan et al., 2007). Pignolo *et al.* (1992) compared replicative life span *in vitro* of skin fibroblasts derived from Fischer 344 rats of 6, 24, and 29 months of age and found there was decreasing replicative capacity and more rapid induction of senescence with age of donor, suggesting that skin fibroblasts *in situ* in rats lose their replicative capacity with age. For human skin fibroblast, initial studies suggested an inverse relationship between donor age and replicative lifespan but the health status of the donors was unknown. Determination of replicative lifespans of 124 skin fibroblast cell lines from donors of different ages in the Baltimore Longitudinal Study of Aging where donors were healthy found no correlation between the proliferative potential of the cell lines and donor age (Cristofalo et al., 1998). A subsequent study however revealed that replicative fibroblasts isolated from young, middle-age, and old-age humans and humans with progeria, a rare genetic disorder characterized by accelerated aging, had changes in gene expression associated with the ageing phenotype and progeria. This suggested increasing errors in the mitotic control of dividing cells in the post-reproductive stage of life is linked to the aging process (Ly et al., 2000). Moreover, a study of cells from healthy donors and donors with the adult progeria, Werner’s syndrome, of the same age revealed that cells from donors with Werner’s syndrome had decrease proliferative capacity compared to normal donor cells (Martin et al., 1970). Despite the *in vivo* nature of senescence, this model is used in order to get insight on the ageing process. In fact, *in vivo* ageing markers are expressed *in vitro* and cell proliferation seems to be a key element in ageing as seen in senescence studies (Cristofalo and Pignolo, 1993).

1.2.1 The Hayflick Limit

Ageing at the cellular level is often referred to as ‘cellular senescence’. The concept of cellular senescence lays on the idea that proliferation of normal diploid cells can only be achieved for a limited period of time after which, cells stop dividing (Cristofalo and Pignolo, 1993). This limitation of lifespan for *in vitro* cell cultures was first described by Leonard Hayflick in 1961, going against the theory formulated by Alexis Carrel claiming that cells kept in culture have an unlimited potential for division (Carrel and Ebeling, 1921). Indeed, Hayflick and Moorhead demonstrated that culture of normal human fibroblasts followed a pattern consisting of 3 phases (Figure 7).

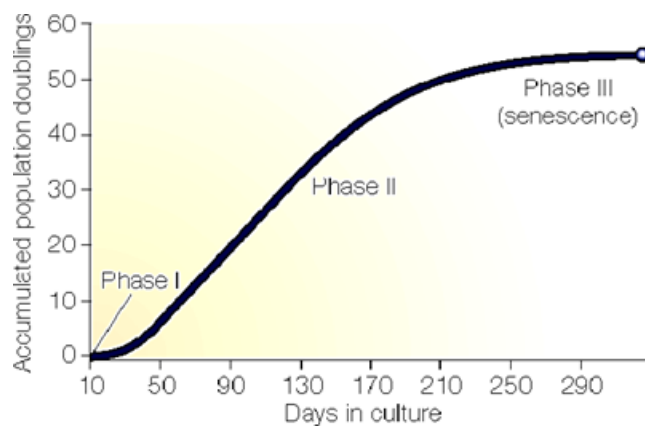


Figure 7. The 3 phases of cell culture as described by Hayflick and Moorhead.

Phase I refers to the primary culture, Phase II is characterised by an abundant exponential cell growth and Phase III is defined as the time period during which cell growth decreases and ultimately comes to an arrest (Hayflick and Moorhead, 1961; Wright and Shay, 2000).

At the start of his research on human foetal fibroblasts culture, Hayflick defined Phase 1 as the primary culture. This phase is followed by Phase II which refers to the time at which cells divide exponentially and profusely. Finally, cells enter Phase III in which they divide much slowly and eventually stop dividing (Hayflick and Moorhead, 1961). This later phase is also referred to as the ‘senescent’ phase. Moreover, the term replicative senescence (RS) was brought

about after the observation that senescence can be triggered by cell-intrinsic mechanisms after extensive proliferation (Ben-Porath and Weinberg, 2005).

Having challenged the undisputed ideas of Alexis Carrel, and described the 3 phases of cellular culture, Hayflick's onset of Phase III is now more commonly known as the Hayflick Limit. The Hayflick limit is defined as the number of times a normal cell population can divide before it comes to a point of cell growth arrest (Masaro, 2006). Indeed, Hayflick established that normal human foetal cells in culture can divide up to around 50 times after which they reach the Hayflick limit (Hayflick and Moorhead, 1961).

It is now known that the protective termini of chromosomal DNA, telomeres, are progressively shortened with the propagation of human cells in culture which ultimately causes cells to reach their Hayflick limit. Attrition of telomeres occurs due to DNA polymerase failing to completely replicate the lagging strands (Watson, 1972). Telomere length reflects the replicative history of cells in primary culture (Harley et al., 1990).

1.2.2 Markers of cell senescence

Although markers of cell senescence are numerous, their specificity is yet to be exclusive and they need to be chosen with caution when used to determine cell senescence in cultures. These markers can be phenotypic or molecular and examples are shown in Table 1.

Table 1. Phenotypic and molecular markers of cellular senescence.

Source: Salama et al., 2014.

Markers
Phenotypic markers
Lack of cell proliferation
Large and flat morphology of cells
Lack of response to growth factors
SA- β -Gal (senescence-associated β -galactosidase activity)
PML nuclear bodies
SAHF (senescence-associated heterochromatic foci)
SASP (senescence-associated secretory phenotype)
TIF (telomere dysfunction-induced foci)
TAF (telomere-associated foci)
DNA-SCARS (DNA segments with chromatin alterations reinforcing senescence)
Molecular markers
CDKIs (p16, p21, etc.)
p53
ARF
DEC1 (BHLHE40)
DCR2 (TNFRSF10D)
DDR (ATM, 53BP1, γ -H2AX, MBS1, CHK2, etc.)
SASP factors and receptors (IL6, IL8, IL1, MMPs, PAI1, etc.)
HMGA proteins
Heterochromatin markers (HP1, H3K9me3, etc.)
Lamin B1 reduction

Some markers, such as DEC1, DCR2, and heterochromatin markers, are less commonly used than others.

1.2.2.1 Exit from the cell cycle

Long-term exit from the cell cycle is a necessary marker of cell senescence *in vitro* and *in vivo*. However, this is not a unique phenomenon as terminal differentiation of cells causes the same effect. Differentiation is triggered by physiological factors which does not involve the activation of tumor suppressor networks. To prevent or delay senescence – as attempted in this study – added compounds will need to delay or weaken engagement of cells in senescence pathways or block their mediators (Kuilman et al., 2010).

1.2.2.2 Changes in cell morphology

It is long established that when cells reach senescence, an increase in cell size and heterogeneity can be observed (Greenberg et al., 1977). Alongside this cell expansion, the size of senescent human fibroblasts nucleolus and nucleus has been observed to increase as the ageing process progresses (Mitsuishi et al., 2010). As shown in Figure 8, senescent human fibroblasts display prominent morphological alterations. Moreover, the lysosome and Golgi apparatus of senescent cells appear larger than in younger cells (Brandes et al., 1972).

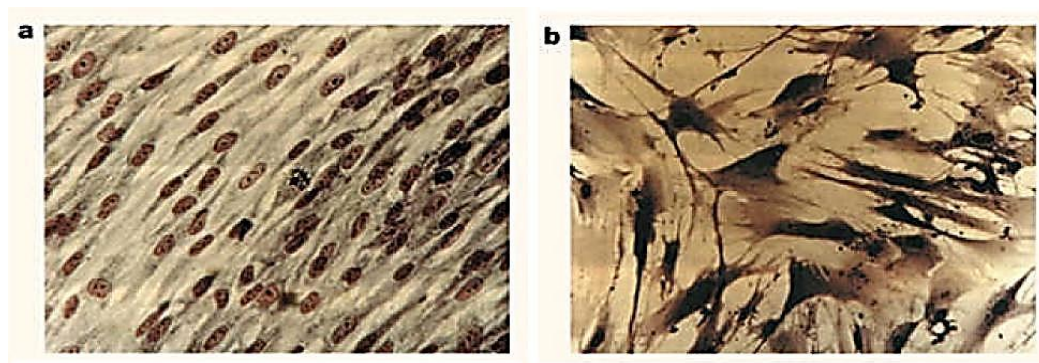


Figure 8. Morphological changes observed in WI-38 fibroblast.

Observations at (a) population doubling 20 and (b) population doubling 40 (Shay and Wright, 2000).

Other morphological changes include a displacement of the endoplasmic reticulum (ER) as well as changes in the cytosol such as an accumulation of cytoplasmic microfilaments (Lipetz and Cristofalo, 1972). Finally, cells reaching senescence display a decreased density at harvest which is accompanied by a rarefaction of cell to cell contact (Cristofalo et al., 1998).

1.2.2.3 Beta-galactosidase

Beta-galactosidase (SA- β -Gal) is the most commonly used marker to quantify senescence at the cellular level. The SA- β -Gal assay was first described in 1995 by Dimri *et al.* in which they observed that at pH 6.0, senescent cells expressed the β -galactosidase enzyme in the cytosol when compared with fibroblasts from young donors (Dimri et al., 1995). In this assay, the cleavage of 5-bromo-4-chloro-3-indolyl-beta-D-galactopyranoside (X-Gal) is performed by β -galactosidase (Figure 9).

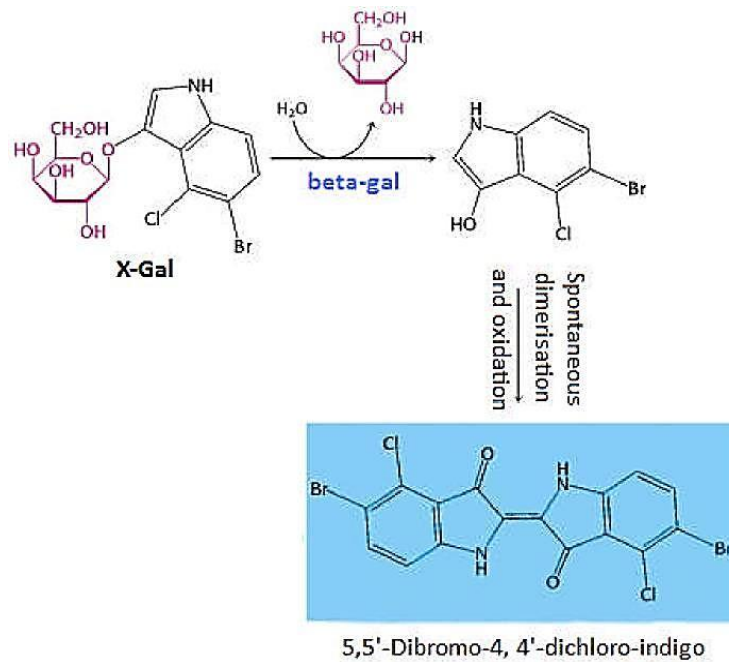
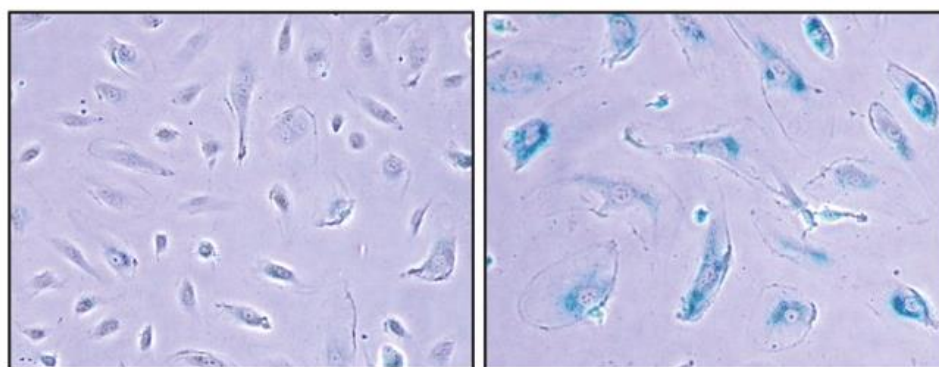


Figure 9. The β -Galactosidase reaction with chromogenic substrate.

X-Gal is cleaved by the enzyme β -galactosidase which leads to the formation of galactose and 5-bromo-4-chloro-3-hydroxyindole. This later product then undergoes spontaneous dimerization and oxidation from which the insoluble blue dye 5,5'-dibromo-4,4'-dichloro-indigo is produced. Senescent cells express β -galactosidase and are easily quantified by counting cells which produce the blue dye. Modified from Berg et al., 2002.

The end result of this reaction is the formation of a characteristic dark blue colour which is easily detectable on senescent cells (Figure 10).



Non-senescent cells

Replicative senescent cells

Figure 10. Senescence detected by beta-galactosidase activity staining in replicative senescent and non-senescent WI-38 human foetal lung fibroblasts.

Source: Debacq-Chainiaux et al., 2009.

1.2.2.4 Lipofuscin

The pigment lipofuscin (LF) was first discovered in 1842 by Hannover (O'Donovan and Tully, 1996). Since over a century, LF pigments deposits is considered to be a characteristic of ageing (Jung et al., 2009) as its accumulation seems to follow a linear trend when plotted against age of the donor. LF is a complex mixture of fluorophores of excitation and emission wavelength ranges 340 – 390 nm and 430 – 490 nm, respectively - some formed oxidatively, others non-oxidatively and also endogenous fluorophoric metabolites (Li et al., 2006; Na et al., 2000; Sohal, 1981; Xue et al., 2008a).

1.2.2.5 Activation of tumor suppressor networks

p53 and p16INK4A–RB signal transduction cascades commonly mediate the activation of the senescence program (Lowe et al., 2004) and therefore components of these pathways have been proposed as biomarkers of cell senescence. In human fibroblasts undergoing RS, an active, hypophosphorylated form of RB accumulates (Stein et al., 1990). Moreover, p53 shows increased activity and/or levels in human fibroblasts undergoing RS (Atadja et al., 1995). An activator of RB, p16INK4A, is induced in senescent cells in vitro. Moreover, other proteins such as p21CIP1 and p15INK4B accumulate in cells undergoing senescence. These proteins are part of the p16INK4A–RB and p53 pathways (Kuilman et al., 2010). The wingless-type mouse mammary tumor virus (MMTV) integration site family member 16B (WNT16B) has been found to be a specific marker of senescence (Binet et al., 2009). WNT16B is one of two ligand isoforms of the WNT family of seven transmembrane receptors and is implicated in tumorigenesis and development (Nusse, 2005). The WNT family has been shown to be involved in senescence (Maiese et al., 2008) and although WNT16B structure and mechanism pathway is yet to be fully understood, it has been found to be specifically overexpressed in RS of skin fibroblasts (Binet et al., 2009).

Immortalisation of HDFs has also been achieved by inactivation of p53 and pRb (de Magalhaes, 2004). p53 and pRb are both tumour suppressor proteins which are involved in the prevention of cancer by suppression of apoptosis (Ben-Porath and Weinberg, 2005; Matlashewski et al., 1984). The p53/p21 and Rb/p16 pathways are thought to be the central pathways for senescence activation (Ben-

Porath and Weinberg, 2005). p53 is encoded by the TP53 gene and is often referred to as the ‘guardian of the genome’ (Matlashewski et al., 1984). Indeed, the main purpose of p53 is to conserve genome stability (Strachan and Read, 1999). The structural organisation of p53 (Figure 11) is defined by four small nodes and four large nodes, the latest forming the four cores of the structure, and an N- and C-terminal (Aramayo et al., 2011).

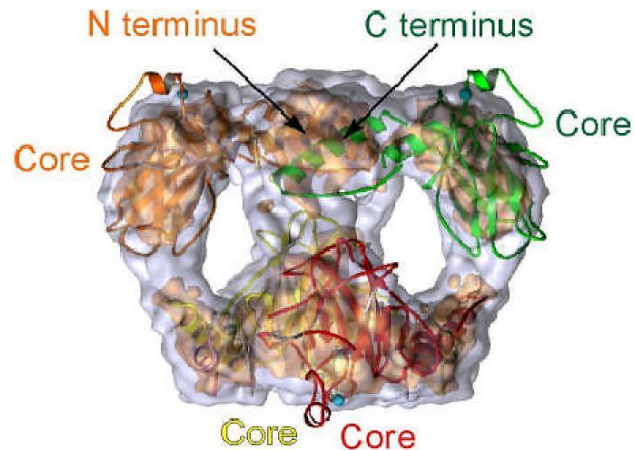


Figure 11. The structural organisation of the tumour suppressor protein p53. Four cores are part of the eight nodes that constitute the general structure of p53 as well as an N- and C-terminal. Source: Aramayo et al., 2011.

The retinoblastoma protein Rb is encoded by the RB1 gene and is considered a tumour suppressive factor due to its ability to inhibit cell cycle progression (Xiao et al., 2003). pRb has an 18 helixes structure contained in two domains: Rb-A and Rb-B (Lee et al., 1998). These two domains form a pocket (Figure 12) to which the transcription factor E2F binds, allowing for effective transcription of genes involved in DNA replication and cell cycle progression (Xiao et al., 2003)

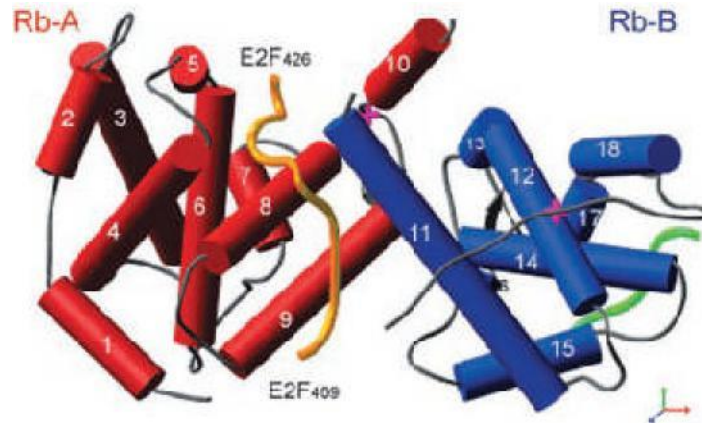


Figure 12. The structural organisation of the tumour suppressor protein pRb.

Eighteen helices constitute the two domains of pRb which form a groove allowing the transcription factor E2F to bind for effective transcription of genes involved in cell cycle progression and DNA replication. Source: Xiao et al., 2003.

Activation of tumour suppressor protein P19^{ARF}, coupled to the Mdm2 protein, leads to the degradation of p53. This, in turn, leads to direct onset of senescence (Lowe et al., 2004) or activation of the cyclin-dependent kinase inhibitor 1 (p21), leading to inactivation of the cyclinE/cyclin dependent kinase 2 (cdk2) complex (Chuaire-Noack et al., 2010). This later results in the inactivation of Rb and subsequently triggers senescence as well as inactivation of E2F (Gewirtz et al., 2008). Moreover, senescence activating factors can also turn on the p16^{lnk4a} cyclin dependent kinase inhibitor which leads to inhibition of the cyclinD/cdk4,6 complex (Roninson, 2003). This later event results in indirect cell growth arrest through inhibition of the Rb/E2F complex and leads to senescence (Chuaire-Noack et al., 2010).

1.2.3 Replicative senescence *in vivo*

Application of biomarkers of senescence to pre-clinical *in vivo* and clinical studies have suggested RS occurs *in vivo*. An increase in SA- β -Gal activity was detected in the skin of elderly people (Dimri et al., 1995) and a decrease in telomere length was found in some cell types in aged tissue (Cristofalo et al., 2004). Later studies have shown increased DNA damage at telomeres and heterochromatinization markers (53BP1, γ -H2AX, phospho-Ser 1981-ATM, HP-1b, and HIRA) were increased in dermal fibroblasts from aging

baboons (Herbig et al., 2006). Moreover, cellular senescence is detected in mitotic tissues of aging primates (Jeyapalan et al., 2007) and senescent cells have also been detected in intestine, kidney, and spleen of mice (Cosme-Blanco et al., 2007). There is also evidence of increased cell senescence in disease. For example, in atherosclerosis there is induction of SA- β -Gal activity (Minamino et al., 2002) and telomere shortening (Foreman and Tang, 2003). Senescent cells have also been observed in osteoarthritis (Price et al., 2002). These observations are in accordance with the proposal that RS contributes to age-related disease (Campisi, 2005). Finally, there has also been findings supporting the suggestion by Hayflick that replicative senescence limits tumorigenesis (Hayflick, 1965; Kuilman et al., 2010).

1.2.4 Mechanism of cell senescence

One of the most important triggers for the onset of RS is the shortening of telomeres. Telomeres are found in eukaryotes and are nucleo-protein structures capping the end of chromosomes in order to conserve normal chromosomal function (Foyer et al., 2009). These TTAGGG repeats (Figure 13) are associated with an assortment of proteins involved in replication, chromosome maintenance and nuclear attachment (Kanoh and Ishikawa, 2003).

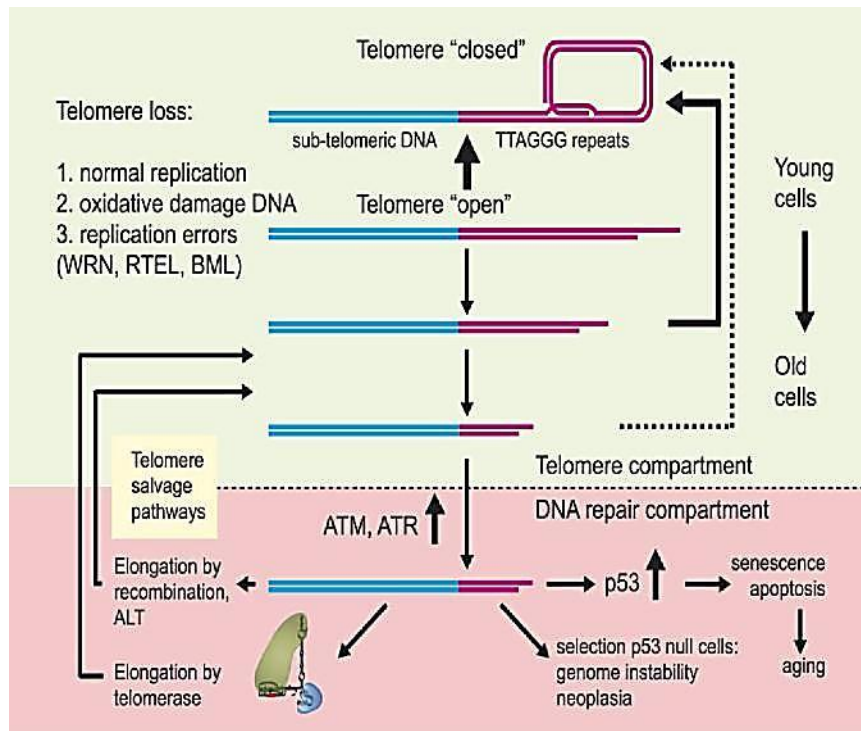


Figure 13. The telomere shortening process.

Telomere shortening occurs as a result of normal cell replication, oxidative DNA damage and replication errors. In this process, when elongation with telomerase is no longer possible, telomeres shortening occurs as cells go through the ageing process. ATM: ataxia telangiectasia mutated kinase, ATR: Rad3-related protein. Source: Jiang et al., 2007.

Activation of RS in response to telomere DNA damage provides a mechanism of cell autonomous RS. Since the observation in the early 1990s that telomeres shorten as RS progresses (Harley et al., 1990), the involvement of the enzyme telomerase for the control of telomere lengthening as well as the expression of the catalytic subunit of human telomerase (hTERT) has been suggested (Bodnar et al., 1998). Indeed, some studies even suggest that induction of hTERT in ageing human diploid fibroblasts (HDFs) could overcome progression of RS (Funk et al., 2000). Rarefaction of the enzyme telomerase, responsible for maintaining telomere length, has been observed at the onset and throughout the process of senescence (Ahmed and Tollefsbol, 2001). Moreover, these observations have been strengthened by the observation that exogenous supplementation of telomerase in cell cultures showed beneficial effects in terms of cell longevity and viability (Bodnar et al., 1998).

The protective ability of telomeres is disturbed when they reach a dangerous minimal length. This critical minimal length then leads to the activation of a DNA damage response (DDR) which is characterised by the formation of foci (Kuilman et al., 2010). These foci are quantified by positive staining to the phosphorylated form of the histone variant H2AX (g-H2AX) and proteins 53BP1, NBS1, and MDC1. Moreover, DNA damage kinases ATM and ATR are activated in senescent cells (d'Adda di Fagagna et al., 2003). These kinases activate CHK1 and CHK2 kinases and link with cell cycle proteins such as the CDC25 family of phosphatases and p53 (Fujita et al., 2009). Transient proliferation arrest for repair of damage is induced but if the DNA damage exceeds a critical threshold apoptosis, senescence is activated (d'Adda di Fagagna et al., 2003). This triggering of cellular senescence by telomere dysfunction, radiation, oncogenes activation and tumour suppressor activation is schematised in Figure 14 below.

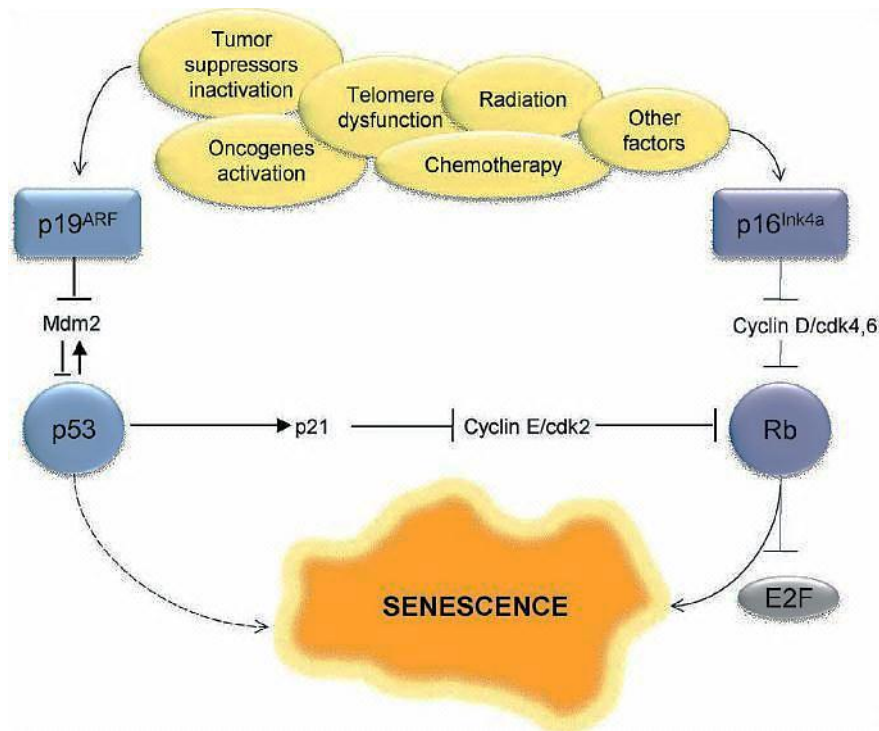


Figure 14. Activating pathways of senescence.

The mechanisms underlying senescence are triggered by factors such as telomere dysfunction, radiation, oncogenes activation and tumour suppressor activation. Source: Chuaire-Noack et al., 2010.

1.2.4.1 Senescence-associated secretory phenotype

There are, however, non-cell-autonomous effects observed in cell senescence – such as senescence-associated secretory phenotype (SASP) – which are linked to functional changes in pathophysiology and likely contribute to declining organ function with aging. Senescence may not be a singular state but rather a heterogeneous phenotype driven by diverse stresses and multiple effector programs in a functional network. Indeed, late passage human fibroblasts or fibroblasts derived from subjects with premature aging syndromes secrete proteins such as plasminogen activator inhibitor type-1 (PAI-1), a range of cytokines, chemokines and proteases (Campisi, 2005; Kuilman and Peeper, 2009). Therefore, as seen in Figure 15, cellular senescence supports a range of functions, including autocrine and paracrine signalling, protumorigenic and tumor-suppressive effects, and pro- and anti-inflammatory signalling (Salama et al., 2014). Indeed, transcription factors, NF- κ B and C/EBP β , act cooperatively to regulate inflammatory components of SASP whilst IL6 and IL8 enhance senescence.

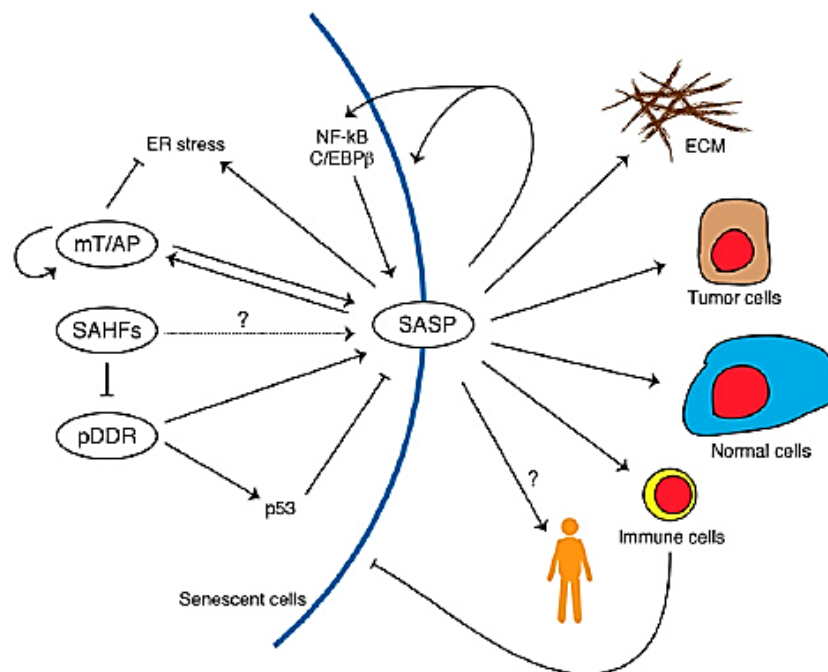


Figure 15. Schematic model of senescence and its biological functions.
Source: Salama et al., 2014.

1.2.4.2 Senescence and changes in cellular metabolism - Protein degradation pathways

Autophagy is a cytoplasmic degradation mechanism for usually large proteins and organelles (Badadani, 2012). The basal level of autophagy plays an important role for quality control of macromolecules and energy homeostasis but it can also be induced in response to cytotoxic stresses. Indeed, a gradual shift in protein degradation from polyubiquitination of the proteasome pathway to autophagy was found in human skin fibroblasts during RS linked to SASP (Gamerding et al., 2009). mTOR is a nutrient-sensitive kinase which inhibits the initial step of autophagy but is involved in facilitating later stages of the process using autolysosomes. Moreover, proteasomal protein degradation also plays important roles in senescence. Therefore, highly active SASP may overwhelm the cellular capacity for synthesis and the processing of secretory proteins, leading to proteotoxic stress.

1.2.4.3 Senescence and changes in cellular metabolism - Mitochondria metabolism

Partial uncoupling of oxidative phosphorylation in mitochondria is found in RS of human skin fibroblasts (Hutter et al., 2004). Indeed, glycolysis and oxygen consumption were shown to be enhanced in RS and that enhanced energy production is critical for progression of RS (Hutter et al., 2004). Finally, most studies also claim that up-regulation of reactive oxygen species (ROS) is a critical mediator of senescence (Lu and Finkel, 2008).

1.2.5 Theories of ageing as applied to cell senescence – accumulation of macromolecular damage

Ageing is associated with the accumulation of macromolecular damage - protein, lipid and DNA damaged by spontaneous modifications. This processes linked to the formation of macromolecular damage in the onset and progression of senescence are thought to be oxidation, glycation, metabolic stress, lipogenic stress and failure of clearance mechanisms for macromolecular damage.

1.2.5.1 Oxidative damage

In 1956, Denham Harman established the theory that ageing is caused by an accretion of reactive oxygen species (ROS) in cells (Harman, 1956). The oxidation of proteins, lipids, saccharides and nucleotides in physiological systems occurs by interaction with oxidizing agents such as hydrogen peroxide H_2O_2 , hydroperoxides ROOH, hypochlorite ClO^- , peroxynitrite and other oxidizing reactive intermediates (hydroxyl radical HO^\bullet , carbonate radical anion $CO_3^{\bullet-}$, and others) (Finkel and Holbrook, 2000). These processes may be catalysed by trace redox active metal ions such as iron (III) or ferric ion Fe^{3+} , and Cu (II) or cupric Cu^{2+} ion (Castellani et al., 2004). Hydrogen peroxide in physiological systems originates mainly from the dismutation of superoxide $O_2^{\bullet-}$ formed by inefficiency of mitochondrial respiration (Chance et al., 1979), superoxide-forming enzymes – such as phagocyte and vascular NADPH oxidases (Lassegue and Clempus, 2003), uncoupling of enzymatic reactions (for example, nitric oxide synthases) (Du et al., 1999), and autoxidation of reducing metabolites (Finkel and Holbrook, 2000). Hypochlorite is formed by the enzymatic reaction of myeloperoxidase in neutrophils (Naskalski et al., 2002). Extracellular proteins are more susceptible to oxidation than cellular proteins because the non-enzymatic and enzymatic activities of antioxidants have mostly an intracellular location. However, one of the sources of highest flux of hydrogen peroxide generation, mitochondria (Murphy, 2009), is also intracellular. Although the cytoplasm in physiological systems is maintained under reducing conditions by the presence of high concentrations of low molecular mass peptide thiols (usually glutathione, GSH), there is nevertheless a residual low level of oxidative damage to proteins, lipids, saccharides and nucleotides in cellular and extracellular compartments. Oxidative damage to proteins forms oxidised amino acid residues (Thornalley and Rabbani, 2014) and are shown in Figure 16. Oxidative damage to lipids forms lipid peroxidation products such as F2-isoprostanes, 4-hydroxynonenal and malondialdehyde (Negre-Salvayre et al., 2010) and oxidative damage to saccharides may form dicarbonyl glycating agents – see below, and oxidation of DNA forms 8-dihydro-8-oxo-2'-deoxyguanosine (8-OxodG) (Cooke et al., 2008).

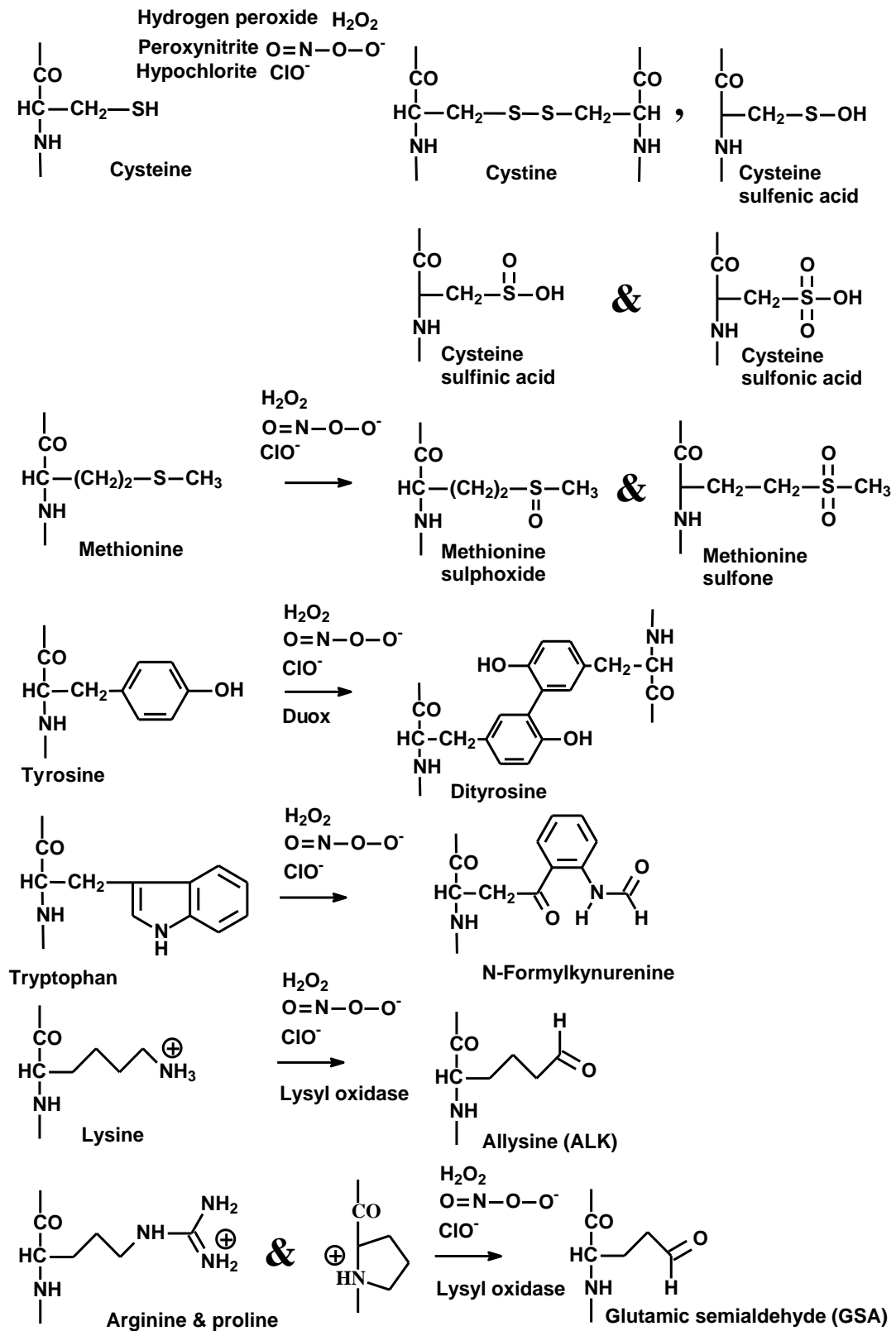


Figure 16. Formation of oxidised amino acid residues from oxidative damage to proteins.

Source: Thornalley and Rabbani, 2014.

The notion of oxidative stress emerged from the concept that ROS become excessively available in cells, leading to impaired cellular functions and senescence (Balaban et al., 2005). Oxidative stress is defined as an imbalance of oxidants and antioxidants in favour of the former potentially leading to cell damage (Sies, 1993). The production of ROS is triggered by endogenous sources (mitochondria, lipoxygenases, peroxisomes, autoxidation of thiol and other reducing metabolites) and exogenous sources (UV light, environmental toxins) – Figure 17. Moreover, oxidative damage is thought to be caused by an imbalance of the enzymatic members of the anti-oxidant defence such as catalase (CAT), glutathione peroxidase (GPx) and superoxide dismutase (SOD) (Finkel, 1998) and non-enzymatic members such as Vitamin A, C and E as well as the tripeptide glutathione (GSH) (Finkel and Holbrook, 2000).

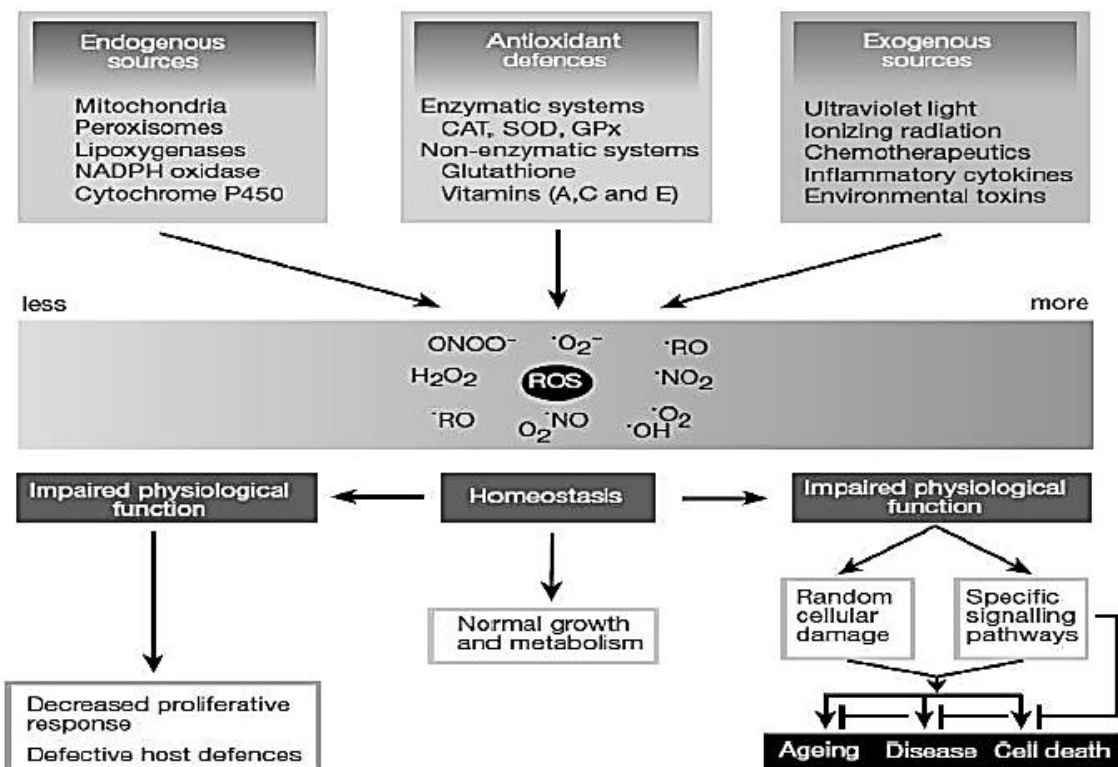


Figure 17. Mechanisms of oxidative damage involved in the ageing process.
Source: Xue et al., 2008a.

1.2.5.2 Glycation

Glycation is a process which relies upon the non-enzymatic attachment of a reducing sugar or sugar derivative to a protein but this process is not available to non-reducing oligosaccharides such as sucrose, in which aldehyde or ketone groups of component monosaccharides have been converted to ketal and acetal groups (Thornalley and Rabbani, 2014). Recently, the glycation of arginine residues by dicarbonyl metabolites has been found to be a major feature of protein glycation in physiological systems and evidence is also pointing towards an involvement of cysteine residues. Protein glycation is possible through sequential and parallel reactions known as the Maillard reaction (Thornalley and Rabbani, 2014). Amongst the adducts formed through glycation are the early glycation adducts and the advanced glycation endproducts (AGEs). Early glycation adducts are Schiff's base and Amadori products or fructosamine residues formed at early stages of glycation processes whereas AGEs are formed in both early and advanced stages (Rabbani and Thornalley, 2012a). Non-oxidative processes allow for the formation of the major glycation adducts N_ε-fructosyl-lysine (FL) residues and methylglyoxal derived hydroimidazolone N_δ-(5-hydro-5-methyl-4-imidazolone-2-yl)ornithine (MG-H1) in physiological systems. Finally, the glycoxidation products N_ε-carboxymethyl-lysine (CML) and pentosidine are AGEs formed using oxidative processes (Thornalley and Rabbani, 2014).

Glycation accounts for 0.1 to 0.2% of cellular arginine and lysine residues in the body (Thornalley et al., 2003). This physiological process causes damage to proteins and results in the formation of glycated amino-acid residues (Xue et al., 2008a). These residues are formed by the spontaneous reaction between monosaccharide and proteins. Glycating agents are formed from the degradation of glycated proteins and lipid peroxidation and include dicarbonyls such as methylglyoxal, glyoxal and 3-deoxyglucosone (3-DG) (Thornalley et al., 2003) which act as precursors for advanced glycation end products (AGEs) directly linked with senescence progression.

Glucose modifies the N-terminal and lysine residue amino groups of proteins forming mainly fructosamine derivatives (Bookchin and Gallop, 1968). This glycation is repaired enzymatically by fructosamine-3-phosphokinase

(F3PK) (Delpierre et al., 2000). Gene deletion of F3PK produces marked increased in fructosyl-lysine with little adverse effect (Veiga da-Cunha et al., 2006), suggesting this type of glycation has little effect on ageing and senescence. In quantitative assessments of advanced glycation endproducts (AGEs) in physiological systems from 2003, it became clear that glycation of proteins by the physiological metabolite methylglyoxal (MG) produces levels of cellular and extracellular proteins modification approaching and sometimes exceeding that of glucose (Thornalley et al., 2003). In contrast to glycation by glucose, protein glycation by MG is directed to arginine residues forming hydroimidazolone N δ -(5-hydro-5-methyl-4-imidazol-2-yl)ornithine (MG-H1) residues. MG glycation also forms AGEs in DNA by glycation of deoxyguanosine bases, forming MG-derived imidazopurinone, 3-(2'-deoxyriboseyl)-6,7-dihydro-6,7-dihydroxy-6/7-methylimidazo-[2,3-b]purine-9(8)one isomers (MGdG). MGdG is a quantitatively major type of DNA damage *in vivo*, often exceeding that of the oxidative marker 8-oxo-7,8-dihydro-2'-deoxyguanosine (8-OxodG) (Thornalley et al., 2010). MG is mainly metabolised by glyoxalase 1 (Glo1) of the glyoxalase system (Thornalley, 1993). Gene deletion of GLO1 is lethal to the embryo and GLO1 silencing and chemical inhibition increases MG concentration, increases MG-H1 residues of cellular and extracellular proteins and MGdG adducts of DNA and is associated with cell dysfunction, premature ageing and development of vascular disease (Giacco et al., 2014; Morcos et al., 2008). Overexpression of Glo1 decreased MG-H1 residue content of protein and increased longevity - exemplified by life extension of Glo1 transgenic *Caenorhabditis elegans* (Morcos et al., 2008). Induction of Glo1 expression decreases cellular and extracellular concentration of MG, decreased glycation and prevented MG-induced mutagenesis and cell dysfunction (Xue et al., 2012b). MG glycation is therefore particularly insidious. As seen in Figure 18 and 19 below, recent research is shedding light on the reasons for which these events happen and point out the benefits available if Glo1 inducers can be developed and deployed.

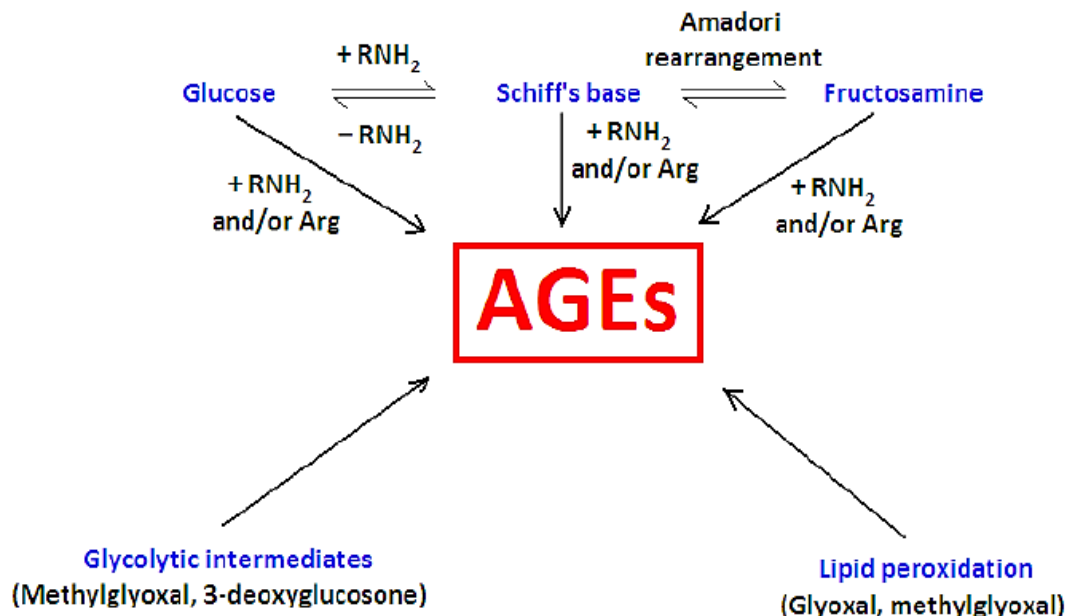


Figure 18. Mechanisms of formation of AGEs from glucose, glycolytic intermediates and lipid peroxidation.
 Source: Xue *et al.*, 2008.

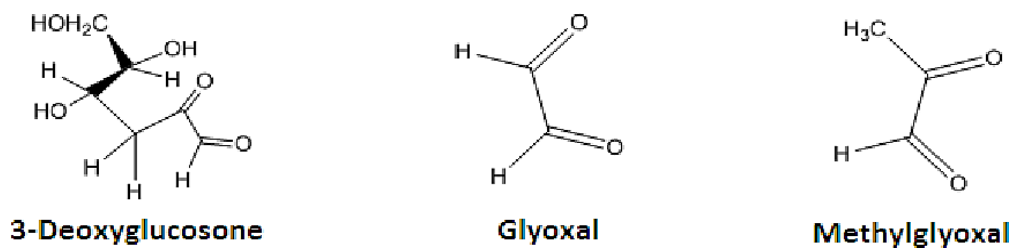


Figure 19. Molecular structure of the physiologically reactive glycating dicarbonyls 3-deoxyglucosone (3-DG), glyoxal and methylglyoxal.
 Source: Xue *et al.*, 2008.

The involvement of the reactive glycating species in the ageing process is summarised in Figure 20 where their fluctuation is triggered by endogenous sources and exogenous sources as well as impairment of the anti-glycation defence. The resulting impairment of physiological functions leads to an increase in hotspot modification at functional sites which contributes to the ageing process.

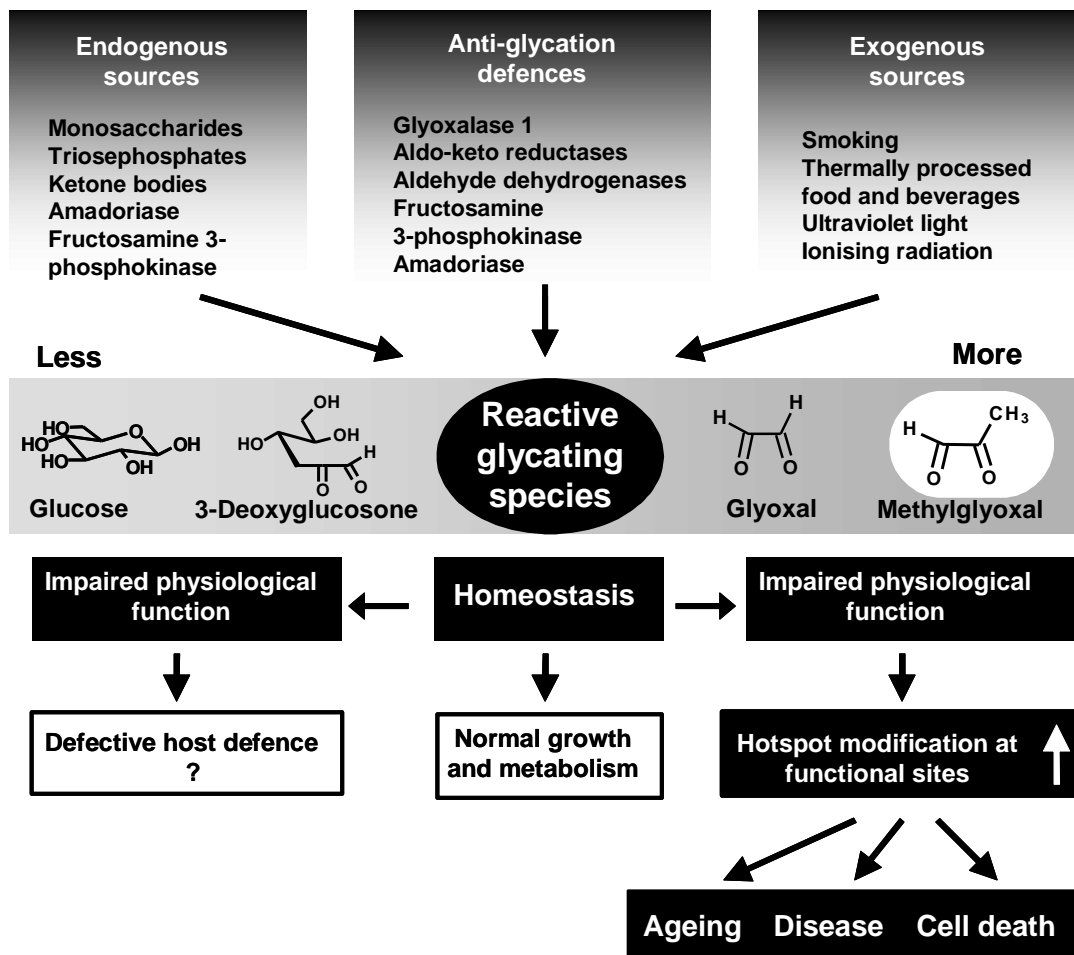


Figure 20. Reactive glycating species function in the ageing process.

Source: Xue *et al.*, 2008.

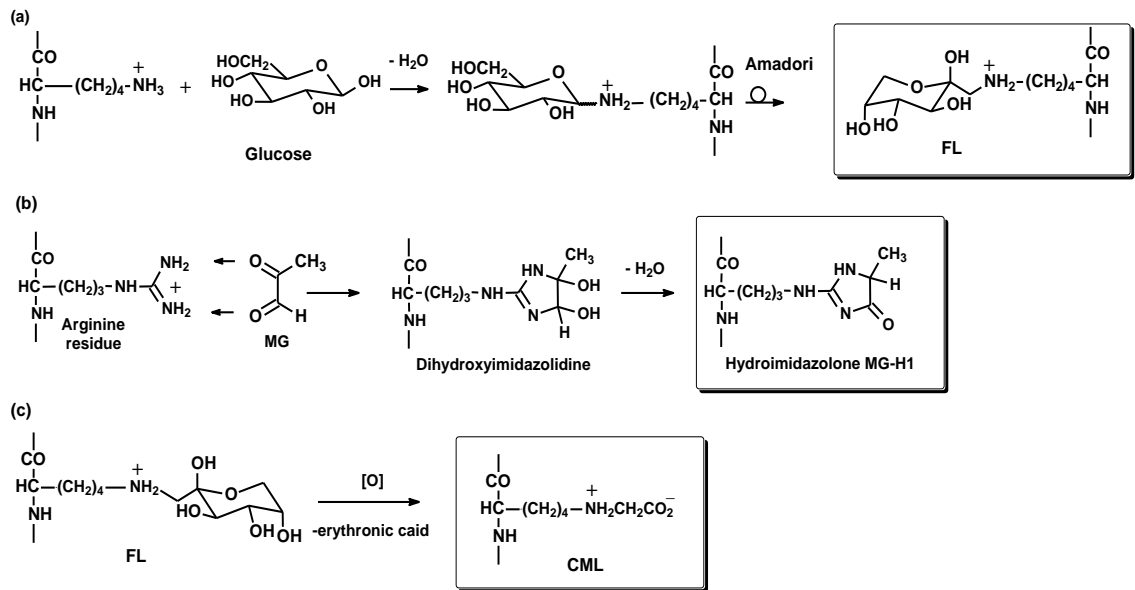


Figure 21. Mechanism of formation of major protein glycation adducts.

a. N ϵ -fructosyl-lysine. b. hydroimidazolone and c. N δ -(5-hydro-5-methyl-4-imidazolone-2-yl)ornithine (MG-H1).

Source: Rabbani and Thornalley, 2012b.

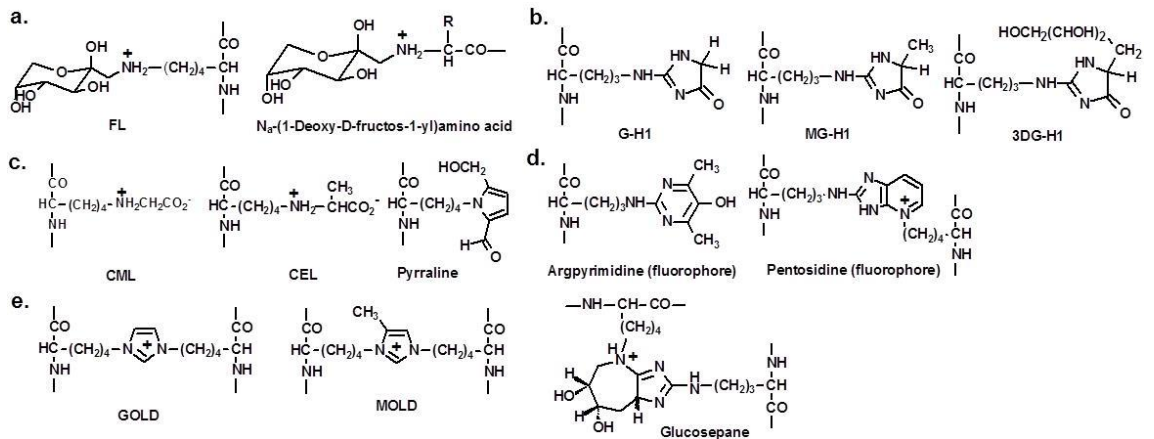


Figure 22. Protein glycation adduct residues in physiological systems.

a. Early glycation adducts – FL and N α -(1-deoxy-D-fructos-1-yl)amino acid residues. Advanced glycation endproducts: b. Hydroimidazolones, c. Monolysyl d. Fluorophorescent AGEs, and e. Non-fluorescent crosslinks. For the corresponding free adducts at physiological pH, the N-terminal amino group is protonated $-\text{NH}_3^+$ and the C-terminal carbonyl is a carboxylate $-\text{CO}_2^-$ moiety. Source: Rabbani and Thornalley, 2012b.

Methylglyoxal glycation of protein is damaging to cells as a positive charge is lost during the modification process of MG to MG-H1. Indeed, this causes a loss in the electrostatic interactions with surrounding ligands and groups

linked to arginine residues (Rabbani and Thornalley, 2014) – Figure 21 and 22. However, fructosamine residues formed as a result of glucose glycation leads to the acquisition of a positive charge on the lysine residue on the amino group. Therefore, damage to arginine is one of the main cause by which MG glycation is damaging as (i) modification is directed to arginine residues which have the highest probability of any amino acid residue for location at functional sites of proteins (predicted probability that a functional site amino acid residue is arginine = 20%); (ii) functionally important arginine residues are often hotspots for dicarbonyl glycation; and (iii) MG-H1 is one of the most quantitatively important, spontaneous irreversible modifications of the proteome in health and disease (Rabbani and Thornalley, 2014).

1.3 The Nrf2 system

One of the key triggers influential for the development of senescence is oxidative stress. In relation to this is the Keap1-Nrf2-antioxidant response element (ARE) signalling pathway and its role in senescence.

Stress responsive signalling coordinated by nuclear factor erythroid 2-related factor 2 (Nrf2) provides an adaptive response for protection of cells against toxic insults, oxidative stress and metabolic dysfunction – Figure 23. Nrf2 regulates a battery of protective genes by binding to regulatory anti-oxidant response elements (AREs). Nrf2 regulates the cellular expression of a battery of protective genes countering oxidative stress, environment toxic insults, lipid peroxidation, macromolecular damage, metabolic dysfunction and cell senescence (Kapeta et al., 2010; Malhotra et al., 2010; Taguchi et al., 2011; Xue et al., 2013).

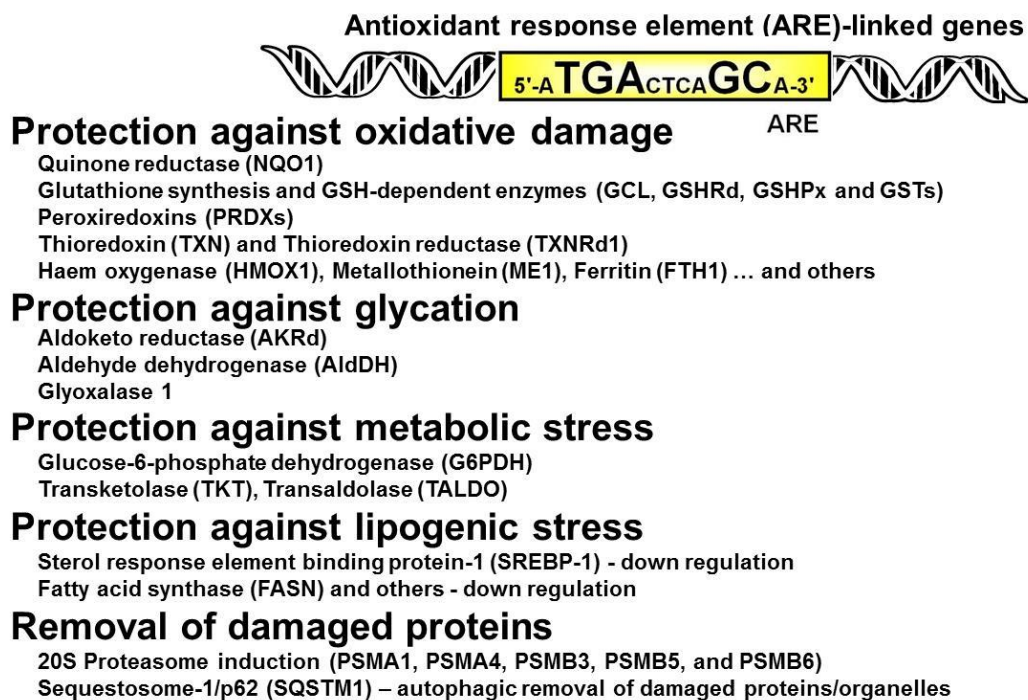


Figure 23. Examples of the battery of protective genes regulated by the Nrf2 system and their role in the anti-stress gene response.

Provided by Professor Paul J. Thornalley.

The Nrf2 system senses challenges to homeostasis in the cell cytoplasm and activates a protective transcriptional response. Such stress-responsive signalling is vital in resisting oxidative damage, cell dysfunction, cytotoxicity and mutagenesis, thereby contributing to resistance to drug toxicity, wound healing and decreasing risk of diabetes, vascular and neurodegenerative disease and ageing-related disease (Collins et al., 2009; Hayashi et al., 2013; Okawa et al., 2006; Pearson et al., 2008). Improved manipulation of the Nrf2 system would likely lead to more effective deployment of micronutrient Nrf2 activators in functional foods to support healthy ageing where delay of cell senescence may be a contributory factor.

Human Nrf2 is a protein of 68 kDa which is detected in SDS-PAGE as a band at 98 kDa of a dominant phosphorylated form (Lau et al., 2013; Xue et al., 2008b). According to current understanding, under basal conditions, Nrf2 transactivational activity is repressed by binding to Kelch-like erythroid cell-

derived protein with CNC homology-associated protein 1 (Keap1). This acts as an inhibitor holding Nrf2 in the cytoplasm and facilitating its degradation. Keap1 is a substrate adaptor protein for Cullin-3 (Cul3)-dependent E2 ubiquitin ligase complex, directing Nrf2 for degradation by the 26S proteasome (Cullinan et al., 2004). Keap1 and Nrf2 are held together with the protein threonine phosphatase, PGAM5, which tethers Keap1 and Nrf2 to the outer mitochondrial membrane (Lo and Hannink, 2008).

The mechanisms of stress sensing and surveillance by the Nrf2 system are uncertain but under conditions of oxidative and electrophilic stress Nrf2 is released from Keap1. Nrf2 is phosphorylated by casein kinase-2 (CK2) (Apopa et al., 2008), translocates to the nucleus via importins $\alpha 5$ and $\beta 1$ (Theodore et al., 2008) and therein activates its target genes by binding to regulatory AREs (Pi et al., 2007). Thereafter Nrf2 is phosphorylated by Fyn kinase and expelled from the nucleus via the nuclear membrane export channel exportin-1/crm1 and degraded (Jain et al., 2005) – Figure 24. Endogenous activators are lipid peroxidation and arachidonic acid oxidation products, 4-hydroxynonenal and J₃-isoprostanes (Gao et al., 2007; Ishii et al., 2004) and exogenous activators are typically bioactive compounds from fruits and vegetables such as glucosinolates-derived isothiocyanates, disulfides, polyphenols, flavonoids, carotenoids and triterpenoids, for example - R-sulforaphane (SFN) found in broccoli, diallyldisulfide found in garlic, quercetin found in onions, resveratrol found in red grapes, and oleanolic acid found in apple, grape and olive pomace (Thimmulappa et al., 2002; Chen et al., 2004; Tanigawa et al., 2007; Rubiolo et al., 2008; Dinkova-Kostova et al., 2005). As Nrf2 is activated in response to toxicity, careful distinction between pharmacological activation of Nrf2 and indirect activation of Nrf2 in response to chemical toxicity is required.

Research on the control of Nrf2 has focussed on binding and chemical modification of its inhibitor Keap1 by activators, stabilising Nrf2 to proteolysis thus increasing cellular Nrf2 protein content (Kobayashi et al., 2006). Studies in this group, however, showed that activation of cells to produce half-maximal ARE-linked transcriptional response elicited no significant change in Nrf2 protein concentration – although markedly higher and often toxic concentrations of activators did so (Tanigawa et al., 2007; Jeong et al., 2005). Under physiological and health beneficial conditions, therefore, Nrf2 activation status may be encoded

in the time dependence of subcellular Nrf2 location rather than its resistance to proteolysis. We found that Nrf2 undergoes translocational oscillations from the cytoplasm to the nucleus in the basal state. When stimulated at physiological levels, the translocational oscillations of Nrf2 increase in frequency, decrease in amplitude and activate ARE-regulated genes. We presented a mechanism to explain this where Nrf2 functionality is linked to reactivation on return to the cytoplasm or “refresh rate” which links protective transactivational response to increased frequency of direct surveillance of the cytoplasm (Xue et al., 2012) – Figure 25.

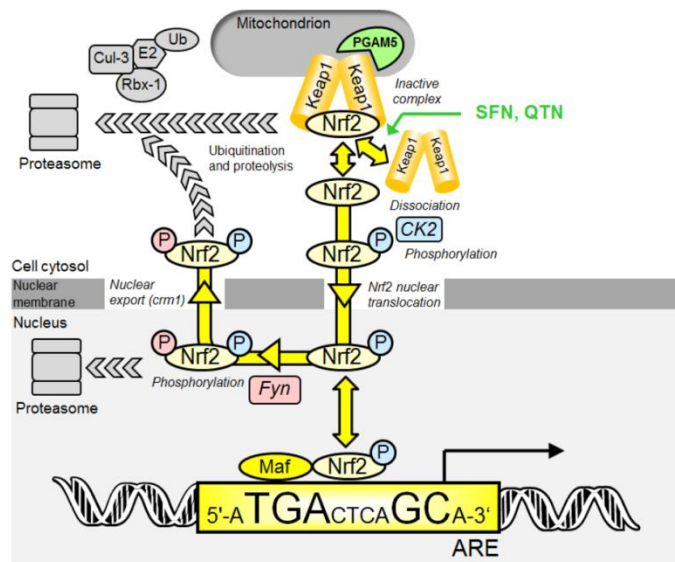


Figure 24. Current understanding of transcriptional control of ARE-linked gene expression by the Nrf2/Keap1 system.

Key: P, phosphorylation (coloured-coded for CK2 or Fyn catalysed modification). In quiescence, Nrf2 in the cytoplasm is complexed to Keap1 in association with Cul-3-Rbx-1 attracting co-association of E2 ubiquitin ligase, Nrf2 ubiquitination and proteolysis. Upon activation (yellow arrows), Nrf2 dissociates from Keap1 and is phosphorylated by CK2; phosphorylated Nrf2 enters the nucleus and binds with accessory Maf protein to AREs. Thereafter, Nrf2 is phosphorylated by Fyn, exported from the nucleus and degraded by the proteasomal system. SFN and QTN are thought to activate Nrf2 by disrupting the Nrf2-Keap1 complex and stabilising Nrf2 from proteolysis (Thimmulappa et al., 2002; Tanigawa et al., 2007). Diagram provided by Professor Paul J. Thornalley.

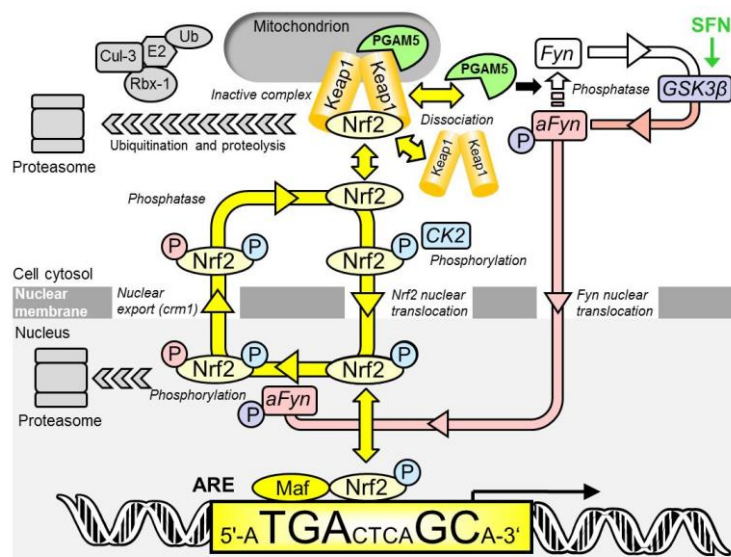


Figure 25. Cell signalling sustaining Nrf2 translocational oscillations for control of ARE-linked gene expression.

Negative feedback is provided by successive de-phosphorylation and phosphorylation steps, which induce ultra-sensitivity in Fyn activation and the Fyn phosphorylation of nuclear Nrf2 and which produce a delay between Nrf2 nuclear entry and the Fyn phosphorylation which drives nuclear export. Figure provided by Professor Paul J. Thornalley.

1.3.1 Antioxidant response element

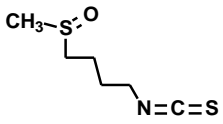
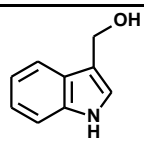
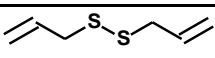
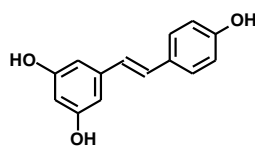
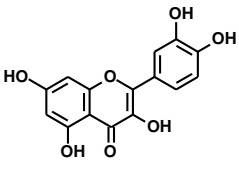
The ARE was first thought to be involved in regulation of the expression of genes encoding enzymes that catalyse drug metabolism phase II conjugation reactions such as glutathione S-transferases (GSTs) and UDP glucuronyl transferase (Rushmore et al., 1991). AREs are conserved cis-acting regulatory elements in the promoter region of these and other genes with expression regulated by Nrf2. ARE gene transcription results in increased production of antioxidant proteins and related enzymes and other protective gene products, and suppression of the expression of lipogenic genes. The Nrf2/Keap1/ARE system regulates a large number of genes in mammals - basal expression of *ca.* 640 genes, inducible expression of 650 genes and basal and inducible expression of *ca.* 240 genes has been discovered (Malhotra et al., 2010). The consensus ARE is shown in Figure 23.

1.3.2 The Nrf2 system in ageing and senescence

Lifespan extension has been shown in mice models where increased activity of Nrf2-dependent enzymes involved in the antioxidant response has been observed (Brown-Borg and Rakoczy, 2005). Moreover, in *C. elegans*, knockout of the Nrf2 gene homologue SKN-1 was proven to shorten life span (Bishop and Guarante, 2007). These data demonstrate that increased longevity is maintained by the Nrf2 system. Studies on the *Drosophila melanogaster* in which Nrf2 was overexpressed (Orr et al., 2005) or Keap1 allele modified for overexpression of glutathione-S-transferase D1 (GSTD1) responsible for the detoxifying response in cells (Sykiotis and Bohmann, 2008) both resulted in extended life span. This suggests that the Nrf2 system is capable of increasing lifespan but it is no clear if delayed cell senescence contributes to these effects.

Dietary activators such as carotenoids (Ben Dor et al., 2005), omega-3 fatty acids (Gao et al., 2007), isoflavones (Mann et al., 2007) and others, have been shown to activate Nrf2 but the challenge lays in the discovery of dietary bioactives that would be able to promote healthy ageing (Xue et al., 2008). Examples of such dietary bioactivators are shown in Table 2.

Table 2. Dietary activators of nrf2.

Dietary bioactive	Example	Dietary sources
Glucosinolate-derived isothiocyanates	<p>Sulforaphane</p> 	Brassica vegetables (broccoli, cabbage, cauliflower, Brussel sprouts and other), rocket salad.
Glucosinolate-derived indoles	<p>Indole-3-carbinol</p> 	Brassica vegetables (broccoli, cabbage, cauliflower, Brussel sprouts and other), rocket salad.
Thioethers and disulfides	<p>Diallyldisulfide</p> 	Garlic, onions and others.
Polyphenols and flavonoids	<p>Resveratrol</p>  <p>Quercetin</p> 	Grape juice, onions, other fruits and vegetables.

Sulforaphane (2 μM) delayed senescence of IMR-90 lung fibroblast cells *in vitro* (Hintze et al., 2008). Trans-Resveratrol (1 and 52 μM) delayed senescence of human MRC5 lung fibroblast cells *in vitro* (Giovanelli et al., 2011). Resveratrol (5 μM) decreased development of SASP in MRC5 fibroblasts *in vitro*, decreasing expression and secretion of pro-inflammatory cytokines; 1 μM resveratrol had a similar but weaker effect. Cell spreading and plating efficiency were increased with type I collagen expression remaining at presenescent levels (Pitozzi et al., 2013). Higher concentrations trans-resveratrol ($\geq 25 \mu\text{M}$) increased fibroblast senescence *in vitro* (Faragher et al., 2011). In human skin fibroblasts, the triterpenoid and Nrf2 activators 18 β -glycyrrhetic acid (4 μM) was found to delay RS. This was associated with induction of proteasomal activity (Kapeta et al., 2010).

2. Project-specific background

2.1 The human fibroblast model in cellular senescence research

Fibroblasts are crucial in order to maintain the homeostasis of connective tissues (Robert et al., 1992) and several humoral and cellular factors may activate or inhibit fibroblast activity or, after being released from fibroblasts, they may reciprocally act on other mesenchymal (Zalatnai, 2006) and epithelial cells (Abraham et al., 1989) contributing to the complex network that modulates connective tissue homeostasis in physiological as well as in pathological conditions, such as during wound healing, inflammation or cancer (Robert and Labat-Robert, 2000). Cultured fibroblasts represent a widespread *in vitro* model for investigating genetic and acquired disorders and for exploring the importance of specific molecular pathways leading to differentiation, ageing and death (Holbrook and Byers, 1989; Van Ganser and Van Lerberghe, 1987). The use of a cell culture model for the study of ageing has many advantages such as the ability to provide a controlled environment for the study of diverse cellular phenomenon (Barnett and Barnett, 2000). Since the 1960s and the discovery of the Hayflick Limit (Hayflick and Moorhead, 1961), diploid fibroblast culture has been at the heart of cellular ageing studies. Indeed, cultured fibroblast cells are capable of sustained proliferative activity *in vitro* (Norwood and Pendergrass, 1992) which represents one of the main advantages for using this type of cells in the study of replicative senescence. Moreover, as described by Cristofalo and colleagues (Cristofalo et al., 2003), fibroblasts in culture express human genetic, metabolic, and regulatory behaviour allowing cells to undergo changes in a predictable and reproducibly constant environment.

Although human fibroblasts are commonly used for *in vitro* studies, their phenotype remains poorly defined. Indeed, beside their ability to attach to plastic cell culture vessel, elongated spindle-shaped morphology and absence of markers for other cell lineages (Chang et al., 2002), human fibroblasts phenotypes differ due to their diversity in gene expression profiles. As explained by Chang and colleagues (2002), the combination of specific groups of genes, rather than a single gene type, differentiates fibroblasts depending on their tissue of origin –

Figure 26.

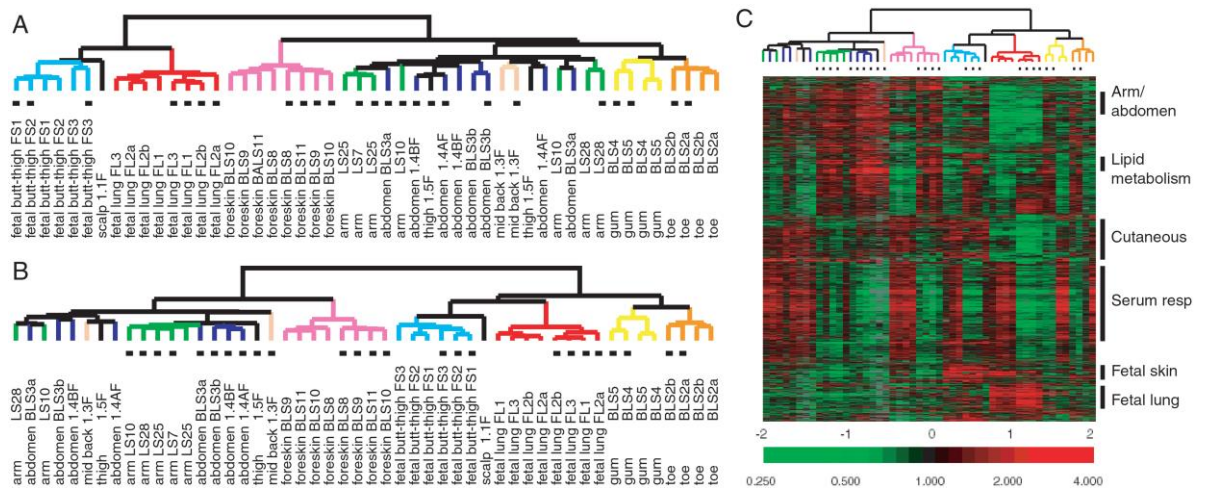


Figure 26. Topographic differentiation of fibroblasts.

(A) Global gene expression patterns of 50 fibroblast cultures were sorted based on similarity by hierarchical clustering. The site of origin of each fibroblast culture is indicated and color-coded. Fibroblasts cultured in minimal-serum medium. (B) Supervised hierarchical clustering of cultured fibroblasts was performed by using approximately 1,600 genes that varied according to fibroblast site of origin. (C) Topography transcriptome of fibroblasts. The variation in expression of approximately 1,600 genes described in B are shown in matrix format. Source: Chang *et al.*, 2002.

2.1.1 Human fetal lung MRC-5 fibroblasts

In 1966, Jacobs and colleagues developed the MRC-5 strain of fibroblasts derived from foetal lung tissue, taken from a 14-week male foetus removed for psychiatric reasons from a 27 year old woman with a genetically normal family history and no sign of neoplastic disease both at abortion and for at least three years afterwards (Jacobs *et al.*, 1970). The MRC-5 fibroblast cell line is a normal diploid human cell line with a Chromosome Frequency Distribution (CFD) of 50 cells: $2n=46$ and $46,XY$ karyotype (Holliday and Tarrant, 1972). Moreover, this adherent cell line is susceptible to viruses such as herpes simplex, human poliovirus 1 and vesicular stomatitis (Indiana strain) and is capable of going through 42 to 46 population doublings before the onset of senescence (Lawless *et al.*, 2010). The human lung fibroblast cell line MRC-5 constitutively produces a megakaryocyte potentiator activity, identified in murine bone marrow liquid culture assays for acetylcholinesterase and megakaryocyte colony assays in the presence of low concentrations of IL-3 (Yamamoto *et al.*, 1990). Finally, MRC-5 fibroblasts are widely used for the development of vaccines (Jacobs, 1976; Jacobs *et al.*, 1970) as well as senescence and ageing studies (Sitte *et al.*, 2000).

2.1.2 Human foreskin BJ fibroblasts

The BJ fibroblast cell line is established from normal human foreskin and has an adherent culture property. These cells have a reported normal diploid karyotype at population doubling 61 but an abnormal karyotype at population doubling 82.

Moreover, BJ fibroblasts are telomerase negative and have the capacity to proliferate to a maximum of 72 - 90 population doublings before the onset of senescence with a telomere-shortening rate of only 15–20 bp/PD (Huot et al., 2002; Lorenz et al., 2001). Ectopic expression of human telomerase (hTERT) in BJ cells extended lifespan (Morales et al., 1999). BJ cells had low levels of ROS formation - as assessed by fluorescence development with dihydrochlorofluorescein, low levels of protein carbonyl – although the method used in their assay lacked robust quantitation, and low steady-state lipofuscin content as compared to other primary human fibroblasts. BJ cells immortalized by transfection with hTERT had the same telomere-shortening rate as in parental cells is observed over a long time despite strong telomerase activity. Hyperoxia induced oxidative stress and accelerated telomere shortening in a variety of human fibroblast strains but did not in BJ cells *in vitro* (Lorenz et al., 2001). Extracellular superoxide dismutase was a major antioxidant in BJ fibroblasts and slowed telomere shortening (Serra et al., 2003). BJ senescence was associated with damage in both telomeric and non-telomeric DNA (Nakamura et al., 2008). Genetic manipulation to decrease the removal of 8-hydroxydeoxyguanosine - oxidative damage to DNA, increased the rate of development of senescence which was suppressed by culture under low 3% oxygen atmosphere (Rai et al., 2009). Basal levels of DNA-binding activity of NF- κ B and phosphorylated ATF-2 were different in BJ and hTERT-BJ1 cells and both cell lines displayed a higher DNA-binding activity of p53 and HIF-1 72 h after exposure to hydrogen peroxide (de Magalhes et al., 2002). Microarray analysis showed strong inflammatory-type response in senescent fibroblasts - MCP-1, IL-15 and IL-1b, Toll-4 (TLR-4) receptor and intercellular adhesion molecule-1 (ICAM-1), and proteins linked to the cell cycle – CDK inhibitor p21, growth-arrest-specific protein 1 (Gas1) and growth-arrest and DNA-damage inducible protein 153 (GADD153). Insulin-like growth factor binding proteins 2 and 5 (IGF-BP2, IGF-BP5), stanniocalcin, cathepsin O, and levels of peptidyl- α amidating monooxygenase (PAM) were all

increased in senescence (Shelton et al., 1999). During proliferative senescence there was a decline in proteasome activity and oxidized and cross-linked proteins (Sitte et al., 2000a; Sitte et al, 2000b) – although assessment of damaged proteins lacked robust quantitation (Table 3).

Table 3. Comparison of proliferative senescence and the ageing of non-dividing BJ fibroblasts.

Source: Sitte et al., 2000a; Sitte et al, 2000b.

Parameter	Senescence of nondividing cells after 20 wk of hyperoxia				
	Proliferative senescence		Quiescent cells		Postmitotic cells
	PD 46	PD 74	PD 46	PD 62	PD 74
Overall cellular proteolysis	100%	45%	25%	17%	18%
Proteasome activities					
Chymotrypsin-like activity	100%	39%	55%	26%	16%
Trypsin-like activity	100%	34%	45%	20%	20%
Peptidyl-glutamyl-hydrolyzing activity	100%	19%	18%	10%	0
Activity of lysosomal cathepsins	100%	37%	160%	120%	31%
Oxidized/cross-linked proteins					
Green fluorescence	100%	151%	267%	274%	357%
Red fluorescence	100%	148%	252%	286%	354%
Protein carbonyls	100%	155%	133%	166%	182%

2.2 Interventions for healthy ageing

Changes in diet and lifestyle could potentially increase human lifespan by suppressing development of disease that is the major cause of mortality in the ageing population. For the human population in the developed world major causes of mortality are cardiovascular disease and cancer. Healthspan, the period of life during which people are healthy and free from serious disease, may be extended by also decreasing the impact of these and diseases which contribute to years of morbidity and disability – such as skeletal diseases, osteoarthritis and rheumatoid arthritis. Impact of disease on health is compared by calculating disability-adjusted life years (DALYs) where one DALY is one year of healthy life lost through premature death or disability. The total DALYs for a population is the burden of disease - the difference between current health status and an ideal health situation where the whole population lives to an advanced age, free of disease and disability. In 2010 the 3 most important causes of DALYs were: ischaemic heart disease, respiratory tract infections and cerebrovascular disease. The leading risk factors for DALYs were: high blood pressure, *ca.* 7%, smoking *ca.* 6% and ischaemic heart disease *ca.* 5% (IHME, 2013). In 20 years from 1990 – 2010, the contribution of risk factors to disease burden has changed from communicable diseases in children towards non-communicable diseases in adults. For ischaemic

heart disease, a significant majority of associated DALYs is linked to dietary factors: for example, a diet low in nuts and seeds, 40%, a diet low in fruit – 30%, and a diet low in vegetables, 12% (Lim et al, 2010). Nuts, seeds, fruits and vegetables are dietary sources of antioxidants and so this may support the free-radical theory of ageing. The antioxidants vitamin C, vitamin E and carotenoids have shown to inhibit lipid peroxidation (Niki et al., 1995) but since these supplements have been found, in certain cases, to increase mortality (Bjelakovic et al., 2007). However, meta-analysis of outcomes of randomized controlled trails with antioxidants suggests there is no significant benefit of antioxidant supplementation (Ye et al., 2013). The free-radical theory of ageing states that an accumulation of oxidative damage through respiration leads to ageing and, as a result, decreased lifespan (Beckman and Ames, 1998). The link of dietary factors to DALYs appears to be more complex than a simple supplement of antioxidants.

The concept of vitagenes – genes influential in lifespan – based on the idea that certain genes encoding for heat-shock proteins thioredoxin and sirtuins are responsible for maintaining homeostasis in response to oxidative stress (Calabrese et al., 2009) , emerged as a broader concept in the healthy ageing process. Based on these observations, antioxidants supplementation were predicted to extend human lifespan by either removal of free-radicals or activation of vitagenes.

One of the recent controversies in the debate surrounds the phytoalexin found in grapes, resveratrol (Valenzano et al., 2006). The initial claims that resveratrol extends lifespan in experimental models of ageing have not been confirmed (Agarwal and Baur, 2011). To date, the only intervention known to successfully delay ageing is caloric restriction in animal studies, as mentioned previously, but evidence in humans is still unavailable.

2.3 Experimental interventions: caloric restriction mimetic for increased lifespan and decreased senescence

2.3.1 Caloric restriction and delay of ageing

The concept of caloric restriction (CR) for life extension has been part of the literature since the 1930s. Extension of lifespan and delay of the onset of age-associated pathologies was first shown in rodents (McCay et al., 1989) and particular focus was put on the definition of CR without malnutrition. This “undernutrition without malnutrition” typically implies that 10-30% of total calorie intake is reduced whilst the physical environment is controlled (Hursting et al., 2003). Although CR literature related to ageing is extensive, the debate still remains on whether or not CR slows down the ageing process (Masaro, 2005). Indeed, this is dependent on the method by which this process is investigated and the most accepted method of determining if CR has an effect on ageing is by Gompertz parameters analysis (Simons et al., 2013) which is a mathematical model based on a sigmoid function representing slower growth at the beginning and end of a defined time frame. Several ageing studies in rats based on Gompertz analysis have supported the theory of ageing delay in relation to CR (Holehan and Merry, 1986; Lewis et al., 1985; Pletcher et al., 2000; Yu et al., 1982). Moreover, Mair and colleagues (2003) have reported that *Drosophila* flies under CR diet at any stage of their normal ageing process exhibit the same delay of ageing as *Drosophila* fed CR diets throughout their whole life (Mair et al., 2003).

Many hypotheses on the mechanism of action of CR on delay of ageing have been put forward since the 1930s. The *Retardation of Growth Hypothesis* rests on the principle that CR increases longevity by delaying growth, therefore assuming that ageing is an impairment of continuous development (McCay et al., 1989). However, this theory was refuted due to the fact that in mouse and rat studies, CR at a later development compared to initiation at birth had the strongest beneficial effect in delaying ageing (Weindruch and Walford, 1982; Yu et al., 1982). Another once popular hypothesis on the mechanism of action of CR on delay of ageing is the *Reduction of Body Fat Hypothesis*. As described by Berg and Simms (1960), delay of ageing by CR is due to a decrease in body fat content (Berg and Simms, 1960). This hypothesis has been supported by experimental evidence obtained in mice and rat studies showing that CR leads to a reduction in

body fat content (Bertrand et al., 1980; Garthwaite et al., 1986, Harrison et al., 1984). Moreover, the *Reduction of Body Fat Hypothesis* has similarly been demonstrated in rhesus and cynomolgus monkeys (Cefalu et al., 1997; Colman et al., 1999; Lane et al., 1995). Table 4 summarises the effects of CR on selected parameters of morphology, physiology, ageing, and disease in rhesus monkeys.

Table 4. Effects of CR on selected parameters of morphology, physiology, ageing, and disease in rhesus monkeys.

Source: Lane et al., 2007.

Category/parameter	Decrease	Increase	No change
Body Composition			
Body weight	X		
Fat and lean mass	X		
Trunk: leg fat ratio	X		
Height	X		
Development			
Time to sexual maturity		X	
Time to skeletal maturity		X	
Metabolism			
Metabolic rate (short-term)	X		
Metabolic rate (long-term)			X
Metabolic rate (long-term:nighttime)	X		
Body temperature	X		
Thriiodothyronine (T3)	X		
Thyroxin (T4)			X
Thyroid Stimulating Hormone (TSH)			X
Leptin	X		
Endocrinology			
Fasting glucose/insulin	X		
IGF-1/Growth Hormone	X		
Insulin sensitivity		X	
Age-Related Maintenance of Melatonin and DHEAs		X	
Testosterone; Estradiol			X
Cardiovascular Parameters			
Systolic blood pressure	X		
Heart rate	X		
Serum triglycerides	X		
Serum HDL2B		X	
LDL interaction with proteoglycans	X		
Lipoprotein(a)	X		
Immunological Parameters			
IL-6	X		
IL-10	X		
Interferon- γ		X	
Oxidative Stress			
Oxidative damage to skeletal muscle	X		
Cell Biology			
Proliferative capacity of fibroblasts		X	
Glycation products	X		
Functional Measures			
Locomotor activity			X
Acoustic responses		X	

*"X" notes whether caloric restriction has been shown to decrease, increase, or produce no change in the selected parameters.

Anderson and Weindruch (2007) proposed metabolic reprogramming may be one of the pathways by which CR exerts its delay of ageing effect (Anderson and Weindruch, 2007). Indeed, the *Reduction in Metabolic Rate Hypothesis* is based on experimental human and animal data showing that a decrease in food intake is directly related to a decrease in metabolic rate per kilogram body mass (Garrow, 1974; Pearl, 1928). However, this hypothesis has been disputed. Indeed, the “rate of living theory of ageing” is challenged by studies done in primates indicating that metabolic rate per gram of lean body mass is decreased following initiation of CR but gradually increases to the metabolic rate per gram of lean body mass of primates that have not been subjected to CR (Lane et al., 1996; Ramsey et al., 1996). Moreover, the method used to normalize for body size in CR studies does not take into account metabolic rate measurements for individual organs and tissues and has been heavily criticised (Gallagher et al., 2003; Speakman et al., 2004). Another theory by which CR is thought to delay ageing is through the decrease of accumulation of oxidative damage. This *Oxidative Damage Attenuation Hypothesis* has been shown to be relevant in rodents (Yu, 1996) as well as primate models (Zainal et al., 2000). Moreover, CR leads to an increase in the levels of reduced glutathione (GSH) (Someya et al., 2010) as well as increase in oxidative DNA damage repair and decrease in protein damage expression (Lambert et al., 2004). However, studies using long-lived *Drosophila* disagree with these findings as they show no increase in antioxidant enzymes (Orr et al., 2003). The effect of lifelong CR on plasma concentrations of glucose and insulin has been linked with delay of ageing through the *Altered Glucose-Insulin System Hypothesis*. Indeed, CR has been found to increase insulin sensitivity and lower blood glucose levels in rhesus monkeys (Kemnitz et al., 1994) and loss-of-function mutations of the insulin signaling systems have been shown to result in life extension of *C. elegans* (Kenyon et al., 1993), *Drosophila Melanogaster* (Wolkow et al., 2000) and mice (Clancy et al., 2001).

2.3.2 Caloric restriction mimetic compounds

Caloric restriction mimetic (CRM) was a term first described by Lane and colleagues (1998) as a hypothetical class of drugs which imitates the anti-ageing effects associated with CR *in vivo* and which would act upon the same metabolic

pathways without the need for a decrease in caloric intake. CRM have been proposed to regulate a vast number of pathways associated with energy metabolism (Lane *et al.*, 2007). Indeed, inhibitors of glycolysis have been shown to mimic metabolic and protective effects of CR (Guo *et al.*, 2001). Also, sirtuin regulators have been shown to delay the ageing process and extend lifespan in short-lived organisms (Guarente and Picard, 2005). Finally, insulin sensitizers have been explored as possible CRM due to the fact that insulin sensitivity has been shown to increase in animal CR studies (Kemnitz *et al.*, 1994; Kenyon *et al.*, 1993; Wolkow *et al.*, 2000; Clancy *et al.*, 2001). However, this theory has been disputed for the compound phenformin, a treatment for diabetes, due to the fact that *in vivo* treatment failed to show markers related to CR and lifespan (Lane *et al.*, 2007). However, particular attention has been given to the compound *trans*-resveratrol (3,4',5-trihydroxy-*trans*-stilbene, RES) – Figure 27 – and rapamycin over the past 10 years with regards to their caloric restriction mimetics effect. Indeed the beneficial properties of RES have been known since the 1940s when this polyphenolic compound was first isolated from white hellebore (Baur and Sinclair, 2006).

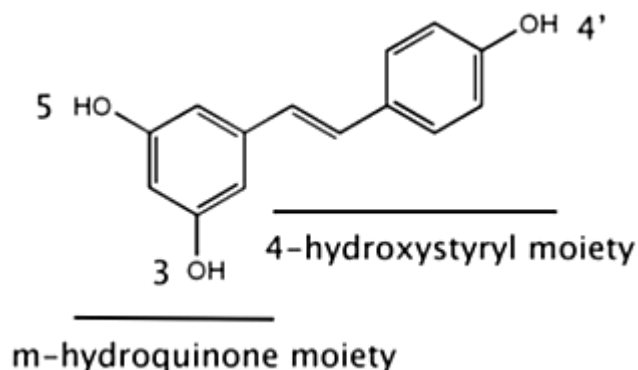


Figure 27. Chemical structure of resveratrol.

Source: Pirola and Frojdo, 2008.

Moreover, this phytoalexin is commonly found in nuts, berries and in grape skin and has been often mediatised as the source of the “French paradox” as moderate wine consumption has been shown to inhibit platelet activity (Demrow *et al.*, 1995) as well as induce nitric oxide, protein kinase C and adenosine, all of which are responsible for cardiac preconditioning (Das and Maulik, 2006). Over the past decade, RES mechanism of action has been linked as a CRM for the prolongation of longevity. Indeed, RES has been shown to improve insulin

sensitivity which in turn leads to a decrease in glucose and insulin in the body (Bauer *et al.*, 2006; Bluher *et al.*, 2003; Lagouge *et al.*, 2006). However, the mechanism by which RES is thought to act as a CRM involved in the delay of ageing is through the activation of the NAD-dependent deacetylase sirtuin-1 (Sirt1). Indeed, RES was found to be the most potent Sirt1 activator (Howitz *et al.*, 2003) in *S. Cerevisiae* whereas in aging delay studies conducted in metazoans, Sir2 seemed to be activated by RES (Wood *et al.*, 2004). However, this delay of ageing and CRM with RES through the activation of Sir2 and Sirt1 is still unclear and has been refuted on many occasions (Bass *et al.*, 2007; Kaeberlein *et al.*, 2005). Nonetheless, RES is thought to improve mitochondrial function and glucose tolerance in an AMP-activated kinase (AMPK) manner. Indeed, as seen in Figure 28, upon caloric restriction and fasting, the levels of glucagon and catecholamines increase which then binds to their receptors and increases cAMP production. This increase in cAMP production then activates adenylate cyclase. Resveratrol acts by increasing cAMP levels by inhibiting cAMP phosphodiesterases (PDEs) (Chung *et al.*, 2012).

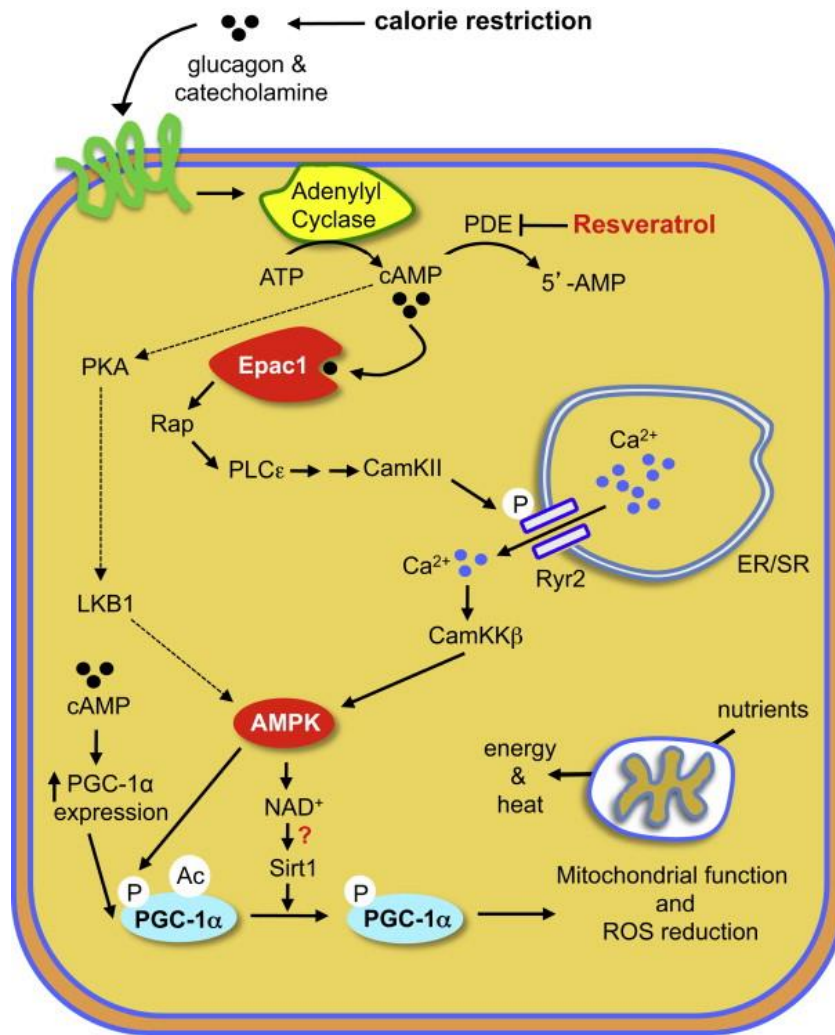


Figure 28. Resveratrol mimics caloric restriction by inhibiting cAMP phosphodiesterases (PDEs).

Source: Chung *et al.*, 2012.

Another CRM that has been persistently studied in anti-ageing research is rapamycin. This compound (Figure 29) is an immunosuppressant drug used to prevent organ rejection after organ transplantation and is a non-competitive and specific inhibitor of the nutrient-responsive mammalian target of rapamycin (mTOR) kinase (Dazer and Hall, 2011).

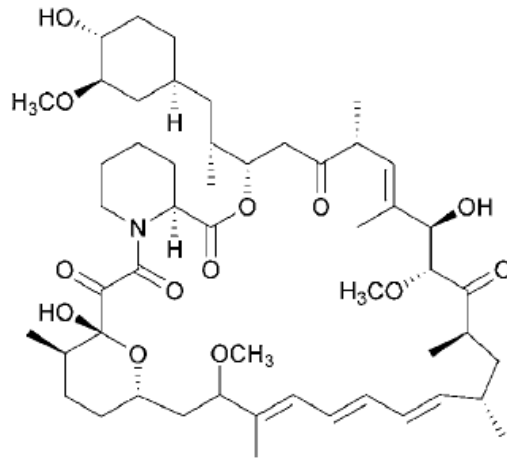


Figure 29. Molecular structure of rapamycin.

Source: Argyropoulos *et al.*, 2013.

The role of the target of rapamycin (TOR) in the delay of ageing was first demonstrated in *Drosophila* and *C. elegans* in which its down-regulation was associated with an extension of lifespan (Passtoors *et al.*, 2013). Moreover, this effect was also shown to be replicable in mouse models (Selman *et al.*, 2009) and with treatment with rapamycin (Harrison *et al.*, 2009). Although there is no primate evidence for delay of ageing through the mTOR pathway with rapamycin treatment, it was recently shown that mTOR signalling gene downregulation is associated with life extension as seen in a Dutch cohort of families with extended life-span (Passtoors *et al.*, 2013). The nutrient-responsive mammalian target of rapamycin (mTOR) is composed of two distinct complexes: the mTOR complex 1 (mTORC1) which is rapamycin sensitive and contains Raptor (rapamycin-sensitive adaptor protein of mTOR) and the mTOR complex 2 (mTORC2) which is rapamycin insensitive and which contains Rictor (Testa *et al.*, 2014). Moreover, mTORC1 encourages cell proliferation and protein synthesis as well as inhibits autophagy (Wullschleger *et al.*, 2006). CR and rapamycin treatment acts by downregulation of insulin-like growth factor (IGF-1) which in turn leads to SIT1 and AMPK activation and consequent inactivation of the TSC1/TSC2 complex. Upon inactivation of the TSC1/TSC2 complex, the bonds between Guanosine-5'-triphosphate (GTP) and Rheb protein cannot be broken which leads to an increase in GTP-Rheb complexes therefore activating mTORC1 and increasing cell proliferation and protein synthesis as well as inhibition of autophagy (Testa *et al.*, 2014). Activators of TOR (rapamycin), sirtuins (resveratrol), AMPK (metformin),

autophagy inhibitors (spermidine) as well as activators of antioxidative gene translation (curcumin, quercetin and others) have been proposed as CRMs (Argyropoulos *et al.*, 2013) – Figure 30.

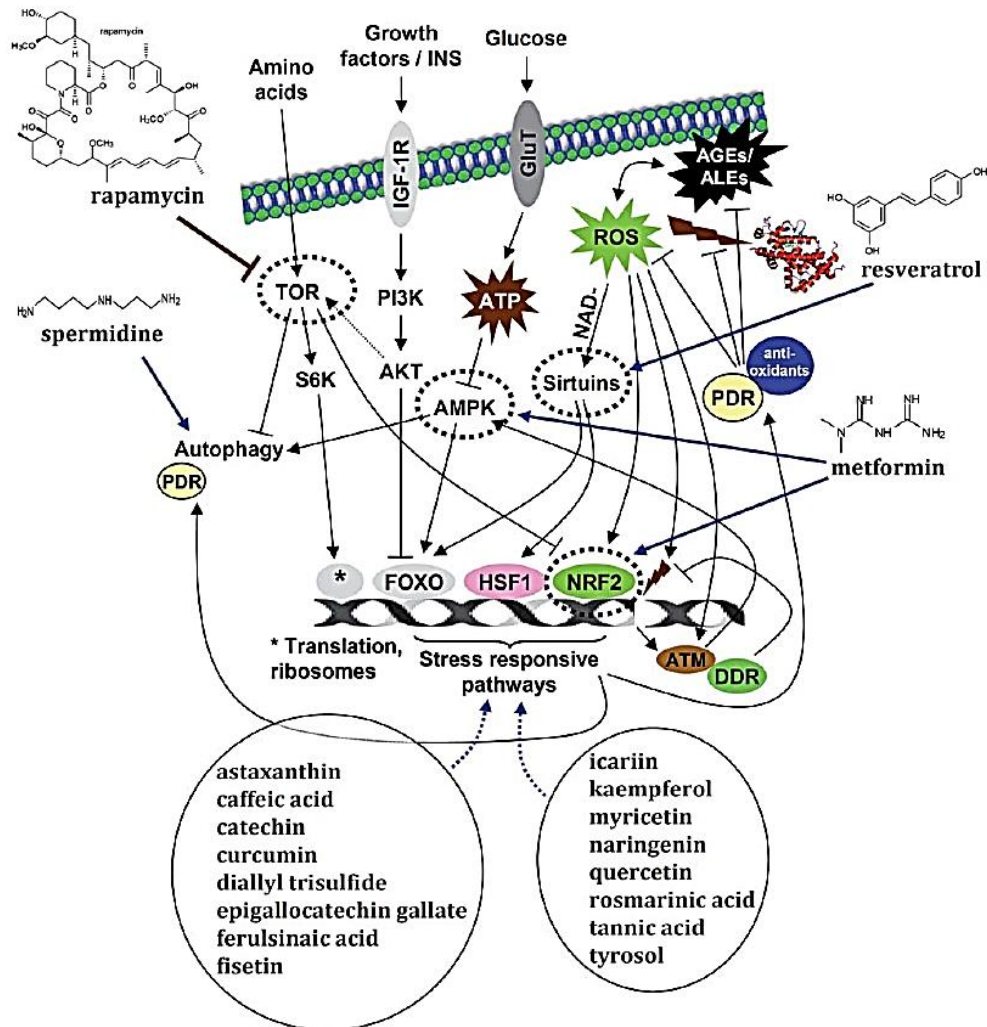


Figure 30. Summary of the main signalling pathways responsible for the delay of ageing by diverse dietary activators.
Source: Argyropoulos *et al.*, 2013.

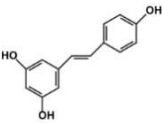
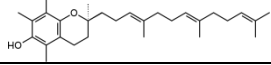
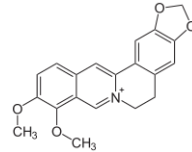
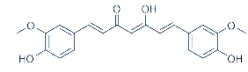
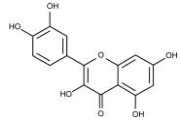
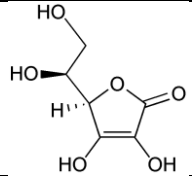
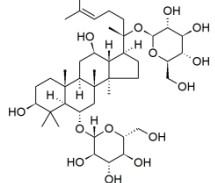
Although RES and rapamycin have been the focus of many anti-ageing studies considering their CRM effect, these two compounds are often used at such high concentration that their effect cannot be replicated using normal physiological conditions and their beneficial outcome is therefore lacking strong scientific evidence. Many studies in human subjects with RES are on-going. Resveratrol (150 mg/day) given to 11 healthy obese men in a randomized double-

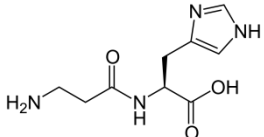
blind crossover study for 30 days decreased sleeping and resting metabolic rate. In muscle it activated AMPK, increased SIRT1 and PGC-1a protein levels, increased citrate synthase activity without change in mitochondrial content, and improved muscle mitochondrial respiration on a fatty acid-derived substrate. It also elevated intramyocellular lipid levels and decreased intrahepatic lipid content, circulating glucose, triglycerides, alanine-aminotransferase, and inflammation markers. Systolic blood pressure decreased and HOMA index improved after resveratrol. In the postprandial state, adipose tissue lipolysis and plasma fatty acid and glycerol decreased (Timmers et al., 2011). Many of these effects were small however and RES has shown beneficial effects on glucose and lipid metabolism in some, but not all studies. Currently, despite the strong preclinical evidence of potential beneficial effects for cardiovascular health, RES benefit in human subjects remains uncertain (Pollack et al., 2013).

2.3.3 Nrf2 activation by dietary activators

The main hypothesis of this project proposes that genes regulated by transcription factor Nrf2 have a key role in cell senescence and Nrf2 activators may thereby delay senescence. If correct and translated clinically, functional foods may be formulated to support healthy ageing. The main focus of this study is to assess if an established Nrf2 activator, dietary isothiocyanate sulforaphane (SFN), may delay cell senescence and, if so, identify the mechanism of action. Other compounds have been found to delay senescence – Table 5.

Table 5. Examples of divergent effects of dietary bioactive and other compounds on human cellular senescence in vitro.
Modified from: Malavolta *et al.*, 2014.

Compound	Molecular structure	Effect	Model & type of senescence	Concentration (timing)	Reference
Resveratrol		D	MSC (RS)	0.1 μ M (30d)	Peltz <i>et al.</i> , 2012
		D	Tenocytes (SIPS)	30 μ M (72 hr in SIPS)	Carroll <i>et al.</i> , 2011
		I	MSC	>10 μ M (4d)	Peltz <i>et al.</i> , 2012
		I	EC	10 μ M (chronic)	Schilder <i>et al.</i> , 2009
Tocotrienol		D/R	Fibroblasts (RS)	Gold Tri E 50, 0.5 mg/ml	Makpol <i>et al.</i> , 2011
Berberine		D	hF (RS)	60 μ M (24h)	Halicka <i>et al.</i> , 2012
Curcumin		D	Fibroblasts (SIPS)	20 μ M (pre-treatment 48 h)	Li <i>et al.</i> , 2013
Quercetin		D/R	Fibroblasts (RS/SIPS)	6-7 μ M (chronic)	Chondrogianni <i>et al.</i> , 2010
Vitamin C		D (RS)	EmC, fibroblasts	0.2 mM (chronic)	Kashino <i>et al.</i> , 2003
		D (RS)	EC	0.13 mM (chronic)	Furumoto <i>et al.</i> , 1998
Ginsenoside Rg1		D(SIPS)	Fibroblasts	5-20 μ M (chronic pretreatment from 24-30 PD)	Chen <i>et al.</i> , 2008

L-Carnosine		D/R	Fibroblasts (RS)	20-50 mM (chronic)	McFarland and Holliday, 1999
-------------	---	-----	------------------	--------------------	------------------------------

*Model: MSC = mesenchymal stem cells; EC = endothelial cells; EmC = embryonic cells. **Type of senescence: SIPS = stress induced premature senescence; RS = replicative senescence. ***Effect: I = inducer of a senescent-like phenotype; R = rejuvenator of the senescent state; D = delayer of senescence markers onset.

The Nrf2 system has been implicated in longevity studies using *C. elegans* through the activation of the transcription factor Skn-1 which is responsible for mesodermal development and also is an orthologue of Nrf2 in mammalian cells (An et al. 2005; Tullet et al. 2008). Moreover, Skn-1 activation is crucial in the delay of ageing caused by CR in *C. elegans* (Bishop and Guarente 2007) and long-lived *C. elegans* models show upregulated expression of Skn-1-dependent enzymes (Jasper, 2008). The link between Nrf2 activation and lifespan extension has been seen in the *Drosophila melanogaster* in which the deletion of Keap1 allele has led to the increase in the expression of glutathione transferase D1 (GST D1) (Sykiotis and Bohmann, 2008). Finally, studies in the nematode and fruit flies have shown that the overexpression of the downstream components of the Nrf2 signalling pathway extend their lifespan, and decrease of lifespan is observed when homologues of Nrf2 are knocked out in both species (Orr et al. 2005; Bishop and Guarente, 2007). Therefore, by taking into consideration the *in vivo* studies linking Nrf2 activation, CR and extension of lifespan, the Nrf2-ARE ought to be considered as a major target for CRM.

Several dietary bioactives that delay cellular senescence are Nrf2 activators. Fruit and vegetable-derived bioactive compounds often exert their antioxidant activity indirectly through Nrf2 signalling (Jung and Kwak, 2010). Surh *et al.* (2008) have shown that isothiocyanates, dithiolethiones, RES, curcumin, caffeic acid phenethyl ester (CAPE; from honey), epigallocatechin gallate (from green tea), allyl sulfides (from garlic), xanthohumols (from hops), and cinnamaldehyde are activators of Nrf2. Many studies with putative Nrf2 activators have, however, used high concentrations which are not translatable clinically and/or activate Nrf2 within the toxic concentration range. In the latter case toxicity prevents use of such compounds and activation of Nrf2 is likely as part of the response to toxicity rather than a direct agonism of the Nrf2 system. For some Nrf2 activators the optimum dietary dose range (Figure 31) may be narrow and very low concentrations or very high concentrations of compound administration can lead to an exponential increase in the risk of developing chronic diseases (Argyropoulou et al., 2013).

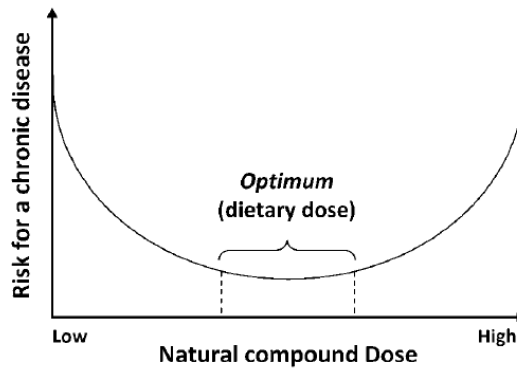


Figure 31. Dose-response of natural compounds against risk of chronic disease.

Source: Argyropoulou et al., 2013.

Moreover, the current *in vitro* and *in vivo* models of Nrf2 activation have so far not been able to explain the exact mechanism by which Nrf2 is activated – see Chapter 1.3.

2.4 Dietary bioactive compounds: Sulforaphane (SFN) and Hesperetin (HESP)

2.4.1 Sulforaphane (SFN)

SFN is an alkyl isothiocyanate formed by hydrolysis of its glucoside derivative, glucoraphanin, by the enzyme myrosinase. Glucoraphanin is a glucosinolate enriched in the plant family of Brassicaceae and present in high concentration in broccoli. SFN inhibits phase 1 cytochrome P450 enzymes, induces phase 2 metabolic enzymes, and acts as an antioxidant by increasing reduced glutathione levels as well as inducing cell cycle arrest and apoptosis (Herr and Buchler, 2010). It exhibits anti-inflammatory properties and inhibits angiogenesis (Herr and Buchler, 2010). SFN has also been shown to sensitize pancreatic CSCs by downregulation of NF- κ B along with inhibition of CSC properties (Kallifatidis et al., 2009).

The cruciferae plant family is characterized by a unique phytochemistry: their high content (often several percent by weight) of glucosinolates, which are β -thioglucoside N-hydroxysulfates with more than 120 unique amino acid side chains (Fahey et al., 2001). Sulforaphane and other isothiocyanates are synthesized and stored in plants in the form of the inactive glucosinolate precursors (Figure 32).

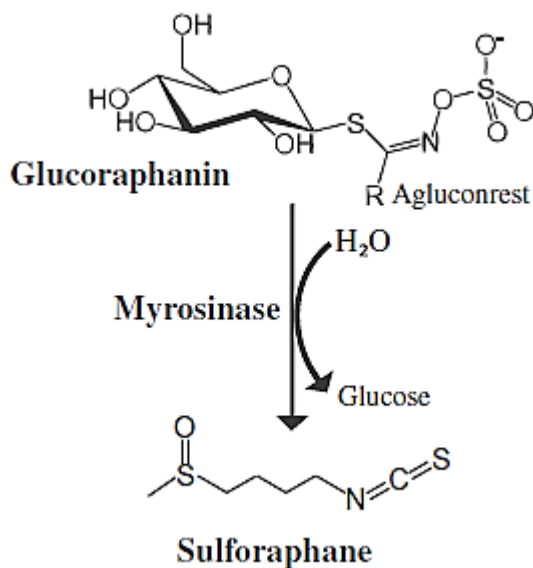


Figure 32. Glucosinolates and myrosinase are stored in separate cell compartments.

Break down of the cell, e.g. by chewing, cutting or boiling, leads to the release of glucosinolates and myrosinase. Myrosinase causes hydrolytic cleavage of glucosinolate. Thereby, preventive or therapeutically active degradation products arise, such the isothiocyanate sulforaphane present in high concentration in broccoli. Source: Herr and Buchler, 2010.

Myrosinase is physically segregated from glucosinolates in plant cells but is released when the cells are damaged, e.g. by microbial attack, insect predation, mechanical food processing, such as by chewing or food preparation (Herr and Buchler, 2010). This hydrolysis can be also mediated by the microflora of the mammalian gastrointestinal tract (Shapiro et al., 1998). Glucoraphanin is the major glucosinolate contained in broccoli (Fahey et al., 1997). Because of the widely varying content of glucoraphanin in mature broccoli, 3-day-old sprouts are commonly used for human delivery of standardized amounts of glucoraphanin and sulforaphane (Herr and Buchler, 2010). Moreover, amongst all the isothiocyanates, L-sulforaphane, which is found in broccoli and broccoli sprouts at particular high levels, has been the most extensively studied (Lampe, 2009). The mechanism of anti-carcinogenic action of SFN probably involves the detoxication of carcinogens and procarcinogens and prevention of procarcinogen activation (Herr and Buchler, 2010). This is mediated by induction of expression of enzymes catalyzing phase II biotransformation enzymes (GSTs, UDP glucuronosyltransferases, etc.) (Clarke et al., 2008) and inhibition of cytochrome P450 system (Shishu et al., 2003), respectively. SFN is readily available in the

healthy diet through the consumption of cruciferous vegetables such as broccoli. SFN reacts with specific thiol groups on Keap1, promoting Nrf2 dissociation from Keap1. Keum and colleagues (2006) found SFN increased expression of heme oxygenase-1 (HO-1) in HepG2 cells *in vitro*. Nrf2-independent effects of SFN have also been found – such as effects on MAP kinases in expression of keratin in skin epithelial cells (Kerns et al., 2010).

2.4.2 Hesperetin (HESP)

Hesperetin is a flavonoid found in citrus fruits (Erlund et al., 2001; Erlund et al., 2004). Several epidemiological studies have suggested a protective effect of these compounds on cardiovascular diseases (Knekt et al., 1996). The flavanones, also called citrus flavonoids, have been studied extensively in the past 20 years as their intake from the diet can be quite high and they exhibit promising biological activities (Erlund et al., 2001). Hesperetin chemical structure is represented in Figure 33.

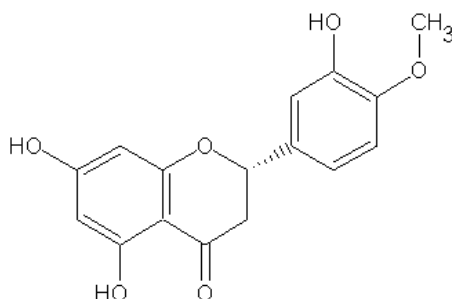


Figure 33. Chemical structure of the bioflavonoid Hesperetin (Mw = 302 g/mol).

Source: Erlund, 2004.

Epidemiological studies indicate a protective relationship between the consumption of citrus fruits or juices and the risk of ischemic stroke (Joshi et al., 1999) and lung cancer (Le Marchand et al., 2000). In the United States, the mean daily individual consumption of citrus fruits and juices has been estimated as 68 g, of which 59 g was consumed as juices (Erlund et al., 2001). The most commonly used citrus juices (i.e., orange and grapefruit juices) contain high amounts of the flavanone hesperetin (Kawaii et al., 1999). Mean dietary intakes of hesperetin were *ca.* 7 mg/day, undetectable in a diet low in fruit and vegetables

and 132 mg in a diet rich in fruit and vegetables (Erlund et al, 2002). Hesperetin is a phytoestrogen, which could affect sex hormone mediated biological responses by several different mechanisms, including binding to oestrogen receptors (Dechaud et al., 1999). The compound also possesses anticarcinogenic (So et al., 1996), antioxidant (van Acker et al., 2000) and blood lipid-lowering (Shin et al., 1999) activities.

Other possible effects of hesperetin and naringenin are on lipid metabolism. They have been reported to regulate apolipoprotein B secretion by HepG2 cells, possibly through inhibition of cholesterol ester synthesis (Borradaile et al., 1999), and to inhibit 3-hydroxy-3 methylglutaryl-coenzyme A reductase and acyl coenzyme A:cholesterol O acyltransferase in rats (Lee et al., 1999). Furthermore, a decrease in plasma low-density lipoprotein levels and hepatic cholesterol levels in rabbits fed a high-cholesterol diet has been observed (Kurowska et al., 2000). An increase of high-density lipoprotein levels in hypercholesterolemic human subjects after consumption of orange juice was also reported (Kurowska et al., 2000). Finally, hesperetin urinary recovery is thought to be 3% in subjects ingesting 500 mg of naringin and 500 mg of hesperidin once and 24% in 5 subjects ingesting 1250 mL of grapefruit juice and 1250 mL of orange juice daily for 4 weeks (Ameer et al., 1996).

2.5 Nutrient sensing via the ChREBP/MondoA–Mlx complex

Multicellular animals sense and control their glucose homeostasis at several levels. Systemic regulation by insulin and glucagon maintains levels of circulating glucose constant during fluctuating nutritional conditions. Upon feeding, elevated circulating glucose is taken up by muscle, liver and adipose tissue through the actions of insulin signaling, while starvation elevates glucagon levels to promote glycogenolysis and gluconeogenesis (Havua and Hietakangas 2012). The intracellular glucose is rapidly converted into glucose-6-phosphate. Through a yet-unknown mechanism, glucose-6-phosphate activates two paralogous basic helix-loop-helix-leucine zipper (bHLHZ) transcription factors (TFs) ChREBP and MondoA, which heterodimerize with their common binding partner Mlx. This bHLHZ complex resembles the evolutionarily related Myc–Max complex. As

shown by Havua and Hietakangas (2012) ChREBP/Mondo–Mlx is known to mediate a majority of the glucose-induced transcriptional response by binding to target gene promoters containing so-called carbohydrate response elements (ChoREs).

As demonstrated by Billin and colleagues (2000), regulation of ChREBP/MondoA–Mlx complexes involves shuttling between cytoplasm and nucleus (Figure 34).

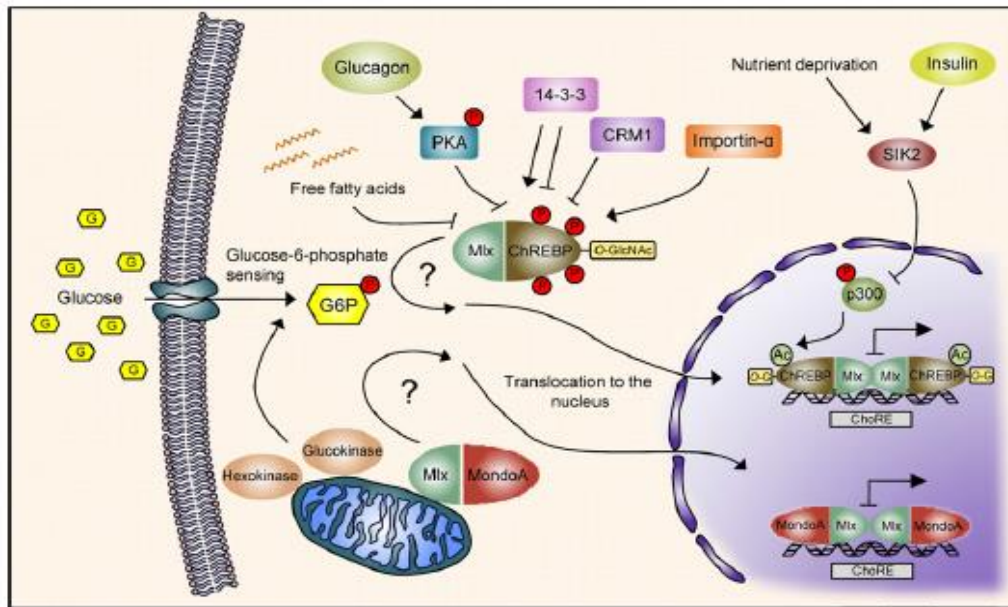


Figure 34. Regulation of ChREBP/MondoA–Mlx activity.
Source: Havua and Hietakangas, 2012.

MondoA–Mlx localizes to the outer mitochondrial membrane (OMM) in its inactive state (Sans et al., 2006). While mitochondrial localization has not been demonstrated for ChREBP, it displays punctuated cytoplasmic localization upon low glucose in hepatocytes (Kawaguchi et al., 2001). In response to elevated glucose, MondoA and ChREBP concentrate strongly into the nucleus (Stoltzman et al., 2008). Heterodimerization of ChREBP/MondoA with Mlx is required for their nuclear entry in response to glucose and is a prerequisite for their binding to ChoREs (Ma et al., 2007). ChREBP and MondoA activity is, however, regulated at several levels, since forced nuclear accumulation of ChREBP or MondoA is insufficient in target gene transactivation (Peterson et al., 2010). Several lines of evidence imply that ChREBP/MondoA–Mlx activation is induced by intracellular glucose-6-phosphate (G6P), the immediate metabolite of glucose (Figure 34) (Stoltzman et al., 2008). The formation of G6P is catalyzed by hexokinases or

glucokinase, which also localize to the OMM (Gerbitz et al., 1996). The responsiveness of MondoA–Mlx to G6P was shown elegantly by the use of a glucose analog 2-deoxyglucose (2-DG). 2-DG is phosphorylated into 2-deoxyglucose-6-phosphate (2-DG6P), but it cannot be processed further, leading to 2-DG6P accumulation (Stoltzman et al., 2008). In response to 2-DG treatment, MondoA–Mlx translocates into the nucleus and strongly transactivates target genes (Havua and Hietakangas, 2012) and furthermore, ChREBP was shown to be activated by fructose 2,6 bisphosphate in hepatocytes.

ChREBP and MondoA are multidomain proteins with highly homologous N- and C terminal regions. They contain a bHLHZ region and a C-terminal dimerization domain mediating DNA binding and heterodimerization with Mlx (Figure 35) (Eilers et al., 2002).

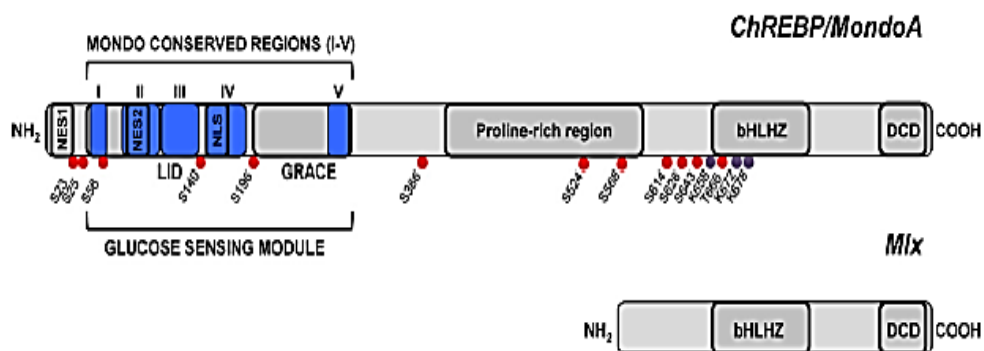


Figure 35. Domain structure of ChREBP/MondoA and Mlx.

The C-termini of ChREBP/MondoA and Mlx are similar and contain a dimerization and cytoplasmic localization domain (DCD) and a basic helix-loop-helix leucine zipper region (bHLHZ). Source: Havua and Hietakangas, 2012.

Both ChREBP and MondoA contain transcriptional activation domains, while Mlx is much shorter and lacks intrinsic transactivation capacity (Billin et al., 2000). The loop region of Mlx bHLHZ domain mediates the interaction between two ChREBP/ MondoA–Mlx heterodimers, stabilizing their binding to the tandem E-boxes in ChoRE (Ma et al., 2007). In terms of glucose sensing the most important region is the highly conserved N-terminal part of MondoA and ChREBP, called Mondo conserved region (MCR) (Billin et al., 2000) or glucose-sensing module (GSM) (Li et al., 2006). Li and colleagues (2006) have shown that the GSM can be functionally divided into low-glucose inhibitory domain (LID)

and glucose-response activation conserved element (GRACE) (Figure 35). LID inhibits the transactivation capacity of GRACE under low glucose conditions and this inhibition can be relieved by high glucose. LID and GRACE are functionally distinct modules as the glucose responsiveness is retained even when the domains are physically separated by intervening GFP. The N terminus is functionally conserved: the MCR/GSM region of ChREBP can be replaced by the corresponding region of MondoA while retaining the glucose responsiveness (Li et al., 2006). Finally, consistent with its role as a regulator of glycolytic genes, MondoA activity corresponds to the rate of glycolysis (Sans et al., 2006).

2.6 Aim and objectives

2.6.1 Aim

The aim of this investigation is to study the prevention of human fibroblasts senescence *in vitro* by chronic treatment with dietary bioactive compounds and to determine the mechanism by which these compounds delay senescence.

2.6.2 Objectives

2.6.2.1 Objective 1: To study the effects of SFN and HESP on MRC-5 and BJ senescence in vitro

Transcription factor Nrf2 regulates the expression of a battery of genes via interaction with one or more AREs that provide protection against proteome, lipidome and genome damage by glycation, oxidation and nitration. In this project, the delay of MRC-5 and BJ senescence by the nrf2-activating dietary bioactive compounds SFN and HESP will be studied. Initially, growth patterns of MRC-5 and BJ fibroblasts will be studied by constructing a growth curve for these two cell types. Moreover, the median growth inhibitory concentration of SFN and HESP will be analysed on MRC-5 and BJ fibroblasts by constructing dose-response curves for these two compounds. The Population Doubling Limit (PDL) as well as cumulative PDL (cPDL) will also be analyzed in order to represent MRC-5 and BJ fibroblast growth as progression of senescence occurred. Moreover, the percentage of cells expressing β -galactosidase and protein

expression of the human β -galactosidase-1 in MRC-5 fibroblasts at early and late passage will be determined in order to evaluate the senescent state of these cells with or without SFN treatment.

2.6.2.2 Objective 2: To characterize gene expression and cell metabolism in cells escaping senescence by treatment with SFN and HESP

Custom real time RT-PCR and antibody arrays will be used to assess expression of ARE-linked genes. Moreover, expression of genes involved in protection against oxidative damage, protection against proteasomal proteolysis, autophagy and glycation, protection against metabolic stress and senescence-linked genes will be determined in young and senescent MRC-5 fibroblasts treated with SFN or HESP using NanoString technology. Proteome, lipidome and genome damage will be assessed by quantitative screening of protein oxidation, nitration and glycation adducts, isoprostanes and deoxyguanosine glycation and oxidation adducts by stable isotopic dilution analysis tandem mass spectrometry. This will allow for the identification of gene expression patterns linked to healthy ageing and dietary bioactives supplementation to be characterized.

2.6.2.3 Objective 3: To characterize the mechanism of decrease glucose metabolism by SFN and HESP action linked to delay of fibroblast senescence

The effect of SFN and HESP treatment on D-glucose consumption in young and senescent MRC-5 fibroblasts will be determined in order to evaluate the caloric restriction mimetic of SFN and HESP linked to delay of fibroblast senescence. This will be further confirmed by analysis of L-lactate production in the cells - leaking into the culture medium of MRC-5 and BJ fibroblasts treated with SFN and HESP. The formation of D-lactate - terminal product of the metabolism of the senescence inducing glycating agent, MG, will also be studied (Sejersen and Rattan, 2009). Moreover, glycolytic intermediates expression in MRC-5 fibroblasts treated with SFN at early and late passage will be analysed by stable isotopic dilution analysis tandem mass spectrometry in order to characterize the mechanism of caloric restriction mimetic further in response to SFN-linked delay of MRC-5 senescence. Finally, glucose sensing by ChREBP/MondoA-Mlx transcription factors in response to SFN treatment in MRC-5 fibroblasts will be

studied by nuclear translocation observations of MondoA using immunostaining analysis.

3. Materials and Methods

3.1 Materials

3.1.1 Human fibroblasts

Human foetal lung MRC-5 fibroblasts, human foreskin BJ fibroblasts and human leukemia HL60 leukemia cells were purchased from the European Collection of Animal Cell Cultures (ECACC, Porton Down, U.K), London, United Kingdom (U.K.).

MRC-5 and BJ cells were grown in Eagle's Minimum Essential Medium (MEM) purchased from Invitrogen (Paisley, Scotland). MEM culture media contained non-essential amino acids (NEAA) and was supplemented with 10% foetal bovine serum (FBS) (Biosera; UK agent - Labtech International Ltd, Uckfield, UK), 1% penicillin-streptomycin (Sigma-Aldrich, Poole, Dorset, UK), 2 mM L-glutamine and 100 mM sodium pyruvate (Invitrogen). The solution of trypsin-ethylenediaminetetra-acetic acid trypsin-EDTA (trypsin, 0.25%, EDTA, 0.02% (w/v)) was purchased from Sigma-Aldrich (Poole, Dorset, U.K.). Phosphate-buffered-saline (PBS) was prepared in-house by the technical staff and had composition: 137 mM NaCl, 2.7 mM KCl, 10 mM Na₂HPO₄ and 2 mM KH₂PO₄. MRC-5 and BJ fibroblasts were passaged every 7 days: seeding density 10,000- 40,000 cells/cm² for MRC-5 fibroblasts and 10,000 - 30,000 cells/cm² for BJ fibroblasts. MRC-5 and BJ fibroblasts were harvested with trypsin-EDTA. Cells were all passaged using the following method. Conditioned medium was removed from above the cells adhered to the bottom of the culture flask, the cells were gently rinsed with PBS at 37°C. Approximately 1 ml/25 cm² of trypsin-EDTA solution (0.25% trypsin, 0.02% EDTA) was then added to each flask and cells returned to the 37°C incubator for 3 - 5 min until cells acquired a rounded appearance when viewed under an inverted microscope. Trypsin was then neutralised with 4 ml/25 cm² of fresh cell culture medium. Cells were sedimented by centrifugation (125g, 10 min, 25°C) and the supernatant removed. Cells were then re-suspended in culture media and assessed for cell viability for seeding. Unless mentioned otherwise, all cell types were passaged in the above conditions.

3.1.2 Human leukaemia 60 cells

Human leukaemia 60 (HL60) cells were used to prepare ¹³C-labelled glycolytic intermediates. They were grown in Roswell Park Memorial Institute (RPMI) 1640 medium purchased from Invitrogen (UK) supplemented with 10% FBS (complete medium). RPMI 1640 medium without glucose was purchased from Invitrogen (UK) and used to make HL60 for cell growth with serum-free medium (defined medium). This defined medium was supplemented with 10.0 mM 4-(2-hydroxyethyl) piperazine-1-ethanesulfonic acid HEPES (Fisher Scientific, Loughborough, UK) and 1 mM sodium pyruvate, 25 mM D-Glucose, 5 µg/ml human insulin and 5 µg/ml human transferrin - all purchased from Sigma-Aldrich (Poole, Dorset, UK).

3.1.3 Cell viability

Cell viability was assessed by the Trypan blue dye exclusion technique (Kenyon et al., 1993). Cell suspension (20 µl) containing 1 - 10 x 10⁴ cells was mixed with 20 µl 0.4% solution of Trypan blue in buffered isotonic salt solution (PBS), pH 7.2 to 7.3. Viability was then determined using a Neubauer haemocytometer ensuring a total count of 100 – 200 cells. The number of cells excluding Trypan blue gives the viable cell count N and the number of cells stained with Trypan blue gives the non-viable cell count NV. Percentage cell viability is given by $V/(V+NV) \times 100$. All experiments were performed with cell viability of 98% or more.

3.1.4 Enzymes, substrates, co-factors, antibodies, primers, other biochemical and miscellaneous reagents

3.1.4.1 Enzymes, co-factors and substrates

D-Lactic dehydrogenase enzyme (from *Staphylococcus epidermidis*, ≥80 units/mg activity, lyophilized powder) and L-lactic dehydrogenase (from rabbit muscle), pepsin (from porcine stomach mucosa, specific activity 3460 units/mg protein), pronase E (from bacterial *Streptomyces griseus*, specific activity 4.4 units/mg protein), leucine aminopeptidase type VI (from porcine kidney microsomes, specific activity 22 units/mg protein) and prolidase (from porcine

kidney, specific activity 145 units/mg protein), nicotinamide adenine dinucleotide-oxidised form (NAD⁺), sodium L-lactate and L-lactic acid sodium D-lactate ($\geq 99.0\%$) was purchased from Sigma-Aldrich.

3.1.4.2 Antibodies and primers for RT-PCR

Rabbit polyclonal anti- β -galactosidase (BGAL) antibody (supplied as 1 mg IgG in 100 μ l of 1% BSA, 0.15 M sodium chloride, 20 mM potassium phosphate buffer, pH 7.2), rabbit polyclonal anti-MLX-interacting protein (MondoA) antibody and rabbit polyclonal anti- β -actin antibody were purchased from Abcam (Cambridge, UK). Alexa fluor 488 goat anti-rabbit IgG conjugate was purchased from Molecular Probes (Paisley, Scotland).

RT-PCR primers for β -actin (ACTB), NAD(P)H:quinone oxidoreductase-1 (NQO1), nuclear factor (erythroid-derived 2)-like 2 (NFE2L2), transketolase (TKT), glyoxalase 1 (GLO1), aldoketo-reductase B1 (AKRB1), Kelch-like ECH-associated protein 1 (KEAP1), γ -glutamylcysteine ligase – catalytic subunit (GCLC), γ -glutamylcysteine ligase – modulatory subunit (GCLM), carbonyl reductase-1 (CBR1), transaldolase-1 (TALDO1), glutathione reductase (GSR), haem oxygenase-1 (HMOX1), aldoketo-reductase B2 (AKRB2) and thioredoxin (TXN) were all purchased from Sigma-Aldrich. BioScriptTM (Moloney murine leukaemia virus reverse transcriptase), Oligo(dT)18, Rnase inhibitor, buffer RT and master mixture/50 SYBR Green were all purchased from BioLine (London, U.K).

3.1.4.3 Reagents for Agilent one-colour microarray-based gene expression analysis

The following reagents were purchased from Agilent Technologies UK Ltd. (Wokingham, Berkshire) and provided by Unilever Laboratories (Colworth, UK): One-colour Spike-Mix stock, Dilution Buffer, T7 Promoter primer, 5X first strand buffer, DTT, dNTP mix, MMLV-RT, RNase out, 50% PEG, 4X transcription buffer, NTP mix, inorganic pyrophosphatase, T7 RNA Polymerase, Cyanine 3-CTP, Cyanine 3 dye absorbance, 10X Blocking Agent from Agilent Gene Expression Hybridization Kit, 25X Fragmentation Buffer, 2X GEX Hybridization Buffer HI-RPM, GE wash buffer 1, GE wash buffer 2, acetonitrile ,

Stabilization and Drying solution. Qiagen RNeasy mini spin columns was purchased from Qiagen (West Sussex, U.K).

3.1.4.4 Other biochemical and miscellaneous reagents

The senescence cells staining kit (cat. no. CS0030) and glucose assay kit for the hexokinase method (cat. no. GAHK20) was obtained from Sigma Aldrich. The RNeasy Mini Kit was purchased from Qiagen (West Sussex, U.K). Bovine Serum Albumin (BSA) was purchased from Sigma-Aldrich (Poole, Dorset, U.K). R-Sulforaphane (SFN, $\geq 95\%$) was purchased from Sigma-Aldrich and hesperetin ((2S)-2,3-dihydro-5,7-dihydroxy-2-(3-hydroxy-4-methoxyphenyl)-4H-1-benzopyran-4-one, $\geq 95\%$) from LKT Laboratories – UK distributors: Cambridge Bioscience Ltd (Cambridge, UK). Sodium glycinate, perchloric acid, sodium chloride, potassium bicarbonate, glycine and HPLC methanol and acetonitrile were all purchased from Fisher Scientific (Loughborough, UK). All other reagents, acids, salts, buffers and based were analytical grade reagents and purchased from Fisher Scientific (Loughborough, U.K) and Sigma-Aldrich.

3.1.5 Immunocytochemistry, electrophoresis and Western blotting reagents

Glass bottom dishes (35 mm, round, cat. no. P35GC-1.5-14-C) were from MatTek Corporation (Ashland, Massachusetts, U.S.A) and glass coverslips (13 mm, round, cat. no. 631-0149) from VWR International (Lutterworth, Leicestershire, UK). Mounting medium containing 4',6-diamidino-2-phenylindole (DAPI) was purchased from Vector Laboratories (Peterborough, UK).

For electrophoresis, acrylamide:N,N'-methylenebisacrylamide solution (30% w/v, 37.5: 1, Ultrapure grade), 4 X Protogel resolving buffer (0.375 M Tris-HCl and 0.1% SDS, pH 8.8), protogel stacking buffer (0.125 M Tris-HCl and 0.1% SDS, pH 6.8), and 10 X Tris/glycine electroblotting buffer containing 0.25 M Tris base and 1.92 M glycine (Ultrapure, electrophoresis grade) were all purchased from National Diagnostics (Hessle, UK). Tween-20, N,N,N',N'-tetramethylethylene-1,2-diamine (TEMED, $\geq 99\%$ electrophoresis grade), β -mercaptoethanol, 3', 3'', 5', 5''-tetrabromophenolsulfonphthalein sodium salt (bromophenol blue, electrophoresis grade) and protease inhibitor cocktail

containing 104 mM 4-(2-aminoethyl) benzenesulfonyl fluoride hydrochloride (AEBSF), 80 μ M aprotinin, 4 mM bestatin, 1.4 mM E-64, 2 mM leupeptin and 1.5 mM pepstatin A were all purchased from Sigma-Aldrich. Coomassie Brilliant Blue G-250 (analytical grade) was purchased from Fluka (Poole, UK). Polyvinyl difluoride (PVDF) membrane and photographic film were purchased from GE Healthcare (Little Chalfont, UK). SpectroTM multicolor broad range protein ladder (10-260 kDa, for 4 – 20% Tris-glycine SDS-PAGE) used for western-blotting was purchased from Fisher Scientific.

3.1.6 Analytical standards for stable isotopic analysis of metabolites

3.1.6.1 GSH and GSSG

GSH, GSSG and [*glycine*-¹³C₂,¹⁵N₁]Glutathione (99%; [¹³C₂,¹⁵N₁]GSH) were purchased from Sigma Aldrich. [¹³C₄¹⁵N₂]GSSG was synthesised from [*glycine*-¹³C₂,¹⁵N₁]GSH – Figure 36. Briefly, [¹³C₂¹⁵N₁]GSH was oxidised using diamide to form [¹³C₄¹⁵N₂]GSSG for use in the LC-MS/MS method to quantify cellular GSSG. An aliquot of [¹³C₂¹⁵N₁]GSH solution (3.2 mM, 100 μ l) and 10 mM diamide in methanol (30 μ l) was added to 100 μ l of 10 mM sodium phosphate buffer, pH 7.4 and incubated at 37°C for 30 min. The product mixture was purified by elution onto a strong anion-exchange solid-phase extraction (SAX SPE) cartridge, 500 mg, formate form. [¹³C₄¹⁵N₂]GSSG was retained on the SAX-SPE cartridge whereas diamide and reduced diamide were not. The SAX-SPE cartridge was washed with 10 mL water to remove the diamide and residual GSH. [¹³C₄¹⁵N₂]GSSG was collected by elution from the SAX-SPE cartridge with 5 ml 100 mM formic acid. The solution was lyophilised to dryness, reconstituted in water (1 ml) and filtered through a 0.2 μ m nylon filter. The concentration of [¹³C₄¹⁵N₂]GSSG was deduced by isotopic dilution analysis with known amounts of GSSG. The yield was 28%.

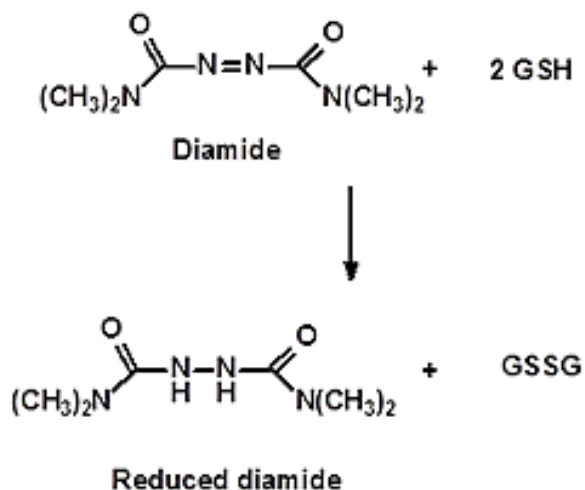


Figure 36. Oxidation of glutathione by diamide.

3.1.6.2 Glyoxal, methylglyoxal and 3-deoxyglucosone

Normal and isotopic standards for assay of dicarbonyl metabolites, glyoxal, MG and 3-DG, were available in house. Glyoxal (8.8 M aqueous solution) was purchased from Sigma and [$^{13}\text{C}_2$]glyoxal was prepared from [$^{13}\text{C}_2$]ethylene glycol by alcohol oxidase in the presence of catalase (Isobe and Nishise, 1994). High purity methylglyoxal and [$^{13}\text{C}_3$]methylglyoxal were available in house, prepared and purified as described (McLellan and Thornalley, 1992). [$^{13}\text{C}_3$]MG was prepared from [$^{13}\text{C}_3$]acetone by oxidation with selenium dioxide and purified by distillation (Clelland and Thornalley, 1990). 3-DG and [$^{13}\text{C}_6$]3-DG were synthesised from glucose and [$^{13}\text{C}_6$]glucose as described (Madson and Feather, 1981). [$^{13}\text{C}_2$]Ethylene glycol and [$^{13}\text{C}_3$]acetone were purchased from Sigma and [$^{13}\text{C}_6$]Glucose Cambridge Isotope Laboratories (Andover, MA, USA).

3.1.6.3 Amino acids and glycated, oxidized and nitrated derivatives

L-Amino acids were purchased from Sigma, stable isotope-substituted amino acids were purchased from Cambridge Isotope Laboratories (Andover, MA, USA) and 2,5,5- $^2\text{H}_3$]DL- α -amino adipic acid (d_3 -AAA) was purchased from CDN Isotopes (Quebec, Canada). Glycated, oxidized and nitrated amino acid derivatives and stable isotope-substituted isotopomers were available in house, prepared and purified as described (Kenyon et al., 1993)(Kenyon et al., 1993). ϵ -(γ -L-glutamyl)-L-lysine was purchased from Bachem AG (Bubendorf,

Switzerland) and [$^{13}\text{C}_5$] ϵ -(γ -L-glutamyl)-L-lysine was available in house, prepared and purified as described .

3.1.6.4 ^{13}C -Labelled glycolytic intermediate isotopomers

HL60 cells (1×10^6) were seeded in T-175 flasks in 30 ml of complete media – see section 3.1.2. Cells cultured in these conditions were passaged for four or more passages when exponential growth of cultures free of cell debris was attained. HL60 cells (1×10^6) were then seeded in T-175 flasks in 30 ml defined media for 5 days until cells reached 80-90% confluence according to the method described by Breitman et al. (1980). The resulting culture was used to seed 6 further cultures of 1×10^6 cells in 30 ml of RPMI 1640 medium without glucose supplemented with 10.0 mM HEPES, 1 mM sodium pyruvate, 25 mM [$^{13}\text{C}_6$]glucose, 5 $\mu\text{g/ml}$ insulin and 5 $\mu\text{g/ml}$ transferrin. After 5 days in culture, the cells were collected by centrifugation (200g, 10 min), washed twice with ice-cold PBS and cell pellets (3×10^6 cells) were collected and stored at -80°C as stock $^{13}\text{C}_6$ -labelled glycolytic intermediates.

3.1.7 Equipment, instrumentation and software

The Neubauer Haemocytometer used for cell counting was from Marienfield (Germany). Water used for all experiments was filtered through a Milli-Q Advantage A-10 System from Millipore (Watford, UK). The inverted microscope Nikon Eclipse TE2000-S (U.S.A) was used for picture recording. The FLUOstar OPTIMA microplate reader (BMG Labtech, U.K) was used for the enzymatic assays. LC- MS/MS was performed with a AcquityTM ultra high performance liquid chromatography (UPLC) system with a Quattro Premier XE Tandem mass spectrometer or an AcquityTM UPLC system with a Xevo-TQS Quattro tandem mass spectrometer (Waters, Elstree, U.K.). Enzymatic hydrolysis was performed using a CTC-PAL Automation System (CTC-Analytics, Zwingen, Switzerland). The 7500 Fast Real - Time PCR system (Applied Biosystem by Life Technologies, U.K) was used for gene expression analysis and the Nanodrop Spectrophotometer ND- 1000 (Labtech International, U.K) was used to determine protein concentration in media. Confocal microscopy was performed using an

AxioVert 200M laser scanning confocal microscope from Carl Zeiss Microscopy (Thornwood, NY, USA).

Protein expression level was analysed with ImageQuant densitometry software from Amersham Biosciences (Little Chalfont, UK). Related data outputs were processed with software Masslynx version 4.1. Confocal microscopy images were viewed using LSM Image Browser (Carl Zeiss Microscopy, Thornwood, NY, USA). RNA primers were designed using the Oligo perfect design tool (Invitrogen Life Technologies, Paisley, UK) with mRNA and genomic sequences obtained using the University of California, Santa Cruz genome browser tool (Genome Bioinformatics Group, University of California, Santa Cruz). Agilent SureHyb, SureHyb gasket slide, Agilent scanner and Agilent Feature Extraction Software were all purchased from Agilent Technologies UK Ltd. (Wokingham, Berkshire) and provided by Unilever Laboratories (Colworth, UK).

3.2 Cell culture

3.2.1 Effect of sulforaphane treatment on growth of MRC-5 cells *in vitro*.

Human MRC-5 fibroblasts were seeded in 6-well cell culture plates (30,000 cells/well) in 3 ml Eagle's MEM per well with and without 0.5 – 10.0 μM SFN. Stock SFN solution (50 mM) was prepared in DMSO and sterilized in microspin filters (0.2 μm , nylon filters). Immediately before use, an aliquot of the stock solution was diluted 1000-fold and then diluted further to the required concentration. The maximum concentration of vehicle, dimethyl sulfoxide (DMSO), was therefore 0.002% (v/v) and control incubations therefore contained 0.002% DMSO. The cells were cultured for 24 h and 48 h and the viable cell number recorded. Viable cell number - SFN concentration response curves were constructed with data fitted to the logistic equation $V = V_{\text{max}} \times \text{GC}_{50}^n / (\text{GC}_{50}^n + [\text{SFN}]^n)$ where V is the viable cell number, V_{max} the viable cell number of control cultures incubated without SFN, GC_{50} is the median growth inhibitory concentration value, [SFN] the concentration of SFN (0.5 – 10 μM) and n the logistic regression coefficient. Data were fitted by non-linear regression using the ENZFITTER programme (Biosoft, Cambridge, U.K.) solving for GC_{50} and n.

3.2.2 Effect of hesperetin on growth of MRC-5 cells *in vitro*.

Human MRC-5 fibroblasts were seeded in 6-well cell culture plates (30,000 cells/well) in 3 ml Eagle's MEM per well with and without 0.5 – 40.0 μ M hesperetin. Stock hesperetin solution (100 mM) was prepared in DMSO and sterilized in microspin filters (0.2 μ m, nylon filters). Immediately before use, an aliquot of the stock solution was diluted 1000-fold and then diluted further to the required concentration. The maximum concentration of vehicle, DMSO, was therefore 0.005% (v/v) and control incubations therefore contained 0.005% DMSO. The cells were cultured for 24 h and 48 h and the viable cell number recorded. Viable cell number - hesperetin concentration response curves were constructed with data fitted to the logistic equation $V = V_{\max} \times GC_{50}^n / (GC_{50}^n + [\text{Hesperetin}]^n)$ solving for GC_{50} and n .

3.2.3 Effect of chronic treatment with sulforaphane on the development of MRC-5 cell senescence *in vitro*

MRC-5 cells were seeded in T-75 cell culture flasks (300,000 cells/flask) in 5 ml Eagle's MEM per well supplemented with either 1 μ M SFN or with vehicle (0.002% DMSO). Cells cultured in these two conditions were cultured for 7 days and then cell number and viability recorded and passaged. Viable cell counts determined at every passage were used to deduce population doubling level (PDL) and cumulative PDL with passage. $PDL = \ln(N_H/N_S) / \ln 2$, where N_H and N_S are the cell population numbers at harvest and seeding, respectively at each passage. Cell viability was assessed by Trypan blue exclusion.

3.2.4 Effect of chronic treatment with hesperetin on the development of MRC-5 cell senescence *in vitro*.

MRC-5 cells were seeded in T-75 cell culture flasks (300,000 cells/flask) in 5 ml Eagle's MEM per well supplemented with either 5 μ M HESP in DMSO or with vehicle (0.005% DMSO). Cells cultured in these two conditions were passaged and counted every 7 days. Viable cell counts determined at every passage were plotted against number of days in culture to deduce PDL and cumulative PDL. Cell viability was assessed by Trypan blue exclusion.

3.3 Analytical methods

3.3.1 Senescence-associated beta-galactosidase staining

MRC-5 fibroblasts were seeded at a density of 30,000 cells per well in a 12-well plate with 3 ml Eagle's MEM media with 1 μ M SFN or 0.002% DMSO vehicle control. After 24 h, the growth medium was aspirated from the cells. The cells were then washed twice with 1 ml of PBS per well. Residual wash solution was carefully removed by aspiration. The senescence cells staining kit from Sigma-Aldrich was used for the following steps. An aliquot of fixation buffer (0.4 ml, containing 20% formaldehyde, 2% glutaraldehyde, 70.4 mM Na_2HPO_4 , 14.7 mM KH_2PO_4 , 1.37 M NaCl and 26.8 mM KCl) was added per well and the plates were incubated for 6 to 7 min at room temperature. During the fixation process, 7 ml of the staining mixture was prepared as follows: 700 μ l Staining Solution (10-fold concentrated) was added to 87.5 μ l of 400 mM potassium ferricyanide, 87.5 μ l of 400 mM potassium ferrocyanide, 175 μ l of 40 mg/ml 5-bromo-4-chloro-3-indolyl β -D-galactopyranoside (X-gal) solution and 5.95 ml of water. The staining mixtures was then filtered using a 0.2 μ m filter and then an aliquot (0.35 ml) was added to each per well and incubated at 37°C overnight. The senescent cells were stained blue. For long-term storage of the stained plate, and later senescence quantification, the staining mixture was aspirated, and cells were overlaid with 0.4 ml of a 70% glycerol in PBS, and stored at 4°C.

3.3.2 Bradford Assay

Protein concentration in cell lysates was determined by the Bradford method (Bradford, 1976) using bovine serum albumin (BSA) as calibration standard. Stock solutions of BSA were calibrated by spectrophotometry; ϵ_{279} (1%) = 6.59 cm^{-1} (Peters Jr., 1995).

3.3.3 Real-time polymerase chain reaction analysis of mRNA

Human MRC-5 fibroblasts at the end of each passage, processed as described in Section 3.2.3, were collected in 1.5 ml microcentrifuge tubes and washed 3 times with 1 ml ice-cold PBS. After final centrifugation and removal of supernatant PBS, the cell pellets were stored at -80°C for later analysis.

3.3.3.1 Primer design and testing

Primers were designed using the Invitrogen OligoperfectTM designer tool using mRNA and genomic DNA sequences obtained from the University of California, Santa Cruz genome browser. Multiple primer pairs were selected for each gene. Amplicon length (optimal 100-150 base pairs) was considered and primers spanning exon-exon junctions were chosen when possible; this acted as an additional quality control since any contaminant genomic DNA would not act as a template for amplification. Dissociation plots were performed for all primers to test performance. An example of dissociation plot is shown in Figure 37. Dissociation plots were routinely performed for each assay plate; this ensured that the primers performed consistently.

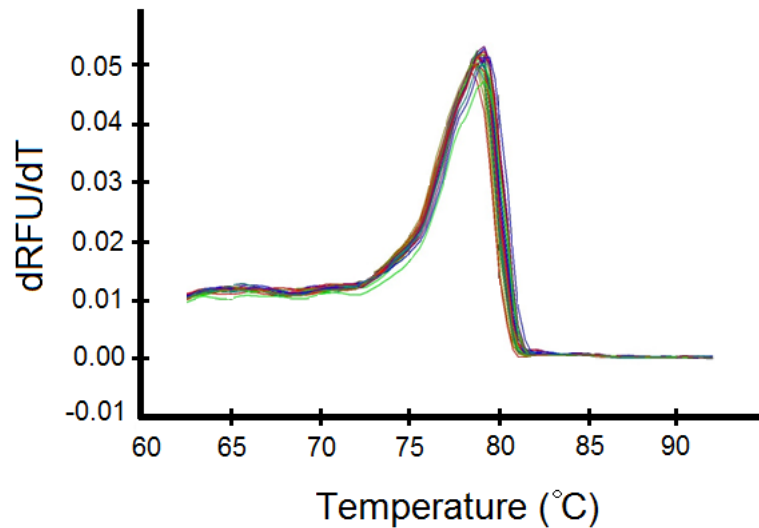


Figure 37. Representative dissociation plot for primers.

Y-axis represents the change in fluorescence with temperature ($dRFU/dT$) and X-axis represents increases in temperature in $^{\circ}C$.

3.3.3.2 RNA extraction

Sedimented cells were re-suspended and homogenized in 350 μ l RLT buffer (RNeasy Mini Kit) and Ethanol (350 μ l) was then added and samples mixed well. Samples were then transferred to an RNeasy column in 2 ml tube and centrifuged (15s, 8000g, room temperature). The eluate was discarded and 700 μ l RW1 buffer (RNeasy Mini Kit) was added to the RNeasy column. The column was centrifuged (8000g, 15s, room temperature) and the eluate was discarded. Buffer RPE (500 μ l, RNeasy Mini Kit) was added to the RNeasy column and centrifugation and flow-through discarding was repeated. This later step was performed a second time. The RNeasy column was then placed in a new 2 ml tube and centrifuged (10,000g, 1 min, room temperature). Finally, the column was placed in a clean 1.5 ml tube and 40 μ l RNase-free water added to the microspin column before centrifugation (8000xg, 1 min, room temperature). The eluate was retained as mRNA extract.

3.3.3.3 RNA quality control

RNA content and purity of samples was determined by nanodrop spectrophotometry. The quality and concentration of RNA was determined spectrophotometrically using the NanoDrop 1000 spectrophotometer. An aliquot

of RNA solution (2 μ l) was used to determine the RNA concentration; the absorbance at 260 nm was measured and RNA concentration deduced – ϵ_{260} (1 mg/ml) = 23 cm^{-1} . The quality of RNA was determined using the A_{260}/A_{280} ratio where a ratio of 1.9 - 2.1 is indicative of high purity (Glasel, 1995).

3.3.3.4 Reverse transcription

Synthesis of cDNA was performed using the BIOLINE cDNA synthesis kit. From the protein concentrations obtained, 0.1 μ g mRNA was mixed with 1.0 μ l Oligo(dT)18 and RNase-free water was added to a total volume of 12 μ l. Samples were then heated at 70 $^{\circ}$ C for 5 min and put on ice immediately thereafter. The following mixture was then added to each sample: 1.0 μ l RNase inhibitor (10 units/ μ l), 1.0 μ l dNTPs (10 mM each), 4.0 μ l 5x Buffer RT, 1.0 μ l BioScriptTM and 1.0 μ l RNase-free water. Samples were then heated at 40 $^{\circ}$ C for 60 min. Finally, 2.0 μ l of sample was loaded in a clear 96-well plate for RT-PCR analysis along with the following mixture: 10 μ l of Master Mixture/50 SYBR Green, 0.5 μ l primer solution of interest and 7.5 μ l nuclease-free water. RNA was quantified as a ratio to β -actin RNA in the sample. Gene expression was recorded using the 7500 Fast Real-Time PCR system described in Materials.

3.3.3.5 Preparation of standards

Samples with the highest mRNA concentration were used to construct the standard curve. A standard curve of serially diluted pooled cDNA over the range 0.1 pg – 1,000 ng was run alongside assay samples and used for quantification using β -actin as a reference gene. A typical standard curve is shown in Figure 38.

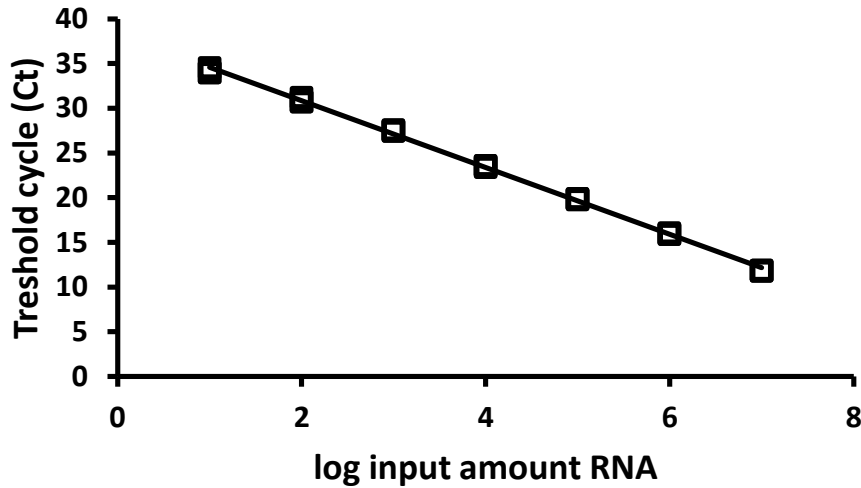


Figure 38. Typical calibration curve for RT-PCR.

Linear regression equation: Threshold cycle = $(-3.73 \pm 0.03) \times \log$ input of mRNA (pg); $R^2=0.999$; $n = 21$.

The following primers were used for analysis: β -actin (ACTB), NAD(P)H: quinone oxidoreductase-1 (NQO1), nuclear factor (erythroid-derived 2)-like 2 (NFE2L2), transketolase (TKT), glyoxalase 1 (GLO1), aldoketo-reductase B1(AKRB1), kelch-like ECH-associated protein 1 (KEAP1), glutamate-cysteine ligase-C (GCLC), glutamate-cysteine ligase-M (GCLM), carbonyl reductase 1 (CBR1), transaldolase 1 (TALDO1), glutathione reductase (GSR), haem oxygenase (decycling) 1 (HMOX1), aldoketo-reductase B2 (AKRB2), thioredoxin (TXN).

3.3.4 Custom mRNA array analysis by the Nanostring method

3.3.4.1 Sample preparation: Time course with SFN treatment on young MRC-5 fibroblasts

MRC-5 fibroblasts after passage 4 were seeded in 6-well plates at a density of 200,000 cells per well. After 24 h, cells were treated with either 1 μ M SFN or vehicle control (0.002% DMSO). The media contained in each well was removed, cells were washed twice with ice cold PBS and the plate was stored at -80°C after rigorous sealing at time points 0, 4, 8, 12, 24, 36, 48 and 72 hours. MRC-5 and BJ fibroblasts treated with 1 μ M SFN or vehicle (0.002% DMSO) at early and late passages were also analysed.

3.3.4.2 Sample preparation: Effect of SFN and HESP treatment on young and senescent MRC-5 fibroblasts

MRC-5 cells were seeded in T-175 cell culture flasks (1 million cells/flask) in 30 ml Eagle's MEM per well supplemented with either 1 μ M SFN or with vehicle (0.002% DMSO). MRC-5 cells were also seeded in T-175 cell culture flasks (1 million cells/flask) in 30 ml Eagle's MEM per well supplemented with either 5 μ M HESP or with vehicle (0.005% DMSO). Cells cultured in these two conditions were cultured for 7 days and then cell number and viability recorded and passaged. MRC-5 fibroblasts treated with SFN after passage 3 and 11 were used and MRC-5 fibroblasts treated with HESP after passage 3 and 9 were used for Nanostring analysis. The media contained in each flask was removed, trypsinised and collected cells were washed twice with ice cold PBS and stored at - 80°C until further analysis.

3.3.4.3 Processing of samples

Total RNA was extracted as described in Method 3.3.3. 2. Total RNA (600 – 800 ng) was analyzed for mRNA copy number of target genes by the NanoString nCounter Gene Expression method (Geiss et al., 2008) - outsourced to Nanostring, Seattle, USA. Two sequence-specific probes were constructed for each gene of interest (Table 6 and 7). The probes were complementary to a 100-base region of the target mRNA. One probe was covalently linked to an oligonucleotide containing biotin (the capture probe), and the other was linked to a color-coded molecular tag that provided the signal (the reporter probe; see Figure 39). In this study, a custom codeset of 47 genes linked to Nrf2 system (anti-glycation related genes, antioxidant related genes, phase II conjugation genes, pentophosphate pathway genes, lipogenesis related genes, proteasome subunit genes and Nrf2 regulation related genes), inflammatory and immune response genes, extracellular matrix regulating genes, lysosomal and plasminogen activator inhibitor genes, senescence-associated genes and three reference genes (β -actin, clathrin heavy chain and β -glucuronidase) was designed. Triplicate samples were used for each treatment and time point. NanoString processing was performed by NanoString TechnologyTM (Seattle, Washington). The response

gives an estimate of relative mRNA copy number. Correction with the reference genes is made by normalizing to the geometric mean of reference genes at baseline – thereby controlling for technical variability in the mRNA copy number response. Data were analyzed using the nCounter™ digital analyser software.

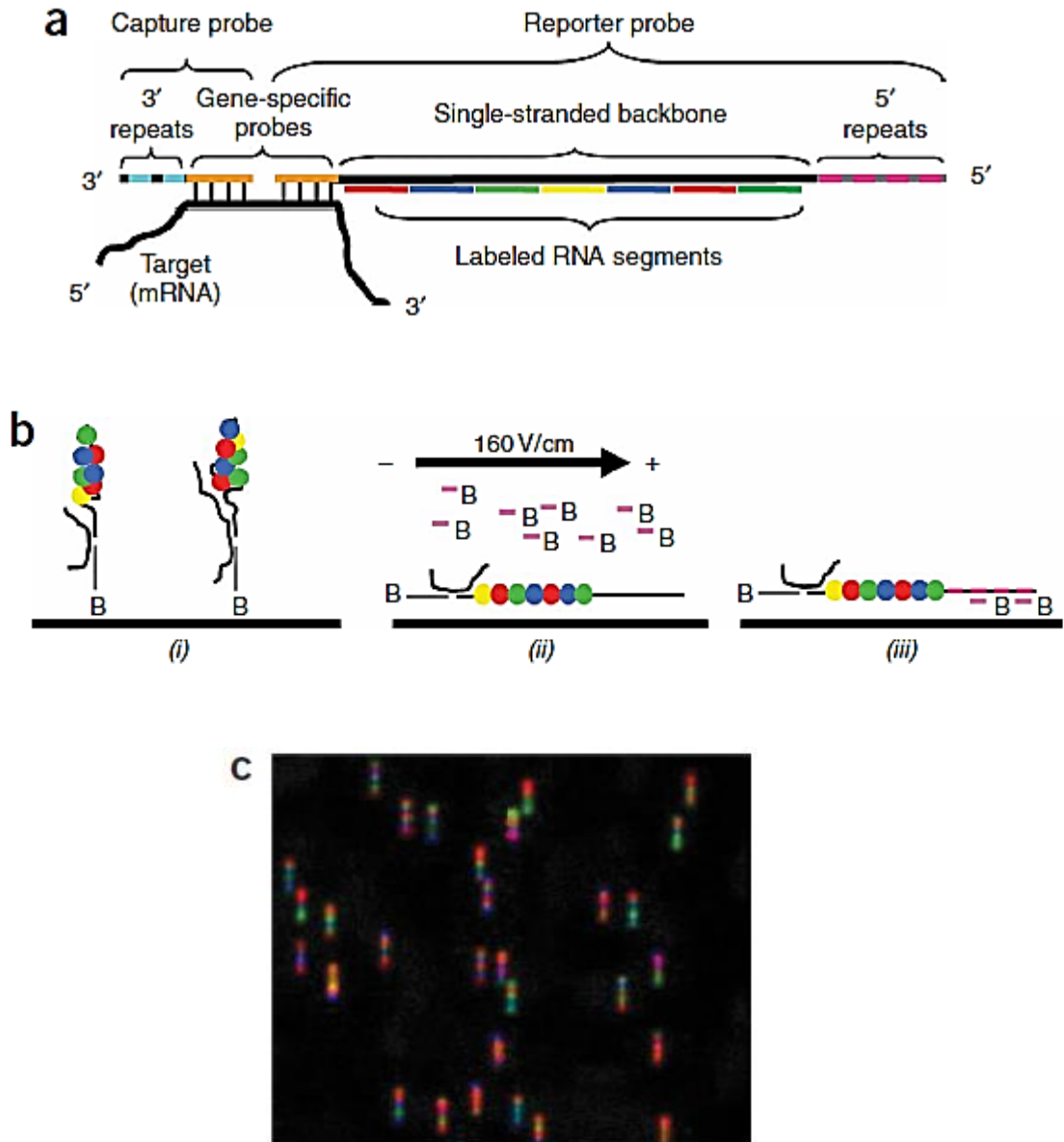


Figure 39. Overview of NanoString nCounter gene expression system.

(a) A schematic representation of the hybridized complex (not to scale). The capture probe and reporter probe hybridize to a complementary target mRNA in solution via the gene-specific sequences. After hybridization, the tripartite molecule is affinity-purified first by the 3'-repeat sequence and then by the 5'-repeat sequence to remove excess reporter and capture probes, respectively. (b) Schematic representation of binding, electrophoresis, and immobilization. (i) The purified complexes are attached to a streptavidin-coated slide via biotinylated capture probes. (ii) Voltage is applied to elongate and align the molecules. Biotinylated anti-5' oligonucleotides that hybridize to the 5'-repeat sequence are added. (iii) The stretched reporters are immobilized by the binding of the anti-5' oligonucleotides to the slide surface via the biotin. Voltage is turned off and the immobilized reporters are prepared for imaging and counting. (c) False-color image of immobilized reporter probes. Source: Geiss et al., 2008.

Table 6. Genes of interest for Nanostring analysis in MRC-5 fibroblasts treated with or without SFN at passage 4.

Gene list for time course of expression analysis in response to sulforaphane
Codeset design included in Appendix A.

	Name	Symbol
Anti-glycation related genes	Aldoketo reductase 1C1	AKR1C1
	Glyoxalase 1	GLO1
Anti-oxidant related genes	Catalase	CAT
	γ -Glu-cys ligase-catalytic subunit	GCLC
	γ -Glu-cys ligase-modulatory subunit	GCLM
	Quinone reductase	NQO1
	Thioredoxin reductase-1	TXNRD1
	Thioredoxin	TXN
	Glutathione reductase	GSR
	Heme oxygenase	HMOX1
	Superoxide dismutase-1	SOD1
	Peroxiredoxin-1	PRDX1
	Glutathione peroxidase-1	GPX1
Ferritin	FTH1	
Phase II conjugation genes	Glutathione transferase P1	GSTP1
	Multidrug resistance-associated protein 2	Mrp2
Pentose phosphate pathway and glycolysis regulation	Transaldolase	TALDO1
	Transketolase	TKT
	Glucose-6-phosphate dehydrogenase	G6PD
Lipogenesis related genes	6-Phosphofructo-2-kinase/fructose-2,6-bisphosphatase-4	PFKFB4
	Sterol response element binding protein-1	SREBF1
Nrf2 regulation related genes	Fatty acid synthase	FASN
	Nrf2	NFE2L2
Proteasome and autophagy genes	Keap1 (inrf2)	KEAP1
	Maf protein-G	MAFG
	Fyn kinase	FYN
	Proteasome subunit A1	PSMA1
Inflammatory and immune response genes	Proteasome subunit B5	PSMB5
	Sequestosome 1	SQSTM1
	Monocyte chemotactic protein-1/Chemokine (C-C motif) ligand 2	CCL2
	GRO-alpha oncogene/Chemokine (C-X-C motif) ligand 1	CXCL1
	Interleukin-15	IL15
	Interleukin 1-beta	IL1B
	Toll-like receptor 4	TLR4
	Transcription factor p65	NFKB3
	Nuclear factor NF-kappa-B p105 subunit/p50	NFKB1
	Intracellular adhesion molecule-1	ICAM1
Matrix regulating genes	Stromelysin-1/matrix metalloproteinase-3	MMP3
	Collagenase-3/matrix	MMP13

	metalloproteinase-13	
	Mitochondrial superoxide dismutase	SOD2
	Elastin	ELN
Lysosome regulating gene	Cathepsin O	CTSO
Plasminogen activator inhibitor genes	Plasminogen activator inhibitor-1	SERPINE1
	Plasminogen activator inhibitor-2	SERPINB2
Senescence-associated genes	Senescence-associated beta-galactosidase	GLB1
	Cyclin-dependent kinase inhibitor 2A/P16INK4a	CDKN2A
	Cyclin-dependent kinase inhibitor 1/p21	CDKN1A
Reference genes	Beta Actin	ACTB
	Clathrin, heavy chain	CLTC
	Beta-glucuronidase	GUSB

Table 7. Genes of interest for Nanostring analysis analysis in MRC-5 fibroblasts treated with or without SFN or HESP at passage 3 and 11.

Gene list for early and late passage expression analysis in response to sulforaphane and hesperetin. Codeset design included in Appendix B.

Name	Symbol
Anti-glycation related genes	
Aldoketo reductase 1C1	AKR1C1
Glyoxalase 1	GLO1
Anti-oxidant related genes	
Catalase	CAT
Gamma-glu-cys ligase-catalytic subunit	GCLC
Gamma-glu-cys ligase-modulatory subunit	GCLM
Quinone reductase	NQO1
Thioredoxin reductase-1	TXNRD1
Thioredoxin	TXN
Glutathione reductase	GSR
Heme oxygenase	HMOX1
Superoxide dismutase-1	SOD1
Peroxiredoxin-1	PRDX1
Glutathione peroxidase-1	GPX1
Ferritin	FTH1
Phase II conjugation genes	
Glutathione transferase P1	GSTP1
Glutathione conjugate transporter (ABCC2)	Mrp2/UGT1A1
UDP glucuronosyltransferase 1	A1
Pentophosphate pathway genes	
Transaldolase	TALDO1
Transketolase	TKT
Glucose-6-phosphate dehydrogenase	G6PD
Lipogenesis related genes	
Sterol response element binding protein-1	SREBF1
Fatty acid synthase	FASN
Nutrient sensing	
6-Phosphofructo-2-kinase/fructose-2,6-bisphosphatase-2	PFKFB2
Thioredoxin interacting protein (Thioredoxin-Binding Protein 2)	TXNIP
MondoA (MLX interacting protein)	MLXIP
Max-Like BHLHZip Protein2	MLX
HIF1- α	HIF1A
Hexokinase-1	HK1
Nrf2 regulation related genes	
Nrf2	NFE2L2
Keap1 (inrf2)	KEAP1
Maf protein-G	MAFG
Proteasome subunits genes (protein turnover)	

	Proteasome subunit A1	PSMA1
	Proteasome subunit B5	PSMB5
	Sequestosome 1	SQSTM1
Inflammatory and immune response genes		
	Monocyte chemoattractant protein-1/Chemokine (C-C motif) ligand 2	CCL2
	Toll-like receptor 4	TLR4
	Transcription factor p65	NFKB3
	Nuclear factor NF-kappa-B p105 subunit/p50	NFKB1
	Intracellular adhesion molecule-1	ICAM1
Extracellular matrix		
	Collagen 1-alpha	COL1A1
Matrix regulating genes		
	Fibroblast collagenase/matrix metalloproteinase-1	MMP1
	Stromelysin-1/matrix metalloproteinase-3	MMP3
	Collagenase-3/matrix metalloproteinase-13	MMP13
	Mitochondrial superoxide dismutase	SOD2
	Elastin	ELN
Plasminogen activator inhibitor genes		
	Plasminogen activator inhibitor-2	SERPIN2
Senescence-associated genes		
	Senescence-associated beta-galactosidase	GLB1
	Cyclin-dependent kinase inhibitor 1/p21	CDKN1A
Reference genes		
	Beta Actin	ACTB
	Clathrin, heavy chain	CLTC
	Beta-glucuronidase	GUSB

3.3.5 Glycation, oxidation and nitration of cellular protein

Protein damage by glycation, oxidation and nitration in MRC-5 cells *in vitro* cultures was assessed by measuring the glycation, oxidation and nitration adduct residues of cell protein and also glycation, oxidation and nitration free adducts (glycated, oxidised and nitrated amino acids) released into the culture medium. The latter also contain contributions from glycation, oxidation and nitration of amino acids in the culture medium. Protein glycation, oxidation and nitration adducts were assayed by stable isotopic dilution analysis liquid chromatography with tandem mass spectrometric detection (LC-MS/MS) . Analytes determined were: the major early glycation adduct N ϵ fructosyllysine (FL); advanced glycation endproducts (AGEs) - the major quantitative advanced glycation endproduct (AGE) methylglyoxal-derived hydroimidazolone (MG-H1) and others; the oxidation marker methionine sulfoxide (MetSO), protein carbonyls - α -amino adipic semialdehyde (AASA) and glutamic semialdehyde (GSA), and others; and the protein nitration marker nitrotyrosine (NT) - Figure 40.

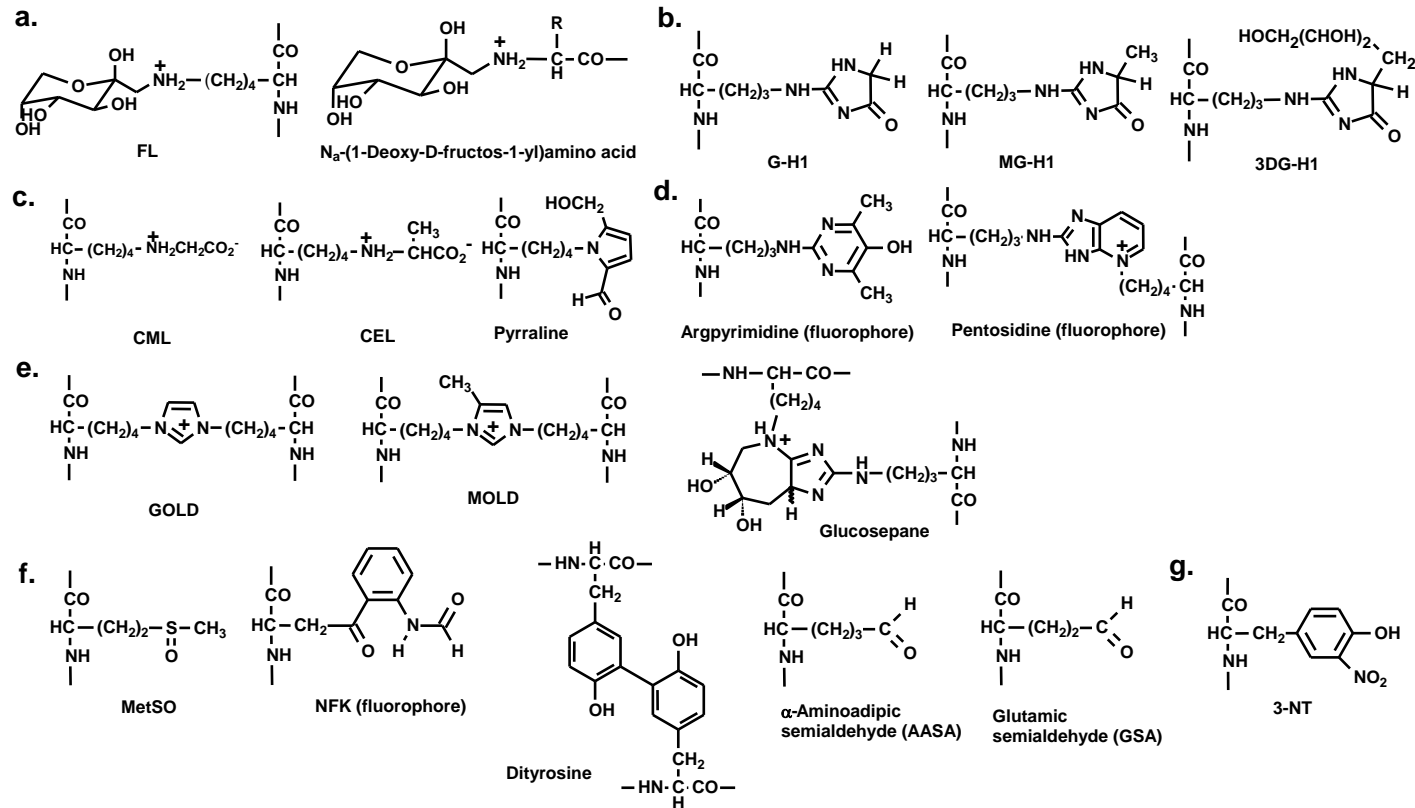


Figure 40. Protein glycation, oxidation and nitration adduct residues in physiological systems.

a. Early glycation adducts – FL and N_{α} -(1-deoxy-D-fructos-1-yl)amino acid residues. Advanced glycation endproducts: **b.** Hydroimidazolones, **c.** Monolysyl **d.** Fluorophores, AGEs, **e.** Non-fluorescent crosslinks, **f.** Oxidation adducts, and **g.** Nitration adduct. Protein glycation, oxidation and nitration adduct residues are shown. For the corresponding free adducts at physiological pH, the N-terminal amino group is protonated $-\text{NH}_3^+$ and the C-terminal carbonyl is a carboxylate $-\text{CO}_2^-$ moiety. Source: Rabbani et al., 2014.

In addition, increased expression of transglutaminase is also implicated in fibroblast senescence (Kim et al., 2001; Dellorco et al., 1985) with expected increased formation of increased Nε(γ-glutamyl)lysine (GEEK) – Figure 41, although protein content of GEEK has not been reported.

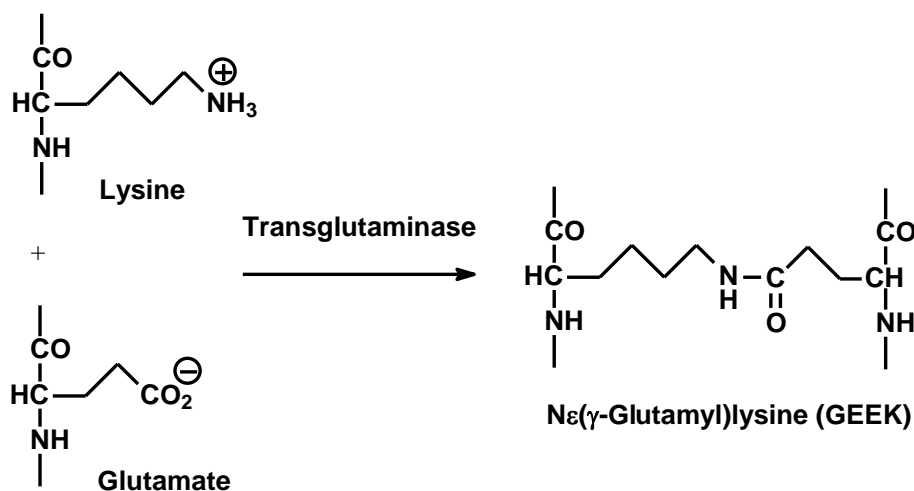


Figure 41. Formation of Nε(γ-glutamyl)lysine (GEEK).

3.3.5.1 Sample preparation: MRC-5 cell protein for adduct residues

MRC-5 Cells (*ca.* 1 x 10⁶) were washed thrice with ice-cold PBS, re-suspended in 10 mM sodium phosphate buffer, pH 7.4 (100 μl), sonicated (100 W, 30 s) and then centrifuged (20,000g, 30 min, 4 °C). The supernatant containing cytosolic protein was washed over 10 kDa cut-off membrane filters, using ice-cold argon purged water by 4 cycles of dilution to 500 μl and concentration to 50 μl by microspin ultrafiltration (10,000g, 1 h, 4 °C). The protein content was assayed by the Bradford method and 100 μg used for exhaustive enzymatic hydrolysis.

Cytosolic protein (100 μg diluted to 25 μl with water) were washed in a glass vial (2 ml vial with 200 μl glass insert). Samples and enzyme reagents were flushed with argon by 3 cycles of applying vacuum (32 mmHg, 1 min, 18 °C) and re-gassing with argon in a centrifugal evaporator. Argon-gassed samples were placed in a robotic processor (PAL HTS9, CTC Analytics, Switzerland) for automated enzymatic hydrolysis. The processor is programmed to perform series of additions as follows:

- a. **Additions 1:** 100 mM HCl (10 μ l), pepsin solution (2 mg/ml in 20 mM HCl; 5 μ l) and thymol solution (2 mg/ml in 20 mM HCl; 5 μ l). The samples were then incubated at 37°C for 24 h.
- b. **Additions 2 (order critical):** 100 mM $\text{KH}_2\text{PO}_4/\text{K}_2\text{HPO}_4$ buffer, pH 7.4 (12.5 μ l); 260 mM KOH (5 μ l). Pronase E solution (2 mg/ml in 10 mM $\text{KH}_2\text{PO}_4/\text{K}_2\text{HPO}_4$ buffer, pH 7.4; 5 μ l) and penicillin-streptomycin solution (1000 U/ml and 1 mg/ml, respectively; 5 μ l). The samples were then incubated at 37°C for 24 h.
- c. **Additions 3:** aminopeptidase solution (2 mg/ml in 10 mM $\text{KH}_2\text{PO}_4/\text{K}_2\text{HPO}_4$ buffer, pH 7.4; 5 μ l) and prolidase solution (2 mg/ml in 10 mM $\text{KH}_2\text{PO}_4/\text{K}_2\text{HPO}_4$ buffer, pH 7.4; 5 μ l). Samples were then incubated at 37°C for 48 h. The final enzymatic hydrolysate (77.5 μ l) is ready for LC-MS/MS analysis.

3.3.5.2 *Sample preparation: culture medium for free adducts*

An aliquot of culture medium (100 μ l), baseline medium and end of passage conditioned medium, was used to prepare ultrafiltrate with a 3 kDa cut-off microspin ultrafilter. An aliquot of the resulting ultrafiltrate (25 μ l) was mixed with 25 μ l of stable isotopic internal standard mixture. An aliquot (50-100 μ l) is filtered by microspin ultrafiltration (10 kDa cut-off, 4 °C). Ultrafiltrate was retained for free adduct analysis. Plasma protein was diluted 5-fold with water and washed by 4 cycles of concentration to 50 μ l and dilution to 500 μ l with ice cold argon purged water over a microspin ultrafilter (10 kDa cut-off) at 4 °C.

3.3.5.3 *LC-MS/MS analysis*

Detection of analytes was performed by LC-MS/MS in electrospray-positive ionization multiple reaction monitoring (MRM) mode. Quantification was performed using stable isotopic dilution analysis. LC-MS/MS was performed using a Waters AcquityTM ultra high performance liquid chromatography (UPLC) system with a Quattro Premier XE tandem mass spectrometer. Chromatography was performed with two Hypercarb columns in series: column 1, 2.1 x 50 mm, 5 μ m particle size; and column 2, 2.1 x 250 mm 5 μ m particle size. The mobile

phase was made of two solvents: Solvent A (0.1% TFA in water) and Solvent B (0.1% TFA in 50% acetonitrile (MeCN)). Solvent A (0.1% TFA in water) and solvent B (0.1% TFA in 50% tetrahydrofuran (THF)) were used for post-run washing. Both solvents were used for 37.5 min and their gradient is shown in Table 8 as well as the column switching programme in Table 9.

Table 8. Gradient table for protein damage analytes detection on LC-MS/MS.

Time (min)	Flow rate (ml/min)	Solvent A 1	Solvent B1 (%)	Solvent B2	Comment
0	0.2	100	0	0	Multi-step linear gradient with column switching. Data collection period: 4 – 35 min.
5	0.2	100	0	0	
8	0.2	97	3	0	
12	0.2	97	3	0	
24	0.2	40	60	0	
24	0.2	97	3	0	
26	0.2	3	0	0	
27	0.2	50	50	0	
35	0.2	50	50	0	
35	0.4	0	0	100	
45	0.4	0	0	100	
45	0.2	100	0	0	Column re-equilibration
57.5	0.2	100	0	0	
57.5	0.4	100	0	0	
72.5	0.4	100	0	0	

Table 9. Column switching programme for protein damage analytes detection on LC-MS/MS.

Time (min)	Columns in-line	Comment
0	1 + 2	Elution of analytes retained only by column 1 and 2 in series
10	1 + 2	
10	1	Elution of analytes retained strongly by only column 1
26	1	
26	1 + 2	Elution of analytes trapped on column 2 during prior column switching
35	1 + 2	
35	1	Washing of column 1
45	1	
45	1 + 2	Washing of action column 2 and re-equilibration
72.5	1 + 2	

Flow from the Column was directed to the MS/MS detector at 4 to 35 min. The ionisation source temperature and desolvation temperatures were set at 120°C and 350°C respectively. The cone gas and desolvation gas flow was set as 99 L/h and 901 L/h. Table 10 shows the optimised molecular ion and fragment ion masses and collision energies for MRM. Typical calibration curves for AGEs is shown in Figure 42.

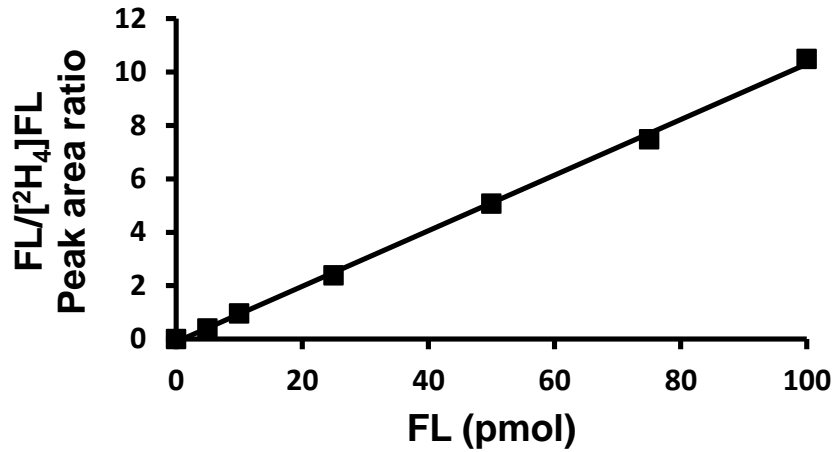
Table 10. Mass spectrometric multiple reaction monitoring detection of protein oxidation and glycation adducts.

Analyte group	Analyte	Rt (min)	Parent ion (Da)	Fragment ion (Da)	CE (eV)	Neutral fragment loss(es)	Isotopic standard
Amino acids							
	Arg	29.2	175.2	70.3	15	H ₂ CO ₂ , NH ₂ C(=NH)NH ₂	[¹⁵ N ₂]arg
	Lys	5.5	147.1	84.3	15	H ₂ CO ₂ , NH ₃	[¹³ C ₆]lys
	Met	29.5	150.0	104.2	11	H ₂ CO ₂	[² H ₃]met
	Tyr	18.3	182.1	136.2	13	H ₂ CO ₂	[² H ₄]tyr
	Trp	23.5	205.0	159.1	15	H ₂ CO ₂	[¹⁵ N ₂]trp
	Val	8.6	117.8	72.0	19	H ₂ CO ₂	[² H ₈]val
Early-stage glycation adduct							
Fructosamines	FL	28.5	291.0	84.3	31	H ₂ CO ₂ , fructosylamine	[² H ₄]FL
AGEs							
Hydroimidazolones [†]	G-H1	12.4	215.0	100.2	14	NH ₂ CH(CO ₂ H)CH ₂ CH=CH ₂	[¹⁵ N ₂]G-H1
	MG-H1	11.6 & 12.5	229.2	114.3	14	NH ₂ CH(CO ₂ H)CH ₂ CH=CH ₂	[¹⁵ N ₂]MG-H1
	3DG-H	11.2, 12.6 & 13.5	319.1	114.8	20	NH ₂ CH(CO ₂ H)CH ₂ CH=CH ₂	[¹⁵ N ₂]3DG-H
Monolysyl AGEs	CEL	28.8	219.2	130.1	13	NH ₂ CH(CH ₃)CO ₂ H	[¹³ C ₆]CEL
	CML	28.5	204.9	130.1	12	NH ₂ CH ₂ CO ₂ H	[¹³ C ₆]CML
	Pyrraline	17.9	255.2	84.3	23	2-CHO-5-HOCH ₂ -pyrrole, H ₂ CO ₂	[¹³ C ₆ , ² N ₂]Pyrraline
Fluorescent AGEs	Argpyrimidine	17.7	255.3	140.3	17	NH ₂ CH(CO ₂ H)CH ₂ CH=CH ₂	[¹⁵ N ₂]argpyrimidine
	Pentosidine [‡]	21.1	379.3	250.4	22	NH ₂ CH(CO ₂ H)CH ₂ CH ₂ CH=CH ₂	[¹³ C ₆]pentosidine
Non-fluorescent crosslinks	MOLD	14.0	341.2	212.3	21	NH ₂ CH(CO ₂ H)CH ₂ CH ₂ CH=CH ₂	[² H ₈]MOLD
	Glucosepane	16.5	429.2	382.1	38	C ₂ H ₅ O	[¹³ C ₆] Glucosepane
Other	CMA	12.1	233.0	70.1	27	H ₂ CO ₂ , NH ₂ C(=NH)NHCH ₂ CO ₂ H	[¹³ C ₂]CMA
	Orn	5.2	133.1	70.1	9	H ₂ CO ₂ , NH ₃	[² H ₆]orn

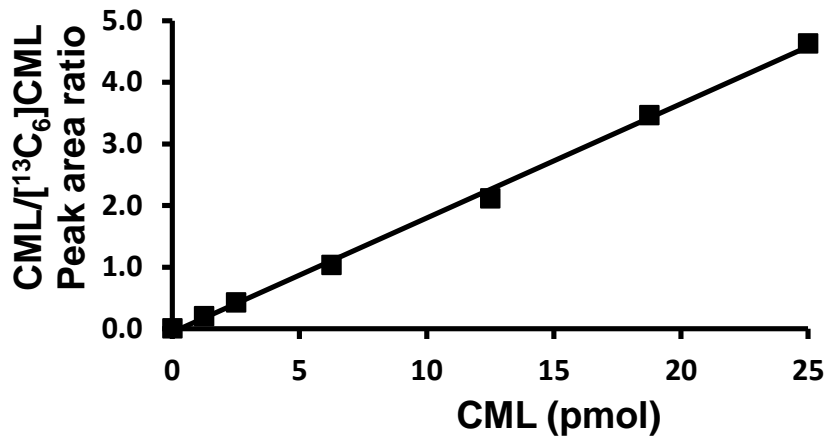
Table 10. (cont.)

Analyte group	Analyte	Rt (min)	Parent ion (Da)	Fragment ion (Da)	CE (eV)	Neutral fragment loss(es)	Isotopic standard
Oxidative damage							
Met oxidation	MetSO	8.7	166.1	102.2	14	CH ₃ -SOH	[² H ₃]MetSO
Tyr oxidation	Dityrosine	19.9	361.2	315.3	15	H ₂ CO ₂	[² H ₆]DT
Tyr oxidation	NFK	21.5	235.8	191.2	18	H ₂ CO ₂	[¹⁵ N ₂]NFK
Lys oxidation	AASA	10.7	128.0	82.0	15	H ₂ CO ₂	AAA (Rt = 29.4)
Arg & Pro oxidation	GSA	32.2	114.0	68.0	15	H ₂ CO ₂	AAA
Nitration damage							
Tyrosine nitration	3-NT	23.2	227.1	181.2	13	H ₂ CO ₂	[² H ₃]3-NT

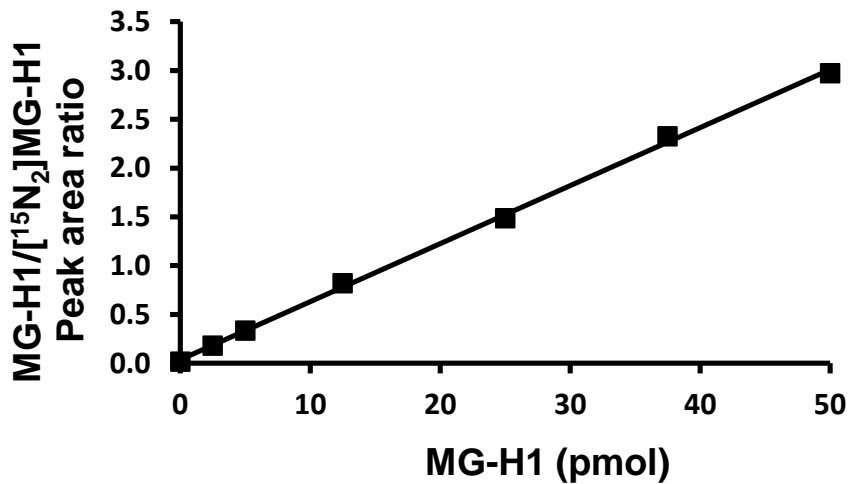
†For hydroimidazolones, R_t values for the 2 epimers if MG-H1 are given and of the 3 structural isomers of 3DG-H, 3DG-H1, 3DG-H2 and 3DG-H3 are all detected.. ‡ Pentosidine is detected to higher sensitivity by in-line fluorimetry, excitation wavelength 320 nm, emission wavelength 365 nm. From: Thornalley, P. J. *et al.* Quantitative screening of advanced glycation endproducts in cellular and extracellular proteins by tandem mass spectrometry. Source: Rabbani et al., 2014.



(a)



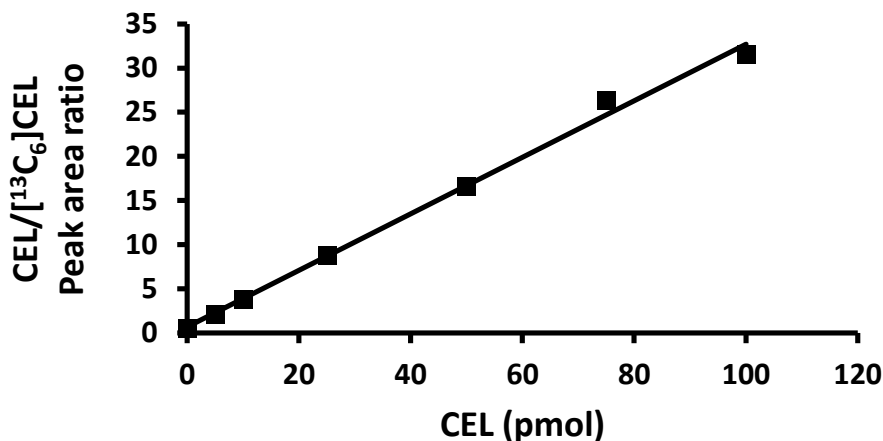
(b)



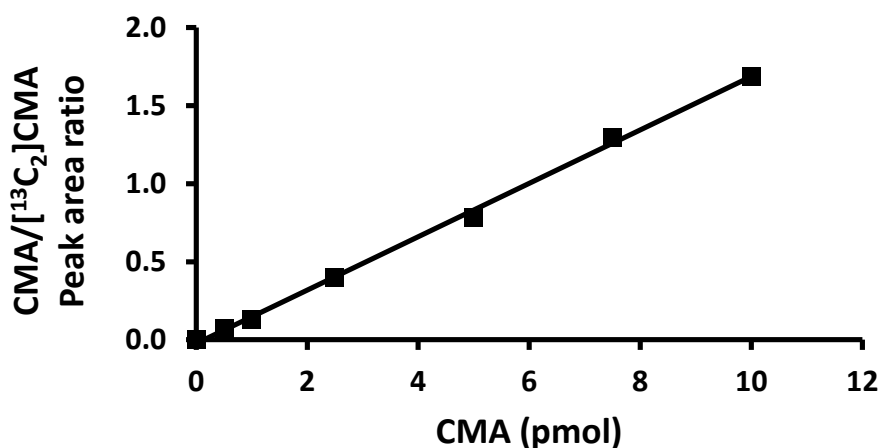
(c)

Figure 42. Typical calibration curves for glycation adducts – AGEs.

(a) Calibration curve for FL. Linear regression equation: FL/[²H₄]FL peak area ratio = $(0.104 \pm 0.002) \times \text{FL (pmol)}$; $R^2 = 0.999$ ($n = 7$). (b) Calibration curve for CML. Linear regression equation: CML/[¹³C₆]CML peak area ratio = $(0.185 \pm 0.004) \times \text{CML (pmol)}$; $R^2 = 0.998$ ($n = 7$). (c) Calibration curve for MG-H1. Linear regression equation: MG-H1/[¹⁵N₂]MG-H1 peak area ratio = $(0.0594 \pm 0.0009) \times \text{MG-H1 (pmol)}$; $R^2 = 0.999$ ($n = 7$).



(d)



(e)

Figure 42. Typical calibration curves for glycation adducts – AGEs (cont²).

(d) Calibration curve for CEL. Linear regression equation: $\text{CEL}/[^{13}\text{C}_6]\text{CEL}$ peak area ratio = $(0.320 \pm 0.010) \times \text{CEL (pmol)}$; $R^2 = 0.996$ ($n = 7$). (e) Calibration curve for CMA. Linear regression equation: $\text{CMA}/[^{13}\text{C}_2]\text{CMA}$ peak area ratio = $(0.171 \pm 0.003) \times \text{CMA (pmol)}$; $R^2 = 0.998$ ($n = 7$).

3.3.5.4 Measurements of protein glycation, oxidation and nitration adduct residues - correction for autohydrolysis in exhaustive enzymatic hydrolysis

In the analysis of protein glycation, oxidation and nitration adduct residues of cell protein, a robust basis for correction of the contribution to protein glycation, oxidation and nitration adducts by autohydrolysis of proteases is required. Hydrolysis in protein free blanks overestimates this contribution since autohydrolysis of proteases is faster when no protein substrate is present. An initial strategy employed was correction from digestion of a polypeptide that could not contain protein glycation, oxidation and nitration adduct residues – such as polythreonine. This only presents the proteases with one type of peptide bond,

however – different from all other samples. The current method uses triplicate digests of zero protein blanks and a known amount of human serum albumin (HSA) and quantitation of an amino acid that is not modified – valine. In the HSA digests the amount of valine detected is that from HSA + autohydrolysis of proteases ($V_{\text{HSA}} + V_{\text{Proteases (Protein)}}$). In the zero protein blanks the valine detected is only from autohydrolysis ($V_{\text{Proteases (Blank)}}$). The valine liberated from proteases in the presence of HSA is decreased by the suppression of autohydrolysis by presence of HSA. The factor $V_{\text{Proteases (Protein)}} / V_{\text{Proteases (Blank)}}$, typically *ca.* 0.7, is applied to the amount of protein glycation, oxidation and nitration adduct quantified in the blank to produce corrections applied to digests of sample protein. That is, the presence of protein substrate slows autohydrolysis of proteases by *ca.* 30%. This correction factor is determined for each samples batch for enzymatic hydrolysis samples.

3.3.6 Analysis of N ϵ -(γ -L-glutamyl)-L-lysine (GEEK)

Analysis of GEEK samples was done by LC-MS/MS using an AcquityTM UPLC system with a Xevo-TQS Quattro tandem mass spectrometer. Samples were prepared as described in section 3.3.5.1 and 3.3.5.2. Standards were prepared as shown in Table 11. – Figure 43 shows a typical calibration curve.

Table 11. Calibration standard-cocktail of stock solution for GEEK analysis.

Calibration no	GEEK	[¹³ C ₅] GEEK
Amount (pmol)		
0	0	10
1	20	10
2	40	10
3	80	10
4	120	10
5	160	10
6	200	10

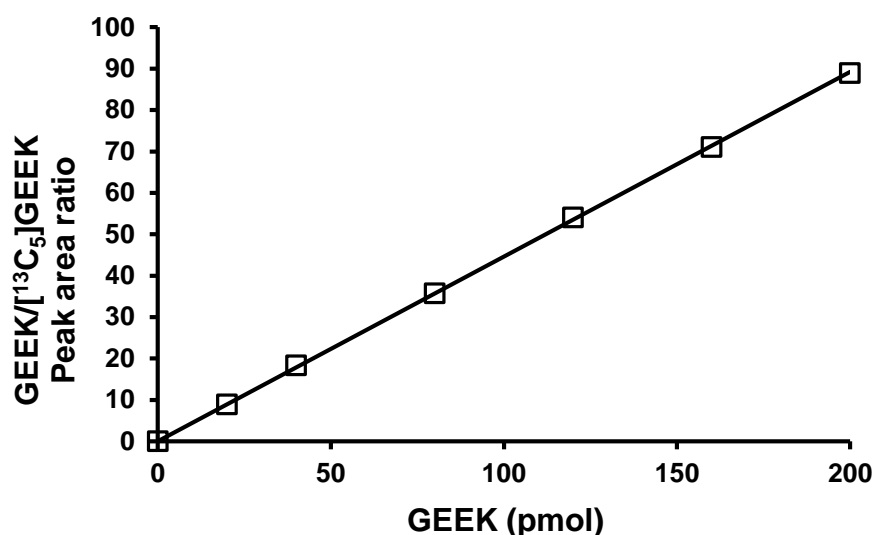


Figure 43. A typical calibration curve for glutamyl lysine.

Linear regression equation: $\text{GEEK}/[^{13}\text{C}_5]\text{GEEK peak area ratio} = (0.446 \pm 0.002) \times \text{GEEK (pmol)}$; $R^2 = 0.999$ ($n = 7$).

A 3 μm particle size Hypercarb columns were used 150 x 2.1 mm. The mobile phase solvent A: 0.1% TFA and 3.75% acetonitrile (CAN) in water and solvent B: 0.1% TFA in 50% THF in water. The gradient is shown in 12. Electrospray positive ionisation mass spectrometric multiple reaction monitoring (MRM) was used to detect all protein damage analytes. The ionisation source temperature and desolvation temperature were 120°C and 350°C, respectively. The cone gas and desolvation gas flow were 96 L/h and 900 L/h, respectively. Optimised molecular ion and fragment ion masses and collision energies for MRM detection are given in Table 13. Masslynx was used to integrate the peaks and GEEK was normalised to lysine.

Table 12. Gradient table for N ϵ -(γ -L-glutamyl)-L-lysine detection on LC-MS/MS.

Time (min)	Flow Rate (ml/min)	Solvent A (%)	Solvent B (%)	Gradient
0	0.2	100	0	
5	0.2	100	0	Isocratic
15	0.2	100	0	Isocratic
35	0.2	0	100	Isocratic
40	0.2	100	0	Isocratic
55	0.4	100	0	Isocratic

Table 13. Mass-spectrometric multiple reaction monitoring detection of Nε-(γ-L-glutamyl)-L-lysine.

Analyte	Rt (min)	Precursor (Da)	Fragment (Da)	CV (V)	CE (eV)
GEEK	9.9	276.1	147.1	32	12
[¹³ C ₅] GEEK	9.9	281.1	147.1	32	12
Lys	5.6	147.1	84.1	20	18
[¹³ C ₆] Lys	5.6	153.1	89.1	20	18

3.3.7 Nucleotide oxidation and glycation

Markers of glycation of DNA by glyoxal and methylglyoxal - 3-(2'-deoxyribose)-6,7-dihydro-6,7-dihydroxyimidazo-[2,3-b]purine-9(8)one (GdG) and 3-(2'-deoxyribose)-6,7-dihydro-6,7-dihydroxy-6/7-methylimidazo-[2,3-b]purine-9(8)one (MGdG) respectively, and DNA oxidation - 7,8-dihydro-8-oxo-2'-deoxyguanosine (Figure 44) - were measured by quantifying the increased concentration of glycated and oxidised nucleosides in the cell culture medium during a passage. Ultrafiltrates of baseline and end of passage conditioned culture medium were prepared by microspin ultrafiltration of medium (3 kDa cut-off, 100 µl), collecting ca. 50 µl ultrafiltrate. For LC-MS/MS, ultrafiltrates (40 µl) were spiked with 10 µl isotopic standard mixture containing: 0.1 nmol [¹³C₁₀,¹⁵N₅]dG, 1 pmol [¹³C₁₀,¹⁵N₅]8-OxodG, 0.73 pmol [¹³C₁₀,¹⁵N₅]MGdG, 0.09 pmol [¹³C₁₀,¹⁵N₅]CEdG and 1.4 pmol [¹³C₁₀,¹⁵N₅]GdG. LC-MS/MS was performed using an Acquity™ UPLC-Quattro Premier tandem mass spectrometer with a BEH C18 1.7 µm particle size, 2.1 x 100 mm column. The mobile phase was 0.1% formic acid with a linear gradient of 0 - 10% acetonitrile from 2 - 10 min and isocratic 10% acetonitrile from 10 -15 min; the flow rate was 0.25 ml/min. After analysis, the column was washed with 50% acetonitrile containing 0.1% formic acid for 10 min and thereafter re-equilibrated with initial mobile phase for 10 min. The column temperature was 10 °C. For GdG, MGdG and 8-OxodG, limits of detection were 0.8, 2.5 and 0.7 fmol; analytical recoveries were 104, 97 and 99%, respectively, and coefficients of variation 2 - 7%. Detection of imidazopurinones and related deoxyguanosine-derived adducts by liquid

chromatography-tandem mass spectrometry multiple reaction monitoring is shown in Table 14.

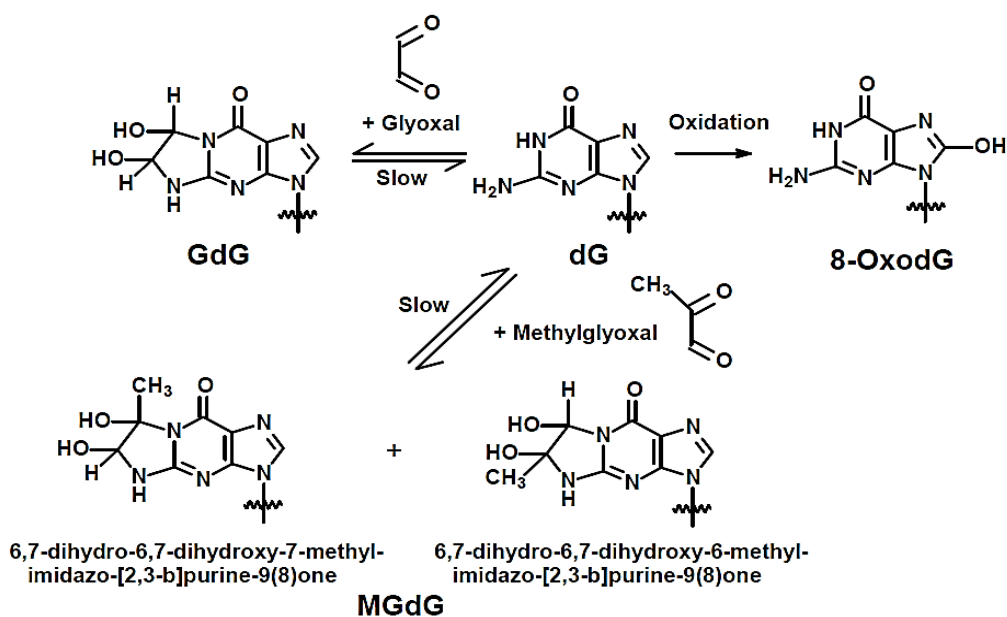


Figure 44. The conversion of GdG into dG and MGdG.

Source: (Lampe, 2009)(Lampe, 2009)(Herr and Buchler, 2010).

Table 14. Detection of imidazopurinones and related deoxyguanosine-derived adducts by liquid chromatography-tandem mass spectrometry multiple reaction monitoring.

Analyte	R _t (min)	Molecular>fragment ion transition (Da)	Collision energy (eV)	Cone voltage (V)
dG	7.3	268.1 > 152.0	37	12
GdG	6.7	325.7 > 209.9	12	12
MGdG†	7.4, 7.8 and 8.4	340.0 > 224.0	12	11
8-OxidG	8.4	283.8 > 168.0	12	12

The neutral fragment loss was 2-dehydro-2-deoxyribose. † Multiple retention times are shown for adduct structural and stereoisomers isomers.

3.3.8 Dicarbonyls analysis

Dicarbonyl metabolites glyoxal, methylglyoxal and 3-deoxyglucosone (3-DG) were assayed by derivatisation with 1,2-diaminobenzene and quantitation of the resulting quinoxaline adducts by stable isotopic dilution analysis LC-MS/MS (Kurz *et al.*, 2010). Media from MRC-5 cell cultures treated with either 1 μ M SFN or vehicle (0.002% DMSO) was collected as mentioned in 3.3.5.1 and, after storage at -80°C, used for analysis.

The media was de-proteinised by addition of 10 μ l of 20% ice-cold trichloroacetic acid (TCA). Stable isotopic standards were then added (2 pmol of each of [$^{13}\text{C}_2$]glyoxal, [$^{13}\text{C}_3$]methylglyoxal and [$^{13}\text{C}_6$]3-DG), the samples mixed and then centrifuged at 10,000xg for 10 min at 4°C. An aliquot of supernatant (35 μ l) was removed and after addition of 5 μ l 3% sodium azide, 10 μ l 0.5 mM 1,2-diaminobenzene solution containing 0.5 mM diethylenetriamine penta-acetic acid (DETAPAC) and 0.2 M HCl were added. The samples were then incubated for 4 h in the dark. The assay was calibrated by concurrent derivatisation of analyte standard: 0 to 10 pmol of glyoxal, MG and 3-DG. The samples were assayed by LC-MS/MS. The column was 100 x 2.1mm, 1.7 μ m particle size BEH C18. The mobile phase contained 0.1% of trifluoroacetic acid (TFA) in water with a linear gradient of 0 to 50% of acetonitrile (MeCN) for 10 min with a 0.2 min/ml flow rate and gradient shown in Table 15.

Table 15. Gradients for the dicarbonyl assay using LC-MS/MS.

Time (min)	Flow rate (ml/min)	Solvent A (%)	Solvent B (%)	Curve
0	0.2	100.0	0.0	0
10.0	0.2	100.0	0.0	6
15.0	0.2	100.0	3.0	1
30.0	0.2	100.0	3.0	1

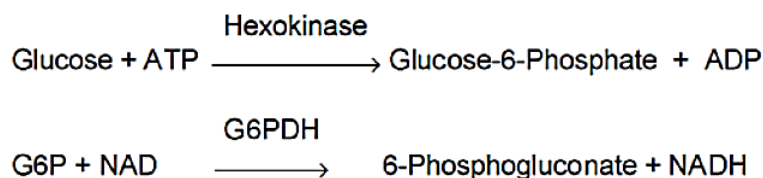
The capillary voltage used for mass spectrometric detection was of 0.6 kV and the ionisation as well as desolvation temperatures used were 120°C and 350°C respectively. The flow for the cone gas was 149 L/h and 901 L/h for desolvation gas flow. The optimised molecular ion and fragment ion masses and collision energies for MRM detection are shown in Table 16.

Table 16. Mass-spectrometric multiple reaction for detection of dicarbonyls.

Analyte	Parent ion (Da)	Fragment ion (Da)	Cone voltage (V)	Collision energy (eV)
MG	145.1	77.1	24	24
3-DG	235.5	199.0	21	15
Glyoxal	131.1	77.1	24	23

3.3.9 Assay of D-glucose

The concentration of glucose in cell culture medium at baseline and end of passage in control and SFN treatment groups was made by end-point enzymatic assay with hexokinase (HK) and glucose-6-phosphate dehydrogenase (G6PDH). The procedure is shown in Figure 45. and based on the following coupled enzymatic reaction.

**Figure 45. Coupled enzymatic assay for glucose – hexokinase method.**

The concentration of glucose is coupled to equimolar formation of NADH. The resulting concentration of NADH is determined spectrophotometrically at 340 nm. Media samples were diluted 3-fold for both treatment groups (SFN and DMSO) and 5-fold for baseline media added at the beginning of each passage. Aliquots of standard and diluted sample (25 µl) were added to wells of a clear 96-well microplate and 225 µl of the assay reagent was added. The HK-based glucose assay reagent was prepared by addition of 20 ml of water to reagent solid mix such that final concentrations of assay components were: 1.5 mM NAD, 1.0 mM ATP, 1.0 U/ml of HK and 1.0 U/ml of G6PDH. The microplate was then incubated at room temperature (18-25°C) for 15 min and absorbance measured using a FLUOstar OPTIMA microplate reader. The concentration of glucose in each sample was deduced

from the standard curve and the glucose standards prepared in the range of 0 to 1.4 mM in water (Figure 46).

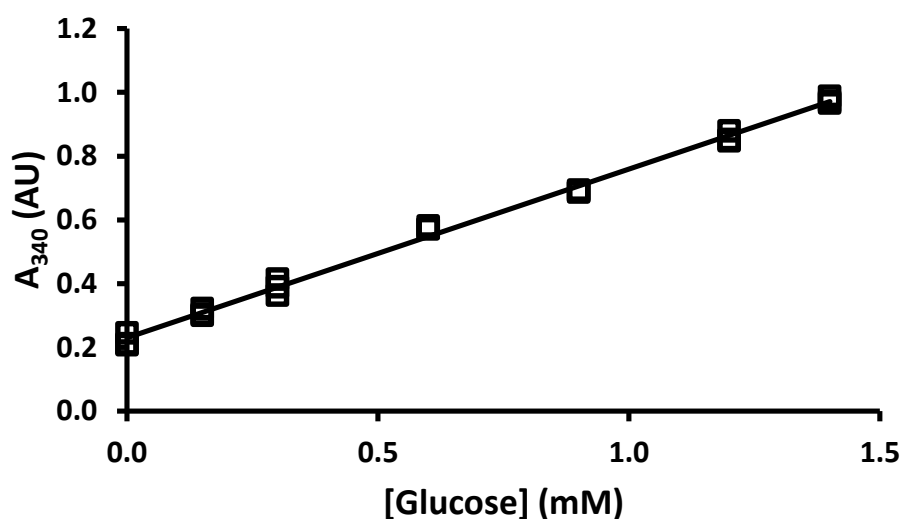


Figure 46. Typical calibration curve for D-glucose.

Linear regression equation: $A_{340} = (0.529 \pm 0.008) \times \text{D-glucose (mM)}$; $R^2 = 0.995$ ($n = 21$).

The absorbance is corrected for absorbance of reagent (reagent blank, y-axis intercept on the calibration curve) and medium (sample blank). The concentration of D-glucose was deduced from the standard curve and is given in mM. The consumption of D-glucose by MRC-5 cells during passage was calculated by subtracting the amount of D-glucose in media at the end of the passage from the amount at baseline and given as nmol/day/ 10^6 cells.

3.3.10 D-Lactate assay

The concentration of D-lactate in culture medium was determined using an end-point enzymatic assay with the enzyme D-Lactic dehydrogenase and microplate fluorimetric detection of NADH formed in the forward reaction. Wavelengths used for the detection of NADH were: excitation, 340 nm, and emission, 460 nm (McLellan et al., 1992). Hydrazine is added to remove pyruvate from the assay reaction equilibrium by formation of pyruvate hydrazone and take the forward assay reaction to completion. The formation of pyruvate by

enzymatic reaction of D-lactate with D-lactic dehydrogenase and reaction with pyruvate is shown in Figure 47.

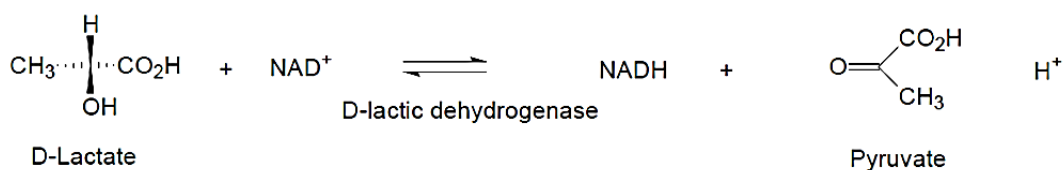


Figure 47. The formation of pyruvate from D-lactate via the enzymatic reaction with D-lactic dehydrogenase.

An aliquot of media (500 μl) was deproteinised by addition of 1.0 ml 0.6M perchloric acid (PCA), mixed well and left on ice for 10 min incubation for protein to precipitate. The precipitate was then sedimented by centrifugation (5 min, 7000g, 4 $^\circ\text{C}$). An aliquot of supernatant (700 μl) was removed and neutralised to pH 7 by addition of 230 μl 2 M potassium bicarbonate and centrifuged again (10 min, 7000g, 4 $^\circ\text{C}$) to sediment the resulting potassium perchlorate precipitate. An aliquot of the neutralised PCA extract (100 μl) was assayed for D-lactate by incubation for 4 h with 100 μl glycine hydrazine buffer (1.2 M glycine, 0.5 M hydrazine dihydrochloride, 2.5 mM DETAPAC, pH 9.2), 25 μl 4 mM NAD^+ and 25 μl 500 U/ml of D-lactic dehydrogenase. Control samples were run in parallel without the enzyme. The calibration curve for D-lactate was constructed in the range 0 - 6 nmol D-lactate (Figure 48).

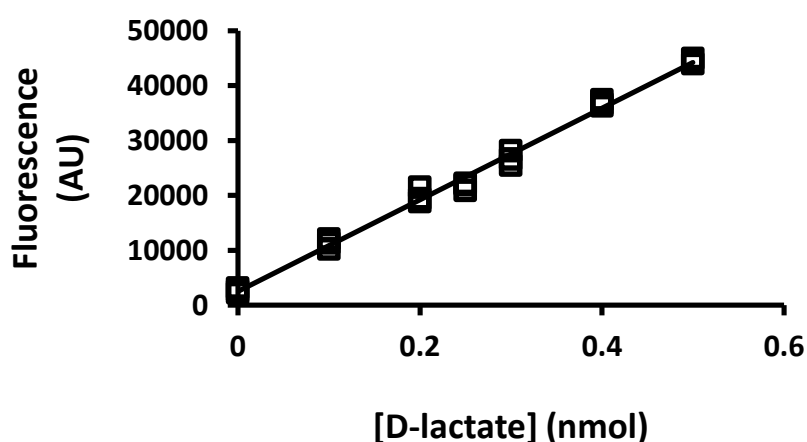


Figure 48. Typical calibration curve for D-lactate.

Linear regression equation: Fluorescence = $(83468 \pm 1779) \times \text{D-lactate (nmol)}$; $R^2 = 0.9919$ ($n = 21$).

3.3.11 L-Lactate assay

L-Lactate was assayed as described for D-lactate but instead using L-lactic dehydrogenase. The sample content of L-lactate is 50-100 folds higher than D-lactate and so media samples were diluted with water prior to assay. L-Lactate calibration standards were prepared over the range 1 - 10 nmol (Figure 49).

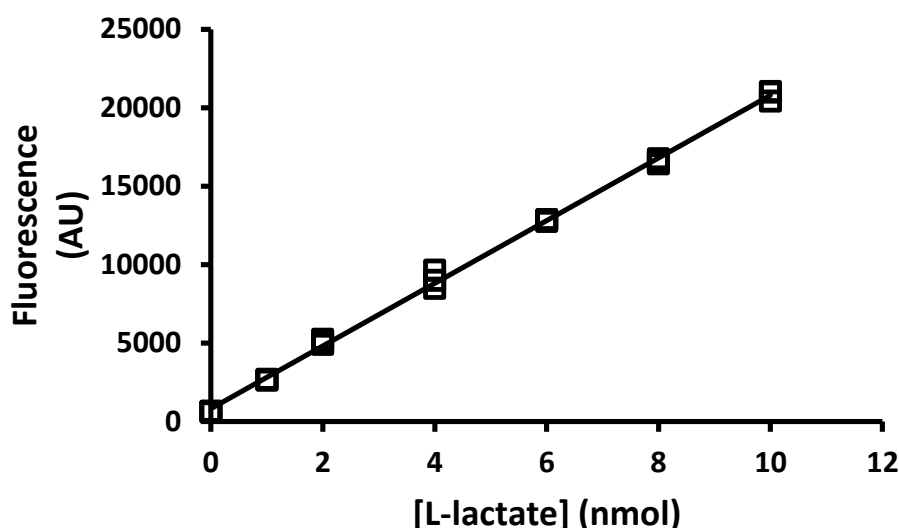


Figure 49. Typical calibration curve for L-lactate.

Linear regression equation: Fluorescence = $(1997 \pm 18) \times$ L-lactate (nmol); $R^2=0.9983$ (n=21).

Samples were prepared and assayed according to the protocol for D-lactate (section 3.3.10).

3.3.12 Assay of cellular reduced and oxidised glutathione and glyoxalase pathway intermediate S-D-lactoylglutathione

MRC-5 cells (1×10^6 cells) were washed 3 times in PBS. The cell pellet was treated with 40 μ l 10% TCA containing 0.15% NaCl and 0.25% sodium azide in water. This solution precipitates proteins and inhibits acid stable, TCA soluble peroxidase activity. Samples were centrifuged (20,000g, 30 min, 4 °C) and aliquots of supernatant (10 μ l) transferred to vials for LC-MS/MS analysis with the addition of 10 μ l isotopic standard cocktail containing 100 pmol [$^{13}\text{C}_2^{15}\text{N}_1$]GSH and 20 pmol [$^{13}\text{C}_4^{15}\text{N}_2$]GSSG. Two graphite Hypercarb HPLC columns were used in series (50 x 2.1 mm and 250 x 2.1 mm, particle size 5 μ m)

with column temperature of 30 °C. Solvents used were 0.1% TFA in water (Solvent A) and 0.1% TFA in 50:50 MeCN: water (Solvent B1) and 0.1% TFA in 50:50 Tetrahydrofuran (THF): water (Solvent B2). The gradients used during the analytical run and post run are displayed in Table 17.

Table 17. UPLC Elution profile for glutathione analysis.

Injection Run					
Time (min)	Flow rate (ml/min)	Solvent A1 (%)	Solvent B1 (%)	Solvent B2 (%)	Gradient
Initial	0.2	100	0	-	Isocratic Linear Isocratic
1	0.2	100	0	-	
15	0.2	40	60	-	
16	0.2	40	60	-	
Postrun					
0	0.4	0	-	100	Column washing
10	0.4	0	-	100	
10	0.4	100	-	0	Re-equilibration
25	0.4	100	-	0	

The eluate from the column was eluted into the electrospray source of the MS/MS detector for 4 - 16 min for data collection. Mass spectrometric analysis was performed using electrospray positive ionisation mode. For mass spectrometric detection, the capillary voltage was 3.4 kV, the ion source temperature 120 °C, the desolvation gas temperature 350 °C and cone and desolvation gas flows 146 and 550 L/h respectively. Table 18 shows the optimised MRM conditions used for detection, along with their retention times, cone voltage and collision energy. Fragmentation analysis of the MRM transitions is detailed in Figure 50.

Table 18. Optimised MRMs for glutathione analysis.

Analyte	Parent ion (Da)	Fragment ion (Da)	Retention time (min)	Cone voltage (V)	Collision energy (eV)
GSH	308.2	179.1	11.7	30	13
[¹³ C ₂ ¹⁵ N ₁]GSH	311.2	182.1	11.7	30	13
GSSG	613.2	483.7	14.4	52	18
[¹³ C ₄ ¹⁵ N ₂]GSSG	619.2	489.7	14.4	52	18
S-D-lactoylglutathione	380.2	76.2	13.1	32	35

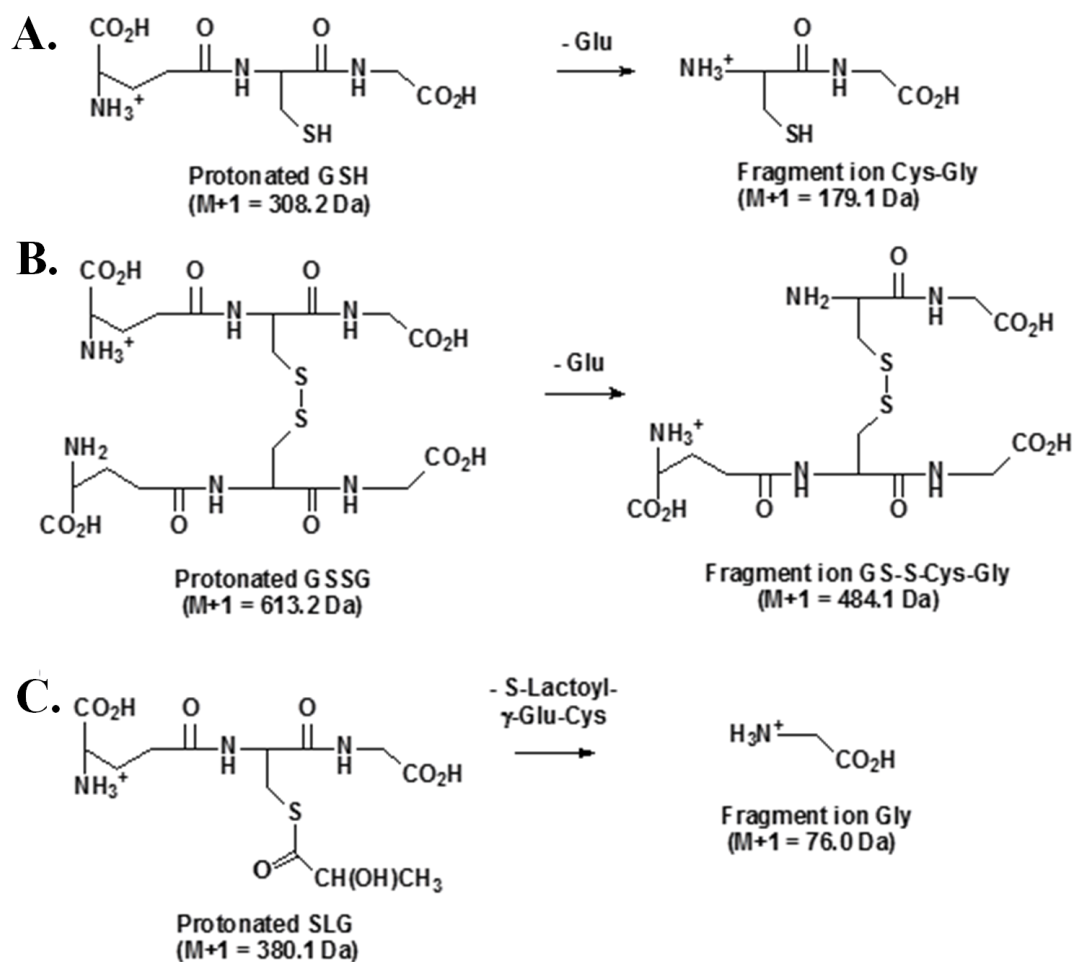


Figure 50. Fragmentation of glutathione in multiple reaction monitoring mass transitions.

A. GSH, B. GSSG and C. S-D-lactoylglutathione.

Data analysis was performed using MassLynx software. Calibration curves were constructed plotting peak area ratio of analyte/isotopic standard against analyte concentration. The amount of glutathione in assayed aliquots was deduced using the peak area ratio and the appropriate calibration curve and the amount in the original sample calculated taking account of any dilution factors.

3.3.13 Immunocytochemistry

MRC-5 fibroblasts were cultured in 4 cm glass bottomed dish (30,000 cells per dish) and incubated for 24 h under normal growth conditions. A total of 8 groups (n = 3 per group) was seeded using the conditions described in Table 19.

Table 19. Immunocytochemistry conditions.

Condition	After 24 h seeding	Treatment next morning
1	Low glucose media	High glucose for 6 hours
2	Low glucose media	High glucose and 1 μ M SFN for 6 hours
3	Low glucose media	High glucose and 2 μ M SFN for 6 hours
4	Normal glucose media	N/A
5	Normal glucose media	High glucose for 6 hours
6	Normal glucose media	High glucose and 1 μ M SFN for 6 hours
7	High glucose media	N/A
8	High glucose media and 1 μ M SFN	N/A

The low glucose media was made with MEM containing: 0.2 mM glucose, non-essential amino acids and supplemented with 2% FBS, 1% penicillin-streptomycin, 2 mM L-glutamine, 100 mM sodium pyruvate. The normal glucose media was made with MEM containing non-essential amino acids and supplemented with 10% FBS, 1% penicillin-streptomycin, 2 mM L-glutamine, 100 mM sodium pyruvate. The high glucose media was made with MEM containing: 20 mM D-glucose, non-essential amino acids and supplemented with 10% FBS, 1% penicillin-streptomycin, 2mM L-glutamine, 100 mM sodium pyruvate. The cells were incubated at 37°C in 5% CO₂ atmosphere. After 6 hours treatment and removal of media, MRC-5 fibroblasts were washed 3 times with PBS. After final aspiration, cells were covered with 250 μ l of a 1:1 acetone/methanol solution for 20 minutes at -20°C. Following aspiration of this fixative, cells were rinsed 3 times in TBST for 5 minutes each. Specimens were then blocked for 60 minutes in a solution of 1% BSA in TBST. Following this procedure, cells were incubated with primary antibody (Mondo A) overnight at 4 °C. Cells were then washed with PBS (2 x 5 min) and incubated with the Alexa labelled secondary antibodies for 1 h at room temperature. Secondary antibody was goat anti-rabbit IgG-Alexa488 conjugate diluted to 5 μ g/mL. Samples were then mounted using mounting medium containing 4',6-diamidino-2-phenylindole (DAPI). Images were acquired under a 63x NA oil immersion objective using a laser scanning Zeiss confocal microscope at 20x zoom.

3.3.14 Western Blotting

MRC-5 fibroblasts samples treated with 1 μ M SFN or 0.002 % DMSO were collected after passage 5 (young) and passage 9 (senescence). Cell pellets were washed 3 times with cold PBS and re-suspended in re-suspension buffer (50 mM Tris-HCl, 3 mM MgCl₂, 2% SDS pH 7.4 at room temperature) with addition of the protease inhibitor cocktail from Sigma (1% in resuspension buffer). Protein extracts were assayed for protein concentration by the Bradford Assay and stored at -80 °C until use.

Total β -galactosidase (BGAL) was measured by Western blotting using anti-BGAL and anti- β -actin antibodies. Protein samples (25 μ g) were separated by SDS-PAGE gel electrophoresis using 12% polyacrylamide gels (Table 20.). Separated proteins were transferred from the gel to PVDF membrane with the semi-dry transfer cell as described in Figure 51. The sandwich containing filter paper, gel and PVDF was immersed with transfer buffer (100 ml 10 X Tris/glycine buffer, 100 ml methanol, top up to 1 L with water) and transferred under 240 mA for 2.5 h.

Table 20. Composition of 10% SDS-PAGE gel for western blotting.

Name of solutions	12% resolving gel (Total volume of 60.66 ml for 2 gels)	5% stacking gel (Total volume of 26.53 ml for 2 gels)
4X Protogel resolving buffer	15 ml	----
Protogel stacking buffer	----	6.4 ml
30% Acrylamide	15 ml	3 ml
10% APS	600 μ l	300 μ l
Water	30 ml	16.8 ml
TEMED	60 μ l	30 μ l



Figure 51. Layout of semi-dry transfer for Western blotting.

The membrane was blocked with 5% BSA in Tris-Buffered Saline with Tween-20 (TBS-T, 30 ml of 5 M NaCl, 10 ml of 1 M Tris-HCl pH 7.6, 0.5 ml Tween-20, top up to 1 L with water) at room temperature on a shaking platform for 1 hr, followed by blotting with anti-BGAL antibody in 1% milk (in TBS-T) at 4°C overnight. The membrane was then washed every 10 min for 3 times and blotted with secondary antibody in 1% milk for 1 h at room temperature. The membrane was washed again for 3 times at 10 min intervals and added with ECL reagent. Photographic films were developed after exposed with the membrane for detection of protein bands. The exposure time was 1 min for BGAL and 10 seconds for β -actin. Protein bands were analysed by densitometry and BGAL (101 kDa) levels were normalised against β -actin (42 kDa) levels.

3.3.15 Assay of glycolytic intermediates in MRC-5 fibroblasts treated with SFN and/or high glucose

3.3.15.1 Cell incubations

MRC-5 cells were seeded in T-175 cell culture flasks (10^6 cells per flask) in 30 ml Eagle's MEM. After 24 h the cultures were supplemented with either 25 mM glucose or 25 mM glucose with 1 μ M SFN and incubated for 6 h. The cells were then trypsinized, collected by centrifugation and washed 3 times in PBS. MRC-5 fibroblasts from previous experiments treated with and without 1 μ M SFN from cPDL *ca.* 33.58 and collected at passage 5 and 9 (see Section 4, Figure 56) were also analysed. Approximately $0.3 - 1.0 \times 10^6$ cells were collected and cell pellets stored at -80°C until sample processing.

3.3.15.2 Sample processing

MRC-5 pellets and HL-60 [^{13}C]glucose labelled cell pellets (Internal Standard - collected in Method 3.1.6.4) were re-suspended in an aliquot of 0.1% TFA (200 μ l). Samples were sonicated for 30 s on ice and cell membranes sedimented by centrifugation (20,000g, 30 min, 4°C). The supernatant was then transferred in 3 kDa microspin filters and centrifuged (14,000g, 1 h, 4°C) and ultrafiltrate

retained. Sample and HL60 cell-derived internal standard ultrafiltrates were stored at -20°C until further analysis.

3.3.15.3 Stable isotopic dilution analysis of glycolytic intermediates

Key intermediates of early-stage glycolysis, glucose-6-phosphate (G6P), fructose-6-phosphate (F6P) and 6-phosphogluconate (PGA) were analysed in cell extracts by modification of the method of Bucholtz *et al.* (2001). Metabolites were detected by fragmentation to phosphate anions and specificity of G6P and F6P detection was further enhanced by concurrent loss of water in the multiple reaction monitoring (MRM) transitions. A aliquot of sample (30 µl) was mixed with internal standard extract (20 µl) and analysed by LC-MS/MS; injection volume 50 µl. Chromatography was performed with two graphite Hypercarb HPLC columns in series (150 x 2.1 mm and 250 mm x 2.1 mm, 5 µm particle size) with column temperature 30 °C. Solvents used were: 0.1% TFA in water (Solvent A1), 0.1% TFA in 50:50 MeCN:water (Solvent B1), and 0.1% TFA in 50:50 tetrahydrofuran:water (Solvent B2). The elution gradient programme used during the analytical run and post run are displayed in Table 21.

Table 21. UPLC Elution profile for glycolytic intermediates analysis.

Analytical run elution gradient programme:

Time (min)	Flow rate (ml/min)	Solvent A1 (%)	Solvent B1 (%)	Solvent B2 (%)	Curve
Initial	0.2	100	0	0	Initial
16	0.2	100	0	0	Linear
40	0.2	40	60	0	Linear

Post-run elution gradient programme:

Time (min)	Flow rate (ml/min)	Solvent A1 (%)	Solvent B1 (%)	Solvent B2 (%)	Column in-line	Curve
0	0.4	0	0	100	1	Initial
10	0.4	0	0	100	1	Isocratic
20	0.2	0	0	100	1 + 2	Immediate change
25	0.2	100	0	0	1 + 2	Immediate change
40	0.4	100	0	0	1 + 2	Immediate change

The eluate from the column was eluted into the electrospray source of the MS/MS detector for 4 - 40 min for data collection in the analytical run. Mass spectrometric analysis was performed using electrospray negative ionisation mode. For mass spectrometric detection, the capillary voltage was 0.60 kV, the ion source temperature 150 °C, the desolvation gas temperature 500 °C and cone and desolvation gas flows 992 and 1000 L/h respectively. Table 22 shows the optimised MRM conditions used for detection, along with their retention times, cone voltage and collision energy.

Table 22. Optimised MRMs for glycolytic intermediates analysis.

Analyte	Parent ion (Da)	Fragment ion (Da)	Fragment	Fragment loss	Retention time (min)	Cone voltage (V)	Collision energy (eV)
F6P	259.0	78.9	H ₂ PO ₄ ⁻	Fructose, H ₂ O	12.9	8	14
[¹³ C ₆]F6P	265.0	78.9	H ₂ PO ₄ ⁻	[¹³ C ₆]Fructose, H ₂ O	12.9	8	14
G6P	259.0	78.9	H ₂ PO ₄ ⁻	Glucose, H ₂ O	14.0	8	32
[¹³ C ₆]G6P	265.0	78.9	H ₂ PO ₄ ⁻	[¹³ C ₆]Glucose, H ₂ O	14.0	8	32
PGA	275.0	96.9	H ₂ PO ₄ ⁻	Gluconic acid	22.2	38	16
[¹³ C ₆]PGA	281.0	96.9	H ₂ PO ₄ ⁻	[¹³ C ₆]Gluconic acid	22.2	38	16

Limits of detection were: F6P, 0.09 pmol, G6P, 0.7 pmol and 3.0 pmol.

3.3.16 Microarray analysis

3.3.16.1 Sample collection

MRC-5 cells were seeded in T-175 cell culture flasks (1 million cells/flask) in 30 ml Eagle's MEM per well supplemented with either 1 μM SFN or with vehicle (0.002% DMSO). Cells cultured in these two conditions were cultured for 7 days and then cell number and viability recorded and passaged. MRC-5 fibroblasts after passage 3 and 11 were used for microarray analysis. The media contained flask was removed, cells were trypsinised and washed twice with

ice cold PBS. Cells were stored at - 80°C after until further analysis. Total RNA was then extracted as described in Method 3.3.3.2.

3.3.16.2 Sample preparation

Total RNA (600 ng) was used for microarray analysis. For this purpose, One-colour Spike-Mix stock was diluted 50 times with dilution buffer and mixed thoroughly. Volume corresponding to 600ng total RNA was added to 3 µl of 1:50 diluted One-colour Spike-Mix and 1.2 µl T7 Promoter primer. Nuclease-free water was added so that total reaction volume was 11.5 µl. The primer and template were then denatured in a Thermocycler at 65°C for 10 min. Samples were then incubated on ice for 5 minutes. In the meantime, the 5X first strand buffer was pre-warmed at 80 °C for 4 min to resuspend. The 5X first strand buffer was then briefly vortexed and span down. This solution was kept at room temperature until needed. cDNA mastermix was then made using the following components for each sample: 4 µl 5X first strand buffer, 2 µl 0.1M DTT, 1 µl 10mM dNTP mix, 1 µl MMLV-RT, 0.5 µl RNase out. A volume of 8.5 µl cDNA master mix was then added to each samples and mixed by pipetting. Samples were then incubated for 2 hrs at 40 °C. Following this 2hrs incubation, samples were incubated at 65 °C for 15 min and incubated at 4 °C for 5 min. In the meantime, 50% PEG was pre-warmed at 40 °C for 1 min. 50% PEG was then briefly vortexed and span down and kept at room temperature until needed. The Transcription Master Mix was then made using the following components for each sample – Table 23.

Table 23. Transcription Master Mix components.

Volumes are expressed per sample.

Component	Per Reaction
Nuclease-free water	15.3 μ l
4X Transcription Buffer	20 μ l
0.1M DTT	6 μ l
NTP mix	8 μ l
50% PEG	6.4 μ l
RNase OUT	0.5 μ l
Inorganic pyrophosphatase	0.6 μ l
T7 RNA Polymerase	0.8 μ l
Cyanine 3-CTP	2.4 μ l
Total Volume	60 μ l

A volume of 60 μ l of Transcription Master Mix was added to each samples and mixed by pipetting. Samples were incubated for 2 hrs at 40 °C.

3.3.16.3 Sample cRNA purification using Quiagen RNeasy mini spin columns

A volume of 20 μ l nuclease-free water and 350 μ l was added to each sample and mixed by pipetting. After quick centrifugation, 250 μ l 70% ethanol was added and mixed by pipetting. The resulting 700 μ l samples were then transferred to RNeasy mini columns in collection tubes. Columns were then span for 30 sec at 13,000 rpm. Flow-through was discarded and collection tube replaced. A volume of 500 μ l of buffer RPE was added and the column was span down for 30 sec at 13,000 rpm. Flow-through was discarded and another 500 μ l buffer RPE was added to the column. The column was then span down at 13,000 rpm for 1 min to dry the column. After discarding of the collection tube, the column was transferred to a clean 1.5 ml collection tube and 40 μ l of RNase-free water was added directly to the column membrane to elute cRNA. After 1 min incubation at room temperature, the column was span for 30 sec at 13,000 rpm to elute. The eluate was then transferred to a 0.5 ml ependorf and kept in the dark. cRNA was then quantified using a UV-VIS Spectrophotometer. The following

values were recorded: RNA absorbance (OD260 nm) and Cyanine 3 dye absorbance (OD550 nm). From these absorbances, the cRNA concentration (ng/μl) and the cyanine 3 dye concentration (pmol/μl) was calculated. Finally, the yield and specific activity for each sample reaction was calculated as follows:

$$\text{Yield } (\mu\text{g cRNA}) = (\text{ng}/\mu\text{l cRNA}) * 30 \mu\text{l elution volume} / 1000$$

$$\text{Specific activity (pmol Cyr3 per } \mu\text{g cRNA)} = (\text{pmol}/\mu\text{l Cyr3}) / (\text{ng}/\mu\text{l cRNA}) * 1000$$

3.3.16.4 Hybridization – 8X60K

A volume of 500 μl nuclease-free water was added to lyophilized 10X Blocking Agent from Agilent Gene Expression Hybridization Kit, and gently vortexed. After equilibration of water bath to 60 °C, 600 ng cyanine 3-labelled cRNA was made to a volume of 19 μl using nuclease-free water. To this cyanine 3-labelled cRNA, 5 μl of 10X Blocking Agent as well as 1 μl of 25X Fragmentation Buffer was added and gently mixed. After 30 min incubation at 60 °C to fragment RNA, the samples were immediately cooled on ice for 1 min. The fragmentation reaction was stopped by addition of 25 μl 2X GEx Hybridization Buffer HI-RPM. After mixing by pipetting, samples were spun 1 min at 13,000 rpm at room temperature and collected.

3.3.16.5 Sample processing

A volume of 40 μl of hybridization sample was loaded on each Agilent SureHyb chamber and SureHyb gasket slide was used to seal. Each sealed slide was placed in a hybridization oven at 65 °C for 17 hrs at 10 rpm. After disassembly of the hybridization chamber, slides were washed 1 min in GE wash buffer 1 at room temperature followed by 1 min wash at 37 °C in GE wash buffer 2, 10 sec wash with acetonitrile at room temperature and finally 20 sec wash with Stabilization and Drying solution at room temperature. Slides were immediately scanned using an Agilent scanner to minimize the impact of environmental oxidants on signal intensities and data was extracted using the Agilent Feature Extraction Software.

3.3.17 Statistical analysis

Experiments were performed using biological replicates in triplicates or greater. Data are presented as mean \pm standard deviation when normally distributed and median (lower – upper quartile) when of nonparametric distribution. Significance testing was performed using Student's t-test (parametric data) and Mann Whitney-U test (non-parametric data). For testing of repeated observations, repeated measures analysis was used. For correlation analysis Pearson correlation was used for parametric data and Spearman correlation for non-parametric data. Statistical significance was performed using the Statistical Package for the Social Sciences (SPSS) Version 17.0 (SPSS Inc). Significance was defined as $p < 0.05$.

4. Results

4.1 Effects of sulforaphane and hesperetin on MRC-5 fibroblast senescence *in vitro*

4.1.1 Growth curve of MRC-5 fibroblasts *in vitro*

MRC-5 fibroblasts were grown in Eagle's MEM medium *in vitro*. The growth curve was done over 5 days and viable cell number was recorder at time 0, 1, 2, 3, 4 and 5. The fibroblast viable cell number increased from 20,000 cells per well at time 0 to 412,000 cells per well after 5 days – Figure 52.

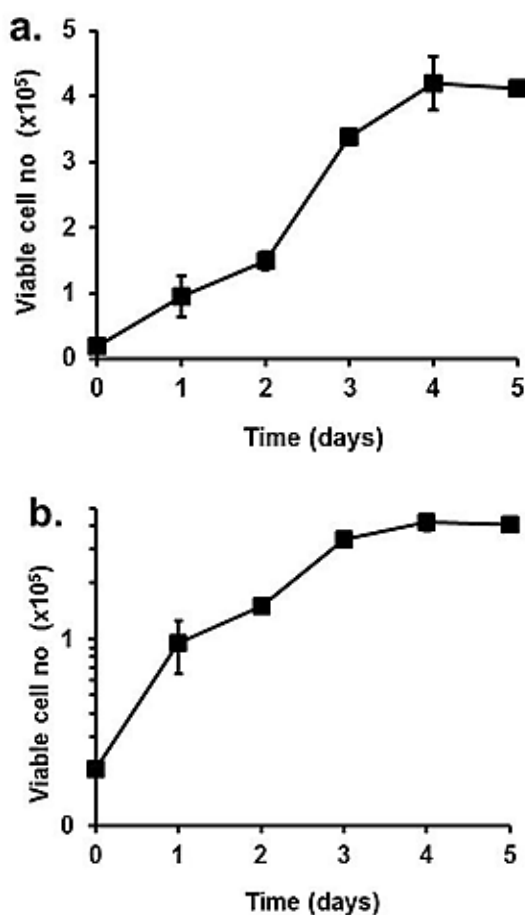


Figure 52. Growth curve for MRC-5 fibroblasts *in vitro*.

a. Growth curve. b. Growth curve with log transformation of viable cell number. Data are mean \pm SD, n = 3.

MRC-5 cells showed an exponential growth curve in the initial 3 days of culture which thereafter slowed to quiescence as the cells reached confluence. Cell viability remained at >98% (Trypan blue exclusion) throughout the culture period.

4.1.2 Dose-response of MRC-5 fibroblasts treated with sulforaphane

MRC-5 cells were incubated with sulforaphane (SFN), 0-8 μM for 48 h. The dose-response curve is shown in Figure 53.

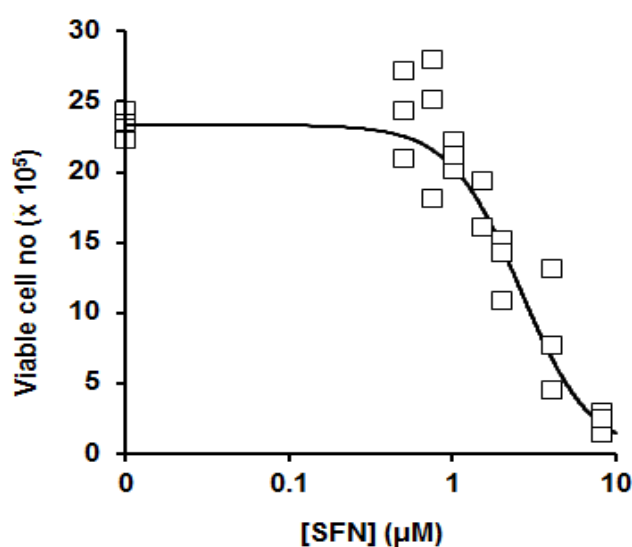


Figure 53. Dose-response curve for the effect of sulforaphane on growth of MRC-5 fibroblasts *in vitro*.

Data were fitted to a logistic regression equation. The median growth inhibitory concentration GC_{50} of SFN was $2.60 \pm 0.03 \mu\text{M}$ and the logistic regression coefficient $n = 2.02 \pm 0.03$ ($N = 21$). Control cell growth was $23.6 \pm 3.1 \times 10^5$ cells ($n = 3$). Legend: \square , viable cell count after 48 h incubation for each cultured well.

From this dose-response curve, the median growth inhibitory concentration GC_{50} value of SFN was $2.60 \pm 0.03 \mu\text{M}$ and the logistic regression coefficient n was 2.02 ± 0.03 . There was no significant inhibition of MRC-5 cell growth at SFN concentrations up to $1.5 \mu\text{M}$ SFN. For all concentrations used, there was negligible toxicity ($< 5\%$). At $\geq 2 \mu\text{M}$ SFN there was growth arrest.

4.1.3 Dose-response of MRC-5 fibroblasts treated with hesperetin

MRC-5 cells were incubated with hesperetin (HESP), 0 - 40 μM , for 48 h. The dose-response curve is shown in Figure 54.

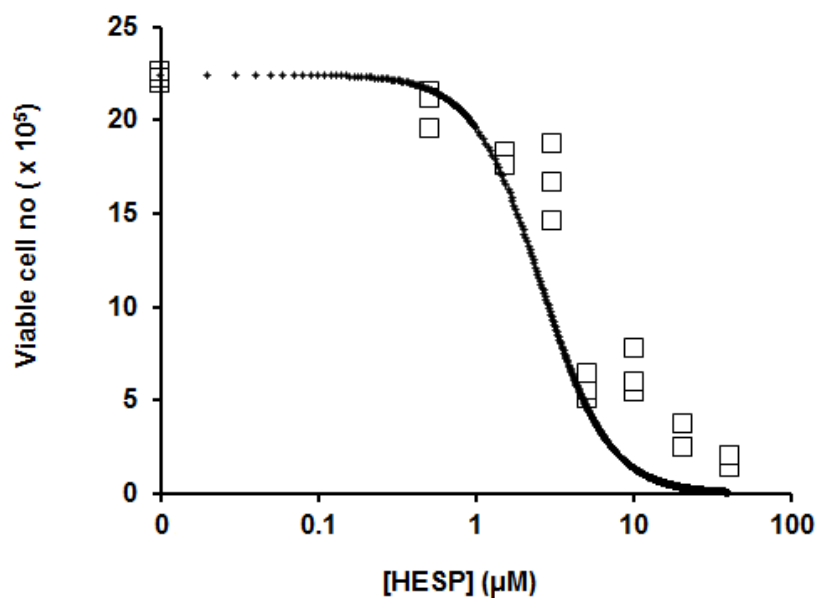


Figure 54. Dose-response curve for the effect of hesperetin on growth of MRC-5 fibroblasts *in vitro*.

Data were fitted to a logistic regression equation. The median growth inhibitory concentration GC_{50} of HESP was $4.83 \pm 0.45 \mu\text{M}$ and the logistic regression coefficient n was 1.38 ± 0.16 ($N = 21$). Control cell growth was $21.5 \pm 1.1 \times 10^5$ cells ($n = 3$). Legend: \square , viable cell count after 48 h incubation for each cultured well.

From this dose-response curve, the median growth inhibitory concentration GC_{50} value of HESP was $4.83 \pm 0.45 \mu\text{M}$ and n was 1.38 ± 0.16 . There was no significant inhibition of MRC-5 cell growth at $1.0 \mu\text{M}$ HESP. For all concentrations used, there was negligible toxicity ($< 5\%$). At higher concentrations, however, HESP decreased MRC-5 cell growth.

4.1.4 Effect of sulforaphane treatment on MRC-5 fibroblasts growth

MRC-5 fibroblasts were grown in Eagle's MEM media supplemented each week with either 0.002% DMSO (control) or $1 \mu\text{M}$ SFN (treatment). The population doubling limit (PDL) as well as cumulative PDL (cPDL) were

analyzed in order to represent MRC-5 fibroblast growth as progression of senescence occurred. Cumulative PDL was calculated from addition of PDL from one passage to another. Three flasks of MRC-5 cells were cultured from cPDL 33.5 for 2 passages, and then each divided into two flasks and one thereafter cultured with 1 μ M SFN added after 24 h and once only during the passage. The cell seeding varied slightly in the early passages and then decreased markedly as cell numbers declined. All changes in seeding density were, however, identical for SFN treated incubations and controls – Table 24 to 27. Data of PDL and cPDL recorded are given in Figure 55 and 56.

Table 24. Seeding density of MRC-5 cells in passages for the sulforaphane treatment study.

Passage no	Cell seeding density (cells/cm ²)	Treatment
1	62400	None
2	26742	“
3	30674	\pm 1 μ M SFN
4	40000	“
5	40000	“
6	11429	“
7	11429	“
8	11429	“
9	11429	“
10	5714	“
11	1714	“
12	1743	“

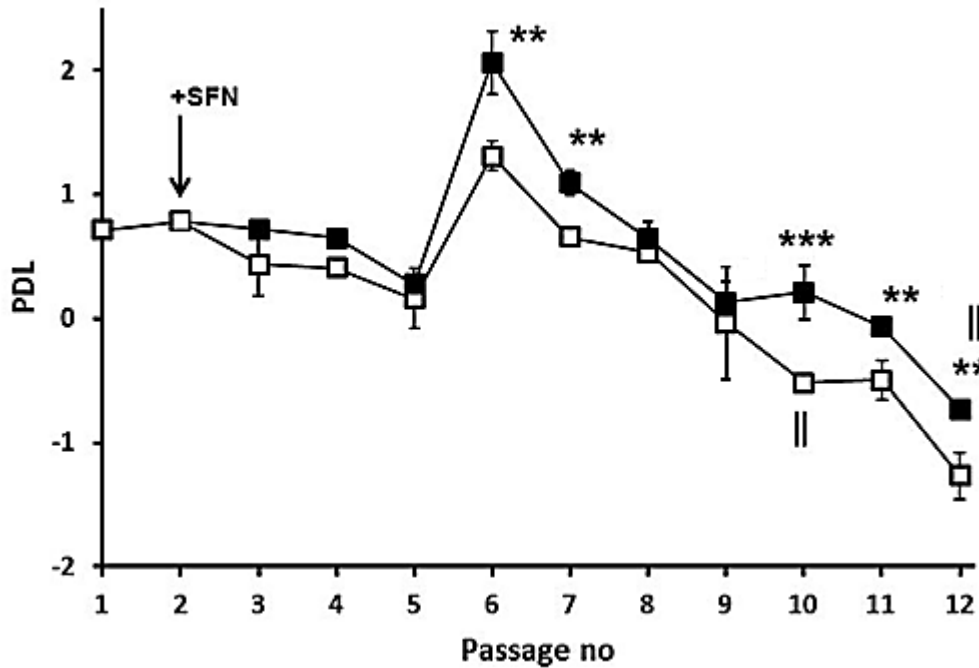


Figure 55. MRC-5 fibroblasts PDL as a function of passage number – Study 1.

Key: □—□, 0.002% DMSO (control), ■—■, + 1 μM SFN. Data are mean ± SD, n = 3. The arrow indicates where SFN treatment was initiated. || indicates cells had stopped growing and were decreasing number (PDL < 0; P<0.05) Significance: ** and ***, P<0.01 and P<0.001, respectively (t-test).

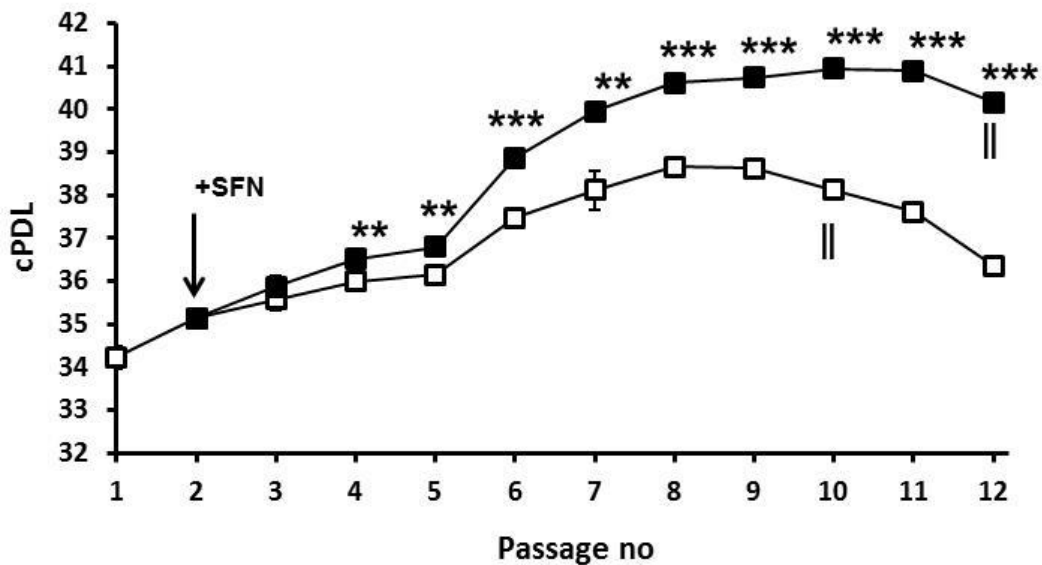


Figure 56. MRC-5 fibroblasts cPDL as a function of passage number – Study 1.

Key: □—□, 0.002% DMSO (control), ■—■, + 1 μM SFN. Data are mean ± SD, n = 3. The arrow indicates where SFN treatment was initiated. || indicates cells stopped growing and were decreasing in number (cPDL decreasing; P<0.05) Significance: ** and ***, P<0.01 and P<0.001, respectively (t-test).

In control cultures, the PDL was initially *ca.* 0.72 and declined to 0.16 at passage 5. When the seeding density was decreased to 11,429 cells/cm² from passages 6 – 9, the initial PDL increased to 1.31 and then decreased to -0.03 by passage 9. At later passages the PDL was negative, indicating that the cells were no longer growing and viable cell number was progressively decreasing. The maximum cPDL of 38.7 ± 0.1 was reached at passage 8. With SFN treatment, the combined increase in PDL over passages 3 – 5 was increased (repeated measures analysis, $P < 0.001$). PDL was also increased in SFN treated cells from passages 6 – 12 – with significance achieved at all passages except 8 and 9 and overall in a combined repeated measures analysis ($P < 0.001$). From regression analysis of PDL on passage number, the rate of decline in PDL per passage with and without SFN was similar (-0.40 ± 0.06 versus -0.40 ± 0.03) whereas the intercept (when PDL = 0) was higher with SFN (4.06 ± 0.29 versus 3.59 ± 0.24 , $P < 0.001$). This suggests the rate of decline in MRC-5 cell growth on approach to senescence with and without SFN is similar; treatment with SFN, however, delayed the onset of approach to senescence. The maximum cPDL with SFN treatment was reached at passage 11 and was higher than in control (40.9 ± 0.2 versus 38.7 ± 0.1 , $P < 0.001$).

Repeat analysis of delay of MRC-5 cell senescence with a similar experimental protocol gave similar results although in one of the three studies the delay of senescence developed late as cPDL progressed. In the four replicate studies, the increase in cPDL achieved with SFN treatment was 2.29, 2.06, 1.56 and 1.99; mean \pm SD, 1.98 ± 0.31 – Figures 57, 58 and 59a. SFN therefore induced a 2 unit increase in cPDL or two additional population doublings. This was achieved by initiation of SFN treatment in the cPDL range 32 – 37. The effect was also investigated of late initiation of SFN treatment at cPDL = 41. Remarkably, this also achieved an increase in cPDL of 1.49 ± 0.13 above control after only treatment of 4 passages – Figure 59b.

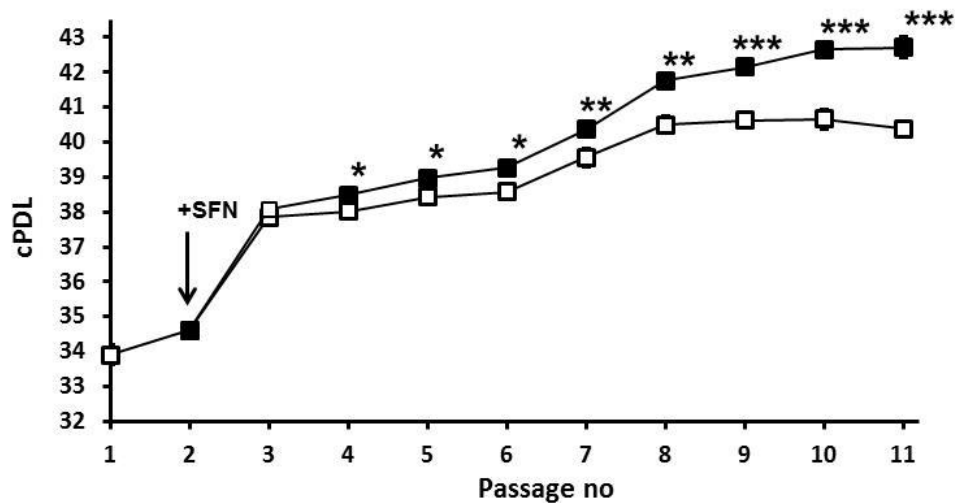


Figure 57. MRC-5 fibroblasts cPDL as a function of passage number. Replicate study 2.

Key: □—□, 0.002% DMSO (control), ■—■, + 1 μM SFN. Data are mean ± SD, n = 3. The arrow indicates where SFN treatment was initiated. || indicates cells stopped growing and were decreasing in number (cPDL decreasing; P<0.05) Significance: *, ** and ***, P<0.05, P<0.01 and P<0.001, respectively (t-test).

Table 25. Seeding density of MRC-5 cells in passages for the sulforaphane treatment study. Replicate study 2.

Passage no	Cell seeding density (cells/cm ²)	Treatment
1	16068	None
2	29088	“
3	46628	± 1 μM SFN
4	3428	“
5	22857	“
6	22857	“
7	22857	“
8	11428	“
9	11428	“
10	11428	“
11	5714	“

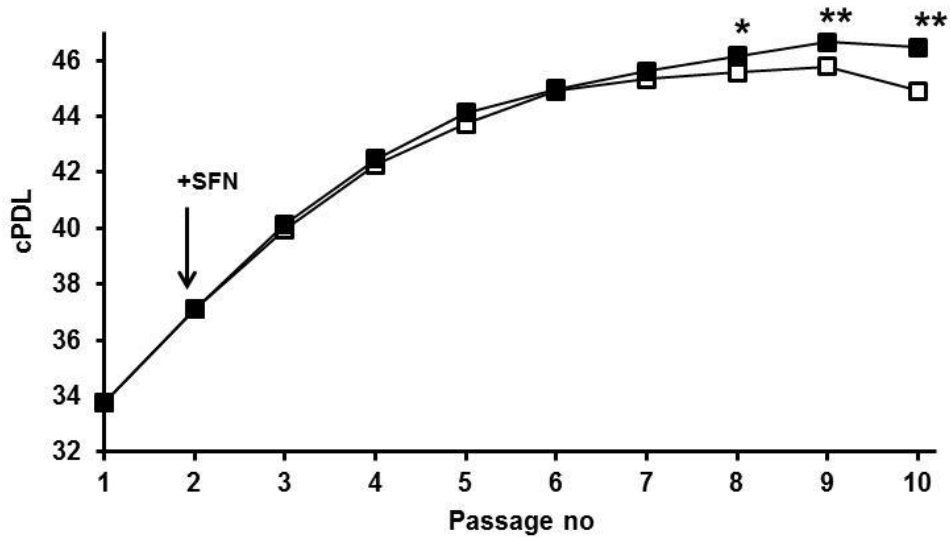


Figure 58. MRC-5 fibroblasts cPDL as a function of passage number. Replicate study 3.

Key: □—□, 0.002% DMSO (control), ■—■, + 1 μM SFN. Data are mean ± SD, n = 3. The arrow indicates where SFN treatment was initiated. † indicates cells stopped growing and were decreasing in number (cPDL decreasing; P<0.05) Significance: * and **, P<0.05 and P<0.01, respectively (t-test).

Table 26. Seeding density of MRC-5 cells in passages for the sulforaphane treatment study. Replicate study 3.

Passage no	Cell seeding density (cells/cm ²)	Treatment
1	12267	None
2	15289	“
3	4000	± 1 μM SFN
4	4000	“
5	4000	“
6	4000	“
7	4000	“
8	4000	“
9	4000	“
10	4000	“

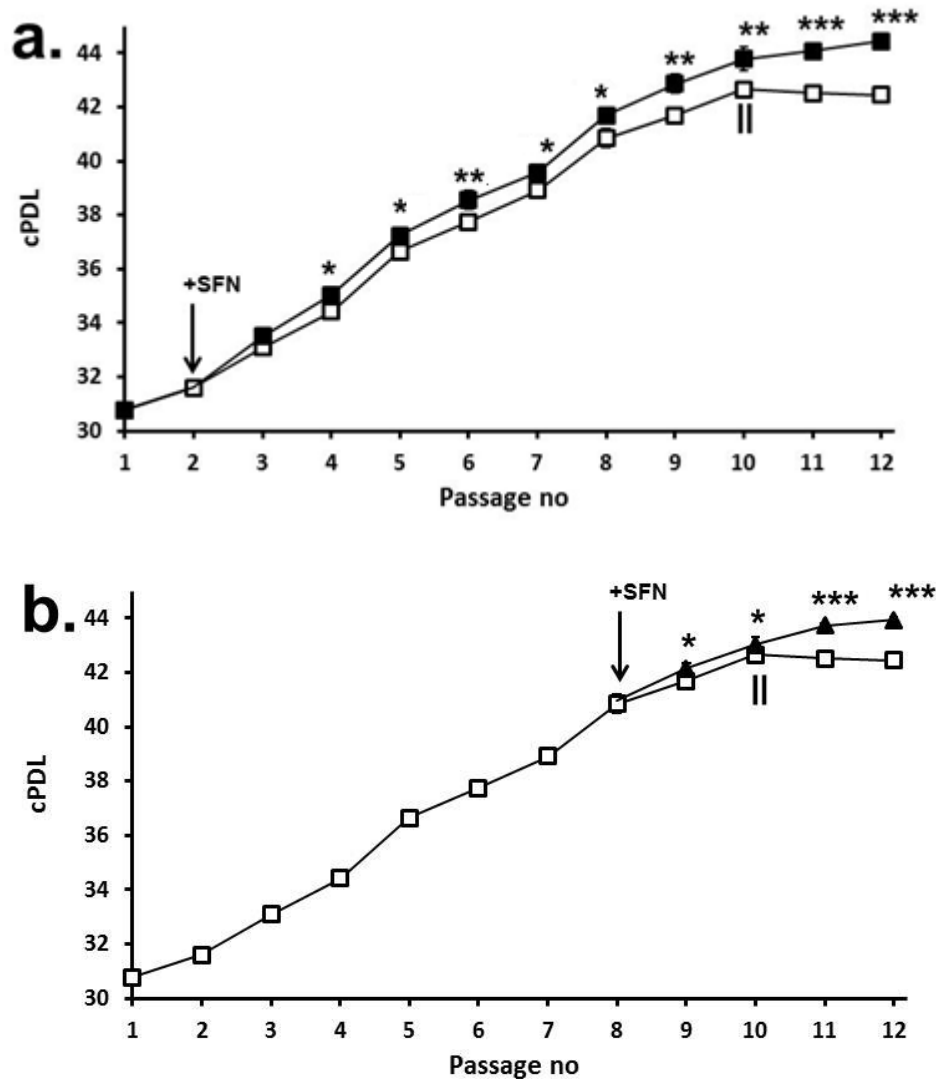


Figure 59. MRC-5 fibroblasts cPDL as a function of passage number. Replicate study 4 – effect of early and late treatment.

a. Early SFN treatment. b. Late SFN treatment. Key: \square — \square , 0.002% DMSO (control), \blacksquare — \blacksquare , +1 μ M SFN from cPDL 31.6. \blacktriangle — \blacktriangle , +1 μ M SFN from cPDL 41.0. Data are mean \pm SD, n = 3. The arrow indicates where SFN treatment was initiated. || indicates cells stopped growing and were decreasing in number thereafter. Significance: *, ** and ***, P<0.05, P<0.01 and P<0.001, respectively (t-test).

Table 27. Seeding density of MRC-5 cells in passages for the sulforaphane treatment study. Replicate study 4.

Passage no	Cell seeding density (cells/cm ²)	Treatment-1	Treatment-2
1	16800	None	None
2	36960	“	“
3	34416	± 1 µM SFN	“
4	24679	“	“
5	11000	“	“
6	11428	“	“
7	11428	“	“
8	5714	“	“
9	11428	“	± 1 µM SFN
10	11428	“	“
11	5714	“	“
12	4000	“	“

4.1.5 Effect of hesperetin treatment on MRC-5 fibroblasts growth

MRC-5 fibroblasts were grown in Eagle’s MEM media supplemented each week with either 0.005% DMSO (control) or 5 µM HESP (treatment). The population doubling limit (PDL) as well as cumulative PDL (cPDL) were analyzed in order to represent MRC-5 fibroblast growth as progression of senescence occurred. Cumulative PDL was calculated from addition of PDL from one passage to another. Three flasks of MRC-5 cells were cultured from cPDL 33.5 for 2 passages, and then each divided into two flasks and one thereafter cultured with 5 µM HESP added after 24 h and once only during the passage. The cell seeding varied slightly and in the early passages and then decreased steadily as cell numbers declined. All changes in seeding density were, however, identical for HESP treated incubations and controls – Table 28. Data of PDL and cPDL recorded are given in Figures 60 and 61.

Table 28. Seeding density of MRC-5 cells in passages for the hesperetin treatment study.

Passage no	Cell seeding density (cells/cm ²)	Treatment
1	17466	None
2	42971	“
3	4000	± 5 µM HESP
4	4000	“
5	3428	“
6	2857	“
7	5714	“
8	2057	“
9	2533	“

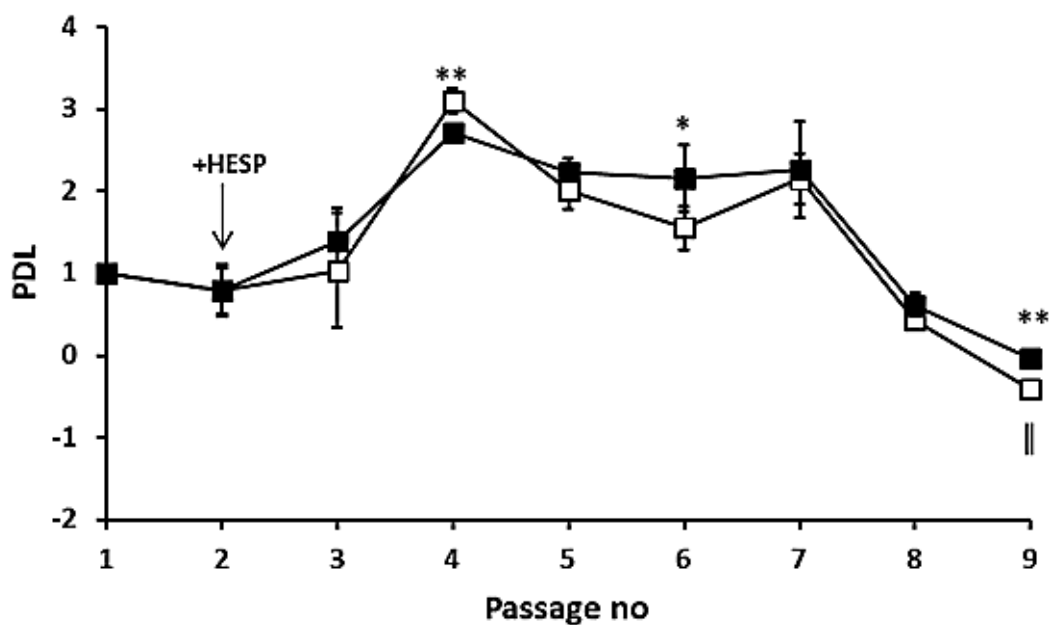


Figure 60. MRC-5 fibroblasts PDL as a function of passage number - HESP study.

Key: □—□, 0.005% DMSO (control), ■—■, + 5 µM HESP. Data are mean ± SD, n = 3. The arrow indicates where HESP treatment was initiated. || indicates cells had stopped growing and were decreasing in number (PDL < 0; P < 0.05)
Significance: * and **, P < 0.05 and P < 0.01, respectively (t-test).

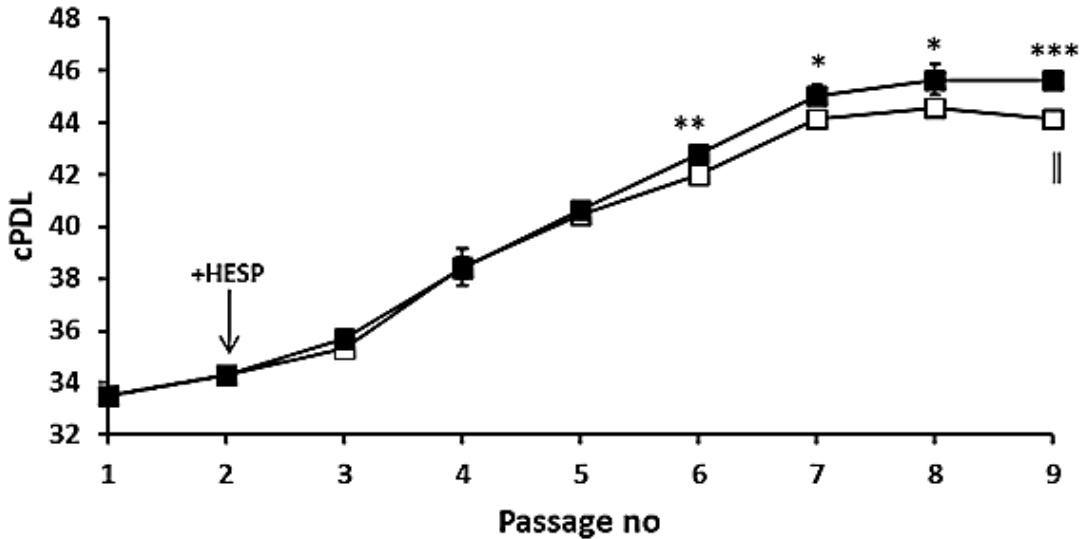


Figure 61. MRC-5 fibroblasts cPDL as a function of passage number - HESP study.

Key: □—□, 0.005% DMSO (control), ■—■, + 5 μM HESP. Data are mean ± SD, n = 3. The arrow indicates where HESP treatment was initiated. || indicates cells stopped growing and were decreasing in number (cPDL decreasing; P<0.05) Significance: *, ** and ***, P<0.05, P<0.01 and P<0.001, respectively (t-test).

In control cultures, the PDL was initially *ca.* 0.98 and increased to 3.10 at passage 4. When the seeding density was decreased to 2,857-3,428 cells/cm² for passages 5 and 6, the initial PDL decreased 1.5-1.9 then increased to 2.1 at passage 7 in accordance with higher seeding density of 5,714 cells/cm². Control PDL then decreased to -0.4 by passage 9. At later passages the PDL was negative, indicating that the cells were no longer growing and viable cell number was progressively decreasing. The maximum cPDL of 44.6 ± 0.3 was reached at passage 8. With HESP treatment, the combined increase in PDL over passages 3 – 6 was increased (repeated measures analysis, P<0.001). PDL was also increased in HESP treated cells at passage 3 and from passages 5 – 9 – with significance achieved at passages 6 and 9 and overall in a combined repeated measures analysis (P<0.001). From regression analysis of PDL on passage number, the rate of decline in PDL per passage with and without HESP was similar (-0.13 ± 0.15 versus -0.17 ± 0.16) whereas the intercept (when PDL = 0) was higher with HESP (2.45 ± 0.05 versus 2.27 ± 0.06, P<0.001). This suggests the rate of decline in MRC-5 cell growth on approach to senescence with and without HESP is similar; treatment with HESP, however, delayed the onset of approach to senescence. The maximum cPDL with

HESP treatment was reached at passage 9 and was higher than in control (45.7 ± 0.2 versus 44.2 ± 0.1 , $P < 0.001$).

4.1.6 Senescence-associated beta-galactosidase staining of MRC-5 fibroblasts treated with SFN

Onset of cell senescence in MRC-5 cells was assessed by staining for the senescence marker, beta-galactosidase. A total of 300 MRC-5 cells were analysed per well, analysing 3 wells per treatment, and the percentage of cells expressing beta-galactosidase (blue stain) determined for passages 4 to 9. Micrographs of characteristic blue staining is shown in Figure 62 and related cell counting quantitation are shown in Figure 63.

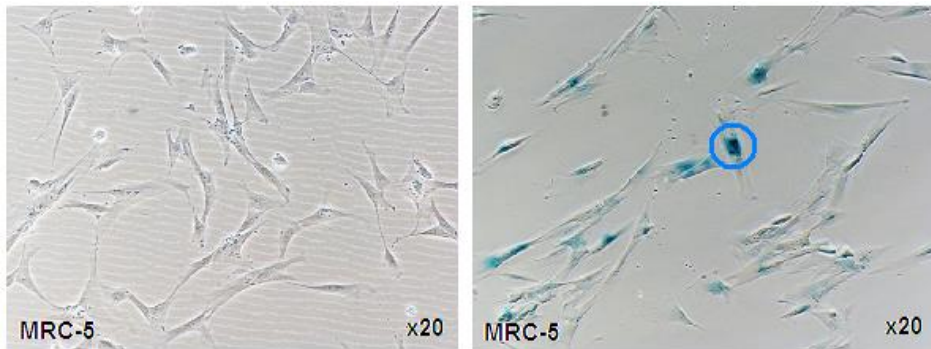


Figure 62. Characteristic blue staining indicating β -galactosidase expression in senescent MRC-5 fibroblasts.

Key: left-hand panel young, non-senescent cells; right-hand panel – old, senescent cells. Inverted microscopy, x20 magnification.

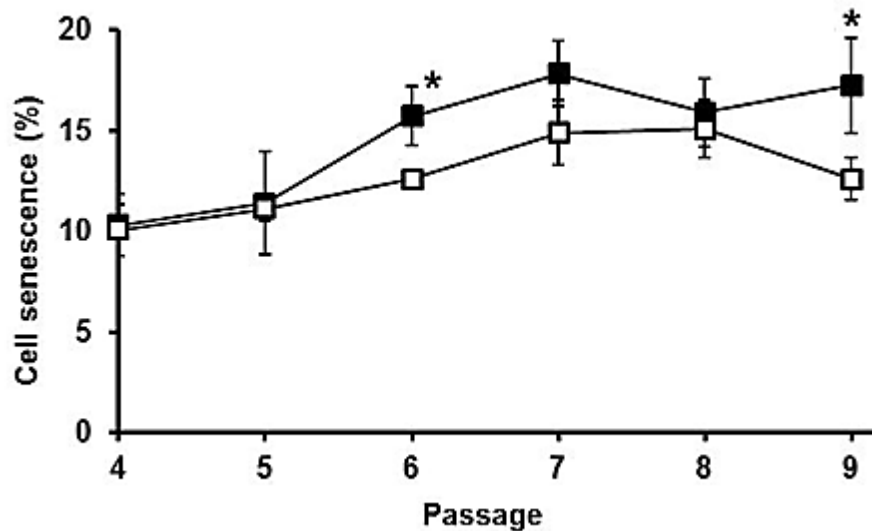


Figure 63. Percentage of senescent MRC-5 fibroblasts as a function of passage.

Key: ■—■, 0.002% DMSO (control), □—□, + 1 μM SFN. Data are mean ± SD, n = 3. Significance: *, P<0.05 (t-test)

Control MRC-5 fibroblasts had a higher percentage of senescent cells in culture than SFN-treated MRC-5 cells at passages 6 and 9 (P<0.05) indicating that treatment delayed senescence marked by decreased β-galactosidase expression compared to control in these two passages.

4.1.7 Cell senescence marker beta-galactosidase – assessment of beta-galactosidase protein

Human β-galactosidase-1 expression in MRC-5 fibroblasts was assessed at the protein level by Western blotting of cell extracts at passage 5 (young) and passage 9 (senescence) treated with either 1 μM SFN or 0.002% DMSO – Figure 64 and 65.

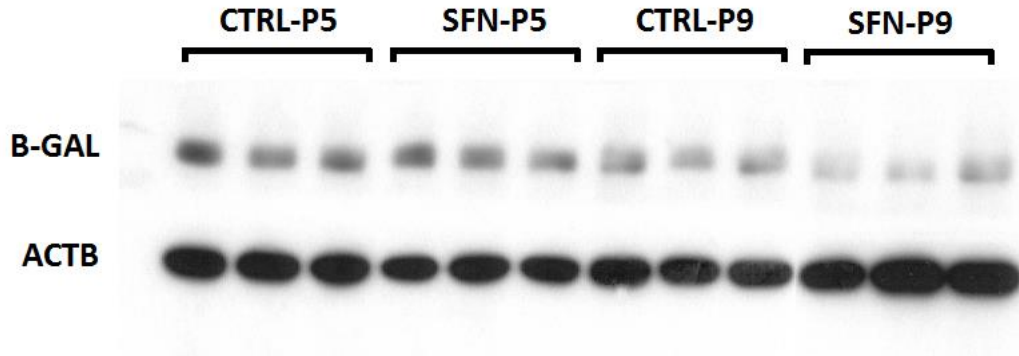


Figure 64. Western blotting of young and senescent MRC-5 fibroblasts for beta-galactosidase.

Key: BGAL, beta-galactosidase protein; and ACTB - β -actin housekeeping protein. SFN-P5 and CTRL-P5, cell extracts from passage 5 treated with and without 1 μ M SFN; and SFN-P9 and CTRL-P9, cell extracts from passage 9 treated with and without 1 μ M SFN.

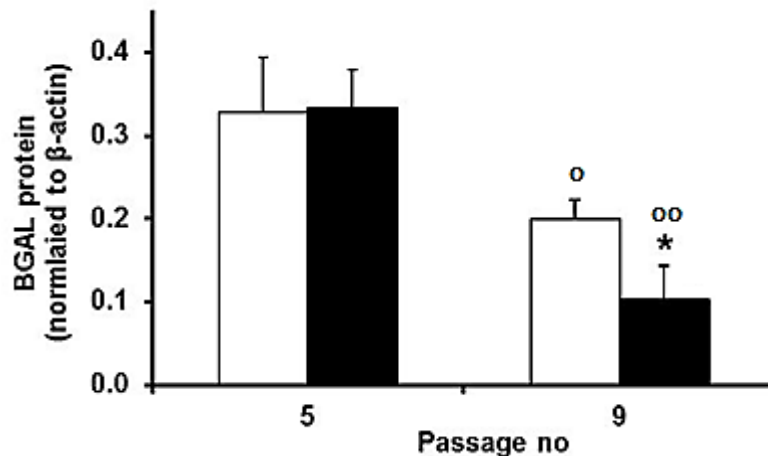


Figure 65. Quantitation of Western blotting of young and senescent MRC-5 fibroblasts for beta-galactosidase.

Key: , control; and + 1 μ M SFN. Data are mean \pm SD (n = 3). Significance: *, P<0.05, SFN treated cells with respect to control; o and oo, P<0.05 and P<0.01, passage 9 with respect passage 5.

Control MRC-5 fibroblasts had a higher expression of β -galactosidase protein compared to the SFN-treated group at passage 9. Unexpectedly β -galactosidase protein, normalized to β -actin, was higher in extracts of cells at passage 5 than at passage 9.

4.1.8 Changes in gene expression induced by sulforaphane in early passage, non-senescent MRC-5 cells *in vitro*.

The time course of changes in gene expression induced by 1 μ M SFN in early passage, non-senescent MRC-5 cells *in vitro* was investigated by quantifying mRNA of genes of selected metabolic pathways with Nrf2 regulated, ARE-linked genes by the Nanostring method – quantifying relative mRNA copy number. The outputs are given in Figures 66-77. Reference genes were β -actin, β -glucosidase and clathrin, heavy chain with responses normalized to the geometric mean of these genes.

SFN induced a 2-fold increase in the Nrf2, ARE-linked transcriptional response marker gene quinone reductase NQO1. For other antioxidant linked genes, there were ca. 2-fold increases in mRNA of γ -glutamylcysteine ligase-modulatory subunit (GCLM), glutathione reductase (GSR), thioredoxin reductase (TXNRD1) and haem oxygenase (HMOX1), and smaller increases in mRNA of ferritin and thioredoxin by SFN. Expression of γ -glutamylcysteine ligase-catalytic subunit, glutathione peroxidase-1, peroxiredoxin-1, superoxide dismutases SOD1 and SOD2 and catalase were little changed. Increased NQO1 mRNA stimulated by SFN maximized after ca. 24 h and remained increased up to 72 h post-stimulation. In contrast, increased GCLM and GSR mRNA maximized after 12 h and returned to baseline levels after 36 – 48 h. The increase in HMOX1 mRNA was even more short-lived, maximizing at 4 h and returning to levels in unstimulated cells by 24 h. SFN also increased mRNA of aldoketo reductase 1C1 but not of glyoxalase 1. It also had little effect on phase II conjugating genes, glutathione transferase P1 and MRP2. Pentosephosphate pathway genes were more responsive, with mRNA of glucose-6-phosphate dehydrogenase (G6PDH), transketolase (TKT) and transaldolase (TALDO) all increasing in SFN stimulated cells. For lipogenic genes, sterol response element binding protein-1 (SREBF1) was decreased in SFN stimulated cells but expression of fatty acid synthase (FASN) was unchanged. The expression of Fructose-2,6-bisphosphate kinase-4 (PFKFBP4) was also unchanged by SFN. For the Nrf2 system itself, SFN did not increase expression of Nrf2, Keap1 nor Fyn kinase but did increase small maf protein-G (MAFG) in the 24 h immediately post-stimulation. Inflammatory gene responses were examined. Monocyte chemoattractant protein-1 (CCL2), chemokine (C-X-C motif) ligand 1 (CXCL1), interleukin-15 (IL15), interleukin 1 β (IL1),

toll-like receptor 4 (TLR4), transcription factor p65 (NFkB3), nuclear factor NF-kappa-B p105 subunit/p50 (NFkB1) and intracellular adhesion molecule-1 (ICAM1) were all unresponsive. Genes associated with extracellular matrix proteolysis, matrix metalloproteinase-3 (MMP3) and matrix metalloproteinase-13 (MMP13), were unchanged whereas the expression of elastin was decreased. The expression of serpins and senescence associated genes, β -galactosidase (GLB1), cyclin-dependent kinase inhibitor 1/p21 (CDKN1A) and cyclin-dependent kinase inhibitor 2A/P16INK4a (CDKN2A), were all unchanged.

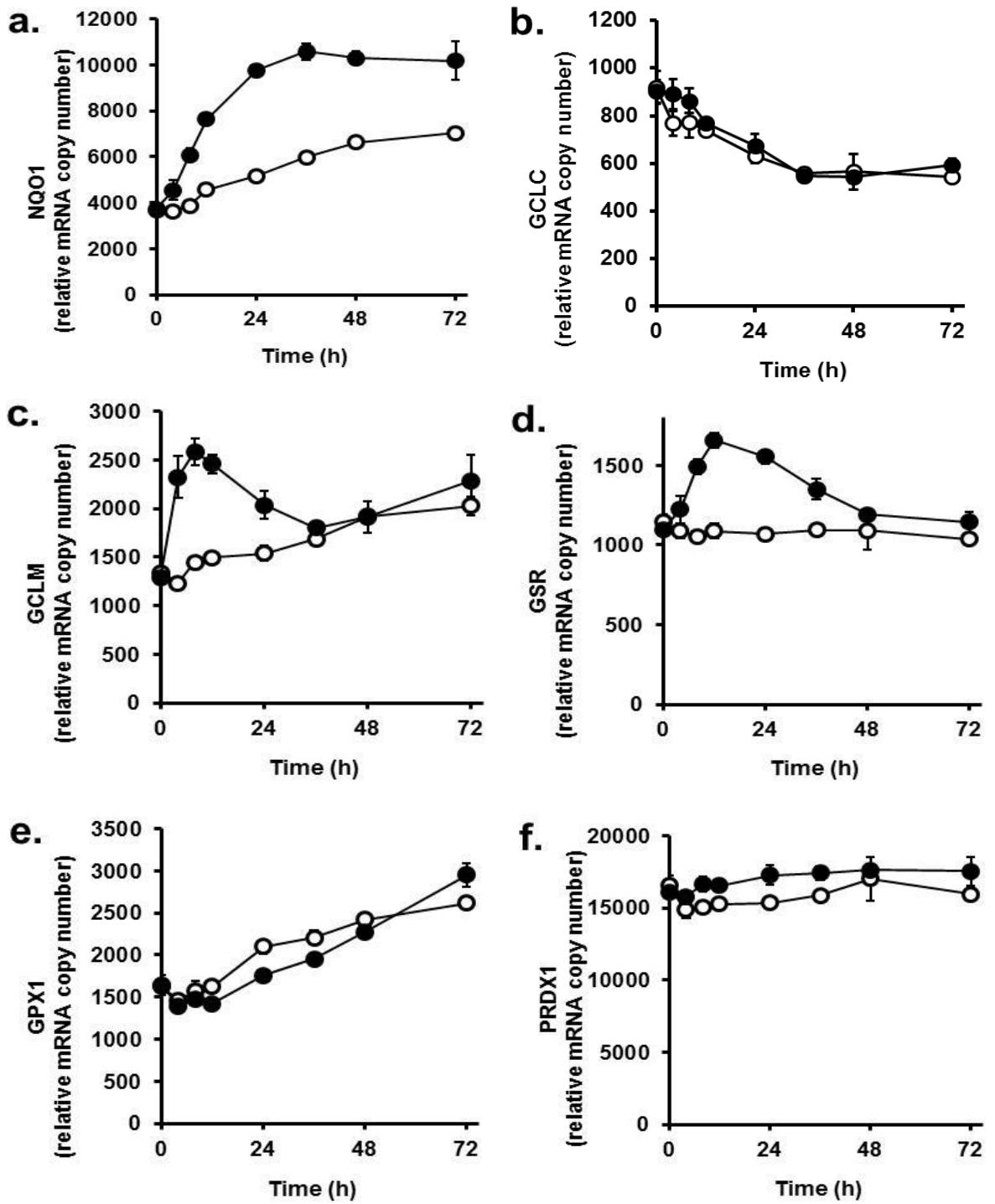


Figure 66. Gene expression of MRC-5 fibroblasts induced by sulforaphane. Nanostring study. Antioxidant genes.

a. Quinone reductase NQO1, b. γ -Glutamylcysteine ligase – catalytic subunit GCLC, c. γ -Glutamylcysteine ligase – modulatory subunit GCLM, d. Glutathione reductase GSR, e. Glutathione peroxidase-1 GPX1, and f. Peroxiredoxin-1 PRDX1. Key: ○—○, control; ●—●, + 1 μ M SFN. Data are mean \pm SD, n = 3.

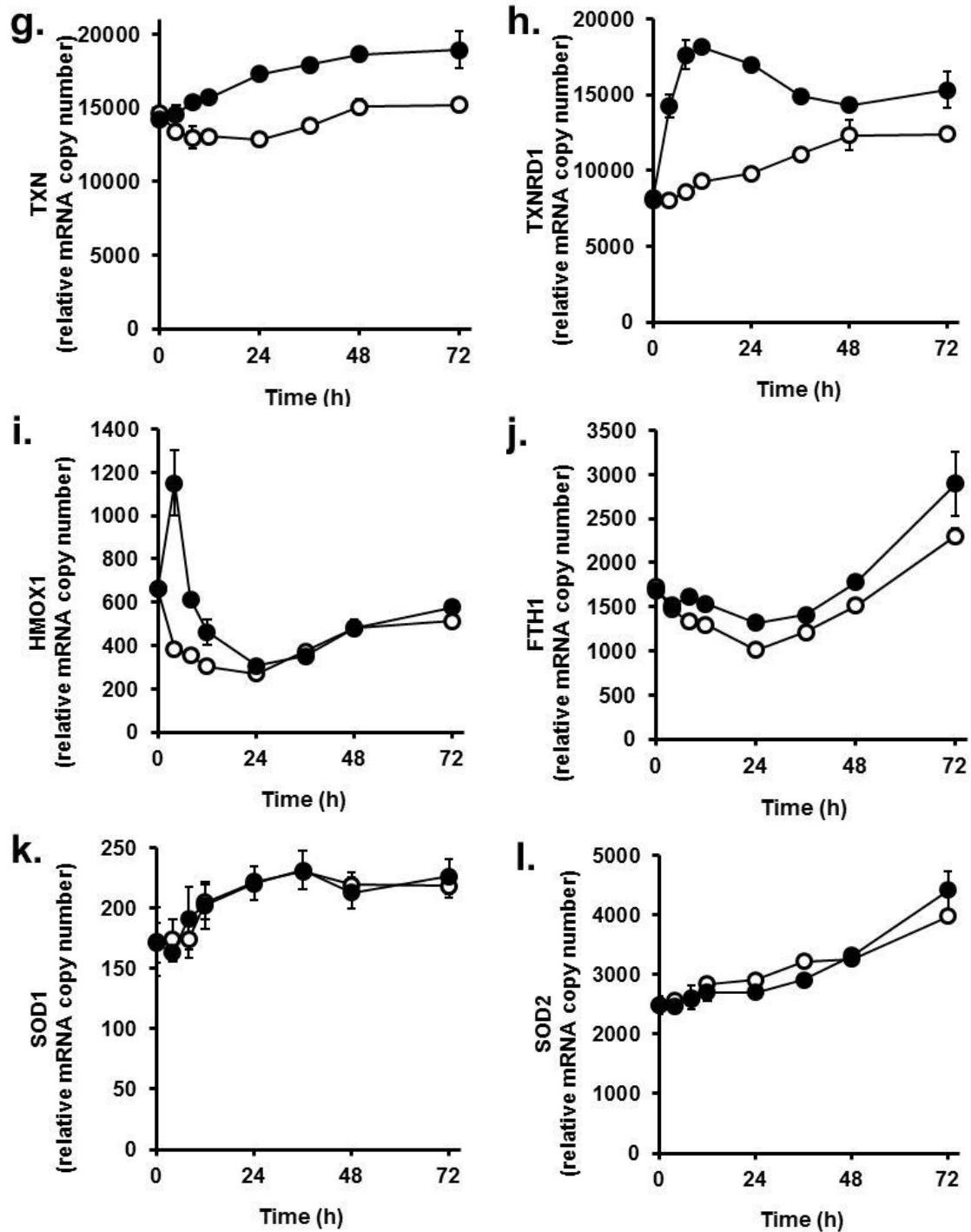


Figure 66. Gene expression of MRC-5 fibroblasts induced by sulforaphane. Nanostring study. Antioxidant genes (cont'd).

g. thioredoxin TXN, h. thioredoxin reductase TXNRD1, i. haem oxygenase HMOX1, j. ferridoxin FTH1, k. Superoxide dismutase-1 SOD1, and l. Superoxide dismutase-2 SOD2. Key: ○—○, control; ●—●, + 1 μM SFN. Data are mean ± SD, n = 3.

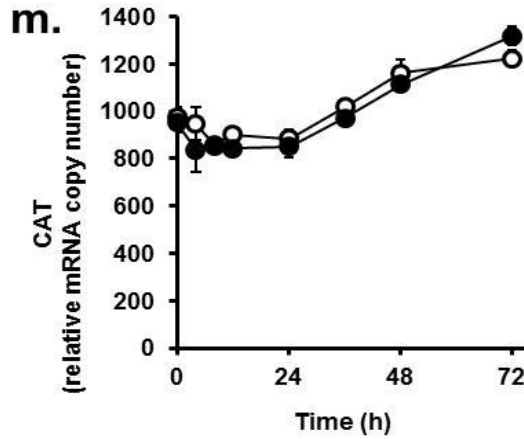


Figure 66. Gene expression of MRC-5 fibroblasts induced by sulforaphane. Nanostring study. Antioxidant genes (cont'd).
 m. Catalase CAT. Key: ○-○, control; ●-●, + 1 μM SFN. Data are mean ± SD, n = 3.

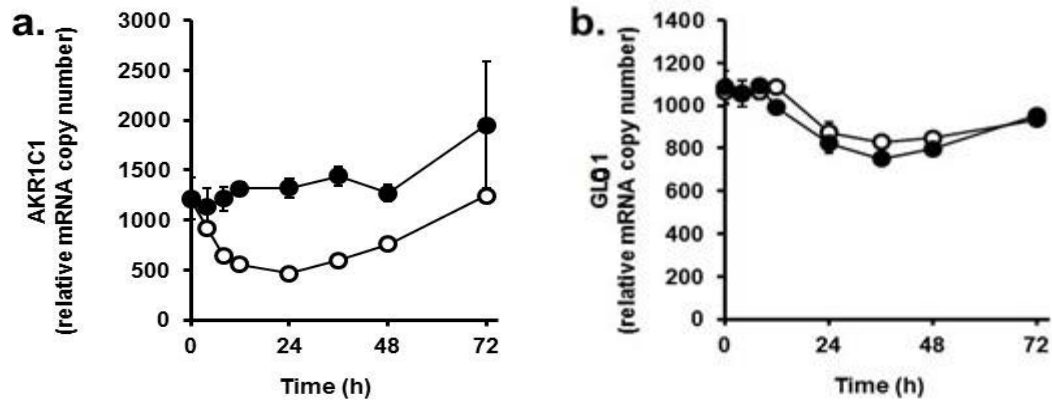


Figure 67. Gene expression of MRC-5 fibroblasts induced by sulforaphane. Nanostring study. Antiglycation genes.
 a. Aldoketo reductase 1C1 (AKR1C1). b. Glyoxalase 1 (GLO1). Key: ○-○, control; ●-●, + 1 μM SFN. Data are mean ± SD, n = 3.

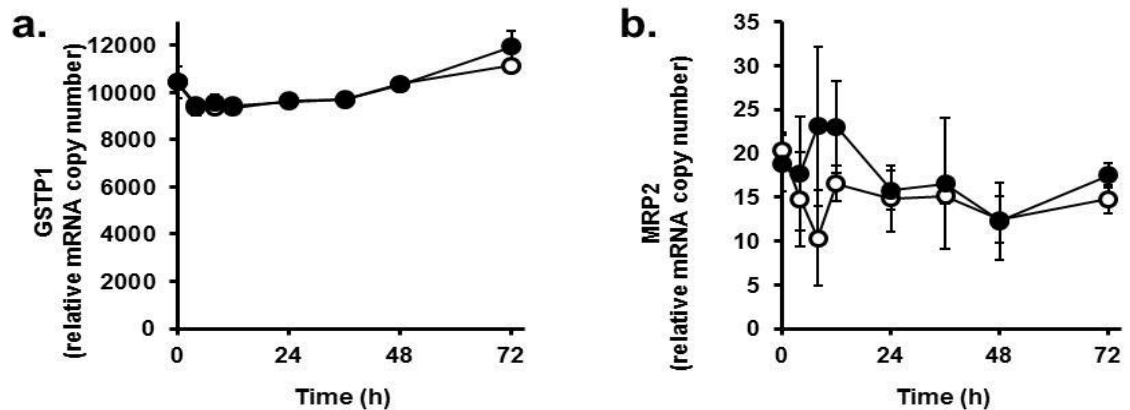


Figure 68. Gene expression of MRC-5 fibroblasts induced by sulforaphane. Nanostring study. Phase II conjugation genes.
 a. Glutathione transferase P1 (GSTP1). b. Glutathione conjugate transporter (ABCC2) MRP2. Key: ○-○, control; ●-●, + 1 μM SFN. Data are mean ± SD, n = 3.

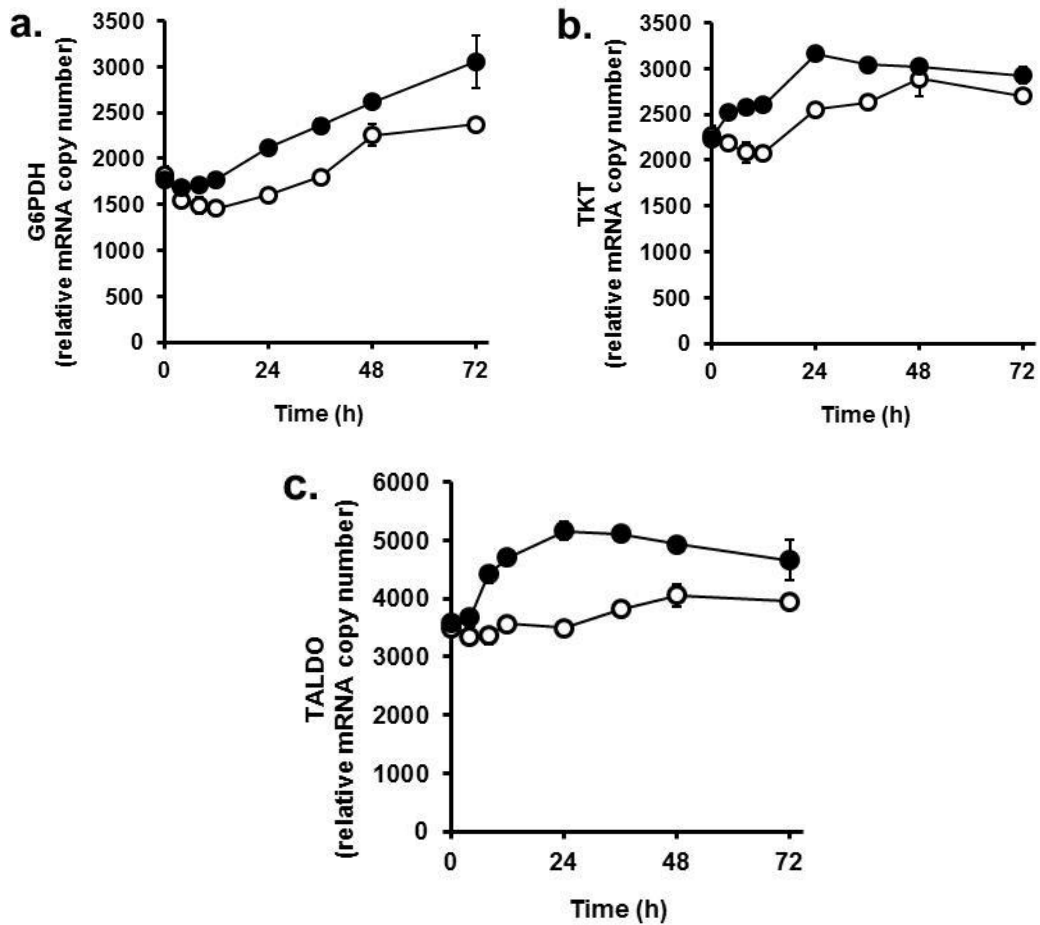


Figure 69. Gene expression of MRC-5 fibroblasts induced by sulforaphane. Nanostring study. Pentophosphate pathway genes.

a. Glucose-6-phosphate dehydrogenase G6PDH. b. Transketolase TKT. c. Transaldolase TALDO. Key: ○—○, control; ●—●, + 1 μM SFN. Data are mean ± SD, n = 3.

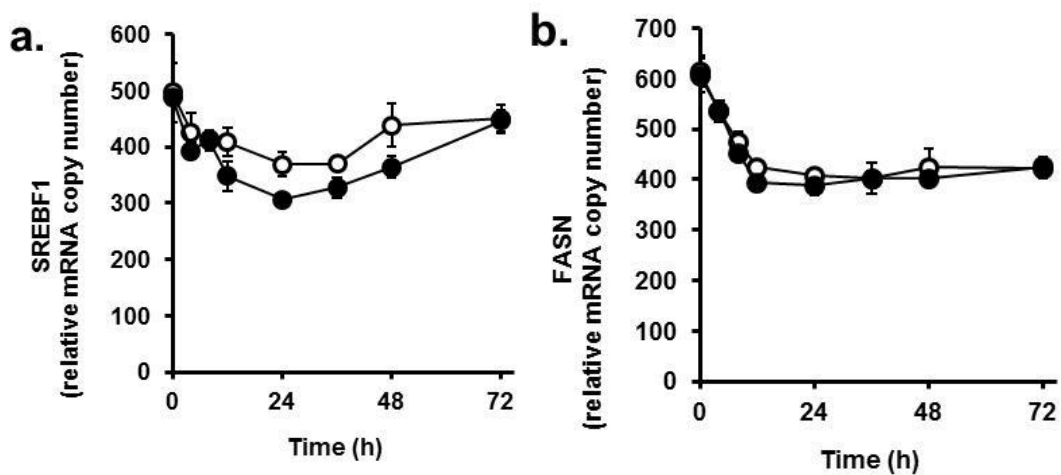


Figure 70. Gene expression of MRC-5 fibroblasts induced by sulforaphane. Nanostring study. Lipogenic and glycolytic regulation genes.

a. Sterol response element binding factor-1 (SREBF1). b. Fatty acid synthase (FASN). Key: ○—○, control; ●—●, + 1 μM SFN. Data are mean ± SD, n = 3.

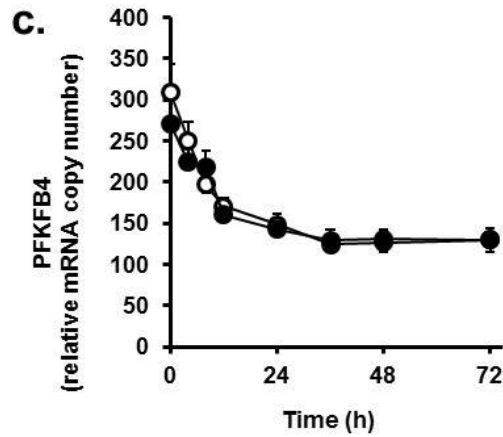


Figure 70. Gene expression of MRC-5 fibroblasts induced by sulforaphane. Nanostring study. Lipogenic and glycolytic regulation genes (cont'd).
 c. Fructose-2,6-bisphosphate kinase-4 (PFKFB4). Key: ○-○, control; ●-●, + 1 μM SFN. Data are mean ± SD, n = 3.

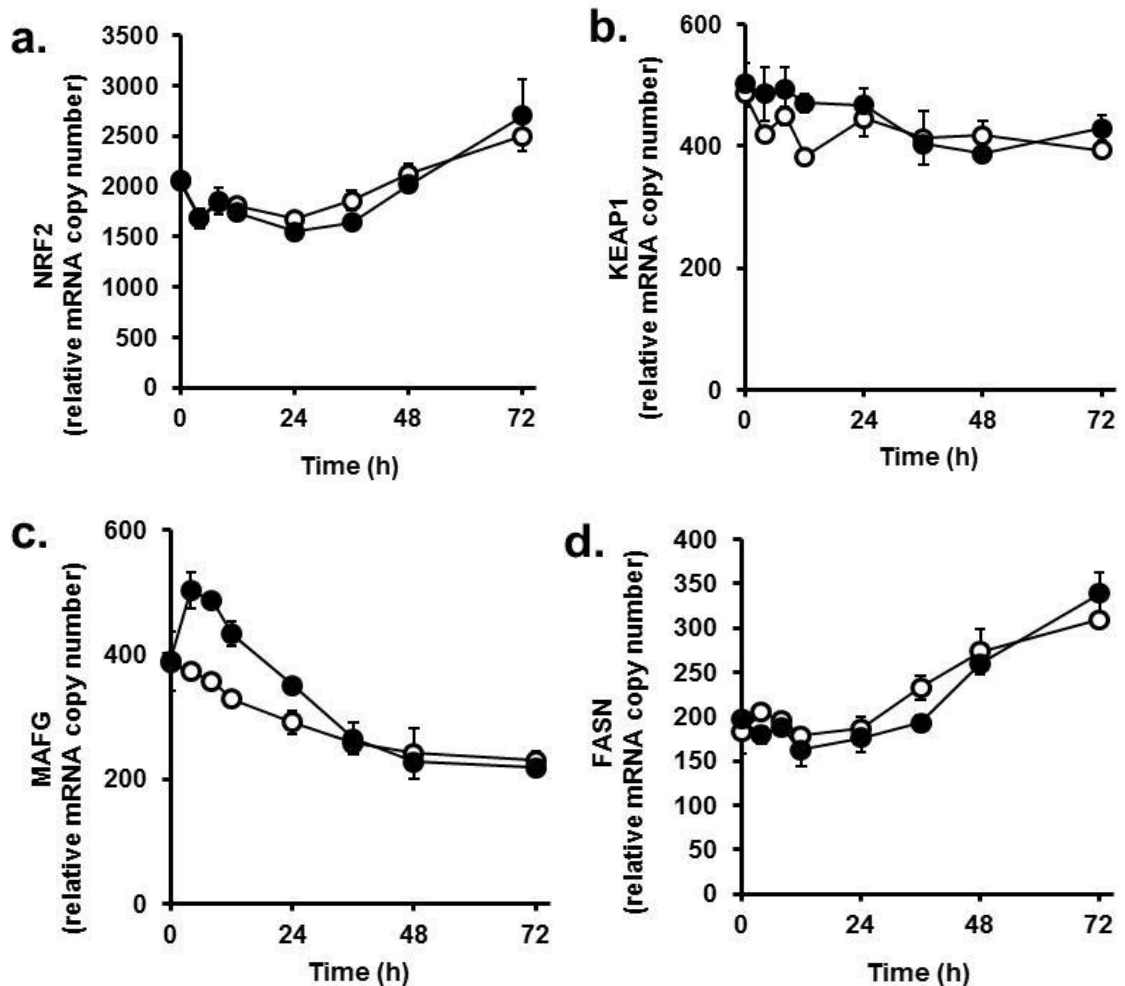


Figure 71. Gene expression of MRC-5 fibroblasts induced by sulforaphane. Nanostring study. Nrf2 regulation genes.
 a. Nrf2. b. Keap1. c. Small maf protein-G MAFG. d. Fyn kinase FYN. Key: ○-○, control; ●-●, + 1 μM SFN. Data are mean ± SD, n = 3.

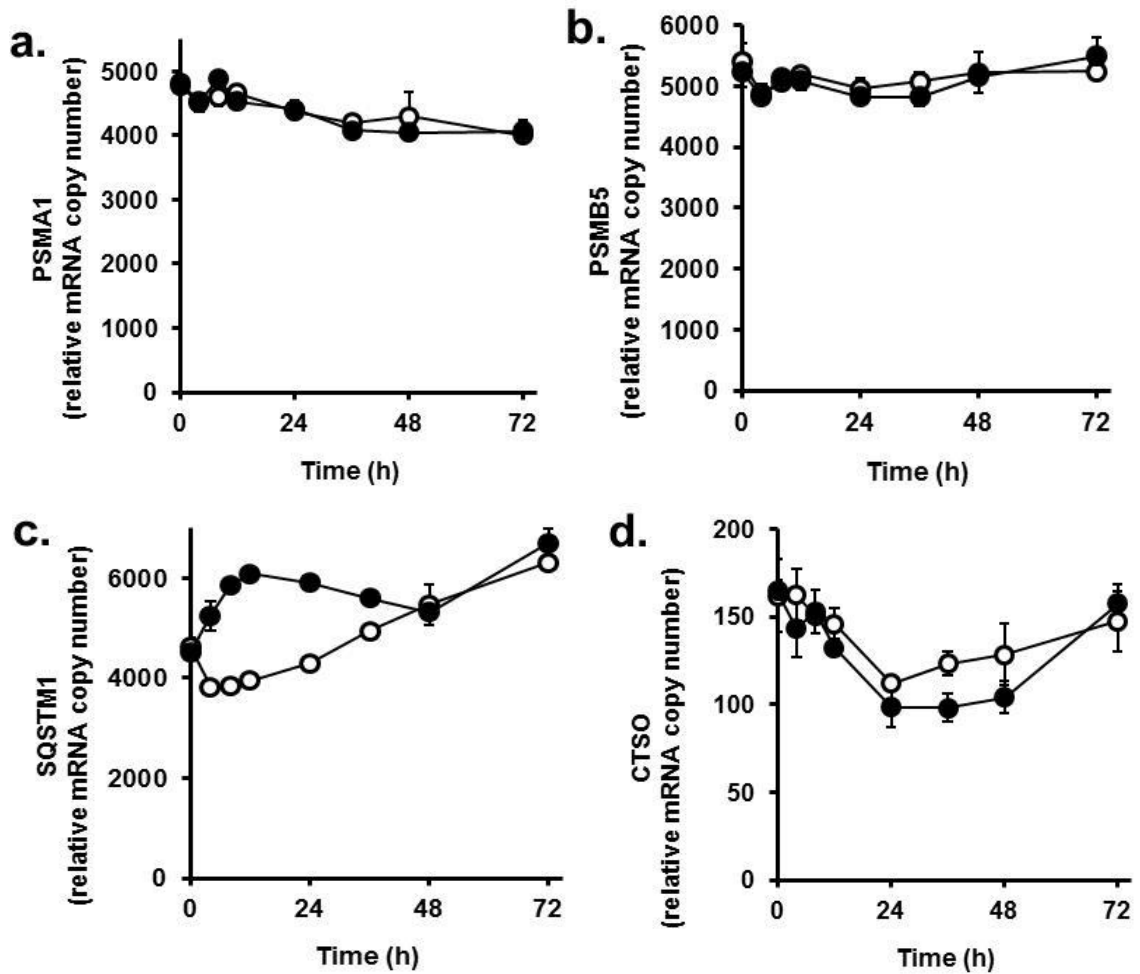


Figure 72. Gene expression of MRC-5 fibroblasts induced by sulforaphane. Nanostring study. Proteolysis related genes.

a. Proteasomal subunit A1 (PSMA1). b. Proteasomal subunit B5 (PSMB5). c. Sequestosome-1/p62 (SQSTM1). d. Cathepsin O (CTSO). Key: ○—○, control; ●—●, + 1 μ M SFN. Data are mean \pm SD, n = 3.

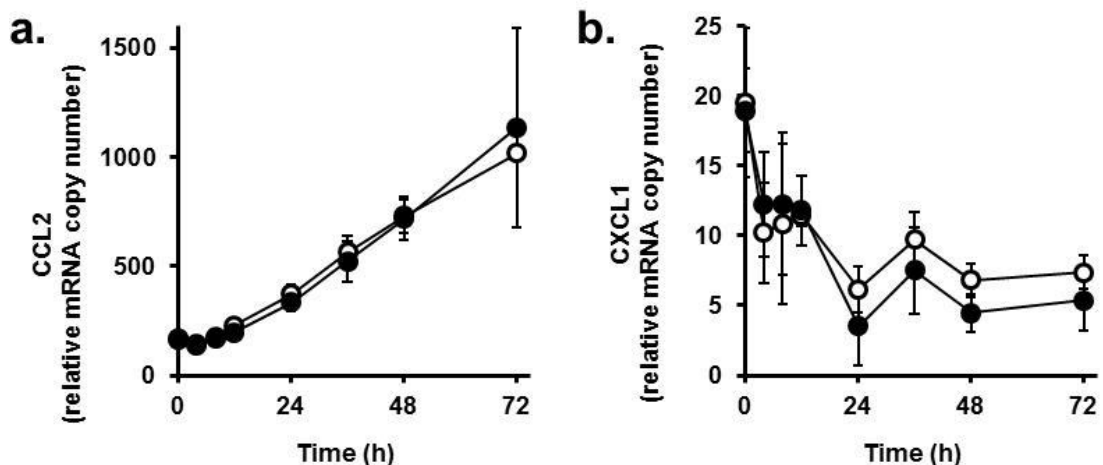


Figure 73. Gene expression of MRC-5 fibroblasts induced by sulforaphane. Nanostring study. Inflammatory/immune response genes.

a. Monocyte chemoattractant protein-1 (CCL2). b. Chemokine (C-X-C motif) ligand 1 (CXCL1). Key: ○—○, control; ●—●, + 1 μ M SFN. Data are mean \pm SD, n = 3.

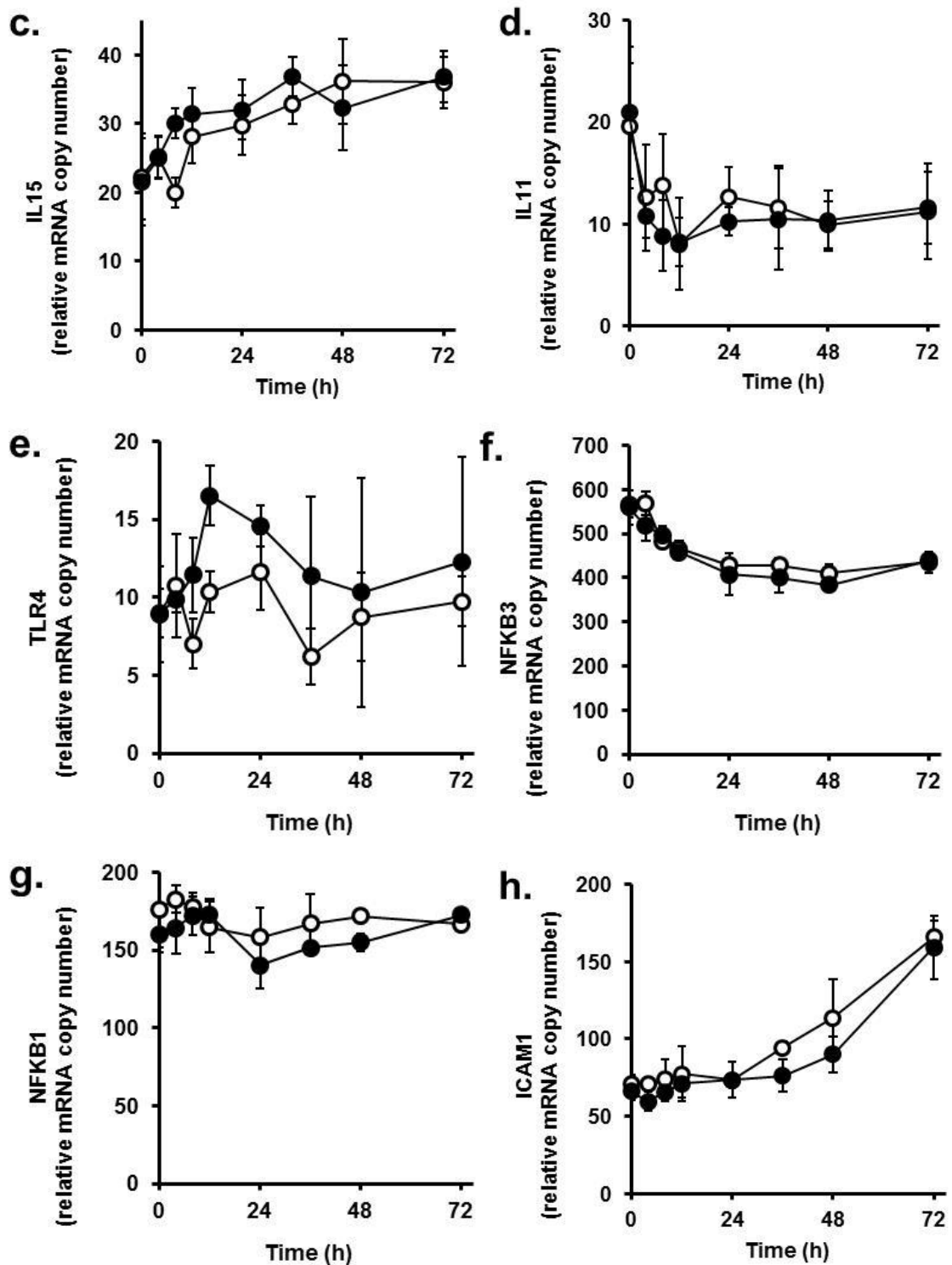


Figure 73. Gene expression of MRC-5 fibroblasts induced by sulforaphane. Nanostring study. Inflammatory/immune response genes (cont'd).
 c. Interleukin-15 (IL15). d. Interleukin 1 β 1 (IL1). e. Toll-like receptor 4 (TLR4), f. Transcription factor p65 (NFKB3), g. Nuclear factor NF-kappa-B p105 subunit/p50 (NFKB1), h. Intracellular adhesion molecule-1 (ICAM1). Key: ○—○, control; ●—●, + 1 μ M SFN. Data are mean \pm SD, n = 3.

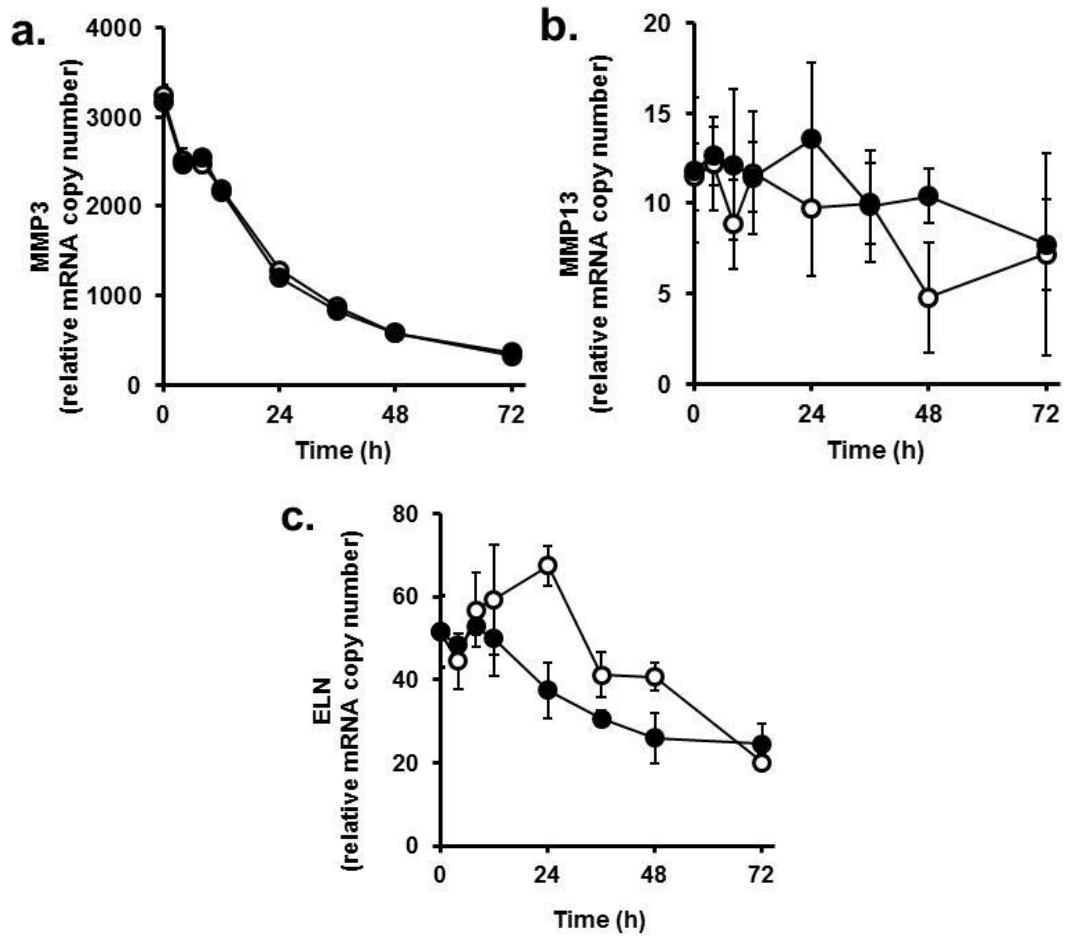


Figure 74. Gene expression of MRC-5 fibroblasts induced by sulforaphane. Nanostring study. Extracellular matrix regulating genes.

a. Matrix metalloproteinase-3 (MMP3). b. Matrix metalloproteinase-13 (MMP13). c. Elastin (ELN). Key: ○—○, control; ●—●, +1 μM SFN. Data are mean ± SD, n = 3.

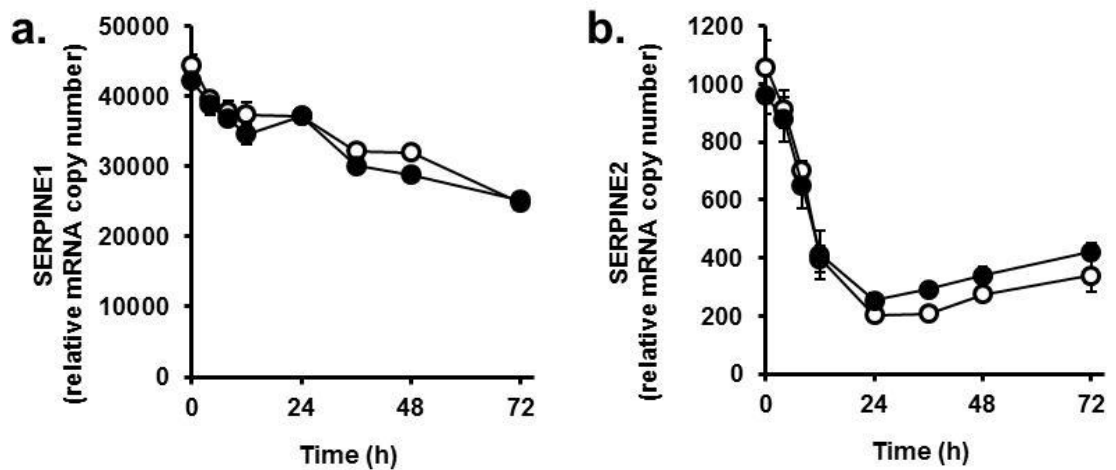


Figure 75. Gene expression of MRC-5 fibroblasts induced by sulforaphane. Nanostring study. Serpines.

a. Plasminogen activator inhibitor-1 (SERPINE1). b. Plasminogen activator inhibitor-2 (SERPINE2). Key: ○—○, control; ●—●, +1 μM SFN. Data are mean ± SD, n = 3.

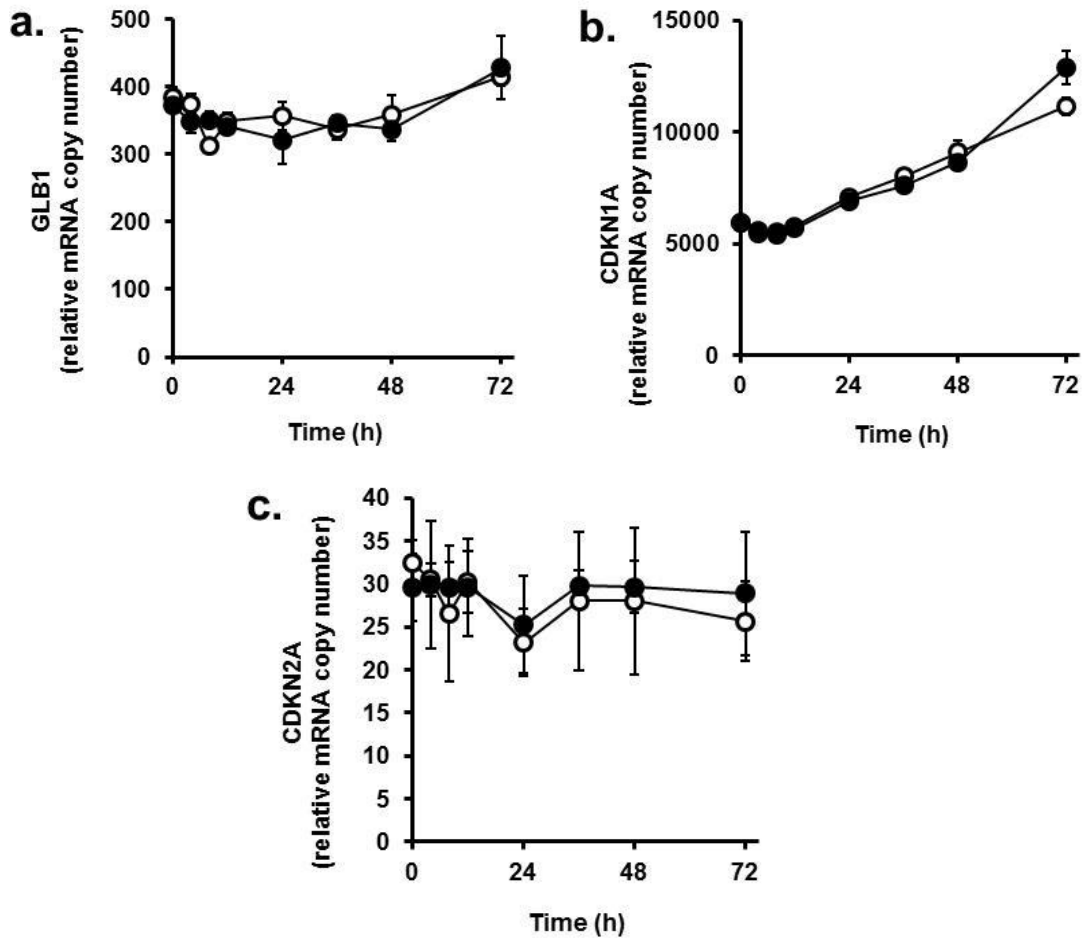


Figure 76. Gene expression of MRC-5 fibroblasts induced by sulforaphane. Nanostring study Senescence-associated genes.

a. β -Galactosidase (GLB1). b. Cyclin-dependent kinase inhibitor 1/p21 (CDKN1A). c. Cyclin-dependent kinase inhibitor 2A/P16INK4a (CDKN2A).

Key: ○—○, control; ●—●, + 1 μ M SFN. Data are mean \pm SD, n = 3.

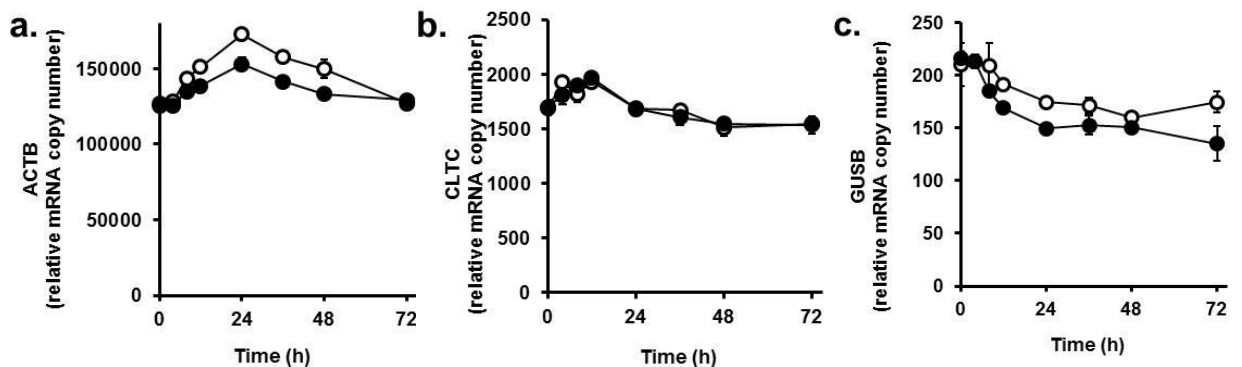


Figure 77. Gene expression of MRC-5 fibroblasts induced by sulforaphane. Nanostring study Reference genes.

a. β -Actin (ACTB). b. Clathrin, heavy chain (CLTC). c. β -glucuronidase (GUSB).

Key: ○—○, control; ●—●, + 1 μ M SFN. Data are mean \pm SD, n = 3.

4.2 Characterization of gene expression and cell metabolism in cells escaping senescence by treatment with sulforaphane and hesperetin.

The changes in gene expression induced by 1 μ M SFN and 5 μ M HESP in young and senescent MRC-5 cells in vitro was investigated by quantifying mRNA of genes of selected metabolic pathways with Nrf2 regulated, ARE-linked genes by the Nanostring method – quantifying relative mRNA copy number. The outputs are given in Table 29 and 30 and most significant changes genes of interest are shown in Figures 78 and 79. The reference gene was clathrin (heavy chain) only as β -actin and β -glucosidase has been shown to change with senescence. Moreover, following analysis of data using a 2-tailed T-test, a Bonferroni correction of 49 was applied in order to account for multiple comparison errors. The Bonferroni correction was set to 49 as the number of genes used for comparison was 49 and did not include the reference gene clathrin in the analysis.

At late passage, when a Bonferroni correction factor of 49 was applied ($P < 0.001$), there was a significant increase in mRNA of the anti-oxidant related gene GCLM in the SFN treatment compared to control. Moreover, using the same inclusion criteria for significance, mRNA of the pentose-phosphate pathway gene glucose-6-phosphate dehydrogenase was significantly ($P < 0.001$) increased in the treatment group compared to the control. The same effect was seen in the expression of the nutrient sensing thioredoxin interacting protein (TXNIP) which was increased by more than 2-fold. Moreover, expression of the extracellular matrix regulator collagen 1-alpha (COL1A1) was significantly increased (Bonferroni correction 49, $P < 0.001$) in the SFN treated group compared to control by 0.5 fold.

Finally the following observations can be made regarding gene expression of both treatment and control in senescence when compared to control at passage 3 with a Bonferroni correction factor of 49 and significance of $P < 0.001$: expression of beta-glucuronidase (GUSB) was significantly halved at passage 11 for both groups compared to control at passage 3. Moreover, expression of the anti-glycation related gene aldoketoreductase 1C1 was reduced by two thirds in both groups at late passage compared to control at passage 3. Expression of the anti-

oxidant related gene GCLM was increased by 3 folds in late passage for the SFN treated group compared to control at early passage. Expression of the anti-oxidant related gene ferritin (FTH1) of both control and treatment group at late passage was halved compared control at passage 3. Moreover, mRNA of the lipogenesis related gene sterol response element binding protein (SREBF1) was decreased by two-thirds in both groups at late passage compared to control at passage 3. Expression of the proteasome subunit gene sequestosome 1 was significantly (Bonferroni correction 49, $P < 0.001$) decreased at late passage by 3 folds in both groups compared to control at early passage.

When Bonferroni correction of 49 ($P < 0.001$) was applied, expression of the antiglycation-related gene glyoxalase 1 (GLO1) did not change with treatment or approach of senescence. This was also the case for the antioxidant-related gene gamma-glutamyl-cys ligase-catalytic subunit (GCLC), the anti-oxidant related gene superoxide dismutase-1 (SOD1), the phase II conjugation gene glutathione conjugate transporter (ABCC2) UDP glucuronosyltransferase (Mrp2/UGT1A1), the inflammatory and immune response genes toll-like receptor 4 (TLR4) and transcription factor p65 (NFkB3) as well as the matrix regulating gene collagenase-3/matrix metalloproteinase-13 (MMP13).

Table 29. Relative mRNA copy number in young (Passage 3) and senescent (Passage 11) MRC-5 fibroblasts with or without treatment with 1 μ M SFN.

Data are presented as mean \pm SD. (n=3)

Gene	Passage 3		Passage 11	
	0.002% DMSO	1 μ M SFN	0.002% DMSO	1 μ M SFN
ACTB	129212 \pm 8628	126896 \pm 10147	89335 \pm 1834	97683 \pm 2191
GUSB	502 \pm 10	444 \pm 29	230 \pm 14 ‡	219 \pm 14 ‡
Anti-glycation related genes				
AKR1C1	3751 \pm 88	5816 \pm 128	1049 \pm 44 ‡	1525 \pm 30 ‡, \diamond
GLO1	1690 \pm 22	1725 \pm 53	1659 \pm 11	1707 \pm 6
Anti-oxidant related genes				
CAT	1199 \pm 50	1188 \pm 62	1420 \pm 29	1725 \pm 64
GCLC	884 \pm 68	857 \pm 2	818 \pm 57	973 \pm 65
GCLM	1579 \pm 108	2033 \pm 67	2610 \pm 7	3490 \pm 41 †, ‡, \diamond
NQO1	4887 \pm 200	6947 \pm 244	3572 \pm 45	5432 \pm 135
TXNRD1	14250 \pm 490	17271 \pm 881	12429 \pm 148	15237 \pm 279
TXN	14505 \pm 332	18269 \pm 807	11887 \pm 151	14742 \pm 298
GSR	1736 \pm 46	2033 \pm 20	1258 \pm 47	1532 \pm 14 \diamond
HMOX1	2104 \pm 118	2435 \pm 35	789 \pm 44	1033 \pm 24 \diamond
SOD1	421 \pm 40	457 \pm 11	331 \pm 13	361 \pm 8
PRDX1	24708 \pm 460	27887 \pm 790	26675 \pm 224	29312 \pm 395
GPX1	2477 \pm 165	2377 \pm 136	1707 \pm 65	1982 \pm 30
FTH1	288261 \pm 8554	349031 \pm 14995	143852 \pm 1002 ‡	159043 \pm 1797 ‡

Phase II conjugation genes				
GSTP1	10935 ± 635	10783 ± 938	6166 ± 150	8053 ± 132
Mrp2/UGT1A1	83 ± 24	68 ± 11	35 ± 3	40 ± 8
Pentosephosphate pathway genes				
TALDO1	6283 ± 129	7292 ± 309	5589 ± 94	6666 ± 28
TKT	6369 ± 430	6384 ± 234	2288 ± 68	2836 ± 47
G6PD	6458 ± 285	7895 ± 278	3036 ± 28	3768 ± 42 [†]
Lipogenesis related genes				
SREBF1	1492 ± 58	1329 ± 194	390 ± 18 [‡]	335 ± 17 [‡]
FASN	2267 ± 71	2220 ± 84	591 ± 22 [‡]	628 ± 8
Nutrient sensing				
PFKFB2	58 ± 10	79 ± 16	25 ± 1	26 ± 3
TXNIP	345 ± 9	356 ± 43	2864 ± 130 [‡]	7076 ± 96 ^{†,◇}
MLXIP	904 ± 114	961 ± 39	518 ± 32	534 ± 4
MLX	1222 ± 11	1264 ± 37	1128 ± 52	1125 ± 20
HIF1A	6084 ± 405	5702 ± 200	5913 ± 124	7236 ± 125
HK1	2078 ± 86	2229 ± 92	1500 ± 42	1529 ± 30
Nrf2 regulation related genes				
NFE2L2	2468 ± 85	2452 ± 81	2808 ± 5	3439 ± 76
KEAP1	289 ± 39	297 ± 23	169 ± 21	169 ± 13
MAFG	691 ± 97	747 ± 53	406 ± 36	386 ± 17

Proteasome subunits genes (protein turnover)				
PSMA1	7060 ± 132	7055 ± 480	5783 ± 68	5622 ± 65
PSMB5	3833 ± 83	4034 ± 59	5291 ± 11	5533 ± 69 †, ◇
SQSTM1	13389 ± 545	14990 ± 764	3881 ± 85 †	3331 ± 57 †, ◇
Inflammatory and immune response genes				
CCL2	904 ± 73	904 ± 92	2150 ± 32 †	1710 ± 52
TLR4	100 ± 38	81 ± 17	33 ± 3	52 ± 7
NFKB1	241 ± 20	235 ± 27	157 ± 13	181 ± 14
NFKB3	368 ± 23	370 ± 25	405 ± 18	402 ± 38
ICAM1	3014 ± 260	2695 ± 53	1604 ± 9	1132 ± 43 ◇
Extracellular matrix				
COL1A1	13812 ± 1079	11901 ± 222	9964 ± 54	12635 ± 75 †
Matrix regulating genes				
MMP1	1096 ± 146	1061 ± 102	986 ± 39	3806 ± 117 †, ‡, ◇
MMP13	31 ± 14	27 ± 7	25 ± 2	24 ± 3
MMP3	86 ± 18	81 ± 13	268 ± 14	339 ± 17
SOD2	14696 ± 134	14842 ± 266	9212 ± 86 †	9362 ± 148 †, ◇
ELN	57 ± 11	21 ± 8	16 ± 3	25 ± 4
Plasminogen activator inhibitor genes				
SERPINB2	2467 ± 339	2828 ± 97	603 ± 24	769 ± 35 ◇

Senescence-associated genes				
CDKN1A	20515 ± 207	22929 ± 968	18695 ± 566	18543 ± 184
GLB1	1835 ± 215	1644 ± 51	1314 ± 43	1292 ± 29

† Significance with respect to treatment control, $p < 0.001$, Bonferroni Correction of 49

‡ Significance with respect to P3 control, $p < 0.001$, Bonferroni Correction of 49

◇ Significance with respect to P3 treated, $p < 0.001$, Bonferroni Correction of 49

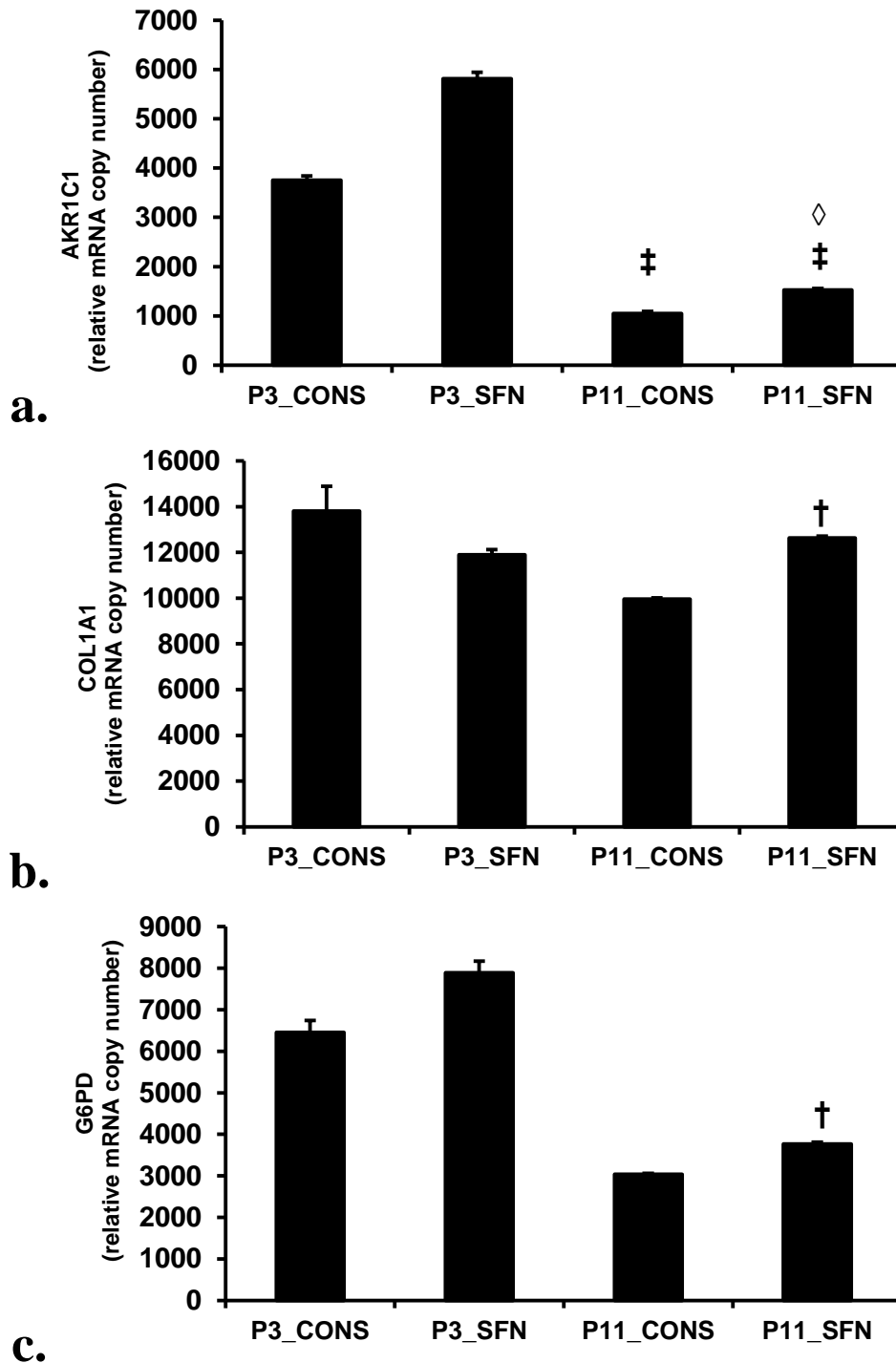


Figure 78. Relative mRNA copy number in young (Passage 3) and senescent (Passage 11) MRC-5 fibroblasts with or without treatment with 1µM SFN after Bonferroni correction of 49.

Data are presented as mean \pm SD. (n=3). a. aldo-ketoreductase 1C1. b. collagen 1-alpha. c. glucose-6-phosphate dehydrogenase. Significance: †, significance with respect to treatment control, $P < 0.001$, Bonferroni Correction of 49; ‡, significance with respect to passage 3 control, $P < 0.001$, Bonferroni Correction of 49; and ◇, significance with respect to passage 3 treated, $P < 0.001$, Bonferroni Correction of 49.

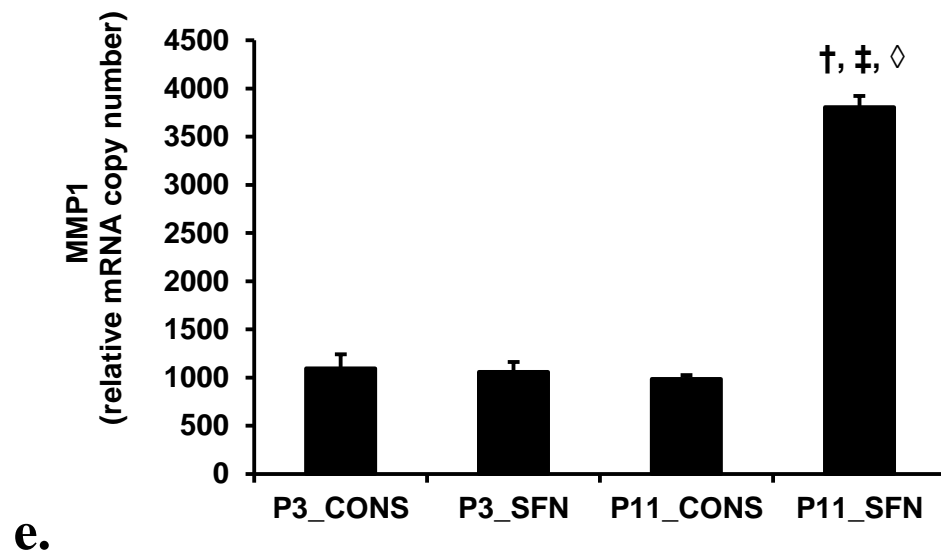
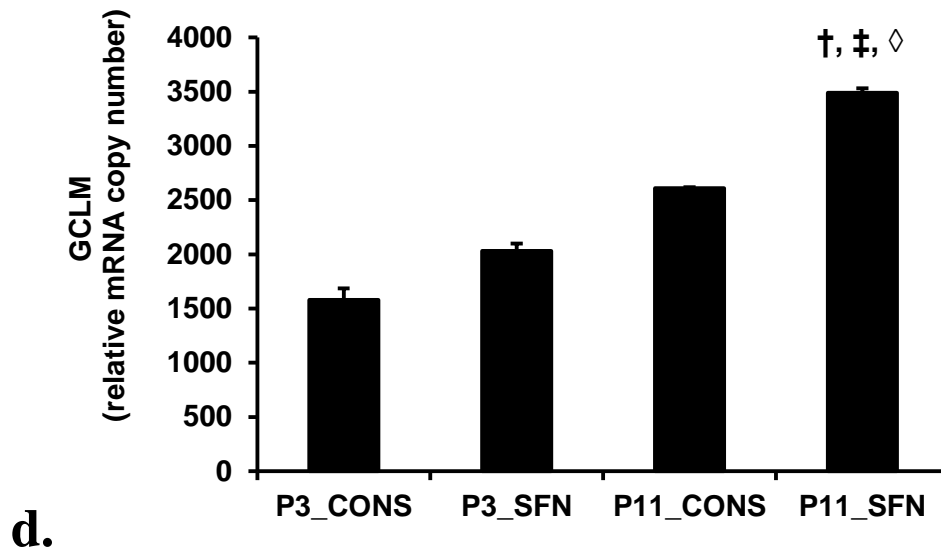


Figure 78. Relative mRNA copy number in young (Passage 3) and senescent (Passage 11) MRC-5 fibroblasts with or without treatment with 1µM SFN after Bonferroni correction of 49 (cont').

Data are presented as mean \pm SD. (n=3).d. gamma-glutamyl-cys-ligase modulatory subunit. e. fibroblast collagenase/matrix metalloproteinase-1. Significance: †, significance with respect to treatment control, P<0.001, Bonferroni Correction of 49; ‡, significance with respect to passage 3 control, P<0.001, Bonferroni Correction of 49; and ◇, significance with respect to passage 3 treated, P<0.001, Bonferroni Correction of 49.

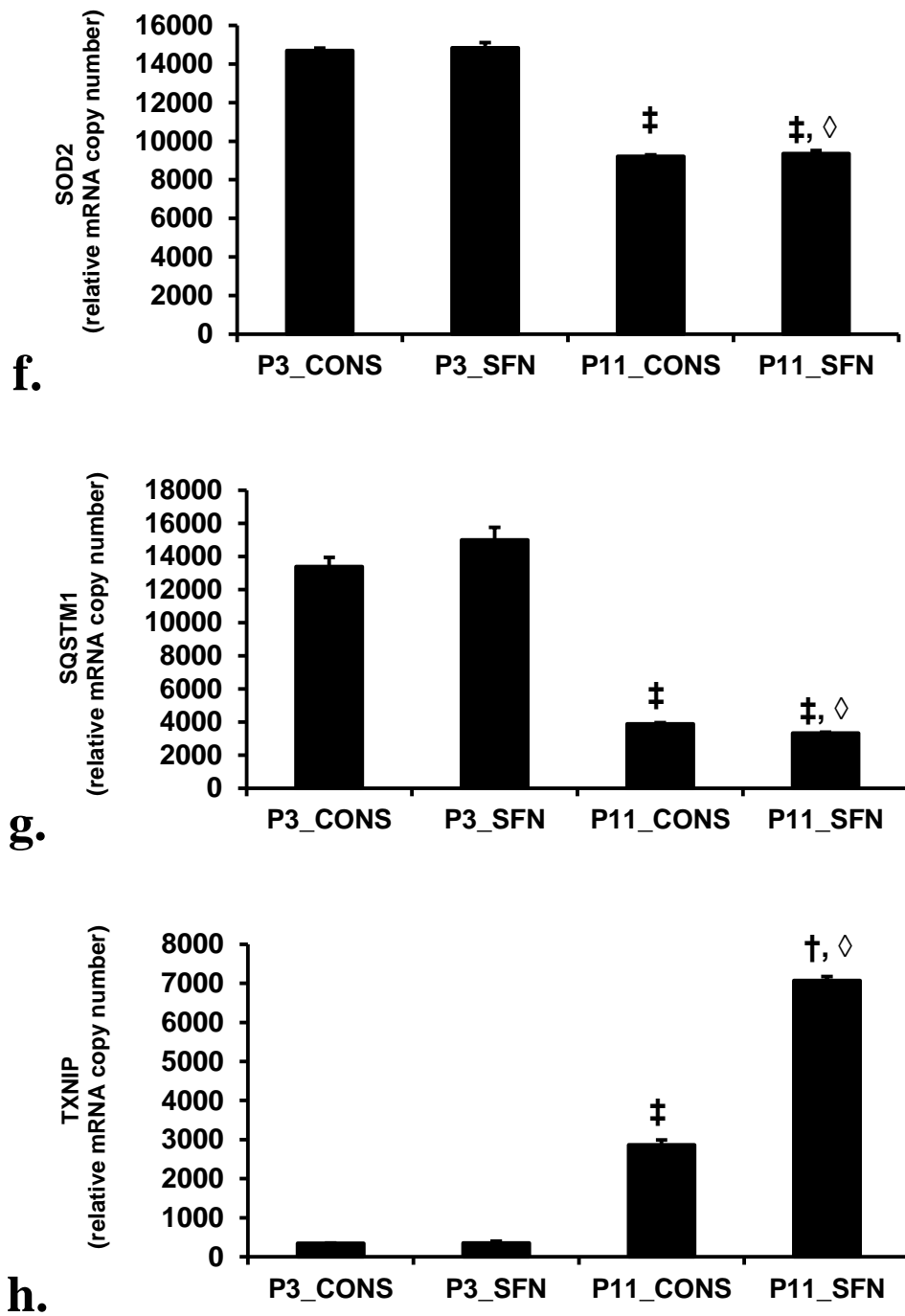


Figure 78. Relative mRNA copy number in young (Passage 3) and senescent (Passage 11) MRC-5 fibroblasts with or without treatment with 1 μ M SFN after Bonferroni correction of 49 (cont').

Data are presented as mean \pm SD. (n=3).f. mitochondrial superoxide dismutase. g. sequestome 1. h. thioredoxin interacting protein. Significance: †, significance with respect to treatment control, P<0.001, Bonferroni Correction of 49; ‡, significance with respect to passage 3 control, P<0.001, Bonferroni Correction of 49; and ◇, significance with respect to passage 3 treated, P<0.001, Bonferroni Correction of 49.

At late passage, when a Bonferroni correction factor of 49 was applied ($P < 0.001$), there was no significant change in mRNA in the HESP treatment compared to control at passage 9. The following observations can be made regarding gene expression of both treatment and control in senescence when compared to control at passage 3 with a Bonferroni correction factor of 49 and significance of $P < 0.001$: expression of the anti-oxidant related gene quinone reductase (NQO1) was decreased by two-fold at passage 11 for both groups compared to control at passage 3. Moreover, expression of the anti-oxidant related gene heme oxygenase (HMOX) was decreased by two-fold in the control group at passage 9 compared to control at passage 3. Expression of the anti-oxidant related gene ferritin (FTH1) was also decreased two-fold in late passage for the SFN treated group compared to control at early passage. Expression of the pentosephosphate pathway gene glucose-6-phosphate dehydrogenase (G6PD) of both control and treatment group at late passage was halved compared control at passage 3.

When Bonferroni correction of 49 ($P < 0.001$) was applied, expression of the anti-oxidant-related gene gamma-glutamyl-cys ligase-catalytic subunit (GCLC) did not change with treatment or approach of senescence. Similar observations were made for the phase II conjugation gene Mrp2/UGT1A1, the nutrient sensing gene Max-Like BHLHZip Protein 2 (MLX), the inflammatory and immune response gene toll-like receptor 4 (TLR4) and transcription factor p65 (NFkB3), the matrix regulating genes collagenase-3/matrix metalloproteinase-13 (MMP13) and elastin (ELN).

Table 30. Relative mRNA copy number in young (Passage 3) and senescent (Passage 9) MRC-5 fibroblasts with or without treatment with 5 μ M HESP.

Data are presented as mean \pm SD. (n=3)

Gene	Passage 3		Passage 9	
	0.005% DMSO	5 μ M HESP	0.005% DMSO	5 μ M HESP
ACTB	73589 \pm 8634	74576 \pm 4894	89839 \pm 7803	99619 \pm 2711
GUSB	359 \pm 37	320 \pm 32	185 \pm 13	175 \pm 5
Anti-glycation related genes				
AKR1C1	3924 \pm 71	3979 \pm 64	2231 \pm 280	1395 \pm 180 \diamond
GLO1	2016 \pm 131	2319 \pm 83	1952 \pm 147	1961 \pm 69
Anti-oxidant related genes				
CAT	1283 \pm 30	1236 \pm 40	1904 \pm 187	2047 \pm 182
GCLC	849 \pm 74	767 \pm 17	867 \pm 53	784 \pm 48
GCLM	1747 \pm 22	1616 \pm 59	3721 \pm 177	3094 \pm 244
NQO1	6629 \pm 211	6612 \pm 249	3401 \pm 109 \ddagger	2378 \pm 161 \diamond
TXNRD1	19382 \pm 140	20450 \pm 823	16797 \pm 1005	14174 \pm 220 \ddagger
TXN	22420 \pm 715	21366 \pm 905	17633 \pm 116	16311 \pm 306
GSR	2141 \pm 29	2309 \pm 82	1494 \pm 52	1388 \pm 83
HMOX1	3830 \pm 73	3884 \pm 41	1975 \pm 93 \ddagger	1879 \pm 240
SOD1	319 \pm 11	363 \pm 9	356 \pm 36	354 \pm 5
PRDX1	23285 \pm 348	22749 \pm 444	30248 \pm 1430	28249 \pm 970
GPX1	1541 \pm 52	1589 \pm 65	2936 \pm 606	3025 \pm 517

FTH1	426109 ± 4407	463248 ± 11526	285456 ± 10673	249220 ± 5761 ‡, ◇
Phase II conjugation genes				
GSTP1	7884 ± 160	8646 ± 355	9154 ± 1101	8518 ± 422
Mrp2/UGT1A1	52 ± 16	56 ± 6	49 ± 8	51 ± 1
Pentosephosphate pathway genes				
TALDO1	6560 ± 150	6916 ± 183	5878 ± 162	4824 ± 242
TKT	6889 ± 273	7833 ± 730	2784 ± 262	2604 ± 118 ‡
G6PD	6382 ± 62	6197 ± 271	3387 ± 178 ‡	2793 ± 178 ‡
Lipogenesis related genes				
SREBF1	1119 ± 28	1171 ± 51	388 ± 62	354 ± 29 ‡, ◇
FASN	1668 ± 120	1990 ± 110	698 ± 22	623 ± 71
Nutrient sensing				
PFKFB2	76 ± 3	81 ± 11	27 ± 7	33 ± 2
TXNIP	90 ± 8	67 ± 10	2849 ± 1769	3619 ± 1636
MLXIP	821 ± 59	802 ± 59	684 ± 37	654 ± 51
MLX	1136 ± 20	1131 ± 36	1157 ± 77	1191 ± 30
HIF1A	7963 ± 415	7590 ± 376	8168 ± 334	9289 ± 439
HK1	1918 ± 143	1887 ± 124	1501 ± 92	1461 ± 32
Nrf2 regulation related genes				
NFE2L2	4026 ± 167	3368 ± 60	4137 ± 306	3133 ± 203
KEAP1	220 ± 21	223 ± 35	164 ± 22	160 ± 20
MAFG	743 ± 57	718 ± 75	354 ± 27	353 ± 30

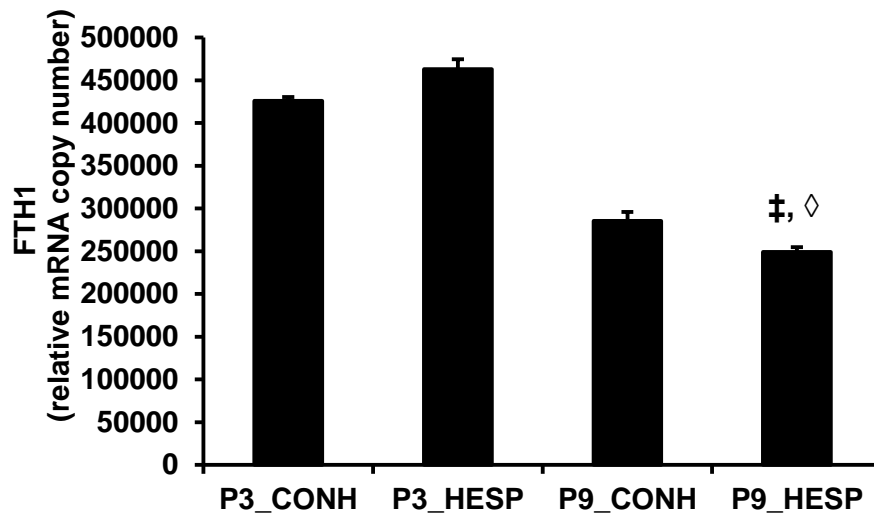
Proteasome subunits genes (protein turnover)				
PSMA1	6969 ± 99	7161 ± 97	5460 ± 198	5421 ± 137
PSMB5	5465 ± 102	5513 ± 132	6669 ± 401	6786 ± 510
SQSTM1	17334 ± 585	19138 ± 636	5968 ± 383 ‡	5232 ± 431 ‡, ◇
Inflammatory and immune response genes				
CCL2	416 ± 77	377 ± 27	2068 ± 395	1404 ± 165
TLR4	55 ± 7	52 ± 14	56 ± 5	48 ± 9
NFKB1	263 ± 16	292 ± 49	209 ± 8	196 ± 13
NFKB3	415 ± 6	428 ± 26	410 ± 12	443 ± 31
ICAM1	2505 ± 137	2854 ± 272	988 ± 59	727 ± 47
Extracellular matrix				
COL1A1	4844 ± 764	3420 ± 463	16782 ± 652	19684 ± 3027
Matrix regulating genes				
MMP1	489 ± 12	474 ± 10	358 ± 77	321 ± 92
MMP13	19 ± 5	19 ± 3	25 ± 4	24 ± 8
MMP3	19 ± 3	22 ± 1	252 ± 38	177 ± 29
SOD2	19182 ± 458	24861 ± 642	11510 ± 327 ‡	10368 ± 725 ◇
ELN	18 ± 6	15 ± 4	15 ± 3	16 ± 6
Plasminogen activator inhibitor genes				
SERPINB2	1112 ± 105	785 ± 13	748 ± 185	327 ± 70

Senescence-associated genes				
CDKN1A	21791 ± 366	21157 ± 864	22774 ± 1545	22812 ± 454
GLB1	1256 ± 51	1178 ± 14	1433 ± 52	1332 ± 28

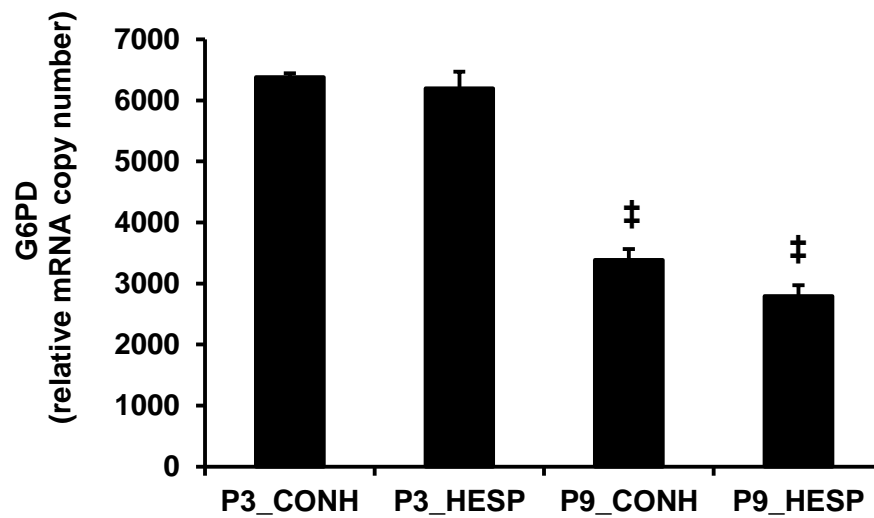
† Significance with respect to treatment control, $p < 0.001$, Bonferroni Correction of 49

‡ Significance with respect to P3 control, $p < 0.001$, Bonferroni Correction of 49

◇ Significance with respect to P3 treated, $p < 0.001$, Bonferroni Correction of 49



a.



b.

Figure 79. Relative mRNA copy number in young (Passage 3) and senescent (Passage 9) MRC-5 fibroblasts with or without treatment with 5µM HESP after Bonferroni correction of 49.

Data are presented as mean \pm SD. (n=3). a. ferritin. b. glucose-6-phosphate dehydrogenase. Significance: ‡, significance with respect to passage 3 control, $P < 0.001$, Bonferroni Correction of 49; and ◇, significance with respect to passage 3 treated, $P < 0.001$, Bonferroni Correction of 49.

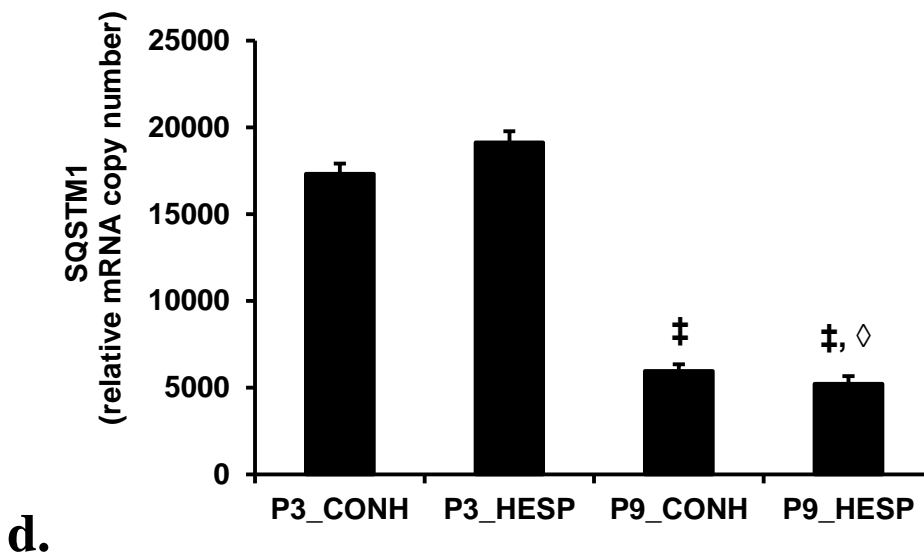
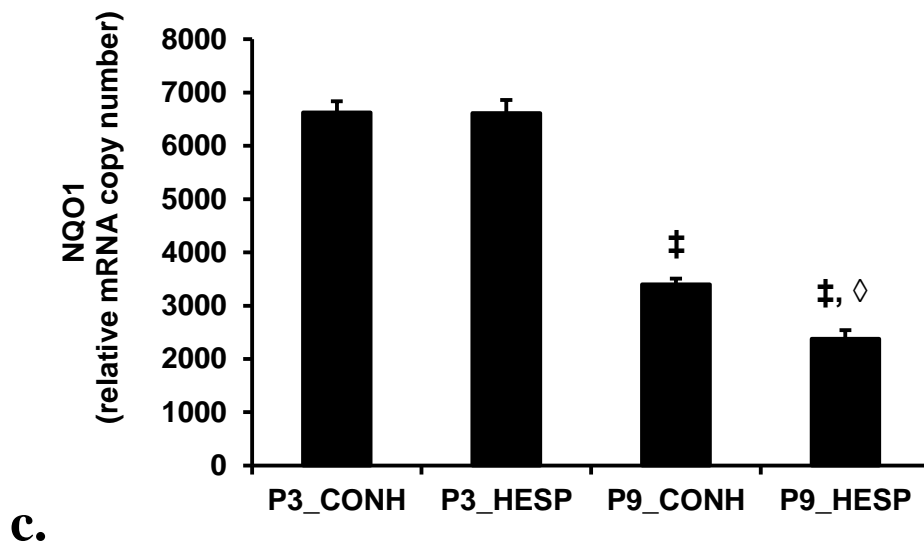


Figure 79. Relative mRNA copy number in young (Passage 3) and senescent (Passage 9) MRC-5 fibroblasts with or without treatment with 5µM HESP after Bonferroni correction of 49 (cont').

Data are presented as mean \pm SD. (n=3).c. quinone reductase. d. sequestosome 1. Significance: ‡, significance with respect to passage 3 control, $P < 0.001$, Bonferroni Correction of 49; and ◇, significance with respect to passage 3 treated, $P < 0.001$, Bonferroni Correction of 49.

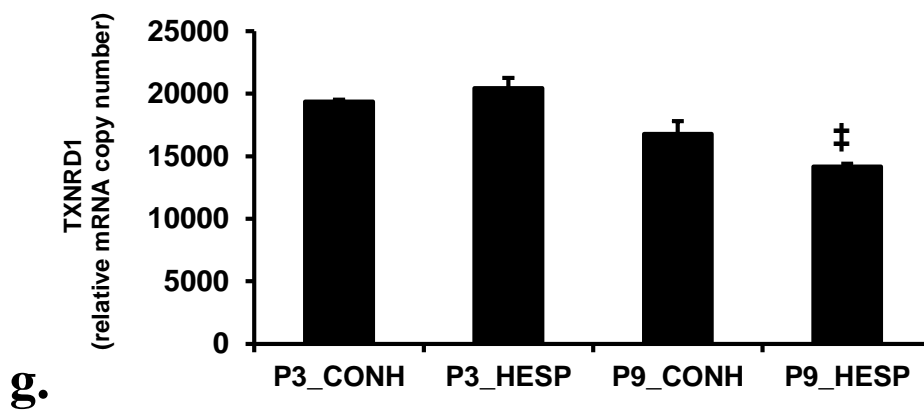
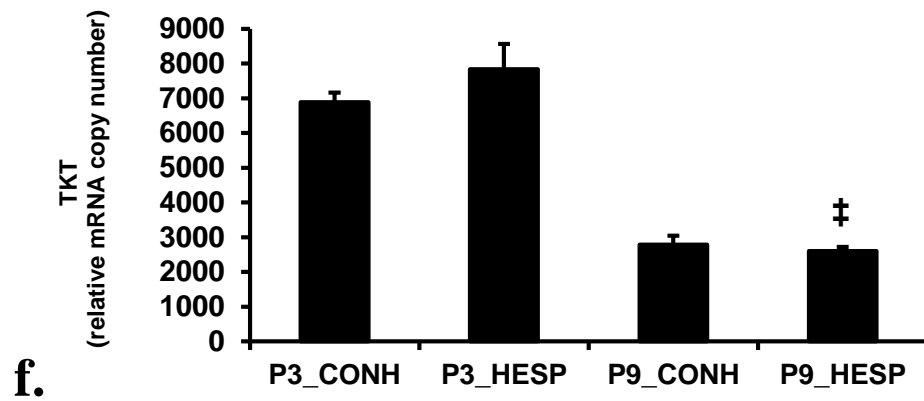
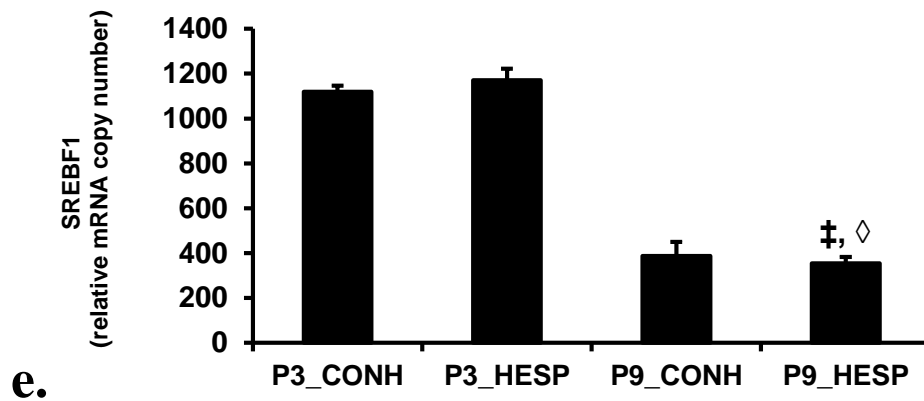


Figure 79. Relative mRNA copy number in young (Passage 3) and senescent (Passage 9) MRC-5 fibroblasts with or without treatment with 5µM HESP after Bonferroni correction of 49 (cont').

Data are presented as mean \pm SD. (n=3). e. sterol response element binding protein-1. f. transketolase. g. thioredoxin reductase-1. Significance: ‡, significance with respect to passage 3 control, $P < 0.001$, Bonferroni Correction of 49; and ◇, significance with respect to passage 3 treated, $P < 0.001$, Bonferroni Correction of 49.

4.3 Characterisation of gene expression in MRC-5 fibroblasts escaping senescence by treatment with sulforaphane using genome-wide microarray analysis

The changes in gene expression induced by 1 μ M SFN treatment in young (passage 3) and senescent (passage 11) MRC-5 cells in vitro was investigated by quantifying mRNA of 20773 genes throughout the whole human genome by the Microarray Agilent method – quantifying total RNA copy number. The outputs are given in Table 31, 32 and 33 in which the most significant changes in gene expression are shown. Moreover, following analysis of data using a 2-tailed T-test, a Bonferroni correction of 20773 was applied in order to account for multiple comparison errors and gene expression was assessed for regulation and downregulation using log₂ differential analysis. The Bonferroni correction was set to 20733 as this represents the number of genes used for comparison.

After Bonferroni factor of 20773 was applied ($P < 0.05$), there was no significant changes in gene expression between the treatment and control group at passage 3. Moreover, the colon-cancer secreted protein 1 (KIAA1199) was the only gene for which expression was significantly different in the treatment and control group at passage 11. Indeed, KIAA1199 was downregulated by 0.6 folds with SFN treatment compared to control in senescence.

Expression of 131 genes (Appendix E.) was significantly changed between controls at passage 3 and passage 11. Table 31 shows gene expression changes of the most significant genes. Indeed, expression of the DnaJ (Hsp40) homolog, subfamily C, member 6 (DNAJC6) was increased 6-fold with senescence in the control group compared to young fibroblasts. Moreover, expression of the C-C chemokine receptor type 11 (CCRL1) was increased 5-folds in the control at passage 11 compared to early passage control. Finally, expression of chemokine (C-X-C motif) ligand (CXCL2) was decreased by 3-folds and expression of Coiled-coil domain containing 144A (CCDC144A) was decreased by 4-fold in senescent controls compared to young controls.

Expression of 18 genes was significantly changed between SFN treated groups at passage 3 and passage 11. As seen in Table 32, all genes were significantly upregulated at passage 11 compared to passage 3 in SFN treated groups apart from Sad1 and UNC84 domain containing 1 (SUN1) which was downregulated by 0.7 folds with senescence. Expression of the C-C chemokine

receptor type 11 (CCRL1) and thioredoxin interacting protein (TXNIP) were amongst the highest upregulated genes in SFN treated senescent cells, increasing 5 and 7 folds respectively.

Expression of 274 genes (Appendix F.) was significantly changed between SFN treated groups at passage 11 and control at passage 3. Table 33 shows gene expression changes of the most significant genes. Indeed, SFN treatment in senescence showed a 5 and 7 fold increase in expression of the major histocompatibility complex, class II, DM beta (HLA-DMB) and nuclear receptor subfamily 5, group A, member 2 (NR5A2) respectively compared to control at passage 3. Moreover, there was a 5-fold decreased in the expression of the small nucleolar RNA, C/D box 99 (SNORD) in the late passage SFN treated group compared to early control.

Unfortunately, when comparing the expression analysis of the 49 genes of interest used in the Nanostring method and the transcriptomic method, it was noticeable that there was considerably less significant changes in gene expression in the SFN treated and control groups at passage 3 and 11 – Table 34.

Table 31. Comparison of significant changes in gene expression in MRC-5 fibroblasts controls at passage 3 and passage 11 using a Bonferroni correction factor of 20773.

Gene ID	Gene Name	Significance with BF correction of 20773	Expression
C11orf70	Chromosome 11 open reading frame 70	1.326E-08	3.873
CXCL2	Chemokine (C-X-C motif) ligand 2	1.945E-08	-3.042
MOB4	MOB family member 4, phocein	2.398E-08	1.810
COL4A3BP	Collagen, type IV, alpha 3 (Goodpasture antigen) binding protein	2.690E-08	0.808
ZMAT2	Zinc finger, matrin-type 2	3.835E-08	1.089
PDE4DIP	Phosphodiesterase 4D interacting protein	6.129E-08	-1.856
SCARNA13	Small Cajal body-specific RNA 13	9.806E-08	-2.984
HLA-E	Major histocompatibility complex, class I, <i>E</i>	1.014E-07	1.248
DNAJC6	DnaJ (Hsp40) homolog, subfamily C, member 6	1.063E-07	6.408
ABTB2	Ankyrin repeat and BTB (POZ) domain containing 2	1.160E-07	0.989
BANK1	B-cell scaffold protein with ankyrin repeats 1	1.211E-07	3.530
CPPED1	Calcineurin-like phosphoesterase domain containing 1	1.405E-07	3.103
CCDC144A	Coiled-coil domain containing 144A	1.457E-07	-3.928
COLEC11	Collectin sub-family member 11	1.556E-07	-1.782
CCRL1	C-C chemokine receptor type 11	1.667E-07	5.636
CCDC144A	Coiled-coil domain containing 144A	1.678E-07	-4.259
HSD11B1L	Hydroxysteroid (11-beta) dehydrogenase 1-like	1.738E-07	0.754

Correlation is significant at the 0.05 level (2-tailed) with Bonferroni correction factor 20773.

Grey areas highlight gene downregulation.

Table 32. Comparison of significant changes in gene expression in MRC-5 fibroblasts SFN treatments at passage 3 and passage 11 using a Bonferroni correction factor of 20773.

Gene ID	Gene Name	Significance with BF correction of 20773	Expression
ARSJ	Arylsulfatase family, member J	1.967E-07	0.897
FZD4	Frizzled family receptor 4	2.280E-07	2.468
MOB4	MOB family member 4, phocein	3.559E-07	1.784
ACTR2	ARP2 actin-related protein 2 homolog	6.857E-07	1.149
MAEA	Macrophage erythroblast attacher	7.728E-07	1.137
VAT1	Vesicle amine transport 1	9.179E-07	1.080
CSNK1G1	Casein kinase 1, gamma 1	1.119E-06	1.499
ACAA2	Acetyl-CoA acyltransferase 2	1.137E-06	2.461
GALC	Galactosylceramidase	1.142E-06	1.103
CCRL1	C-C chemokine receptor type 11	1.170E-06	5.628
SLC46A1	Solute carrier family 46 (folate transporter), member 1	1.665E-06	1.682
C11orf87	Chromosome 11 open reading frame 87	1.878E-06	3.764
TXNIP	Thioredoxin interacting protein	1.898E-06	6.776
SUN1	Sad1 and UNC84 domain containing 1	2.187E-06	-0.713
PRRX2	Paired related homeobox 2	2.234E-06	3.310

Correlation is significant at the 0.05 level (2-tailed) with Bonferroni correction factor 20773.

Grey areas highlight gene downregulation.

Table 33. Comparison of significant changes in gene expression in MRC-5 fibroblasts control at passage 3 and treatment at passage 11 using a Bonferroni correction factor of 20773.

Gene ID	Gene Name	Significance with BF correction of 20773	Expression
FAM46C	Family with sequence similarity 46, member C	4.842E-11	1.645
FAM63A	Family with sequence similarity 63, member A	3.662E-10	1.669
DIXDC1	DIX domain containing 1	9.153E-10	2.502
FAM134A	Family with sequence similarity 134, member A	1.159E-09	1.434
FOSB	FBJ murine osteosarcoma viral oncogene homolog B	4.031E-09	-3.437
KIAA1826	Myb/SANT-like DNA-binding domain containing 4 with coiled-coils	1.935E-08	1.233
NR5A2	Nuclear receptor subfamily 5, group A, member 2	2.379E-08	6.621
DUSP11	Dual specificity phosphatase 11 (RNA/RNP complex 1-interacting)	2.664E-08	2.858
SNORD99	Small nucleolar RNA, C/D box 99	2.724E-08	-4.627
MYO15B	Myosin XVB pseudogene	2.949E-08	-1.737
HLA-DMB	Major histocompatibility complex, class II, DM beta	3.606E-08	5.228
SNORD113-3	Small nucleolar RNA, C/D box 113-3	3.925E-08	-2.784
MOB4	MOB family member 4, phocein	3.939E-08	1.922
FNBP4	Formin binding protein 4	4.649E-08	-1.462
USP39	Ubiquitin specific peptidase 39	6.608E-08	0.898
TPD52L2	Tumor protein D52-like 2	6.789E-08	1.538
INPP5F	Inositol polyphosphate-5-phosphatase F	6.914E-08	1.869
D4S234E	D4S234E p53-responsive gene	7.372E-08	2.701

Correlation is significant at the 0.05 level (2-tailed) with Bonferroni correction factor 20773.

Grey areas highlight gene downregulation.

Table 34. Comparison of significance in gene expression using Microarray and Nanostring methods in MRC-5 fibroblasts treated with SFN at passage 3 and 11.

Gene	SFN_P3 vs CONP3		SFN_P11 vs CON_P11		CONP_11 vs CON_P3		SFN_P11 vs SFN_P3		SFN_P11 vs CON_P3	
	Microarray	Nanostring	Microarray	Nanostring	Microarray	Nanostring	Microarray	Nanostring	Microarray	Nanostring
ACTB	0.5078395	0.778258	0.953887	0.007177	0.111226	0.001436	0.562944	0.008196	0.207102	0.003579
AKR1C1	0.6255313	0.000021 ††	0.668126	0.000103 ††	0.057895	1.157045E-06 †††	0.231992	5.914137E-07 †††	0.023261	1.984714E-06 †††
CAT	0.5300721	0.817453	0.089673	0.001693	0.600443	0.002736	0.093422	0.000477 †	0.008105	0.000364 †
CCL2	0.9089091	0.996076	0.240249	0.000232 †	0.000006	0.000010 †††	0.000144	0.000185 ††	0.000090	0.000096 ††
CDKN1A	0.2325053	0.013422	0.005559	0.680075	0.024883	0.006403	0.255465	0.013423	0.003122	0.000247 †
COL1A1	0.1104167	0.039808	0.361072	9.389386E-07 †††	0.050912	0.003511	0.008947	0.005634	0.002654	0.132615
FASN	0.6129978	0.498363	0.740251	0.050875	0.464149	2.576196E-06 †††	0.746034	0.000847 †	0.904901	0.000542 †
FTH1	0.2159656	0.003660	0.031383	0.000215 †	0.062286	8.369158E-06 †††	0.417169	0.000026 ††	0.010605	0.000013 †††
G6PD	0.3077296	0.003352	0.021608	0.000014 †††	0.955278	0.002125	0.507139	0.001225	0.038012	0.003171
GCLC	0.1193425	0.554664	0.042408	0.036472	0.000201	0.265009	0.000022	0.090946	9.788935E-06 *	0.177840
GCLM	0.5148279	0.003468	0.922263	3.205701E-06 †††	0.000360	0.000079 ††	0.000336	5.500113E-06 †††	0.000589	0.000008 †††
GLB1	0.7161448	0.260062	0.838345	0.520151	0.000134	0.047182	0.000057	0.000478 †	0.000054	0.046080
GLO1	0.5113778	0.346354	0.785427	0.002392	0.003302	0.095323	0.002336	0.584274	0.001712	0.261231
GPX1	0.7613199	0.461273	0.058076	0.002631	0.001774	0.001658	0.003407	0.007914	0.002705	0.006877
GSR	0.0958830	0.000517 †	0.107405	0.000636 ††	0.570153	0.000232 †	0.862327	3.821775E-06 †††	0.031966	0.001869
GSTP1	0.8123289	0.827294	0.047692	0.000081 ††	0.025978	0.000224 †	0.015146	0.007525	0.008579	0.001536

GUSB	0.2238274	0.032612	0.919002	0.365177	0.345490	0.000010 †††	0.780614	0.000273 †	0.174576	8.645483E-06 †††
HIF1A	0.9571877	0.217084	0.074851	0.000199 ††	0.000409	0.523463	0.000047	0.000352 †	0.000000	0.009265
HK1	0.8667444	0.105063	0.178091	0.388649	0.000748	0.000466 †	0.026090	0.000228 †	0.000458	0.000465 †
HMOX1	0.3112500	0.009592	0.065540	0.001097	0.271926	0.000055 ††	0.621719	5.659236E-07 †††	0.122502	0.002985
ICAM1	0.7271304	0.105776	0.018691	0.000048 ††	0.633366	0.011062	0.162345	2.424939E-06 †††	0.022605	0.005293
KEAP1	0.5011426	0.780362	0.217247	0.997422	0.028091	0.009352	0.024264	0.001123	0.000218	0.007372
MAFG	0.4240826	0.437122	0.724163	0.439050	0.019652	0.008836	0.031218	0.000366 †	0.000239	0.005895
MLX	0.5626195	0.134079	0.451840	0.929443	0.001029	0.036205	0.004760	0.004680	0.003644	0.001819
MLXIP	0.8961230	0.458417	0.055415	0.451655	0.003576	0.004809	0.589627	0.002635	0.033436	0.029867
MMP1	0.8135520	0.745987	0.000066	2.465839E-06 †††	0.000876	0.274834	0.000042	6.850904E-06 †††	0.000037	0.000015 †††
MMP13	0.7943929	0.703127	0.577719	0.574042	0.001158	0.516765	0.007542	0.454166	0.000778	0.447737
MMP3	0.5202946	0.715062	0.000986	0.005131	4.622103E-07 *	0.000174 ††	0.000143	0.000029 ††	3.782573E-07 *	0.000063 ††
MRP2/UG	0.6157666	0.375265	0.094351	0.281087	0.342144	0.070467	0.329361	0.026078	0.033357	0.042658
NFE2L2	0.8338989	0.820796	0.731077	0.000137 ††	0.001251	0.019874	0.002102	0.000103	0.000978	0.000122 ††
NFKB1	0.8880151	0.771298	0.053116	0.088329	0.017648	0.003498	0.679392	0.036254	0.733255	0.013064
NFKB3	0.7006818	0.930094	0.370583	0.901248	0.149410	0.093041	0.175023	0.295010	0.021861	0.261105
NQO1	0.0155181	0.000348 †	0.000751	0.000022 ††	0.000479	0.000372 †	0.003905	0.000711 †	8.185903E-06 *	0.017338
PFKFB2	0.8571489	0.115368	0.087489	0.492137	0.190958	0.025668	0.882081	0.004713	0.894420	0.005316
PRDX1	0.4349963	0.003832	0.127454	0.000546 †	0.000382	0.002641	0.000595	0.049059	0.000475	0.000192 ††
PSMA1	0.4542982	0.986704	0.081367	0.041389	0.000039	0.000119 ††	0.000262	0.033438	0.000118	0.000071 ††
PSMB5	0.4442480	0.027065	0.099738	0.023982	0.000562	0.000916 †	0.003041	8.999051E-06 †††	0.000070	0.000010 †††

SERPINB2	0.6386232	0.150557	0.141027	0.002470	0.000338	0.000682	0.057659	4.142766E-06 †††	0.002315	0.000988 †
SOD1	0.4955507	0.198408	0.158794	0.025677	0.913658	0.020292	0.193479	0.000272†	0.037302	0.063683
SOD2	0.4807792	0.442777	0.277868	0.204452	0.298633	4.725874E-07 †††	0.693610	6.275164E-06 †††	0.960254	1.304272E-06 †††
SQSTM1	0.5147259	0.041815	0.749566	0.000739 †	0.027662	7.497274E-06 †††	0.168243	0.000012 †††	0.042220	5.840064E-06 †††
SREBF1	0.4279976	0.233453	0.350304	0.018941	0.028862	6.127240E-06 †††	0.008250	0.000898 †	0.008739	4.916657E-06 †††
TALDO1	0.1087712	0.006461	0.032028	0.000044 ††	0.000059	0.001638	0.001412	0.071569	0.000051	0.007301
TKT	0.4788010	0.959092	0.071636	0.000329 †	0.035752	0.000084 ††	0.570977	0.000993 †	0.195466	0.000145 ††
TLR4	0.3957951	0.478228	0.002563	0.010787	0.000013	0.037159	0.000063	0.051904	0.000003	0.098409
TXN	0.3600658	0.001715	0.013078	0.000121 ††	0.857321	0.000239 †	0.050023	0.002079	0.012978	0.409588
TXNIP	0.2788078	0.683395	0.003598	1.441395E-06 †††	0.000011	4.745044E-06 †††	1.898324 E-06 *	4.038172E-08 †††	6.785231E-07 *	0.000059 ††
TXNRD1	0.1411390	0.006573	0.137183	0.000104 ††	0.028510	0.003527	0.066967	0.018957	0.000115	0.038777

* P<0.05 for transcriptomic analysis with Bonferroni correction factor of 20773

† P<0.05 for nanostring analysis with Bonferroni correction factor of 49

†† P<0.01 for nanostring analysis with Bonferroni correction factor of 49

††† P<0.001 for nanostring analysis with Bonferroni correction factor of 49

4.4 Expression of fructose-2,6-bisphosphate 6-phosphofructo-2-kinase/fructose-2,6-bisphosphatase 2 protein PFKFB2

Human fructose-2,6-bisphosphate 6-phosphofructo-2-kinase/fructose-2,6-bisphosphatase 2 expression in MRC-5 fibroblasts was assessed at the protein level by Western blotting of cell extracts at passage 5 (young) and passage 9 (senescence) treated with either 1 μ M SFN or 0.002% DMSO - Figure 80 and 81.

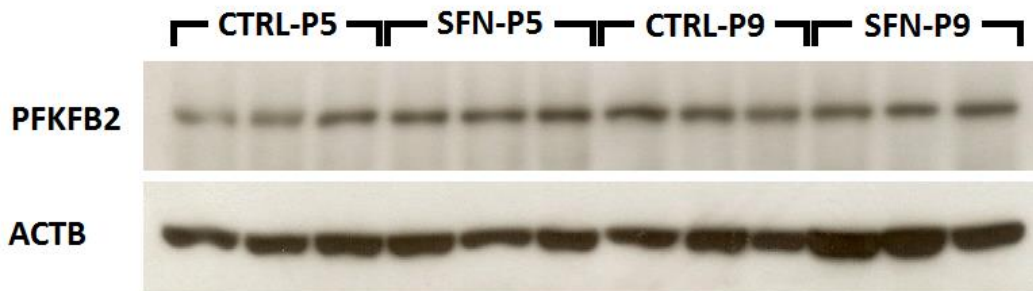


Figure 80. Western blotting of young and senescent MRC-5 fibroblasts for 6-phosphofructo-2-kinase/fructose-2,6-bisphosphatase-2.

Key: PFKFB2, 6-phosphofructo-2-kinase/fructose-2,6-bisphosphatase-2 protein; and ACTB - β -actin housekeeping protein. SFN-P5 and CTRL-P5, cell extracts from passage 5 treated with and without 1 μ M SFN; and SFN-P9 and CTRL-P9, cell extracts from passage 9 treated with and without 1 μ M SFN.

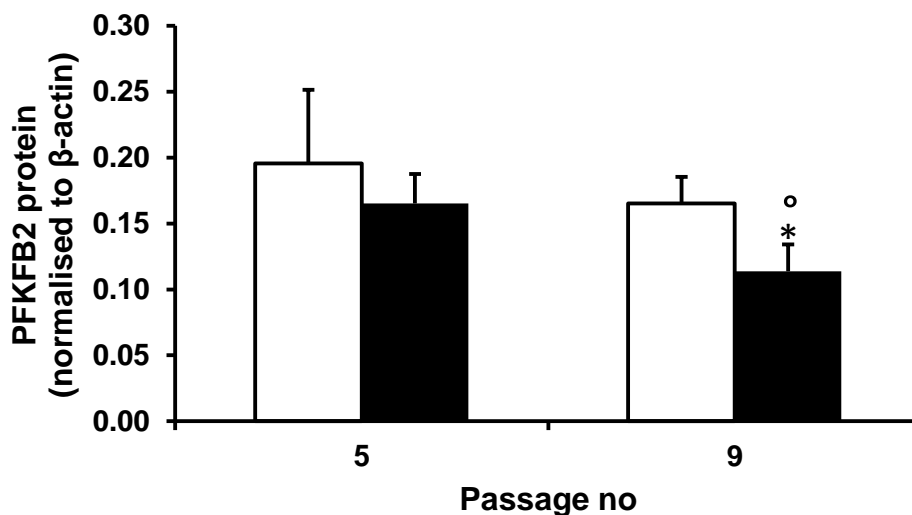


Figure 81. Quantitation of Western blotting of young and senescent MRC-5 fibroblasts for 6-phosphofructo-2-kinase/fructose-2,6-bisphosphatase-2.

Key: , control; and + 1 μ M SFN. Data are mean \pm SD (n = 3). Significance: *, P<0.05, SFN treated cells with respect to control; o, P<0.05, passage 9 SFN with respect passage 5 SFN.

Expression of PFKFB2 protein by western blotting analysis shows that control MRC-5 fibroblasts have a significantly higher expression of PFKFB2 protein compared to the SFN-treated group at later passage (passage 9).

4.5 Change in gene expression of MRC-5 fibroblasts *in vitro* during the approach to senescence

The time course of changes in gene expression of MRC-5 fibroblasts *in vitro* was investigated by quantifying mRNA of genes of selected metabolic pathways with Nrf2 regulated, ARE-linked genes by the RT-PCR method – quantifying relative mRNA expression. The outputs are given in Figures 82-86. The reference gene was β -actin with responses normalized to the relative expression of this gene.

Expression of the anti glycation related gene aldoketo reductase 1B1 (AKR1B1) was significantly decreased ($P<0.001$) by a third of its value in senescence (passage 11) compared to young fibroblasts (passage 3). Expression of AKR1B1 was stable from passage 3 but decreased dramatically after passage 5. Moreover, the expression of the anti-glycation related gene glyoxalase 1 (GLO1) was also decreased significantly ($P<0.01$) with approach to senescence. Expression of GLO1 was stable at passage 3, 5 and 6 but declined rapidly thereafter. At the approach of senescence, the expression of the anti-oxidant related genes thioredoxin (TXN) as well as quinone reductase (NQO1) and heme oxygenase (HMOX1) was significantly decreased ($P<0.001$ and $P<0.05$, respectively) when compared to passage 3. Decline in expression of TXN was steady from passage 3 to 9 but increased slightly at the approach to senescence. Moreover, NQO1 and HMOX1 gene expression decline with approach to senescence was relatively consistent at each passage. Expression of the anti-oxidant related gene gamma-glutamyl-cys ligase-catalytic subunit (GCLC), gamma-glutamyl-cys ligase-modulatory subunit (GCLM) and glutathione reductase (GSR) however did not significantly decline with approach to senescence. Expression of both pentosephosphate pathway genes transaldolase (TALDO1) and transketolase (TKT) was significantly ($P<0.05$) decreased from passage 3 to passage 11, showing almost linear decline with passage. Moreover, expression of the NADPH-dependent oxidoreductase carbonyl reductase 1 (CBR1) was also significantly decreased ($P<0.05$) with approach to senescence.

This decline was drastic from passage 3 to 9 but was steady thereafter until senescence at passage 11. Finally the expression of the Nrf2 regulation related genes Nrf2 was not significantly decreased at passage 11, although 30% decrease in Keap 1 expression at the approach to senescence was very significant ($P < 0.001$).

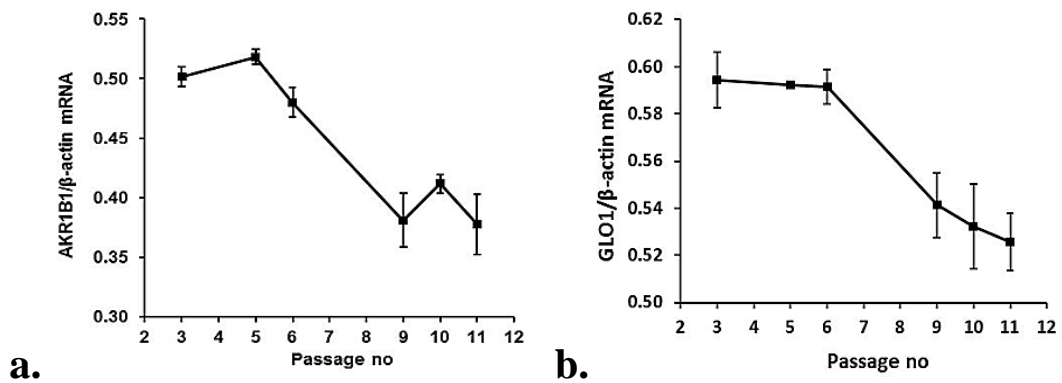


Figure 82. Gene expression of MRC-5 fibroblasts at the approach to senescence. RT-PCR study. Anti-glycation related genes.

a. aldoketo reductase 1B1 (AKR1B1). **b.** glyoxalase 1 (GLO1). Data are mean \pm SD, $n = 3$.

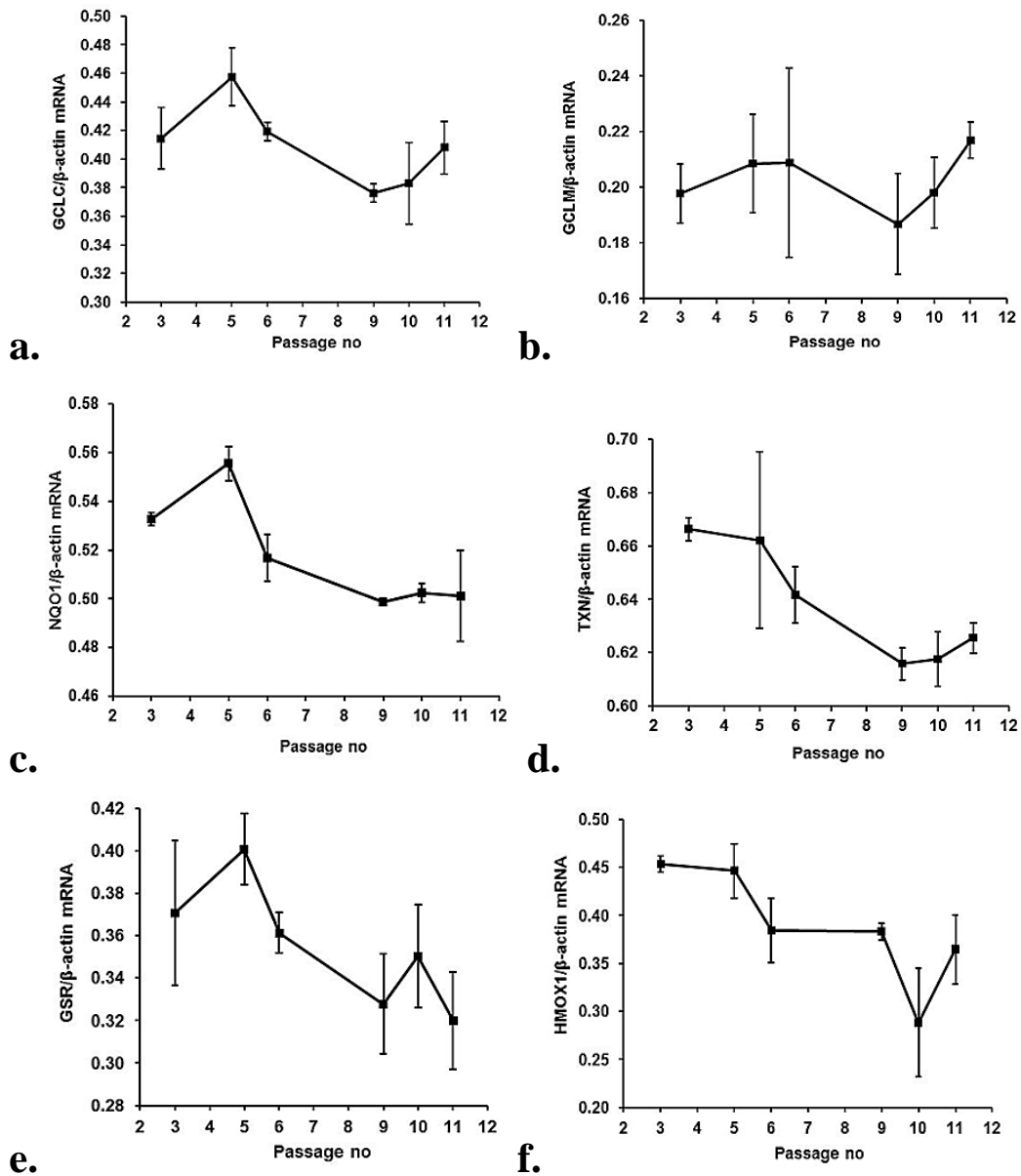


Figure 83. Gene expression of MRC-5 fibroblasts at the approach to senescence. RT-PCR study. Anti-oxidant related genes.

a. gamma-glutamyl-cys ligase-catalytic subunit (GCLC). **b.** gamma-glutamyl-cys ligase-modulatory subunit (GCLM). **c.** quinone reductase (NQO1). **d.** thioredoxin (TXN). **e.** glutathione reductase (GSR). **f.** heme oxygenase (HMOX1). Data are mean \pm SD, n = 3.

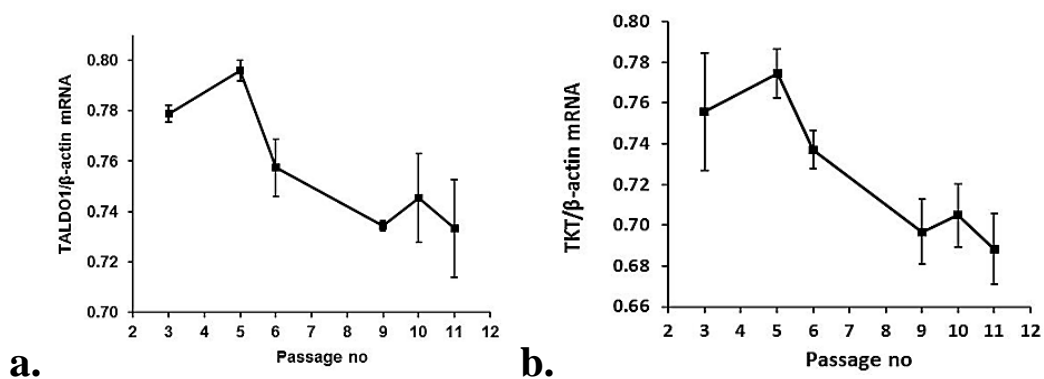


Figure 84. Gene expression of MRC-5 fibroblasts at the approach to senescence. RT-PCR study. Pentosephosphate pathway genes.
 a. transaldolase (TALDO1). b. transketolase (TKT). Data are mean \pm SD, n = 3.

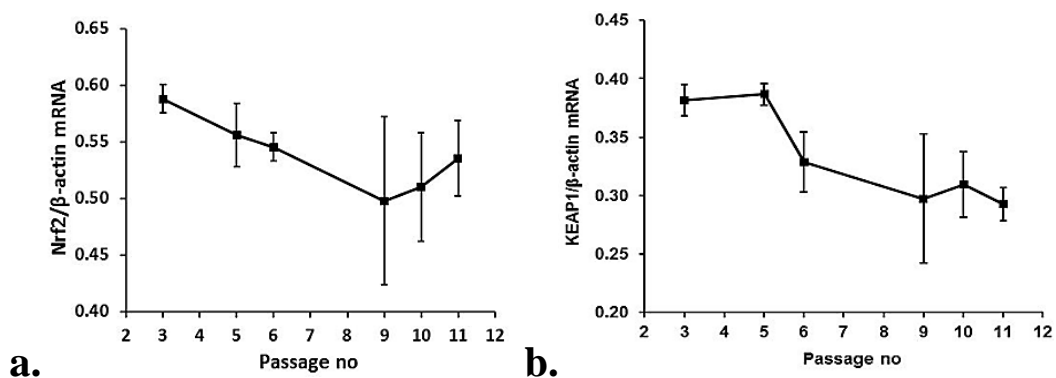


Figure 85. Gene expression of MRC-5 fibroblasts at the approach to senescence. RT-PCR study. Nrf2 regulation related genes.
 a. Nrf2. b. Keap1. Data are mean \pm SD, n = 3.

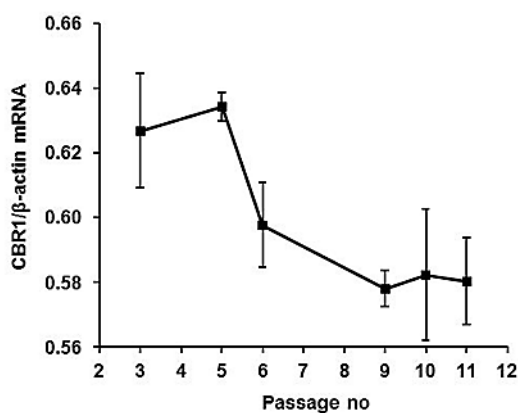


Figure 86. Gene expression of MRC-5 fibroblasts at the approach to senescence. RT-PCR study. NADPH-dependent oxidoreductase genes carbonyl reductase 1 (CBR1).
 Data are mean \pm SD, n = 3.

Analysis of gene expression in MRC-5 cells from passage 3 to 11 showed that, for genes NQO1, NRF2, TKT, GLO1, AKR1B1, KEAP1, CBR-1, TALDO, GSR, HMOX1 and TXN, expression was maintained until passages 5 – 6 and then decline to lower levels at passages 10 – 11. Genes GCLC and GCLM did not change significantly with increased passage. Correlation analysis of gene expression was also performed – Table 35. Changes in expression of many ARE-linked genes, including Nrf2 and Keap1, were highly correlated.

Table 35 Correlation analysis of gene expression in ageing MRC-5 fibroblasts.

NQO1	0.622**											
TKT	0.476*	0.893**										
GLO1	0.595**	0.785**	0.884**									
AKR1B1	0.548*	0.884**	0.847**	0.779**								
KEAP1	0.721**	0.843**	0.769**	0.756**	0.856**							
GCLC	0.544*	0.810**	0.808**	0.715**	0.692**	0.626**						
CBR1	0.723**	0.882**	0.851**	0.785**	0.851**	0.839**	0.806**					
TALDO1	0.602**	0.928**	0.889**	0.767**	0.895**	0.886**	0.773**	0.856**				
GSR		0.802**	0.868**	0.649**	0.763**	0.620**	0.643**	0.707**	0.794**			
HMOX1	0.691**	0.794**	0.745**	0.716**	0.716**	0.777**	0.647**	0.797**	0.748**	0.559*		
AKR1B2	0.626**	0.845**	0.767**	0.775**	0.897**	0.800**	0.773**	0.792**	0.796**	0.612**	0.809**	
TXN	0.662**	0.787**	0.765**	0.728**	0.781**	0.711**	0.765**	0.818**	0.773**	0.525*	0.804**	0.858**
	NFE2L2	NQO1	TKT	GLO1	AKR1B1	KEAP1	GCLC	CBR1	TALDO1	GSR	HMOX1	AKR1B2

*Spearman correlation is significant at the 0.05 level (2-tailed).

** Spearman correlation is significant at the 0.01 level (2-tailed).

4.6 Effect of progression towards senescence and sulforaphane on protein glycation, oxidation and nitration markers in MRC-5 fibroblasts *in vitro*.

Increased damage to the proteome by glycation, oxidation and nitration has been implicated in fibroblast senescence. In this study a comprehensive range of protein damage markers were quantified. Protein damage adduct residues of cell cytosolic protein and flux of free adducts in culture medium were quantified in MRC-5 fibroblasts at passage 4 and 8 after incubation from passage 3 with and without 1 μ M SFN – Table 36 and 37.

Table 36. Protein damage adduct residues of cell cytosolic protein in MRC-5 fibroblasts treated with or without 1 μ M SFN at passage 4 and 8.

Damage marker type	Analyte	Passage 4		Passage 8	
		Control	+ SFN	Control	+ SFN
Early glycation	FL (mmol/mol lys)	5.29 \pm 1.61	4.10 \pm 0.49	5.56 \pm 0.89	2.83 \pm 0.44 ***
AGE	CML (mmol/mol lys)	0.264 \pm 0.085	0.160 \pm 0.020	0.243 \pm 0.028	0.221 \pm 0.051
	CML/FL ratio	0.054 \pm 0.029	0.039 \pm 0.005	0.044 \pm 0.002	0.079 \pm 0.021 *
	3DG-H (mmol/mol arg)	0.249 \pm 0.028	0.313 \pm 0.003**	0.329 \pm 0.043	0.377 \pm 0.051
	MG-H1 (mmol/mol arg)	0.43 \pm 0.10	0.25 \pm 0.01 *	0.35 \pm 0.02	0.35 \pm 0.05
	CMA (mmol/mol arg)	0.093 \pm 0.018	0.054 \pm 0.012 *	0.088 \pm 0.013	0.074 \pm 0.003
	Glucosepane (mmol/mol lys)	0.122 \pm 0.037	0.055 \pm 0.004 *	0.079 \pm 0.016	0.071 \pm 0.025
Oxidation	DT (mmol/mol tyr)	1.23 \pm 0.26	1.71 \pm 0.70	0.89 \pm 0.26	0.77 \pm 0.12 $^{\circ}$
	GSA (mmol/mol arg)	0.219 \pm 0.050	0.112 \pm 0.010 *	0.226 \pm 0.092	0.214 \pm 0.021 $^{\circ\circ}$
Nitration	3-NT (mmol/mol tyr)	0.023 \pm 0.005	0.017 \pm 0.001	0.014 \pm 0.001	0.019 \pm 0.002 *

Significance: *, P<0.05, **, P<0.01 and ***, P<0.001 with respect to DMSO control; $^{\circ}$, P<0.05 and $^{\circ\circ}$, P<0.01 with respect to treatment control at passage 4.

Table 37. Protein damage adduct residues and flux of free adducts in culture medium in MRC-5 fibroblasts treated with or without 1 μ M SFN at passage 4 and 8.

Damage marker type	Analyte flux	Passage 4		Passage 8	
		Control	+ SFN	Control	+ SFN
Early glycation	FL (nmol/day/10 ⁶ cells)			2.32 \pm 0.89	1.16 \pm 0.27
AGE	MG-H1 (nmol/day/10 ⁶ cells)	0.0278 \pm 0.0044	0.0194 \pm 0.0058	0.0838 \pm 0.0086 ^{ooo}	0.0833 \pm 0.0061 ^{ooo}
	CML (nmol/day/10 ⁶ cells)			0.0745 \pm 0.0268	0.0311 \pm 0.0076
	3DG-H (nmol/day/10 ⁶ cells)	0.0155 \pm 0.0039	0.00518 \pm 0.00300 [*]	0.119 \pm 0.023 ^{ooo}	0.0763 \pm 0.0085 ^{*, ooo}
	CMA (nmol/day/10 ⁶ cells)	0.0189 \pm 0.0012	0.0112 \pm 0.0024 ^{***}	0.0611 \pm 0.0060 ^{ooo}	0.0492 \pm 0.0035 ^{**, ooo}
	Glucosepane (pmol/day/10 ⁶ cells)	1.42 \pm 1.33	0.516 \pm 0.056		
Oxidation	DT (nmol/day/10 ⁶ cells)	0.081 \pm 0.115	0.208 \pm 0.059	1.631 \pm 0.866 [°]	1.179 \pm 0.293 ^{oo}
	GSA (nmol/day/10 ⁶ cells)	0.014 \pm 0.015	0.009 \pm 0.013	0.259 \pm 0.076 ^{oo}	0.041 \pm 0.017 ^{**}
Nitration	3-NT (pmol/day/10 ⁶ cells)	0.341 \pm 0.037	0.362 \pm 0.085		

*P<0.05, **P<0.01 and ***P<0.001 with respect to treatment control. ^oP<0.05, ^{oo}P<0.01, ^{ooo}P<0.001 with respect to baseline. (2-tailed t-test)

Areas marked in grey indicate that flux was below limit of detection for this passage.

4.6.1 Protein glycation

Protein glycation adducts studied were the early glycation adduct FL and advanced glycation adducts (AGEs) – hydroimidazolones MG-H1 and 3DG-H, mono-lysine and arginine adducts CML and CMA, and glucosepane. They were determined in cell protein and baseline and end of passage culture medium of MRC-5 cell cultures at passage 4 and passage 8 that had been incubated with and without 1 μ M SFN since passage 3 (when cPDL was 35.8) – Figure 87 to 92. There was no significant change of any protein damage marker at passage 8 compared to passage 4 in control cultures. For protein carbonyls, GSA was detected but AASA was below the limit of detection – indicating that GSA is the major protein carbonyl in MRC-5 cell protein. At passage 4, treatment with SFN decreased residue contents of MG-H1, CMA, glucosepane and GSA but increased residue content of 3DG-H. At passage 8, treatment with SFN decreased residue contents of FL but increased residue content of 3-NT and CML/FL residue content ratio. Treatment with SFN also decreased DT residue content but increased GSA residue content in passage 8 compared to passage 4.

Flux of the following analytes was not calculated as they were below the limit of detection for the given passages: FL (passage 4), CML (passage 4), glucosepane (passage 8) and 3-NT (passage 8). There was a significant ($P < 0.001$) increase in the flux of the AGEs MG-H1, 3DG-H and at passage 8 compared to passage 4 in control cultures. This was also true for the flux of the oxidative damage markers DT and GSA ($P < 0.05$ and $P < 0.01$ respectively). At passage 4, treatment with SFN significantly decreased the flux of 3DG-H and CMA ($P < 0.05$ and $P < 0.01$ respectively). At passage 8, treatment with SFN decreased the flux of AGEs 3DG-H and CMA ($P < 0.05$ and $P < 0.01$ respectively) as well as the flux of the oxidative damage marker GSA ($P < 0.01$).

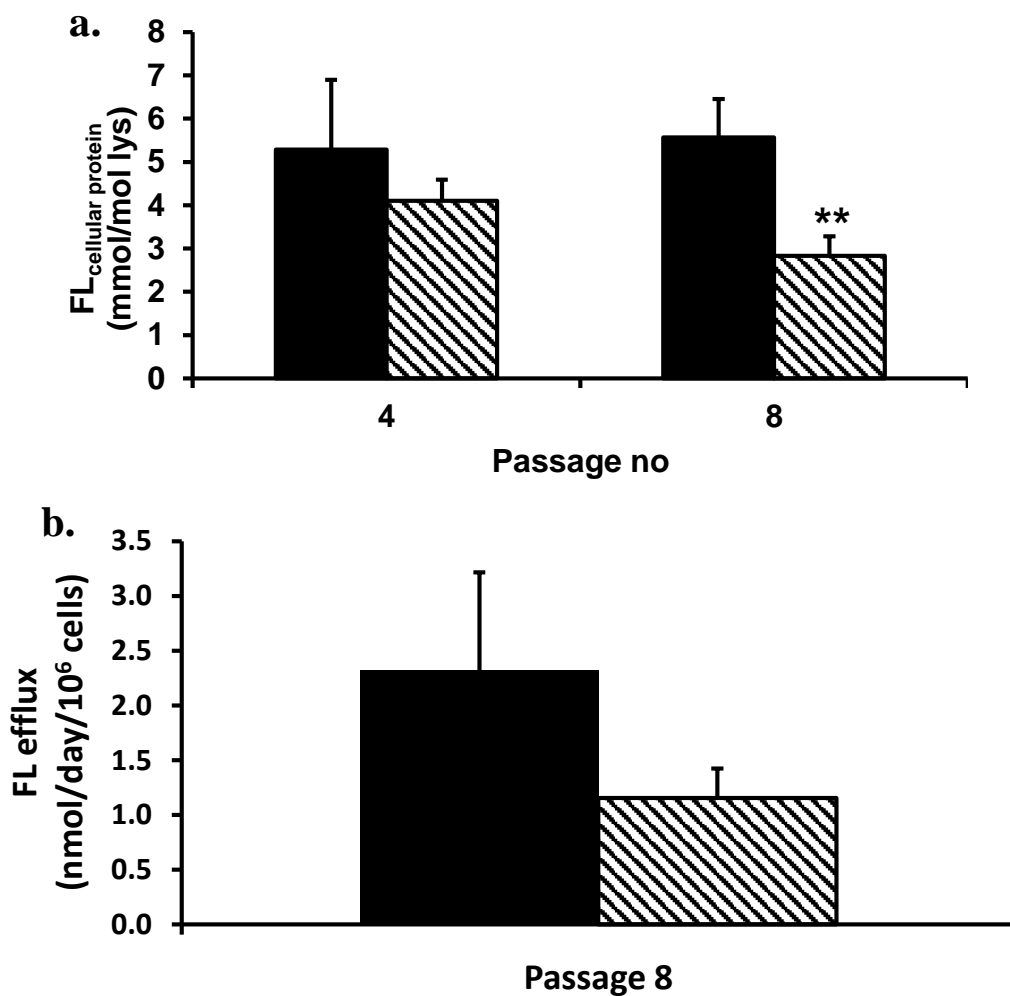


Figure 87. FL residue content of MRC-5 cell protein and flux of formation of FL free adducts.

a. FL residue content of cell protein at passage termination. b. Flux of formation of FL free adduct at passage 8. Key: , – control cultures; , cultures with 1 μM SFN. Data are mean ± SD (n = 3). Significance: **, P<0.01 with respect to DMSO control at respective passages (2-tailed t-test).

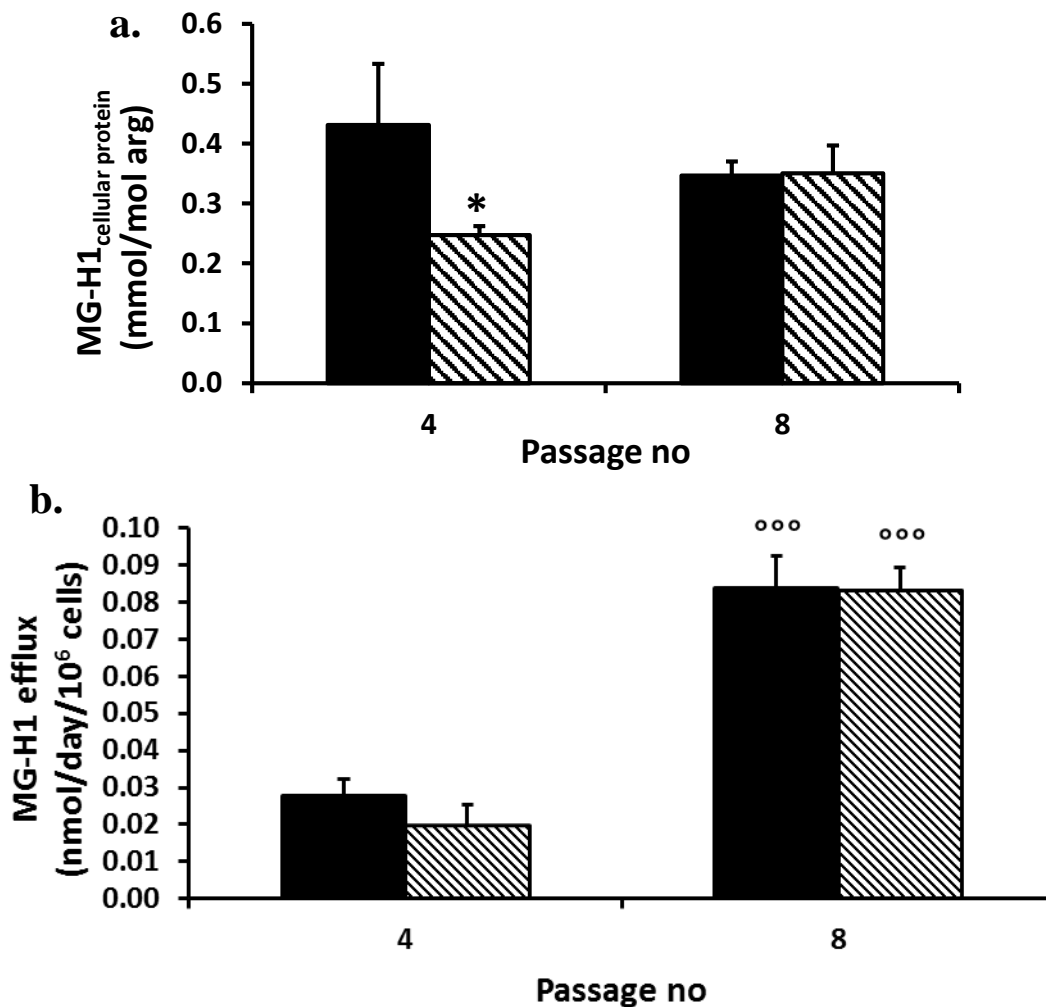


Figure 88. MG-H1 residue content of MRC-5 cell protein and flux of formation of MG-H1 free adducts.

a. MG-H1 residue content of cell protein at passage termination. b. Flux of formation of MG-H1 free adduct. Key: ,— control cultures; , cultures with 1 μM SFN. Data are mean ± SD (n = 3). Significance: *, P<0.05 with respect to DMSO control at respective passages; ooo, P<0.001 with respect to control cultures within same passage (2-tailed t-test).

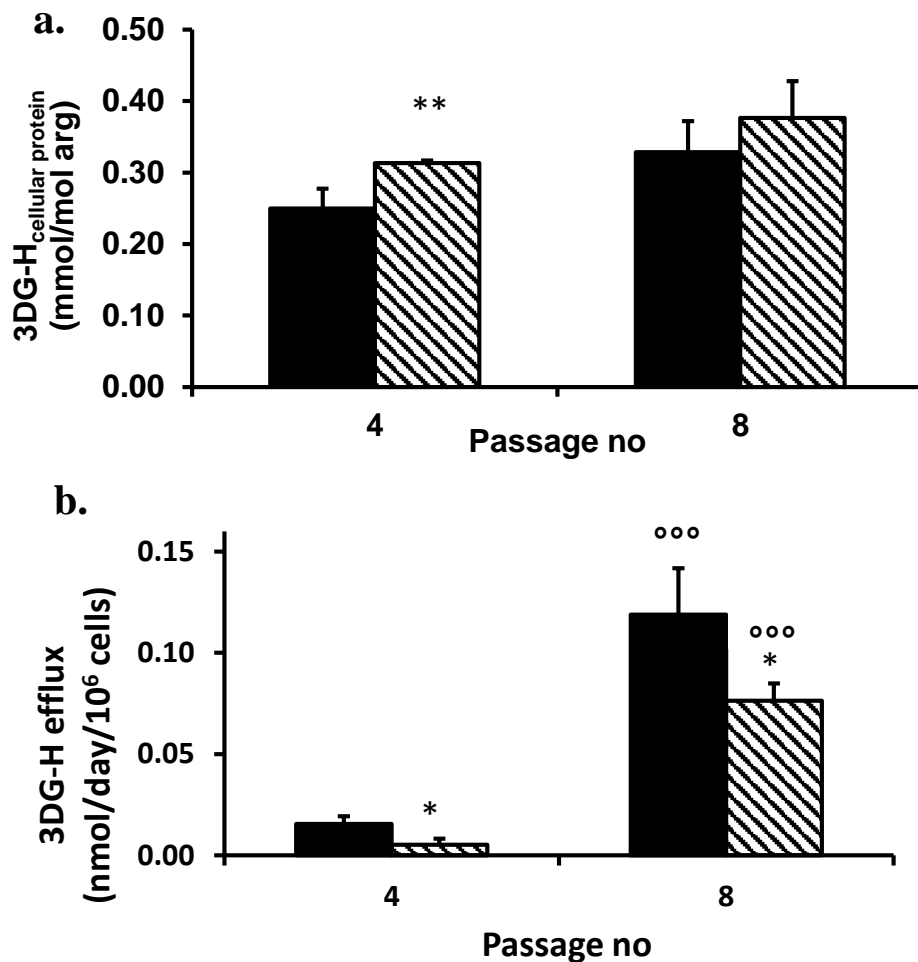


Figure 89. 3DG-H1 residue content of MRC-5 cell protein and flux of formation of 3-DG-H free adducts.

a. 3DG-H1 residue content of cell protein at passage termination. b. Flux of formation of 3DG-H1 free adduct. Key: , - control cultures; , cultures with 1 μ M SFN. Data are mean \pm SD (n = 3). Significance: * and **, P<0.05 and P<0.01 with respect to DMSO control at respective passages; ooo, P<0.001 with respect to control cultures within same passage (2-tailed t-test).

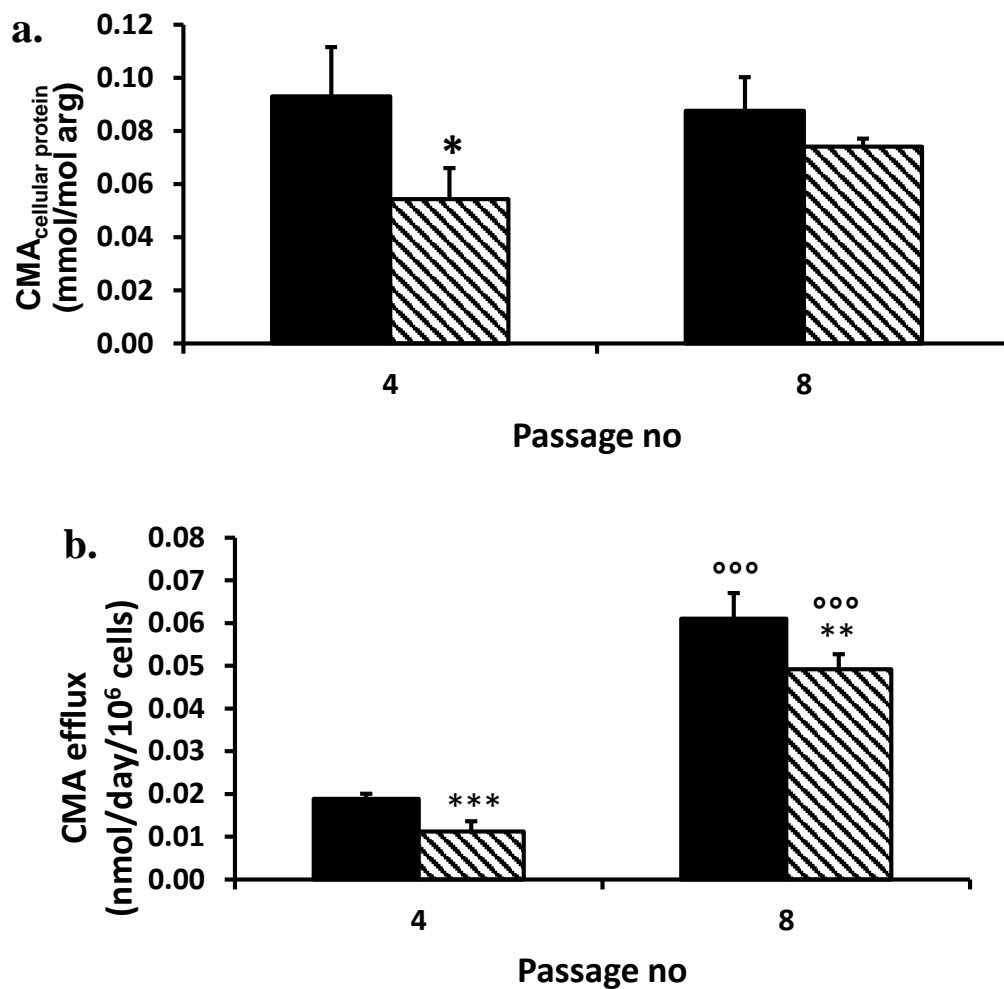


Figure 90. CMA residue content of MRC-5 cell protein and flux of formation of CMA free adducts.

a. CMA residue content of cell protein at passage termination. b. Flux of formation of CMA free adduct. Key: , – control cultures; , cultures with 1 μ M SFN. Data are mean \pm SD (n = 3). Significance: *, **, ***, P<0.05, P<0.01 and P<0.001 with respect to DMSO control at respective passages; ooo, P<0.001 with respect to control cultures within same passage (2-tailed t-test).

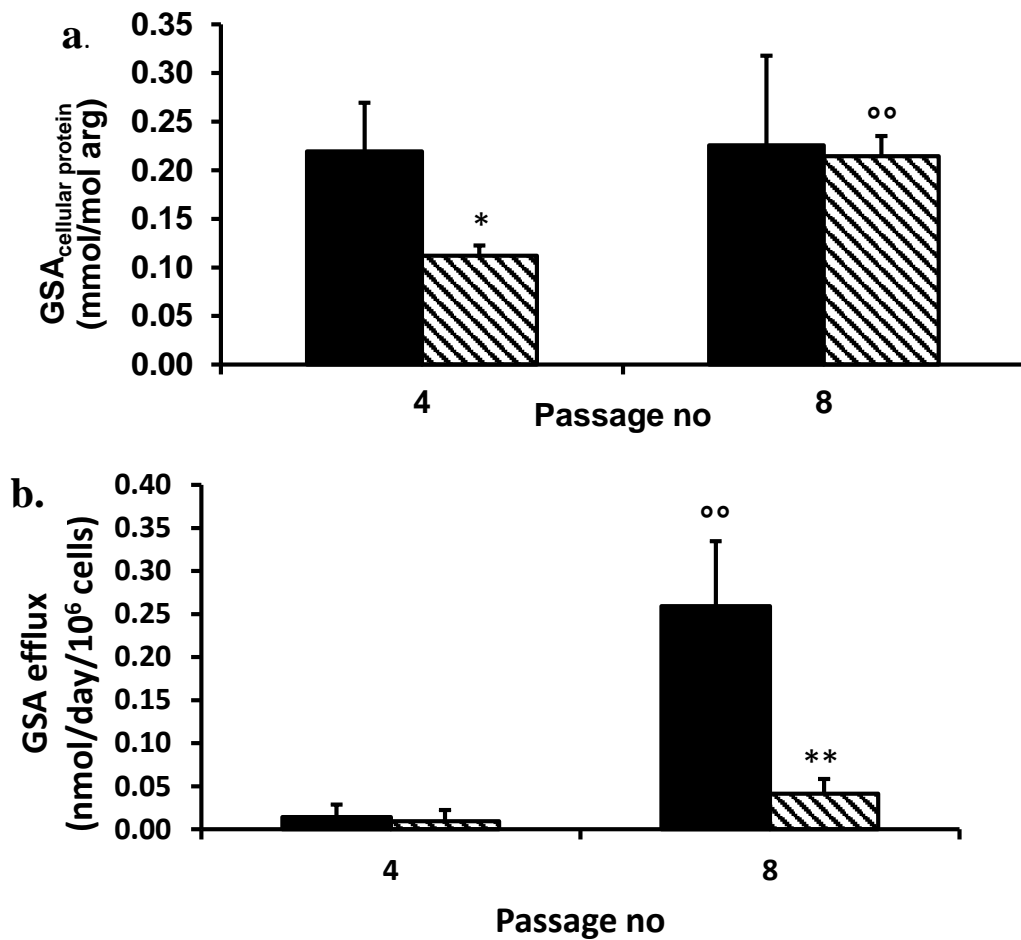


Figure 91. GSA residue content of MRC-5 cell protein and flux of formation of GSA free adducts.

a. GSA residue content of cell protein at passage termination. b. Flux of formation of GSA free adduct. Key: , – control cultures; , cultures with 1 μM SFN. Data are mean ± SD (n = 3). Significance: * and **, P<0.05 and P<0.01 with respect to DMSO control at respective passages; oo, P<0.01 with respect to control cultures within same passage (2-tailed t-test).

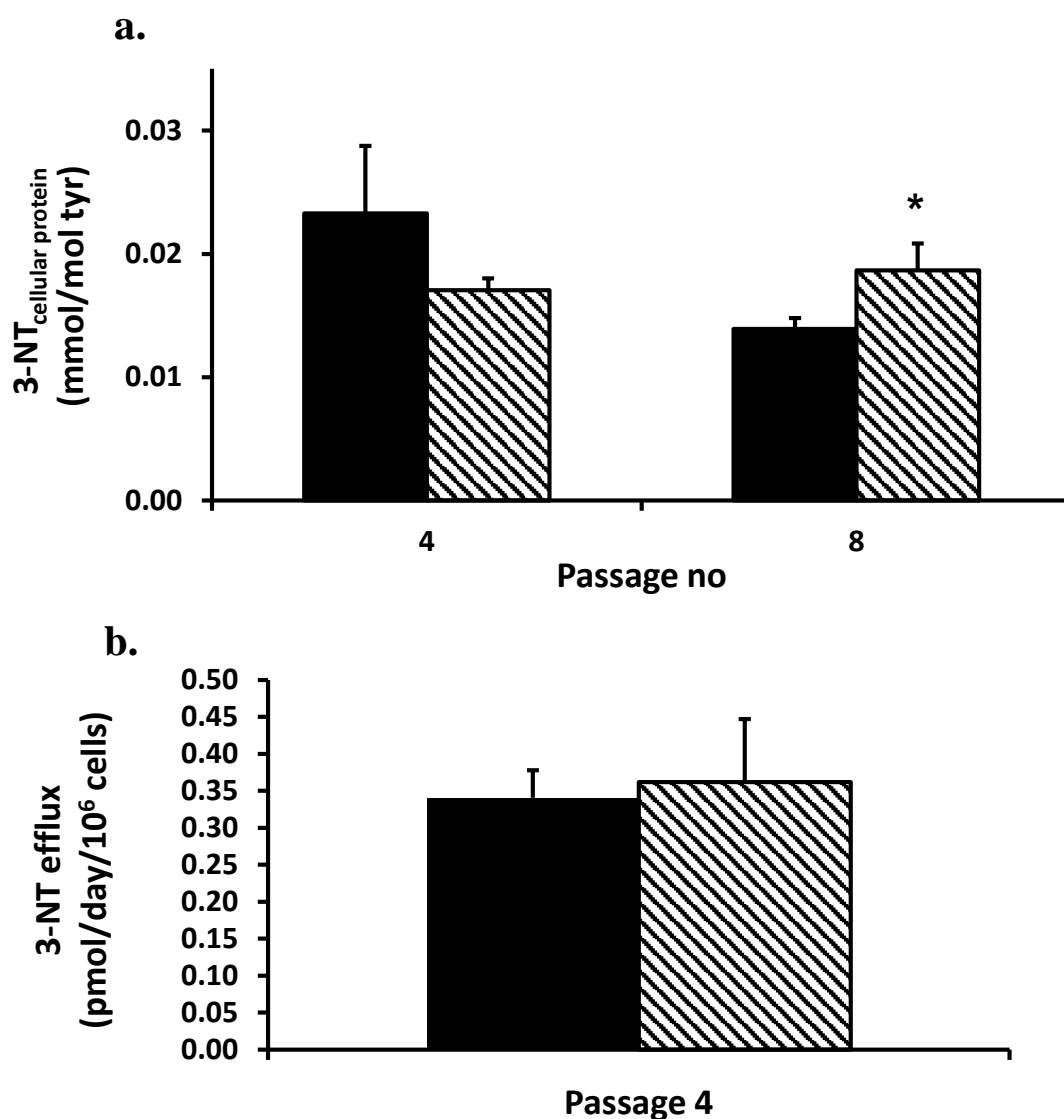


Figure 92. 3-NT residue content of MRC-5 cell protein and flux of formation of 3-NT free adducts.

a. 3-NT residue content of cell protein at passage termination. b. Flux of formation of 3-NT free adduct. Key: , - control cultures; , cultures with 1 μ M SFN. Data are mean \pm SD (n = 3). Significance: *, P<0.05 with respect to DMSO control at respective passages (2-tailed t-test).

4.7 Effect of progression towards senescence and sulforaphane on nucleotide glycation and oxidation in MRC-5 fibroblast cultures.

The concentration of the nucleotide damage markers MGdG, GdG and 8-OxodG in baseline and end of passage conditioned medium at passages 5 and 8 were determined in cultures of MRC-5 cells that had been incubated with and without 1 μ M SFN since passage 3 (when cPDL was 35.8).

For 8-oxodG, typical analytical chromatograms for determination of 8-OxodG in 20 μ l culture medium are given in Figure 93 a. and b. The concentration of 8-oxodG in baseline medium at passage 5 was 8.93 ± 0.63 nM and was not changed significantly at the end of the passage in MRC-5 cells incubated with or without 1 μ M SFN (9.13 ± 1.71 nM and 8.22 ± 1.62 nM respectively; $P > 0.05$). From the data dispersion in estimates of 8-OxodG concentration, the minimum detectable flux of formation of 8-OxodG was 2.3 pmol/million cells/day and hence the actual flux of formation of 8-OxodG is less than this.

At passage 8, however, the concentration of 8-oxodG in baseline medium was 6.16 ± 0.43 nM and was increased at the end of the passage in MRC-5 cells incubated with and without 1 μ M SFN (7.91 ± 0.52 nM and 10.06 ± 1.43 nM, respectively, $P < 0.05$) – Figure 94. The increase in 8-oxodG during the passage was normalized to cell number the mean rates of 8-oxodG formation computed. Incubation with SFN decreased the flux of formation of 8-OxodG: control 3.56 ± 0.44 versus + SFN 2.42 ± 0.30 pmol/day/million cells, $P < 0.05$.

For nucleotide AGEs, GdG, MGdG and CEdG, these analytes were not detectable in fresh or end of passage conditioned medium. The concentrations of these analytes were < 0.04 nM, < 0.13 nM and < 0.11 nM respectively.

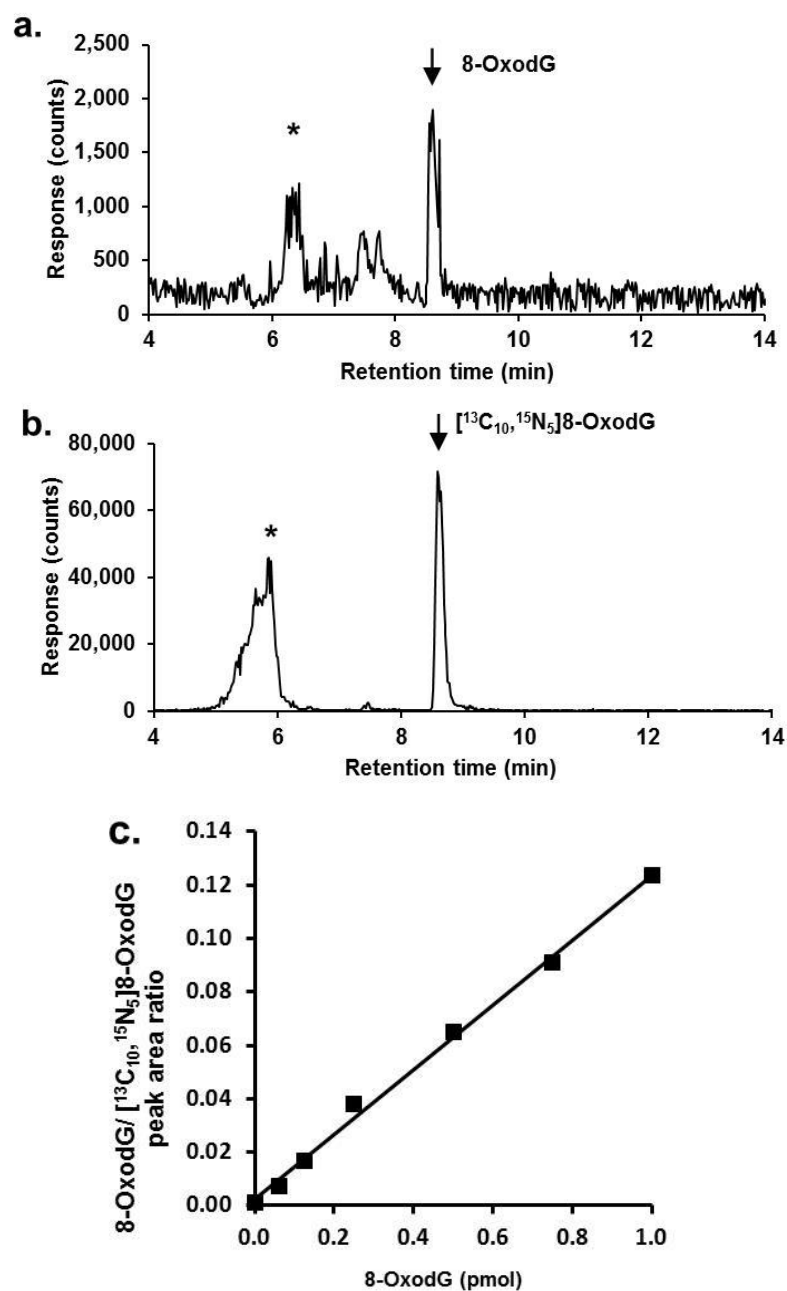


Figure 93. Detection and quantitation of 8-oxodG in culture medium of MRC-5 cell in culture.

a. Detection of 8-OxodG in culture medium. Sample: end of passage 8 with addition of 1 μ M SFN. Injection volume: 20 μ l. **b.** Internal standard (8.24 pmol) [¹³C₁₀, ¹⁵N₅]8-OxodG. **c.** Calibration curve. Regression equation: Peak area ratio = (0.121 \pm 0.003) 8-OxodG (pmol) + (0.0024 \pm 0.017); R = 0.998 (n = 7).

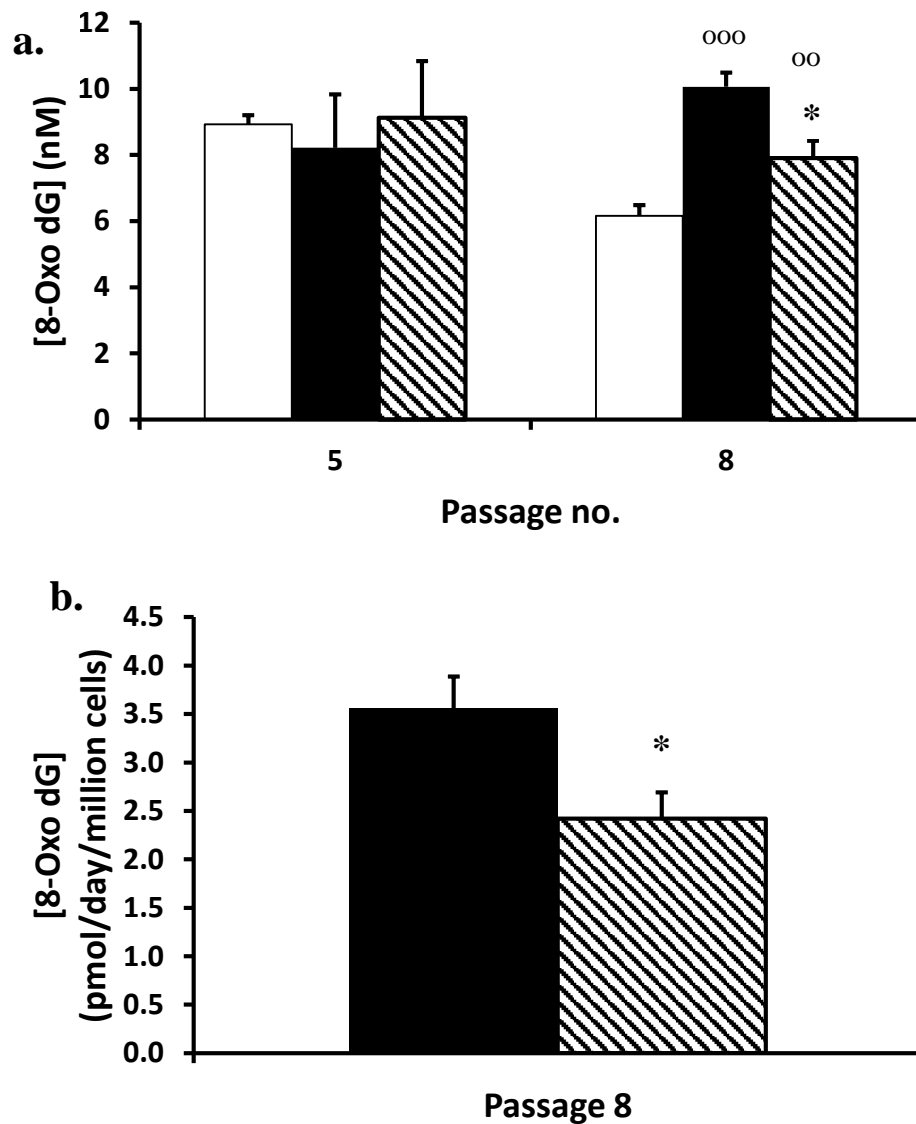





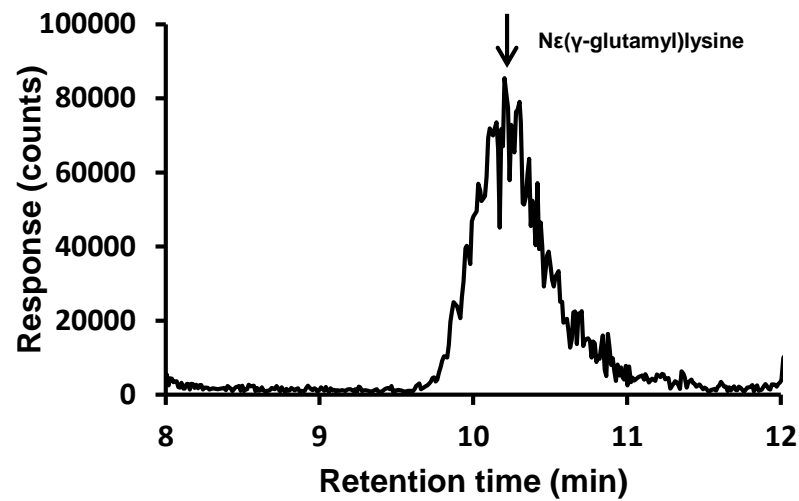
Figure 94. Concentration of 8-oxodG in medium of cultures of MRC-5 cells and 8-oxodG efflux from cells.

a. Concentration of 8-oxoG in culture medium. b. 8-oxodG efflux into the medium from cells at passage termination. Key: , medium at baseline; , medium at passage termination – control cultures; , medium at passage termination – cultures with 1 μ M SFN. Data are mean \pm SD (n = 3). Significance: *, P<0.05 with respect to baseline at respective passages; oo and ooo, P<0.01 and P<0.001 with respect to control cultures (2-tailed t-test).

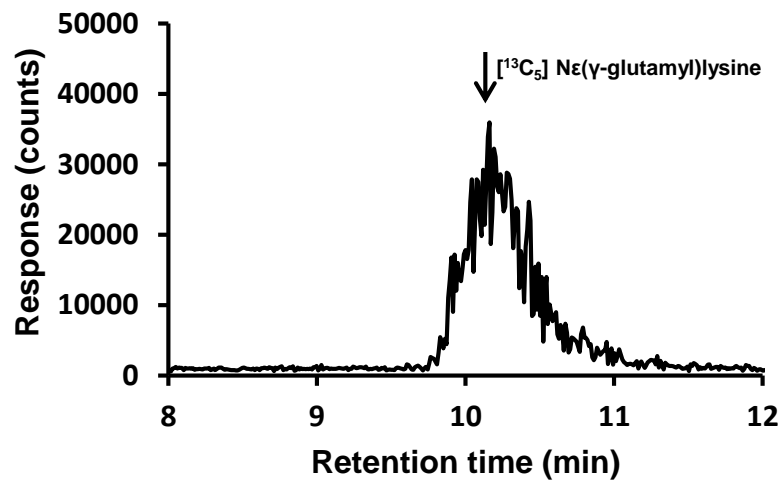
4.8 Effect of progression towards senescence and sulforaphane on formation of Nε(γ-glutamyl)lysine (GEEK) in MRC-5 fibroblast cultures.

Increased expression of transglutaminase is implicated in fibroblast senescence (Kim et al., 2001; Dellorco et al., 1985) with expected increased formation of increased Nε(γ-glutamyl)lysine (GEEK). The cell protein content of GEEK residues and the flux of formation of GEEK released into the culture media in MRC-5 cell cultures at passages 4 and 8 were determined.

Typical analytical chromatograms for determination of GEEK in 20 μl cellular protein are given in Figure 95 (a. and b). The GEEK residue content of cell protein at passage 4 in the control culture and culture treated with 1 μM SFN was 1.11 ± 0.61 mmol/mol lys and 0.91 ± 0.48 mmol/mol lys, respectively, which were not significantly different. At passage 8, however, the GEEK residue content of cell protein in the control cultures was increased by 3-fold compared to passage 4. The GEEK residue content of cell protein of the SFN treatment group was also increased with respect to passage 4 but was decreased *ca.* 45% with respect to control – Figure 97. GEEK free adduct release into culture medium was *ca.* 0.2 nmol/day/10⁶ cells in control and SFN treated cultures at passage 4. By passage 8 this had increased to *ca.* 0.8 nmol/day/10⁶ cells in control and SFN treated cultures with no significant effect on SFN treated cultures – Figure 96.



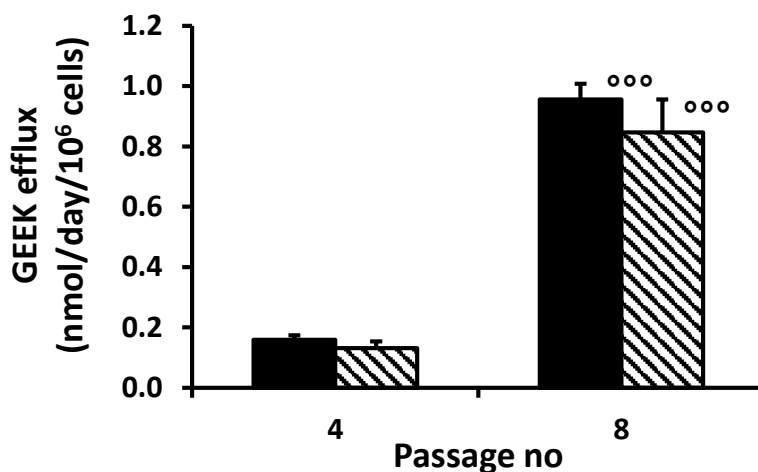
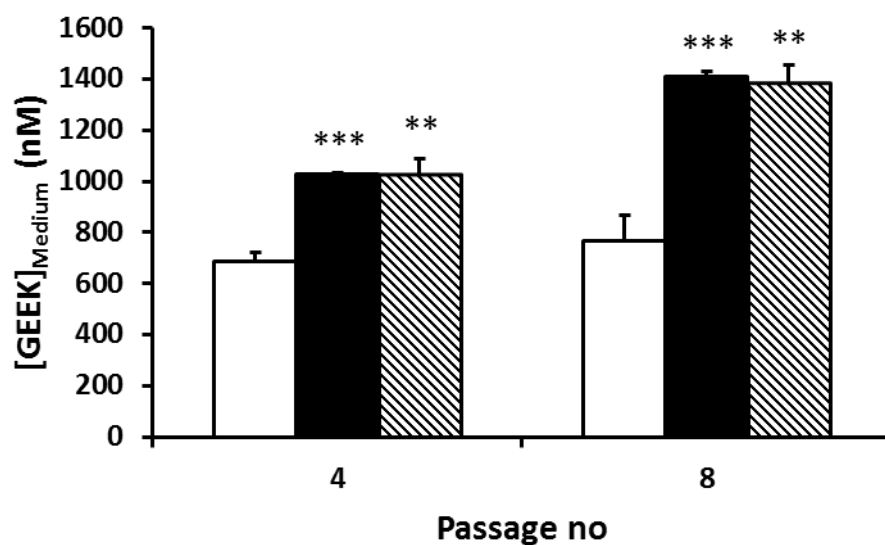
a.



b.


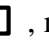

Figure 95. Detection and quantitation of $N\epsilon(\gamma\text{-glutamyl})\text{lysine}$ (GEEK) in cellular protein of MRC-5 cell in culture.

a. Detection of GEEK in cellular protein. Sample: passage 8 with addition of $1\ \mu\text{M}$ SFN. Injection volume: $20\ \mu\text{l}$. **b.** Internal standard ($32.8\ \text{pmol}$) $[^{13}\text{C}_5]\text{GEEK}$.



b.

Figure 96. Concentration of Nε(γ-glutamyl)lysine (GEEK) in medium of cultures of MRC-5 cells and GEEK efflux from cells.

a. Concentration of GEEK in culture medium. b. GEEK efflux into the medium from cells at passage termination. Key:  , medium at baseline;  , medium at passage termination – control cultures;  , medium at passage termination – cultures with 1 μM SFN. Data are mean ± SD (n = 3). Significance: ** and ***, P<0.01 and P<0.001 with respect to baseline at respective passages; ooo, P<0.001 with respect to control cultures (2-tailed t-test).

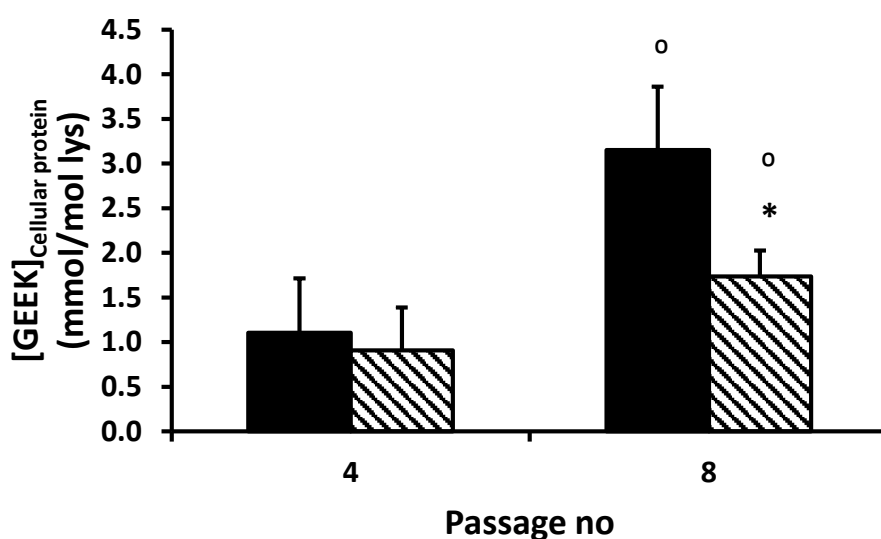


Figure 97. Cellular protein concentration of Nε(γ-glutamyl)lysine (GEEK) in MRC-5 cells at passage 4 and 8 with and without 1μM SFN.

Key: , 0.002% DMSO; , 1 μM SFN. Data are mean ± SD (n = 3).

Significance: *, P<0.05 to control cultures; o, P<0.05 with respect to related control culture at passage 4 (2-tailed t-test).

4.9 Effect of sulforaphane on dicarbonyl precursors of protein and nucleotide glycation in cultures of MRC-5 fibroblasts *in vitro*

Dicarbonyl precursors of glycation, methylglyoxal (MG), 3-deoxyglucosone (3-DG) and glyoxal, were assessed by stable isotopic dilution analysis LC-MS/MS in cell culture media at baseline and at the end of the passage of MRC-5 cell cultures for passages 5, 8 and 11.

For glyoxal, the concentration of glyoxal was decreased at the end of passage with respect to baseline level at passages 8 (-37%, P<0.05) and 11 (-52%, P<0.01) for MRC-5 cells in control cultures but not for MRC-5 cells incubated with SFN. The concentration of glyoxal was decreased at the end of the passage with respect to baseline level in control cultures for all 3 passages combined: 171 ± 53 nM versus 105 ± 45 nM, P<0.05 (n = 9). The concentration of glyoxal in baseline medium for passage 8 was lower than that of medium used for passages 5 and 11: 113 ± 5 nM versus 202 ± 54 nM (P<0.05) and versus 197 ± 27 nM

($P < 0.05$). The concentration of glyoxal in medium of MRC-5 cells in control cultures was decreased at passage 8 with respect to passage 5; 71 ± 20 nM versus 150 ± 47 nM, $P < 0.05$ – Figure 98, a. Glyoxal partitions across the cell plasma membrane where amount of glyoxal in the medium will relate to cell number. Therefore, the efflux of glyoxal from cells at passage termination (pmol per 10^6 cells) was deduced. The efflux of glyoxal was increased in control cultures at passage 11 with respect to passage 5 but not in similar cultures treated with SFN. Combining measurement for passages 8 and 11 as “late passages”, the efflux of glyoxal was increased in control cultures in late passages with respect to passage 5 (4919 ± 1697 versus 1041 ± 413 pmol/ 10^6 cells, $P < 0.01$) but not in similar cultures treated with SFN – Figure 98, b.

For MG, the concentration of MG was decreased at the end of passage with respect to baseline level at passage 5 (-32% , $P < 0.05$) and increased at the end of passage 11 with respect to baseline ($+52\%$, $P < 0.05$) for MRC-5 cells incubated with SFN but was unchanged in MRC-5 cells in control cultures. The concentration of MG in medium of MRC-5 cells in cultures with SFN was increased at passage 8 with respect to passage 5, $P < 0.05$, but was unchanged in control cultures – Figure 99, a. MG partitions across the cell plasma membrane where amount of glyoxal in the medium will relate to cell number. Therefore, the efflux of MG from cells at passage termination (pmol per 10^6 cells) was deduced. The efflux of MG was increased in control cultures at passage 11 with respect to passage 5 and increased at passage 8 with respect to passage 5 in cultures with SFN. Combining measurement for passages 8 and 11 as “late passages”, the efflux of MG was increased in control cultures in late passages with respect to passage 5 (10297 ± 3614 versus 640 ± 230 pmol/ 10^6 cells, $P < 0.01$) and also in cultures treated with SFN (8163 ± 4964 versus 566 ± 79 pmol/ 10^6 cells, $P < 0.01$) – Figure 99, b.

For 3-DG, the concentration of 3-DG was increased at the end of passage with respect to baseline level at passage 5 ($+48\%$, $P < 0.01$), at passage 8 ($+215\%$, $P < 0.001$) and at passage 11 ($+36\%$, $P < 0.05$) for control cultures of MRC-5 cells and increased at passage 8 ($+198\%$, $P < 0.001$) for MRC-5 cells incubated with

SFN. The concentration of 3-DG in cultures at the end of the passage was not changed significantly by addition of SFN for passages 5, 8 and 11. The concentration of 3DG in baseline medium at passage 5 was higher than at passage 8 (268 ± 33 nM versus 163 ± 37 nM, $P < 0.05$) and lower than at passage 11 (268 ± 33 nM versus 383 ± 20 nM, $P < 0.01$) – Figure 100, a. 3-DG partitions across the cell plasma membrane where amount of glyoxal in the medium will relate to cell number. Therefore, the efflux of 3-DG from cells at passage termination (pmol per 10^6 cells) was deduced. The efflux of 3-DG was increased in control cultures at passages 8 and 11 with respect to passage 5 and also increased at passage 11 with respect to passage 8. The efflux of 3-DG was increased at passages 8 with respect to passage 5 in cultures with SFN. Combining measurement for passages 8 and 11 as “late passages”, the efflux of 3-DG was increased in control cultures in late passages with respect to passage 5 (22481 ± 10871 versus 2752 ± 907 pmol/ 10^6 cells, $P < 0.01$) but not in cultures treated with SFN – Figure 100, b.

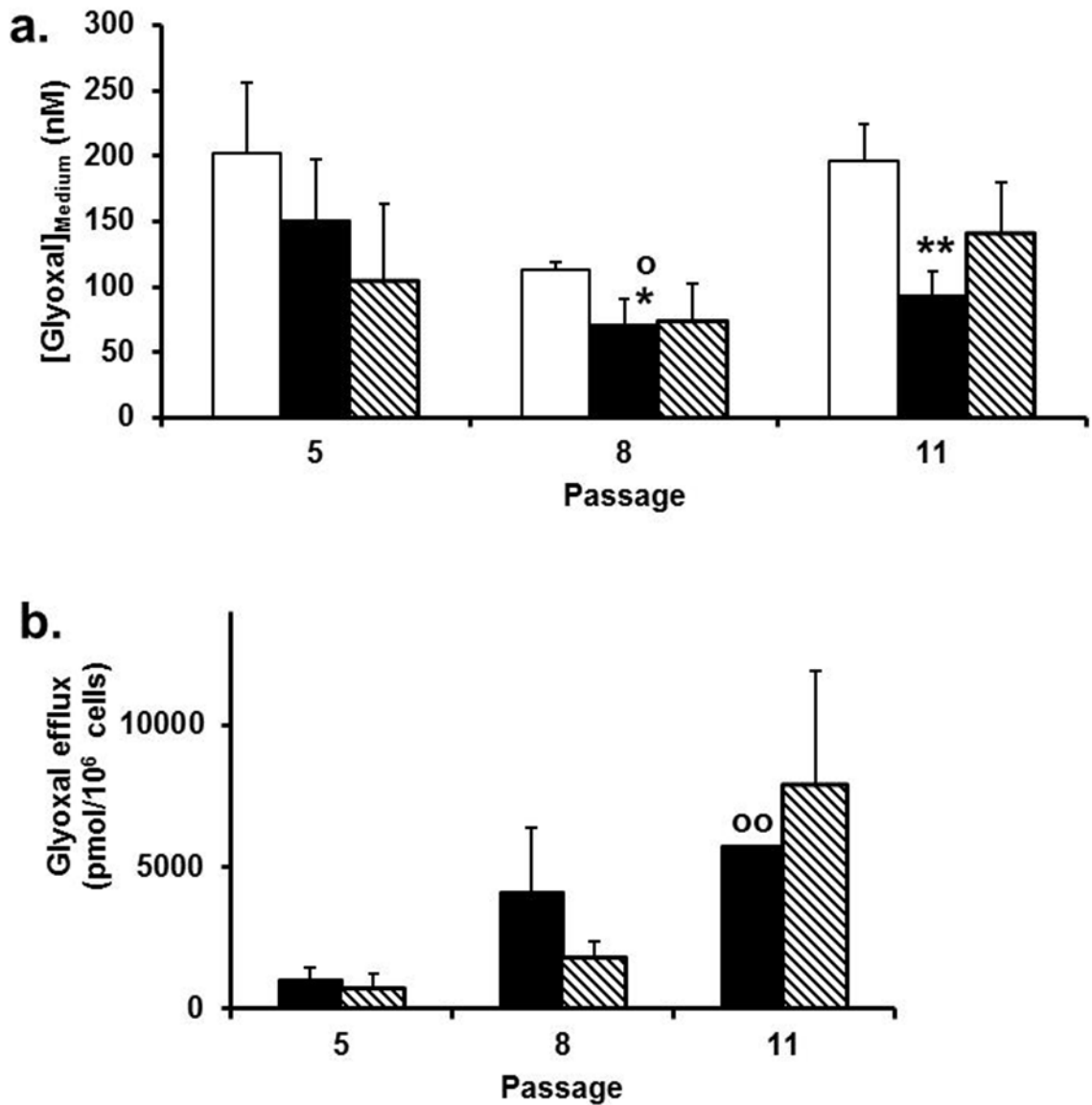


Figure 98. Concentration of glyoxal in medium of cultures of MRC-5 cells and glyoxal efflux from cells.

a. Concentration of glyoxal in culture medium. b. Glyoxal efflux into the medium from cells at passage termination. Key: , medium at baseline; , medium at passage termination – control cultures; , medium at passage termination – cultures with 1 μ M SFN. Data are mean \pm SD (n = 3). Significance: * and **, P<0.05 and P<0.01 with respect to baseline control cultures; ^o and ^{oo}, P<0.05 and P<0.01 with respect to related control culture at passage 5 (t-test and paired t-test, as appropriate).

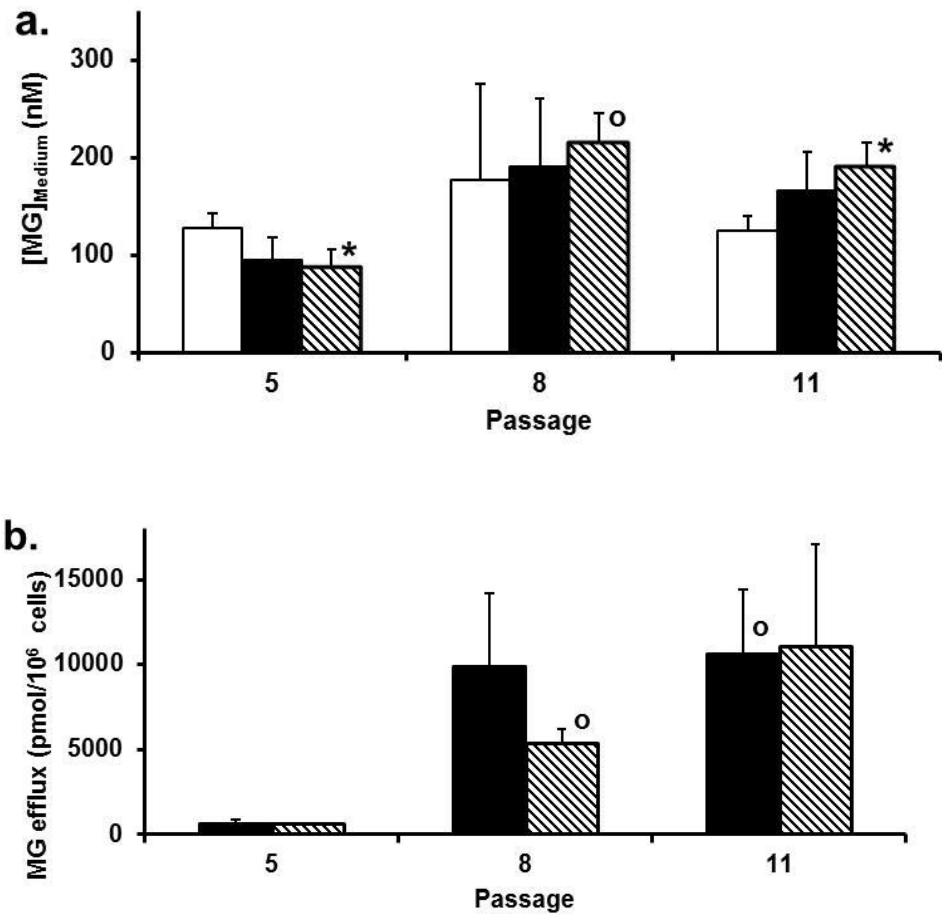





Figure 99. Concentration of methylglyoxal in medium of cultures of MRC-5 cells and methylglyoxal efflux from cells.

a. Concentration of MG in culture medium. b. MG efflux into the medium from cells at passage termination. Key: , medium at baseline; , medium at passage termination – control cultures; , medium at passage termination – cultures with 1 μM SFN. Data are mean ± SD (n = 3). Significance: *, P<0.05 with respect to baseline control cultures; ^o P<0.05 with respect to related control culture at passage 5 (t-test and paired t-test, as appropriate).

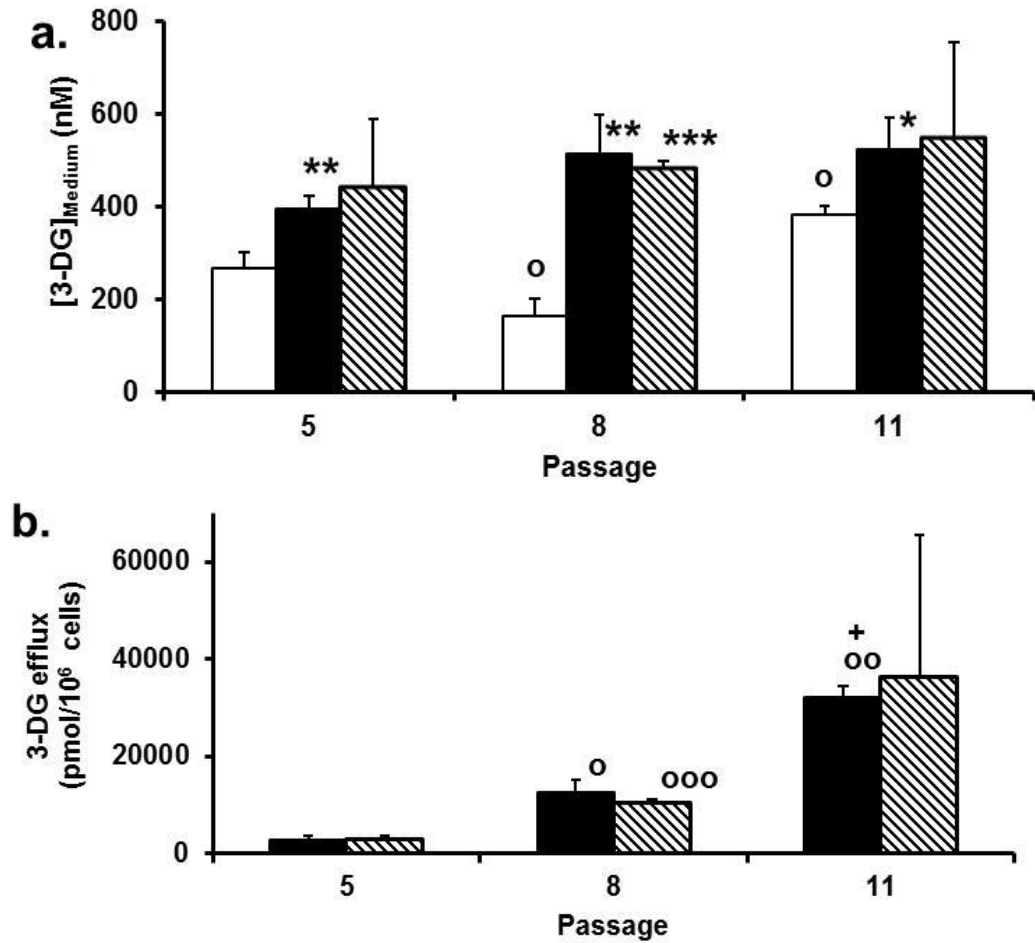


Figure 100. Concentration of 3-deoxyglucosone in medium of cultures of MRC-5 cells and 3-deoxyglucosone efflux from cells.

a. Concentration of 3-DG in culture medium. b. 3-DG efflux into the medium from cells at passage termination. Key: , medium at baseline; , medium at passage termination – control cultures; , medium at passage termination – cultures with 1 μM SFN. Data are mean ± SD (n = 3). Significance: *, ** and ***, P<0.05, P<0.01 and P<0.001 with respect to baseline control cultures; o, oo and ooo, P<0.05, P<0.01 and P<0.001 with respect to related control culture at passage 5; and +, P<0.05 with respect to related control culture at passage 8 (t-test and paired t-test, as appropriate).

4.10 Effect of treatments at the approach to senescence on the consumption of glucose by MRC-5 and BJ fibroblasts *in vitro*

4.10.1 Effect of the approach to senescence and treatment with sulforaphane on the consumption of glucose by MRC-5 fibroblasts *in vitro*

The concentration of glucose in in cultures of MRC-5 fibroblasts at the beginning and end of passages 4, 8 and 12 was determined and the flux of glucose metabolized deduced.

The consumption of glucose increased progressively from 2.59 ± 0.40 μmol per day per 10^6 cells at passage 4 to a maximum of 30.74 ± 2.20 μmol per day per 10^6 cells at passage 12. Incubation with $1 \mu\text{M}$ SFN from passage 3 decreased glucose consumption which was statistically significant at passages 10, 11 and 12 with glucose consumption decreased by 34%, 60% and 53% respectively ($P < 0.01$) – Figure 101.

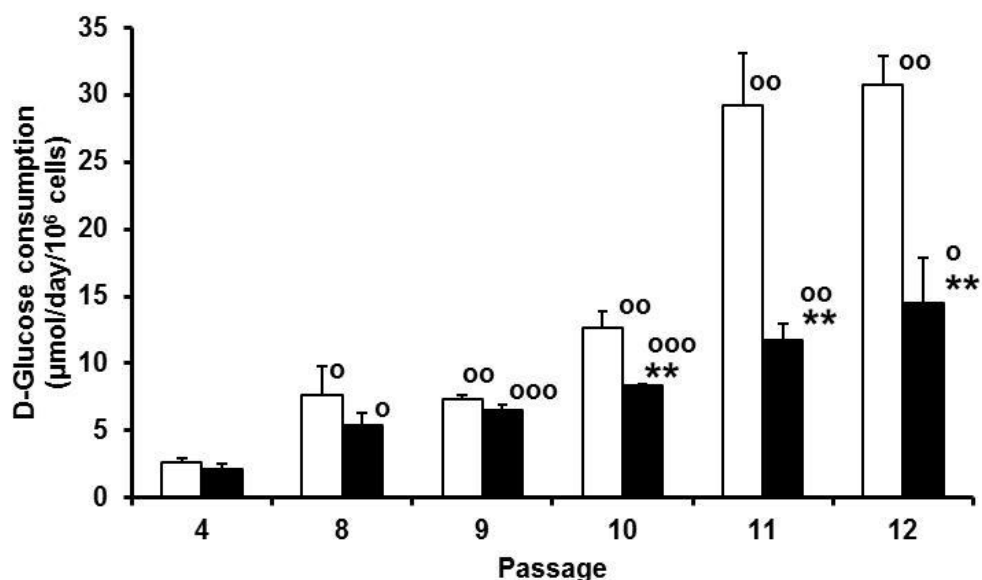


Figure 101. Effect of approach to senescence and sulforaphane on the consumption of D-glucose by MRC-5 fibroblasts *in vitro*.

Data are mean \pm SD ($n = 3$). Key: , control; , + $1 \mu\text{M}$ SFN.

Significance: **, $P < 0.01$ with respect to control cultures; o, oo and ooo, $P < 0.05$, $P < 0.01$ and $P < 0.001$ with respect to related culture at passage 4 (t-test and paired t-test, as appropriate).

4.10.2 Effect of the approach to senescence and treatment with sulforaphane on the consumption of glucose by BJ fibroblasts *in vitro*

Culture media samples were available from a similar study of the approach of human BJ fibroblasts to senescence and delay by treatment with 1 μM SFN. The consumption of glucose increased progressively from 3.48 ± 0.09 μmol per day per 10^6 cells at passage 6 to a maximum of 14.80 ± 1.50 μmol per day per 10^6 cells at passage 19. Incubation with 1 μM SFN from passage 3 decreased glucose consumption by 30% at passage 19 ($P < 0.001$), although at earlier passage treatment with SFN had increased consumption of glucose – Figure 102.

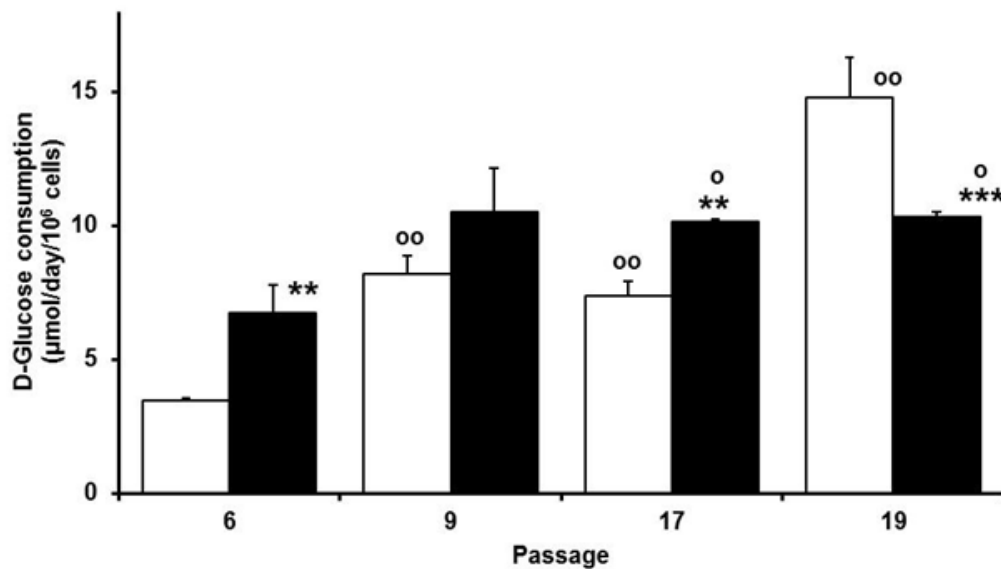


Figure 102. Effect of approach to senescence and sulforaphane on the consumption of D-glucose by BJ fibroblasts *in vitro*.

Data are mean \pm SD ($n = 3$). Key: , control; , + 1 μM SFN.

Significance: ** and ***, $P < 0.01$ and $P < 0.001$ with respect to control cultures; o and oo, $P < 0.05$ and $P < 0.01$ with respect to related culture at passage 6 (t-test and paired t-test, as appropriate).

4.10.3 Effect of the approach to senescence and treatment with hesperetin on the consumption of glucose by MRC-5 fibroblasts *in vitro*

The consumption of glucose increased progressively from 4.11 ± 0.24 μmol per day per 10^6 cells at passage 7 to a maximum of 38.41 ± 4.72 μmol per day per 10^6 cells at passage 9. Incubation with 5 μM hesperetin from passage 3 decreased glucose consumption which was statistically significant at passages 7 and 12 with glucose consumption decreased by 29% and 33% respectively ($P < 0.05$) – Figure 103.

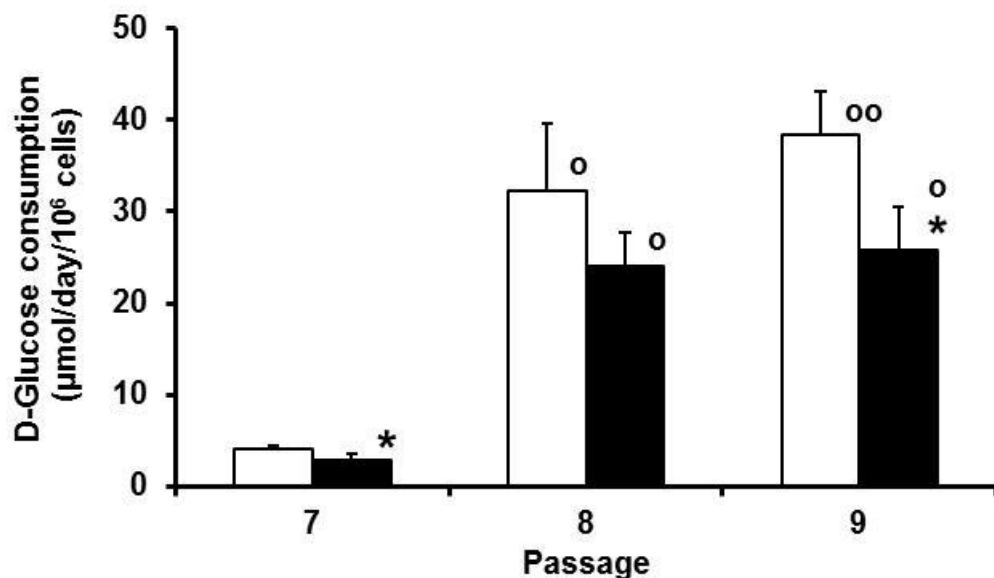


Figure 103. Effect of approach to senescence and hesperetin on the consumption of D-glucose by MRC-5 fibroblasts *in vitro*.

Data are mean \pm SD ($n = 3$). Key: , control; , + 5 μM Hesperetin. Significance: *, $P < 0.05$ with respect to control cultures; o and oo, $P < 0.05$ and $P < 0.01$ with respect to related culture at passage 7 (t-test and paired t-test, as appropriate).

4.11 Effect of approach to senescence and sulforaphane on reduced glutathione concentration in MRC-5 fibroblasts cell pellets

MRC-5 fibroblasts were cultured in media supplemented with and without 1 μ M SFN from passage 3. Cell pellets were collected at the end of passages 4 and 10 and the cell content of GSH was determined by stable isotopic dilution analysis LC-MS/MS. The cellular content of GSH increased ca. 3-fold in control cultures in passage 10 with respect to passage 4. Treatment with SFN did not change the cellular content of GSH at passage 4 but increased cellular content of GSH by 34% at passage 10 – Figure 104.

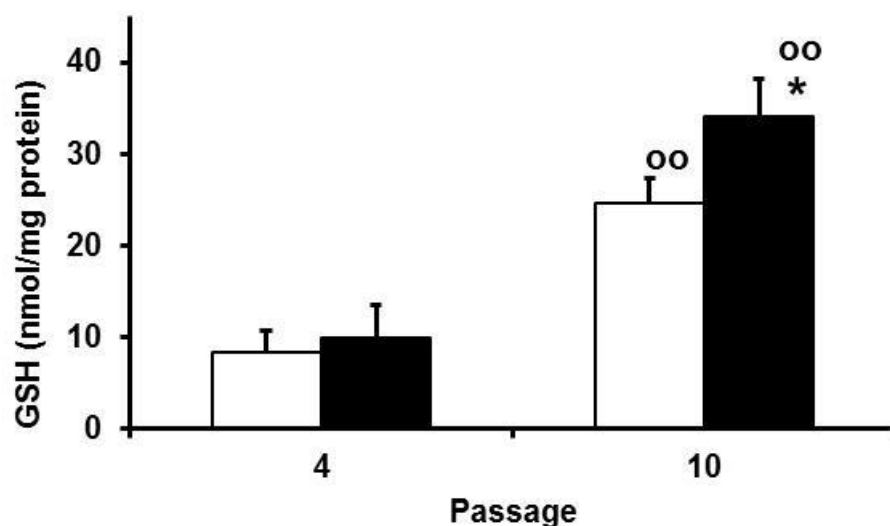


Figure 104. Effect of approach to senescence and sulforaphane on the reduced glutathione content of MRC-5 fibroblasts *in vitro*.

Data are mean \pm SD (n = 3). Key: , control; , + 1 μ M SFN.

Significance: ** and ***, P<0.01 and P<0.001 with respect to control cultures; o and oo, P<0.05 and P<0.01 with respect to related culture at passage 4 (t-test and paired t-test, as appropriate).

4.12 Characterization of the mechanism of decrease glucose metabolism by SFN and HESP action linked to delay of fibroblast senescence

4.12.1 Effect of approach to senescence and sulforaphane on the concentration of L-lactate in cultures of MRC-5 fibroblasts *in vitro*.

L-Lactate is a major metabolite of glucose metabolism and although it is formed and metabolized by MRC-5 cells *in vitro* there was a marked export from cells into the culture medium. In fresh culture medium used for passages 4, 8 and 12, the concentration of L-lactate was 0.31 – 0.93 mM. At the end of the passages this has increased 3 – 4 fold. The flux of L-lactate export into the medium relates to cell number therefore the net increase of L-lactate in cell cultures during the passage was computed from the difference in baseline and end of passage L-lactate concentrations and reported as nmol per day per 10⁶ cells. In control cultures the apparent flux of L-lactate was not increased significantly at passage 8 with respect to passage 4. However, at passage 12 the apparent flux of L-lactate was increased ca. 11 fold with respect to passage 4. In cells treated with SFN the apparent flux of L-lactate was increased similarly excepting a 23% decrease in apparent flux of L-lactate at passage 12 compared to control cultures –Figure 105.

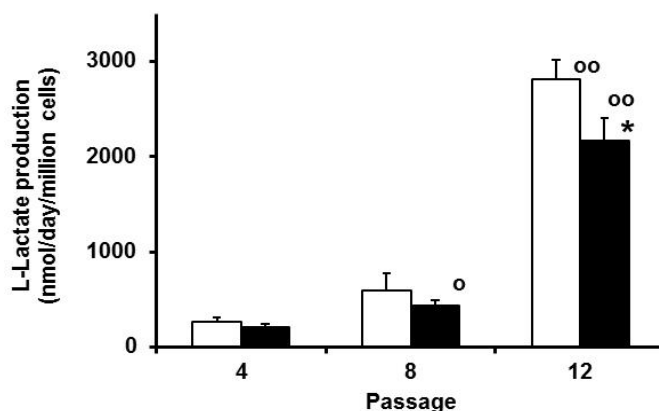


Figure 105. Effect of approach to senescence and sulforaphane on the apparent flux of L-lactate production by MRC-5 cells *in vitro*.

Data are mean ± SD (n = 3). Key: control; , + 1 μM SFN.

Significance: *, P<0.05 with respect to control culture; o and oo, P<0.05 and P<0.01 with respect to related culture at passage 4 (t-test and paired t-test, as appropriate).

4.12.2 Effect of the approach to senescence, sulforaphane and hesperetin on D-lactate production in MRC-5 fibroblasts *in vitro*.

D-Lactate is the terminal product of MG metabolism by the glyoxalase system. It is weakly metabolized in human cells and is a measure of flux of MG formation. The concentration of D-lactate in the medium of cultures at baseline and end of passage were determined and the mean flux of formation of D-lactate deduced. The flux of D-lactate by MRC-5 fibroblasts was 0.31 ± 0.04 nmol per day per 10^6 cells at passage 4 of control cultures. This did not increase significantly at passage 8 but increased 11-fold at passage 12. At passage 12 SFN decreased the flux of formation of D-lactate by 28% - Figure 106.

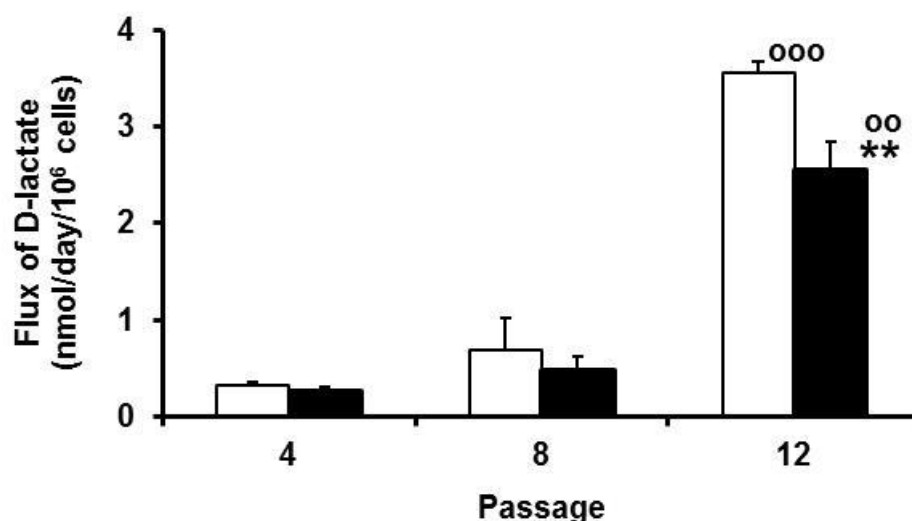


Figure 106. Effect of approach to senescence and sulforaphane on the flux of formation of D-lactate by MRC-5 cells *in vitro*.

Data are mean \pm SD (n = 3). Key: control; + 1 μ M SFN. Significance: **, P<0.01 with respect to control culture; oo and ooo, P<0.01 and P<0.001 with respect to related culture at passage 4 (t-test and paired t-test, as appropriate).

In a similar experiment with and without hesperetin the flux of formation of D-lactate was quantified in MRC-5 cell cultures at passages 7, 8 and 9. The flux of formation of D-lactate increased in control cultures at passage 9 with respect to the flux of formation of D-lactate at passage 7 and in HESP treated cultures at passages 8 and 9 with respect to the flux of formation of D-lactate at

passage 7. However, HESP did not decrease the flux of formation of D-lactate significantly - Figure 107.

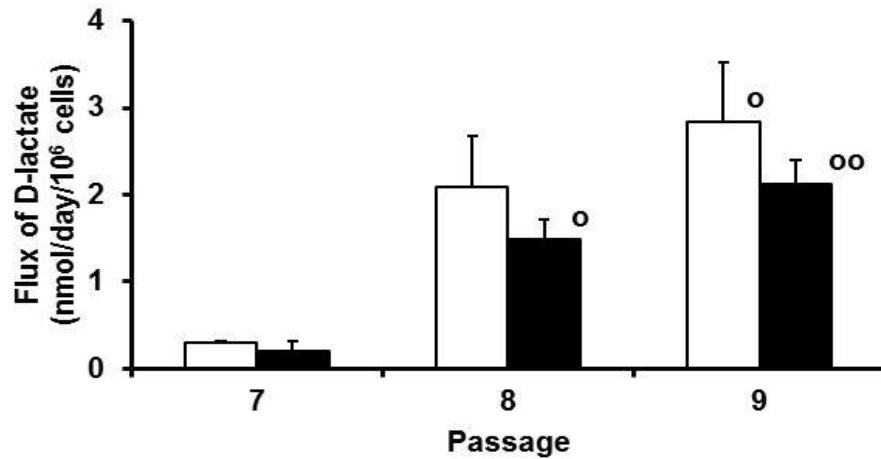


Figure 107. Effect of approach to senescence and hesperetin on the flux of formation of D-lactate by MRC-5 cells *in vitro*.

Data are mean \pm SD (n = 3). Key: control; , + 5 μ M HESP. Significance: o and oo, P<0.05 and P<0.01 with respect to related culture at passage 4 (paired t-test).

4.13 Effect of sulforaphane on the cellular content of glycolytic intermediates

To investigate the effect of SFN on early-stage glycolysis in MRC-5 cells, the changes in the cellular concentrations of glycolytic intermediates were quantified. Key initial intermediates potentially regulated by SFN are G6P, F6P and PGA – Figure 108.

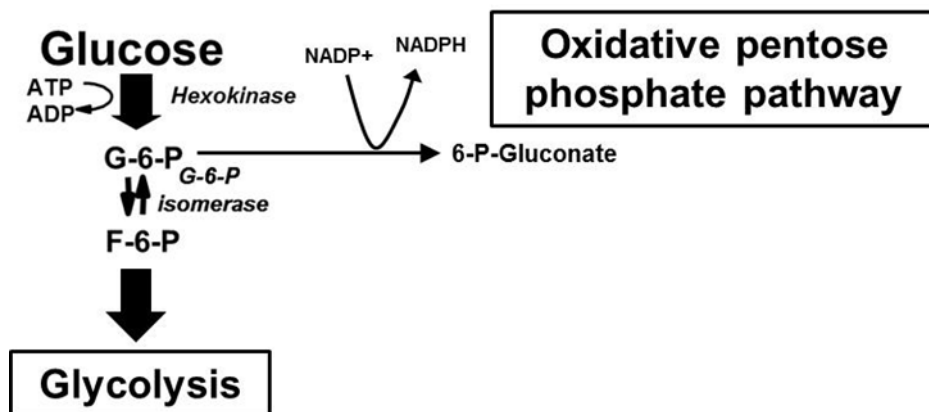


Figure 108. Glycolytic intermediates for entry of glucose into glycolysis and the pentose phosphate pathway.

G6P and F6P are isobaric and hence must be resolved chromatographically before mass spectrometric analysis. This is achieved by retention on Hypercarb graphitic columns – although a substantial column volume is required to achieve this (effectively 400 mm x 2.1 mm column) – Figure 109, a. and c. Stable isotopic standards from prepared [^{13}C]labelled cell extracts provide for robust internal standardisation – Figure 109, b. and d. The calibration curves were linear over a wide dynamic range and the limits of detection appropriate for quantitation in the cell samples – Figure 109, e. and f. G6P, F6P and PGA were quantified in MRC-5 cells with and without SFN treatment – Table 38.

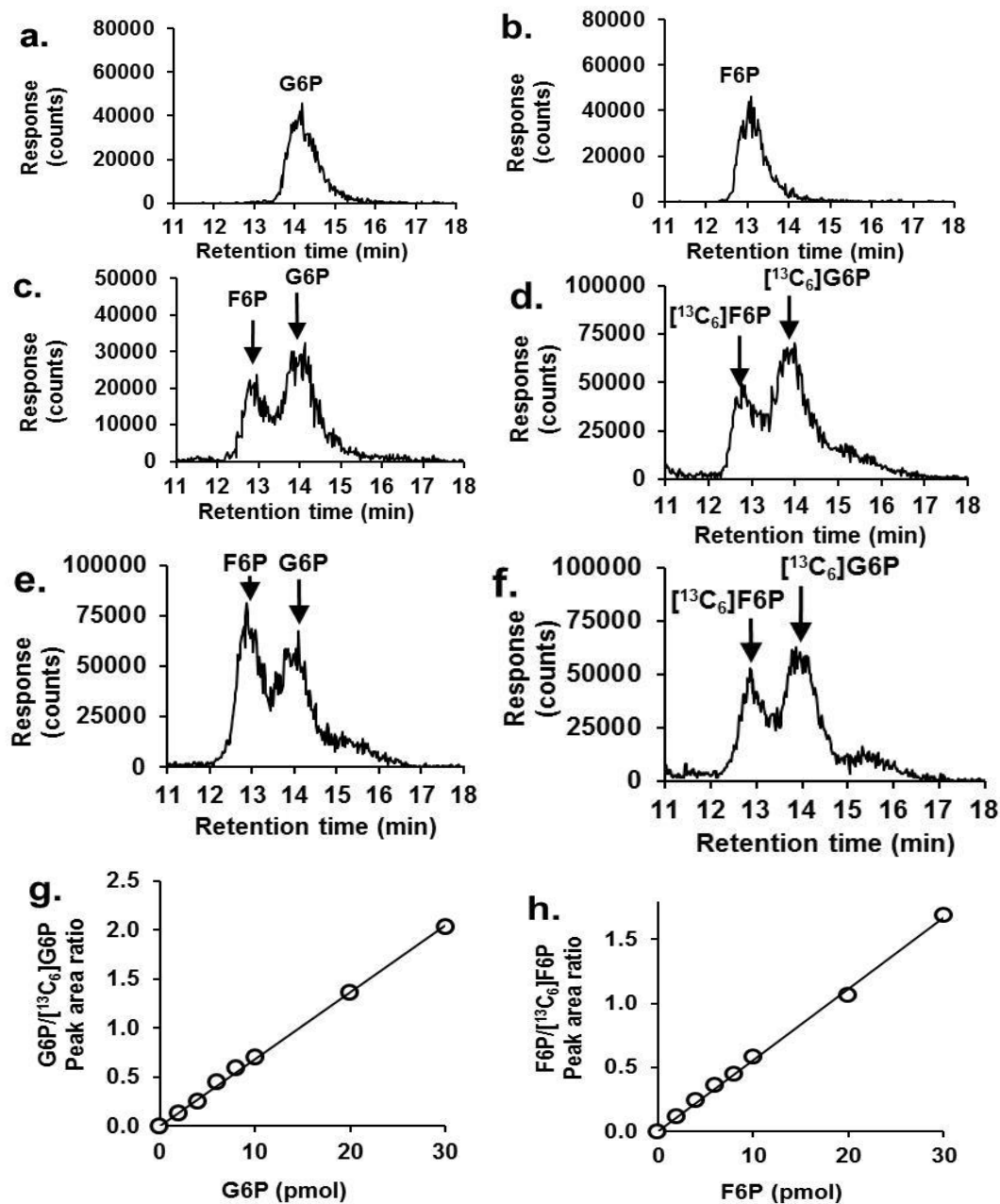


Figure 109. Detection of glucose-6-phosphate and fructose 6-phosphate by liquid chromatography-tandem mass spectrometry. MRM chromatograms. **a.** and **b.** G6P (10 pmol), **b.** F6P (10 pmol). Calibration standard containing 6 pmol G6P, 6 pmol F6P, 14.7 pmol $[^{13}\text{C}_6]\text{G6P}$ and 19.8 pmol $[^{13}\text{C}_6]\text{F6P}$. **c.** Detection of G6P and F6P, MRM transition 259.0 > 78.9 Da. **d.** Detection of $[^{13}\text{C}_6]\text{G6P}$ and $[^{13}\text{C}_6]\text{F6P}$, MRM transition 265.0 > 78.9 Da. **c.** and **d.** quantitation of G6P and F6P in a test samples (MRC-5 cells incubated with SFN). **e.** G6P and F6P, , MRM transition 259.0 > 78.9 Da. **f.** Stable isotopic standards, $[^{13}\text{C}_6]\text{G6P}$ and $[^{13}\text{C}_6]\text{F6P}$, MRM transition 265.0 > 78.9 Da. **g.** and **h.** Calibration curves for the quantitation of G6P and F6P, respectively. **g.** G6P. Regression equation: $\text{G6P}/[^{13}\text{C}_6]\text{G6P}$ peak area ratio = $(0.0680 \pm 0.0006)\text{G6P}$ (pmol). **h.** Regression equation: $\text{F6P}/[^{13}\text{C}_6]\text{F6P}$ peak area ratio = $(0.147 \pm 0.001)\text{F6P}$ (pmol).

Table 38. Effect of sulforaphane on early-stage glycolytic intermediates in MRC-5 cells *in vitro*.

Treatment	G6P (pmol/10 ⁶ cells)	F6P (pmol/10 ⁶ cells)	PGA (pmol/10 ⁶ cells)
Passage 4, 6 h with 25 mM glucose	205 ± 20	877 ± 247	95 ± 13
Passage 4, 6 h with 25 mM glucose + 1 µM SFN	115 ± 40 (P<0.05)	747 ± 61	120 ± 7 (P<0.05)
Passage 5 (Control)	79 ± 1	212 ± 18	89 ± 18
Passage 5, + 1 µM SFN	87 ± 19	160 ± 25 (P<0.05)	70 ± 32
Passage 9 (Control)	293 ± 6	327 ± 29	1104 ± 197
Passage 9, + 1 µM SFN	326 ± 58	329 ± 45	983 ± 185

Short term incubation with SFN in high glucose concentration medium decreased the cellular content of G6P and concurrently increased the cellular content of PGA without change in the cellular content of F6P. The cellular contents of G6P, PGA and F6P were higher in control cells at passage 9 than at passage 5. Addition of SFN decreased F6P in passage 5 but was without effect on other glycolytic intermediate in passage 5 and passage 9. However, it must be noted that the lower concentration of G6P relative to F6P could be due to changes during cell harvesting with trypsin.

4.14 Immunostaining for Mondo A in MRC-5 fibroblasts *in vitro*

A transcription factor sensitive to the cellular content of G6P is carbohydrate response element binding protein or Mondo A in fibroblasts. When Mondo A is activated it binds G6P and translocates to the cell nucleus. To study the effect of SFN on cellular activation of Mondo A, MRC-5 cells were incubated with and without SFN with low and high glucose concentrations. MRC-5 cells were then fixed and immunocytofluorescence microscopy performed to study the subcellular location of Mondo A.

When MRC-5 cells were incubated overnight in low glucose concentration (0.2 mM) followed by 6 h with high glucose concentration (25 mM),

immunostaining for Mondo A showed high intensity staining in the cell nucleus in control cultures which was suppressed by incubation with 1 μ M SFN – Figure 110. Following incubation in normal glucose concentration (5.5 mM) of MRC-5 cells, immunostaining for Mondo A showed no staining in the cell nucleus. However, high intensity staining was seen in the cell nucleus of cultures receiving subsequent treatment with high glucose concentration (25 mM) for 6h. which was then suppressed by incubation with 1 μ M SFN – Figure 111. When MRC-5 cells were incubated overnight in high glucose concentration (25 mM), immunostaining for Mondo A showed no staining in the cell nucleus in control cultures. Surprisingly, in the same cultures, when MRC-5 cells were incubated overnight in high glucose concentration (25 mM) with addition of 1 μ M SFN, immunostaining for Mondo A showed slightly higher intensity staining in the cell nucleus – Figure 112.

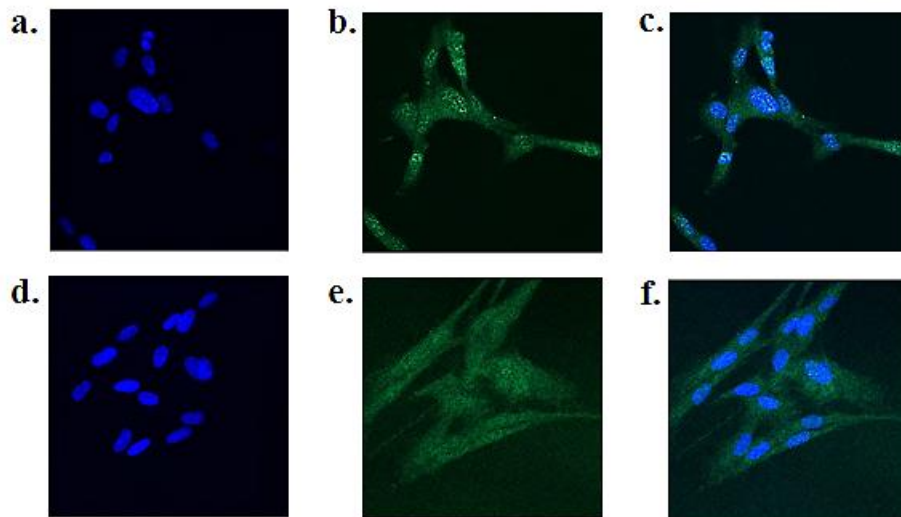


Figure 110. Immunostaining for localization of Mondo A in MRC-5 cells *in vitro*.

Cells were incubated overnight in medium containing 0.2 mM glucose and then incubated with 25 mM glucose for 6 h. Key: **a. – c.** Control, **a.** DAPI nuclear stain, **b.** immunostaining with anti-Mondo A IgG, and **c.** Overlay of **a.** and **b.**; **d. – f.**, + 1 μ M SFN, **d.** DAPI nuclear stain, **e.** immunostaining with anti-Mondo A IgG, and **f.** Overlay of **d.** and **e.**

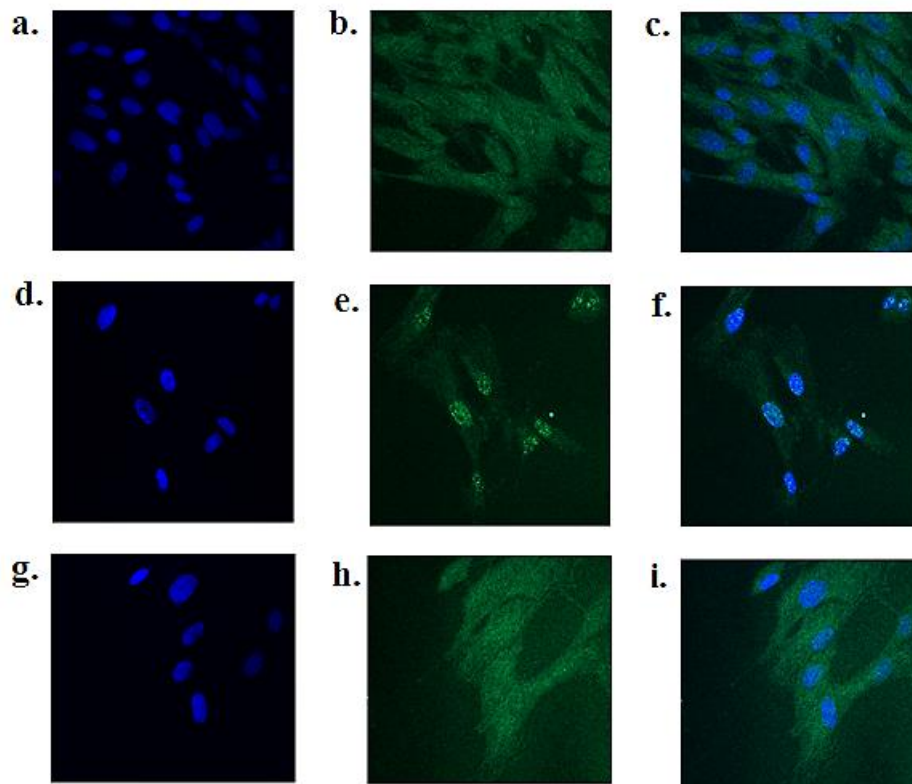


Figure 111. Immunostaining for localization of Mondo A in MRC-5 cells *in vitro*.

Cells were incubated overnight in medium containing 5.5 mM glucose. Key: **a. – c.** Control, **a.** DAPI nuclear stain, **b.** immunostaining with anti-Mondo A IgG, and **c.** Overlay of **a.** and **b.**; **d. – f.**, + 25 mM glucose for 6 h., **d.** DAPI nuclear stain, **e.** immunostaining with anti-Mondo A IgG, and **f.** Overlay of **d.** and **e.**; **g. – i.** + 25 mM glucose and 1 μ M SFN for 6 h. **g.** DAPI nuclear stain, **h.** immunostaining with anti-Mondo A IgG, and **i.** Overlay of **g.** and **h.**

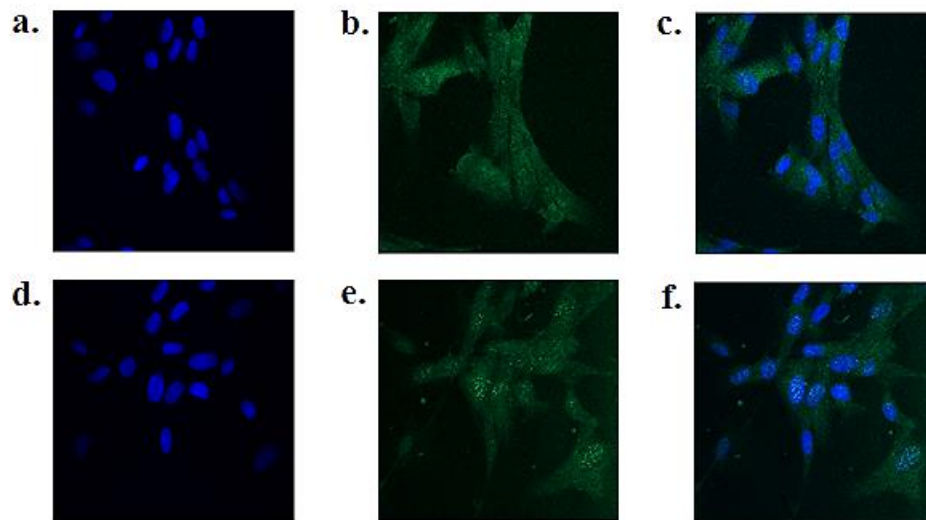


Figure 112. Immunostaining for localization of Mondo A in MRC-5 cells *in vitro*.

Cells were incubated overnight in medium containing 25 mM glucose. Key: **a. – c.** Control, **a.** DAPI nuclear stain, **b.** immunostaining with anti-Mondo A IgG, and **c.** Overlay of **a.** and **b.**; **d. – f.**, + 1 μ M SFN, **d.** DAPI nuclear stain, **e.** immunostaining with anti-Mondo A IgG, and **f.** Overlay of **d.** and **e.**

5. Discussion

The concept of cellular senescence is based on the notion that proliferation of normal diploid cells can only occur for a limited period of time after which cells slowly cease to divide and die (Cristofalo and Pignolo, 1993). This limitation of lifespan for *in vitro* cell cultures was first described by Leonard Hayflick in 1961, going against the theory formulated by Alexis Carrel claiming that cells kept in culture have an unlimited potential for division (Carrel and Ebeling, 1921). Evidence from cell senescence studies have been used to explain the basis of healthy ageing as well as develop food supplements promoting the delay of ageing. Main mechanisms thought to contribute to cellular senescence are thought to include shortening of telomeres, autophagy, as well as mitochondria metabolism. Moreover, theories of ageing as applied to cell senescence are thought to be the result of accumulation of macromolecular damage such as oxidative damage and glycation. Stress responsive signalling coordinated by nuclear factor erythroid 2-related factor 2 (Nrf2) provides an adaptive response for protection of cells against toxic insults, oxidative stress and metabolic dysfunction. Nrf2 regulates a battery of protective genes by binding to regulatory anti-oxidant response elements (AREs). Nrf2 regulates the cellular expression of a battery of protective genes countering oxidative stress, environment toxic insults, lipid peroxidation, macromolecular damage, metabolic dysfunction and cell senescence (Kapeta et al., 2010; Malhotra et al., 2010; Taguchi et al., 2011; Xue et al., 2013).

Since these discoveries, there has been marked expansion of anti-stress gene response research with relation to the role of the transcription factor NF-E2-related factor-2 as well as healthy ageing with regards to dietary activators intake. Dietary activators such as carotenoids (Bishop and Guarente, 2007), omega-3 fatty acids (Orr et al., 2005), isoflavones (Sykiotis and Bohmann, 2008) and others, have been shown to activate Nrf2 but the challenge lays in the discovery of dietary bioactives that would be able to promote healthy ageing (Ben-Dor et al., 2005). Finally, the current Nrf2 system model does not explain how Nrf2 is

activated without change in Nrf2 protein content, how Nrf2 oscillation in and out of the nucleus does not require activation and how Nrf2 is inactivated when trapped in the cell nucleus. This is the rationale of this project for the production of healthy ageing through a better understanding of the activation of the Nrf2 system with dietary bioactive compounds.

5.1 Effects of SFN and HESP on MRC-5 and BJ senescence *in vitro*

5.1.1 Effect of sulforaphane treatment on MRC-5 fibroblasts growth

Transcription factor Nrf2 regulates the expression of a battery of genes via interaction with one or more AREs that provide protection against proteome, lipidome and genome damage by glycation, oxidation and nitration (Kapeta et al., 2010; Malhotra et al., 2010; Tagichi et al., 2011; Xue et al., 2013). The delay of MRC-5 senescence by the Nrf2-activating dietary bioactive compound SFN was studied. Initially, growth patterns of MRC-5 fibroblasts was studied by construction of a growth curve and showed an exponential growth curve in the initial 3 days of culture which thereafter slowed to quiescence as the cells reached confluence. Cell viability remained at >98% (Trypan blue exclusion) throughout the culture period. Moreover, MRC-5 cells were incubated with SFN, 0-8 μM for 48 h and the dose-response curve showed that the median growth inhibitory concentration GC50 value of SFN was $2.60 \pm 0.03 \mu\text{M}$ and the logistic regression coefficient n was 2.02 ± 0.03 . Also, there was no significant inhibition of MRC-5 cell growth at SFN concentrations up to 1.5 μM SFN and negligible toxicity (< 5%) although at $\geq 2 \mu\text{M}$ SFN there was growth arrest. Surh *et al.* (2008) have shown that isothiocyanates are activators of Nrf2. Many studies with putative Nrf2 activators have, however, used high concentrations which are not translatable clinically and/or activate Nrf2 within the toxic concentration range. In the latter case toxicity prevents use of such compounds and activation of Nrf2 is likely as part of the response to toxicity rather than a direct agonism of the Nrf2 system. Therefore, it was crucial to determine toxicity of SFN in MRC-5

fibroblasts prior to use in senescence delay study to avoid toxic effects of the bioactive compounds investigated.

To study the effect of SFN treatment on MRC-5 fibroblasts growth, cells were grown in Eagle's MEM media supplemented each week with or without 1 μM SFN. The population doubling limit (PDL) as well as cumulative PDL (cPDL) were analyzed in order to represent MRC-5 fibroblast growth as progression of senescence occurred and cumulative PDL was calculated from addition of PDL from one passage to another. This work shows that, in four similar experiments, weekly treatment with 1 μM SFN in young MRC-5 fibroblasts in culture treated until the onset of senescence delayed cellular ageing in these cells. Indeed, in control cultures, PDL increased at early passages but decreased progressively by reaching the onset of senescence. At later passages the PDL was negative, indicating that the cells were no longer growing and viable cell number was progressively decreasing. With SFN treatment, the combined increase in PDL over early passage (3 to 5) was significantly increased compared to control cPDL. Indeed, with 1 μM SFN treatment, not only did the maximum cPDL was higher than in control cultures, but also, maximum cPDL was reached at later passage compared to control. From regression analysis of PDL on passage number, the rate of decline in PDL per passage with and without SFN was similar whereas the intercept was higher with SFN in all repeated cultures. This suggests the rate of decline in MRC-5 cell growth on approach to senescence with and without SFN is similar; treatment with SFN, however, delayed the onset of approach to senescence. In the three replicate studies, the increase in cPDL achieved with SFN treatment was a 2 unit increase in cPDL or two additional population doublings. When this effect was also investigated regarding late initiation of SFN treatment at cPDL = 41, this also achieved a significant increase in cPDL compared to control after only treatment of 4 passages. These findings are similar to findings by Hintze and Nabor (2008) who discovered that 2 μM SFN delayed senescence of IMR-90 lung fibroblast cells *in vitro*. The findings herein were demonstrably reproducible using a concentration of SFN that may be readily achieved in plasma by consumption of broccoli. The SFN concentration

was 50% lower than that used by Hintze and Nabor (2008). Herein there was significant decrease of cell growth with 2 μ M SFN. Hintze and Nabor (2008) did not report the effect of 2 μ M SFN on cell growth in their investigation. Use of low concentrations of SFN is important for clinical translation as SFN has a relatively narrow therapeutic concentration range – typically activating Nrf2 and related ARE-linked gene expression at 1 – 2 μ M but decreasing cell growth and viability at concentrations greater than this (Xue et al., 2012). This study is the first to show that SFN delays cell senescence of MRC-5 cells *in vitro*. More extraordinarily, SFN treatment initiated only 2 passages before onset of senescence also delayed senescence. This is innovative and suggests last stage interventions of in senescence-related phenomena may still be effective. This finding holds great hope in ageing research as it would imply that the accumulation of cellular damage as seen in ageing is a reversible process which can be delayed even at later stages in life. Similar work in the host team found the same response in BJ fibroblast *in vitro* (Xue, M and Thornalley, PJ, 2014, unpublished observation).

5.1.2 Effect of hesperetin treatment on MRC-5 fibroblasts growth

The median growth inhibitory concentration GC_{50} value of HESP with MRC-5 cells was 4.83 ± 0.45 μ M. There was no significant inhibition of MRC-5 cell growth at 1.0 μ M HESP and for all concentrations used, there was no toxicity. Low toxicity at higher dose of HESP was expected as intake of flavonoids such as hesperetin from the diet can be quite high but without toxic consequences *in vivo* (Erlund et al., 2001). At higher concentrations, however, our study has shown that HESP decreased MRC-5 cell growth, therefore affecting cellular development and questioning the validity of *in vivo* and *in vitro* studies found in the literature using this compound which do not show dose-response analysis.

To study the effect of HESP treatment on MRC-5 fibroblast growth, cells were grown in Eagle's MEM media supplemented each week with or without 5 μ M HESP. Similarly to our study of SFN, treatment with HESP delayed cell

senescence. The maximum cPDL with HESP treatment increased cPDL by 1.5. The peak plasma concentration of HESP after consumption of orange juice (8 ml/kg) in human subjects was 0.5 – 5 μ M (Erlund et al., 2001), hence hesperetin concentrations from dietary intake of HESP and glycosides may be pharmacologically competent to delay cells senescence.

Although several epidemiological studies have suggested a protective effect of HESP on cardiovascular diseases (Knekt et al., 1996), decrease of risk of ischemic stroke (Joshi-pura et al., 1999) and lung cancer (Le Marchand et al., 2000) as well as anticarcinogenic (So et al., 1996), antioxidant (van Acker et al., 2000) and blood lipid-lowering (Shin et al., 1999) properties, this compound has never been studied individually as part of a senescence-delay study. Indeed, pummelo juice which contains hesperetin amongst other flavonoids, has been shown to delay senescence in the cardiac cell line H9c2 derived from embryonic rat heart (Chularojmontri et al., 2013). However, our findings have not only established that 5 μ M of HESP is suitable for study of senescence in MRC-5 fibroblasts without triggering cell toxicity or growth delay, but also that HESP only successfully delays senescence in these fibroblasts.

5.1.3 Effect of sulforaphane on staining and expression of senescence-associated beta-galactosidase in MRC-5 fibroblasts

Onset of cell senescence in MRC-5 cells was assessed by staining for the senescence marker, beta-galactosidase. For this purpose, the percentage of cells expressing β -galactosidase was determined for passages 4 to 9. Control MRC-5 fibroblasts had a higher percentage of senescent cells in culture than SFN-treated MRC-5 cells at passages 6 and 9 ($P < 0.05$) indicating that treatment delayed senescence marked by decreased β -galactosidase expression compared to control in these two passages. This is an important finding as it supports the findings arising from the performed SFN senescence delay study based on PDL and cPDL. Indeed, beta-galactosidase (SA- β -Gal) is the most commonly used marker to quantify senescence at the cellular level. The SA- β -Gal assay is a

reliable and well established method as it was first described in 1995 by Dimri *et al.* in which they observed that at pH 6.0, senescent cells expressed the β -galactosidase enzyme in the cytosol when compared with fibroblasts from young donors (Dimri et al., 1995). Therefore, this means that not only MRC-5 fibroblasts growth arrest was delayed by SFN treatment but also decreased the expression of beta-galactosidase.

In order to confirm our findings on delay of senescence by SFN treatment on MRC-5 fibroblasts with beta-galactosidase staining experiments, human β -galactosidase-1 expression in MRC-5 fibroblasts was assessed at the protein level by Western blotting of cell extracts at passage 5 (young) and passage 9 (senescence) treated with either 1 μ M SFN or 0.002% DMSO. Control MRC-5 fibroblasts had a higher expression of β -galactosidase protein compared to the SFN-treated group at passage 9. Our findings further supports the argument that SFN acts on RS by delaying the onset of senescence not only targeting the MRC-5 fibroblasts replication ability but also affecting cellular protein levels of human β -galactosidase-1 in senescence. Indeed, as demonstrated by Kurz et al. (2000), β -galactosidase protein content increases with replicative age. However, levels of cellular human β -galactosidase-1 protein were higher in cell at early passages than in cells of later passage approaching senescence. Beta-Galactosidase is considered to reflect lysosomal mass in cells (Kurz et al., 2000). Beta-Galactosidase expression is a marker of senescence but not essential for senescence to occur (Lee et al., 2006). Previous quantitative assessment of beta-galactosidase in MRC-5 cells has shown moderate levels at passage 25 with a *ca.* 40% decline to passage 41 and then a *ca.*10-fold increase in advanced senescence at passage 45 (Lawless et al., 2010). The apparent dichotomy of the well-accepted increase in beta-galactosidase expression in cells senescence with the decrease in beta-galactosidase at passage 9 herein is probably due to cells at passage 9 approaching senescence but not in fully developed senescence when beta-galactosidase increased 10-fold and more than counters the moderate decrease on approach to senescence.

5.2 Characterization of gene expression and cell metabolism in cells escaping senescence by treatment with SFN and HESP *in vitro*

5.2.1 Changes in gene expression induced by sulforaphane in early passage, non-senescent MRC-5 cells *in vitro*.

The time course of changes in gene expression induced by 1 μ M SFN in early passage, non-senescent MRC-5 cells *in vitro* was investigated by quantifying mRNA of genes of selected metabolic pathways with Nrf2 regulated, ARE-linked genes by the Nanostring method – quantifying relative mRNA copy number. One of the key triggers influential for the development of senescence is oxidative stress. In relation to this, the Keap1-Nrf2-antioxidant response element (ARE) signalling pathway has a key role in the delay of senescence. Stress responsive signalling coordinated by nuclear factor erythroid 2-related factor 2 (Nrf2) provides an adaptive response for protection of cells against toxic insults, oxidative stress and metabolic dysfunction. Nrf2 regulates a multitude of protective genes by binding to regulatory anti-oxidant response elements (AREs) (Kapeta et al., 2010; Malhotra et al., 2010; Tagichi et al., 2011; Xue et al., 2013). Our findings showed that SFN induced a 2-fold increase in the Nrf2, ARE-linked transcriptional response marker gene quinone reductase NQO1. For other antioxidant linked genes, there were ca. 2-fold increases in mRNA of γ -glutamylcysteine ligase-modulatory subunit (GCLM), glutathione reductase (GSR), thioredoxin reductase (TXNRD1) and haem oxygenase (HMOX1), and smaller increases in mRNA of ferritin and thioredoxin by SFN. As demonstrated by this mRNA expression study, even in non-senescent young fibroblasts, SFN treatment had the ability to confer protection against oxidative damage by activating their transcription. Moreover, increased expression in NQO1 by SFN acts as a positive control for activation through the Nrf2 system (Jain and Jaiswal, 2007) and confirms its regulation of the ARE. Indeed, expression of anti-oxidant genes (NQO1, GCLM, GSR, TXNRD1 and HMOX1 as well as FTH1 and TXN)

were increased at early passage 4 even though these cells had only been receiving SFN treatment since passage 3. Expression of γ -glutamylcysteine ligase-catalytic subunit, glutathione peroxidase-1, peroxiredoxin-1, superoxide dismutases SOD1 and SOD2 and catalase were little changed. Increased NQO1 mRNA stimulated by SFN maximized after ca. 24 h and remained increased up to 72 h post-stimulation. In contrast, increased GCLM and GSR mRNA maximized after 12 h and returned to baseline levels after 36 – 48 h. The increase in HMOX1 mRNA was even more short-lived, maximizing at 4 h and returning to levels in unstimulated cells by 24 h. SFN also increased mRNA of aldoketo reductase 1C1 but not of glyoxalase 1. It also had little effect on phase II conjugating genes, glutathione transferase P1 and MRP2. Our study showed that pentosephosphate pathway genes were more responsive, with mRNA of glucose-6-phosphate dehydrogenase (G6PDH), transketolase (TKT) and transaldolase (TALDO) all increasing in SFN stimulated cells. This finding has very important implications as although CR studies have consistently shown a beneficial effect towards extended life span in animals (Murphy and Partridge, 2008; Weindruch et al., 1986), the mechanism by which fluctuations of glucose metabolism acts on the Nrf2 system and senescence is still under scrutiny. Indeed, gene array studies reveal that activated Nrf2 regulates clusters of genes involved in lipid and glucose metabolism such as insulin-associated signalling genes and glucose homeostasis regulators (Yates et al., 2009). Moreover, certain cancer cells exploit constructive activation of Nrf2 to reprogram their metabolism for securing optimal supply with biosynthetic building blocks (Mitsuishi et al., 2012). Indeed, proliferating cells take up abundant nutrients, including glucose and glutamine, and shunt their metabolites into anabolic pathways (Mitsuishi et al., 2012). Although the PPP is a well-established metabolic pathway, a direct regulator that activates the PPP during metabolic reprogramming has yet to be identified (Mitsuishi et al., 2012). However, our study indicates that SFN can activate the PPP at very early stages of treatment and increase the transcription of G6PDH, TKT and TALDO, which are therefore contributing to possible delay of senescence and healthy ageing cell programming. For lipogenic genes, sterol response element binding protein-1

(SREBF1) was decreased in SFN stimulated cells but expression of fatty acid synthase (FASN) was unchanged. The expression of Fructose-2,6-bisphosphate kinase-4 (PFKFBP4) was also unchanged by SFN. For the Nrf2 system itself, SFN did not increase expression of Nrf2, Keap1 nor Fyn kinase but did increase small maf protein-G (MAFG) in the 24 h immediately post-stimulation. This increase in MAFG expression is a very important finding in itself as upon activation, Nrf2 dissociates from Keap1, is phosphorylated by CK2 and enters the nucleus and binds with accessory Maf protein to AREs (Jeong et al., 2005; Tanigawa et al., 2007). Therefore our finding indicates that, although Nrf2 and Keap1 mRNA expression are unchanged with SFN-treatment compared to control, MAFG increase in expression is a strong indicator of the activation of the Nrf2 system with SFN-treatment after early stage treatment. When inflammatory gene responses were examined, monocyte chemoattractant protein-1 (CCL2), chemokine (C-X-C motif) ligand 1 (CXCL1), interleukin-15 (IL15), interleukin 1 β (IL1 β), toll-like receptor 4 (TLR4), transcription factor p65 (NF κ B3), nuclear factor NF-kappa-B p105 subunit/p50 (NF κ B1) and intracellular adhesion molecule-1 (ICAM1) were all unresponsive. This may indicate that expression of these genes can only be affected by cumulative treatment with SFN rather than acute treatment. Genes associated with extracellular matrix proteolysis, matrix metalloproteinase-3 (MMP3) and matrix metalloproteinase-13 (MMP13), were unchanged whereas the expression of elastin was decreased. This is probably due to the fact that these MRC-5 fibroblasts are young and therefore the extracellular matrix is not yet damaged by ageing, which means that these fibroblasts do not need to activate extracellular matrix repair. The expression of serpins and senescence associated genes, β -galactosidase (GLB1), cyclin-dependent kinase inhibitor 1/p21 (CDKN1A) and cyclin-dependent kinase inhibitor 2A/P16INK4a (CDKN2A), were all unchanged.

From these mRNA expression results, it can be seen that the Nrf2 system senses challenge to homeostasis in the cell cytoplasm and this could therefore mean that a protective transcriptional response is activated at early passages mainly from the transcription of anti-oxidant genes. Such stress-responsive

signalling is vital in resisting oxidative damage, cell dysfunction, cytotoxicity and mutagenesis, and similar studies have found that decline of these processes contribute to resistance to drug toxicity, wound healing and decreasing risk of diabetes, vascular and neurodegenerative disease and ageing-related disease (Collins et al., 2009; Hayashi et al., 2013; Okawa et al., 2006; Pearson et al., 2008).

5.2.2 Characterization of gene expression and cell metabolism in cells escaping senescence by treatment with sulforaphane and hesperetin.

In order to characterize the expression of genes and cell metabolism in cells escaping senescence by treatment with sulforaphane and hesperetin, the changes in gene expression induced by 1 μM SFN and 5 μM HESP in young and senescent MRC-5 cells *in vitro* was investigated by quantifying mRNA of genes of selected metabolic pathways with Nrf2 regulated, ARE-linked genes by the Nanostring method – quantifying relative mRNA copy number.

At late passage, there was a significant increase in mRNA of the anti-oxidant related gene GCLM in the SFN treatment compared to control. GCLM expression has been linked with extension of life span. Indeed, overexpression of GCLM in fruit flies has been shown to extend mean and maximum life span by up to 50% (Orr et al., 2005). The notion of oxidative stress emerged from the concept that ROS become excessively available in cells, leading to impaired cellular functions and senescence (Balaban et al., 2005). Oxidative stress is defined as an imbalance of oxidants and antioxidants in favour of the former potentially leading to cell damage (Sies, 1993). This increase of the anti-oxidant related gene GCLM with 1 μM SFN treatment therefore counterbalances the normal decrease of anti-oxidant genes with senescence, which ultimately leads to a decrease in oxidative stress and senescence.

Moreover, mRNA of the pentose-phosphate pathway gene glucose-6-phosphate dehydrogenase was significantly ($P < 0.001$) increased in the treatment group compared to the control. As described by Singh et al. (2013), Nrf2

coordinates the regulation of key genes involved in various pathways of glucose metabolism, including the pentose phosphate pathway (PPP), therefore, G6PDH mRNA expression increase with treatment confirms Nrf2 activation with SFN which may affect glucose metabolism in MRC-5 fibroblasts. The same effect was seen in the expression of the nutrient sensing thioredoxin interacting protein (TXNIP) which was increased by more than 2-fold. This finding has been demonstrated to link SFN supplementation to CR mimetics as TXNIP expression increases (Swindell, 2009). Moreover, expression of the extracellular matrix regulator collagen 1-alpha (COL1A1) was significantly increased in the SFN treated group compared to control by 0.5 fold, therefore indicating that SFN treatment at late passage conserves the function of the extracellular matrix hence contributing to delay of RS in these cells.

Oxidative damage is thought to be caused by an imbalance of the enzymatic members of the anti-oxidant defence such as catalase (CAT), glutathione peroxidase (GPx) and superoxide dismutase (SOD) (Finkel, 1998) and non-enzymatic members such as Vitamin A, C and E as well as the tripeptide glutathione (GSH) (Finkel and Holbrook, 2000). At early passage, HESP induced a significant increase ($P < 0.001$) in the expression of the matrix regulating gene mitochondrial superoxide dismutase (SOD2). This means that HESP acts on restoring the balance between oxidative stress and anti-oxidants from the very first attribution of treatment. This increase in gene expression of SOD2 at early passage with HESP treatment has very important implications on HESP effects in delay of ageing. Indeed, SOD2 is an antioxidant, the mitochondrial form of SOD and an important defence against oxidative damage. Evidence from invertebrates suggests it may play a role in ageing as overexpression of SOD2 in flies significantly extends lifespan (Sun et al., 2002) and mice without SOD2 are not viable (Li et al., 1995). Although reducing the activity of SOD2 in mice increases the levels of oxidative damage to DNA but does not affect lifespan (Van Remmen et al., 2003), SOD2 overexpression in mice slightly increases lifespan, while gene deletion in connective tissue only resulted in mutant mice with a reduced lifespan and premature onset of aging-related phenotypes such as weight loss, skin

atrophy, kyphosis, osteoporosis and muscle degeneration (Trieber et al., 2011). At late passage, there was no significant change in mRNA in the HESP treatment compared to control at passage 9. Finally our study showed that gene expression of the anti-oxidant related gene quinone reductase (NQO1) was decreased by two-fold at passage 11 for both treatment and control groups compared to control at passage 3. Moreover, expression of the anti-oxidant related gene heme oxygenase (HMOX) decreased by two-fold the control group at passage 9 compared to control at passage 3. Expression of the anti-oxidant related gene ferritin (FTH1) was also decreased two-fold in late passage for the SFN treated group compared to control at early passage. Expression of the pentosephosphate pathway gene glucose-6-phosphate dehydrogenase (G6PD) of both control and treatment group at late passage was halved compared control at passage 3. Although this gene expression pattern decrease with approach to senescence is expected, Weidrich and colleagues (2001) have shown that they can be counteracted in mice models using CR.

5.2.3 Characterisation of gene expression in MRC-5 fibroblasts escaping senescence by treatment with sulforaphane using genome-wide microarray analysis.

The changes in gene expression induced by 1 μ M SFN treatment in young (passage 3) and senescent (passage 11) MRC-5 cells in vitro was investigated by quantifying mRNA of 20773 genes throughout the whole human genome by the Microarray Agilent method – quantifying total RNA copy number.

The results herein showed that there was no significant changes in gene expression between the SFN treatment and control group at passage 3 detectable by conventional transcriptomic array analysis. Moreover, the colon-cancer secreted protein 1 (KIAA1199) was the only gene for which expression was significantly different in the treatment and control group at passage 11. Indeed, KIAA1199 was downregulated by SFN treatment compared to control in senescence. This result is in accordance with the findings by Michishita et al. (2006) who showed that upregulation of the KIAA1199 gene is associated with

cellular mortality. This, therefore means that treatment of MRC-5 fibroblasts with 1 μ M SFN upon reaching senescence delays cellular mortality in these cells and is strengthened by cPDL decline results obtained on the control group at passage 11. Expression of 131 genes (Appendix E.) was significantly changed between controls at passage 3 and passage 11. Indeed, expression of the DnaJ (Hsp40) homolog, subfamily C, member 6 (DNAJC6) was increased 6-fold with senescence in the control group compared to young fibroblasts. Moreover, expression of the C-C chemokine receptor type 11 (CCRL1) was increased 5-folds in the control at passage 11 compared to early passage control. Finally, expression of chemokine (C-X-C motif) ligand (CXCL2) was decreased by 3-folds and expression of Coiled-coil domain containing 144A (CCDC144A) was decreased by 4-fold in senescent controls compared to young controls.

Expression of 18 genes was significantly changed between SFN treated groups at passage 3 and passage 11. All genes were significantly upregulated at passage 11 compared to passage 3 in SFN treated groups apart from Sad1 and UNC84 domain containing 1 (SUN1) which was downregulated by 0.7 folds with senescence. Expression of the C-C chemokine receptor type 11 (CCRL1) and thioredoxin interacting protein (TXNIP) were amongst the highest upregulated genes in SFN treated senescent cells, increasing 5 and 7 fold respectively.

Expression of 274 genes (Appendix F.) was significantly changed between SFN treated groups at passage 11 and control at passage 3. Indeed, SFN treatment in senescence showed a 5 and 7 fold increase in expression of the major histocompatibility complex, class II, DM beta (HLA-DMB) and nuclear receptor subfamily 5, group A, member 2 (NR5A2) respectively compared to control at passage 3. Moreover, there was a 5-fold decreased in the expression of the small nucleolar RNA, C/D box 99 (SNORD) in the late passage SFN treated group compared to early control.

When comparing the expression analysis of the 49 genes of interest used in the Nanostring method and the transcriptomic method, it was noticeable that there was considerably less significant changes in gene expression in the SFN treated and control groups at passage 3 and 11 using the transcriptomic method.

Measurement of the level of each transcript, by using microarray-based approaches can lead to identification of many pharmacological or toxicological agents which alter gene expression (Kopeck et al. 2012; Yao et al. 2012), and mRNA abundance profiles can be used to create biomarkers of exposure to foreign chemicals as well as to facilitate understanding of mechanisms of basic physiological responses (Van Hummelen and Sasaki 2010; Uehara et al. 2011). However, signal noise, and data-analysis limitations have limited the adoption of transcriptome-wide profiling methods and the limited length of microarray probes (25–100 bp) can result in nonspecific binding of transcripts (Zhang et al. 2002), particularly in disease states. The length of the probes used for NanoString analysis is similar to that used for microarray hybridization; however, the dual-probe system results in more accurate signal capture as ensured by three factors: first, both probes are present in solution, allowing for more direct interaction with targets; second, the reaction is carried through to completion to ensure all targets are counted; and finally, the digital readout provides less noisy results than analog systems (Geiss et al. 2008). Therefore, we recommend the use of NanoString methods rather than Microarray for the successful analysis of biomarkers in response to compounds which are shown to delay senescence *in vitro*.

5.2.4 Characterisation of gene expression in MRC-5 fibroblasts *in vitro* during the approach to senescence.

The time course of changes in gene expression of MRC-5 fibroblasts *in vitro* was investigated by quantifying mRNA of genes of selected metabolic pathways with Nrf2 regulated, ARE-linked genes by the RT-PCR method – quantifying relative mRNA expression. Expression of the anti glycation related gene aldoketo reductase 1B1 (AKR1B1) was significantly decreased ($P < 0.001$) by a third of its value in senescence (passage 11) compared to young fibroblasts (passage 3). Expression of AKR1B1 was stable from passage 3 but decreased dramatically after passage 5. Moreover, the expression of the anti-glycation related gene glyoxalase 1 (GLO1) was also decreased significantly ($P < 0.01$) with approach to senescence. Expression of GLO1 was stable at passage 3, 5 and 6 but declined

rapidly thereafter. At the approach of senescence, the expression of the anti-oxidant related genes thioredoxin (TXN) as well as quinone reductase (NQO1) and heme oxygenase (HMOX1) was significantly decreased ($P < 0.001$ and $P < 0.05$, respectively) when compared to passage 3. Decline in expression of TXN was steady from passage 3 to 9 but increased slightly at the approach to senescence. Moreover, NQO1 and HMOX1 gene expression decline with approach to senescence was relatively consistent at each passage. Expression of the anti-oxidant related gene gamma-glutamyl-cys ligase-catalytic subunit (GCLC), gamma-glutamyl-cys ligase-modulatory subunit (GCLM) and glutathione reductase (GSR) however did not significantly decline with approach to senescence. Expression of both pentosephosphate pathway genes transaldolase (TALDO1) and transketolase (TKT) was significantly ($P < 0.05$) decreased from passage 3 to passage 11, showing almost linear decline with passage. Moreover, expression of the NADPH-dependent oxidoreductase carbonyl reductase 1 (CBR1) was also significantly decreased ($P < 0.05$) with approach to senescence. This decline was drastic from passage 3 to 9 but was steady thereafter until senescence at passage 11. Finally the expression of the Nrf2 regulation related genes Nrf2 was not significantly decreased at passage 11, although 30% decrease in Keap 1 expression at the approach to senescence was very significant ($P < 0.001$). Analysis of gene expression in MRC-5 cells from passage 3 to 11 showed that, for genes NQO1, NRF2, TKT, GLO1, AKR1B1, KEAP1, CBR-1, TALDO, GSR, HMOX1 and TXN, expression was maintained until passages 5 – 6 and then decline to lower levels at passages 10 – 11. These findings confirm similar findings of gene expression decline related to approach to senescence, and also confirms the involvement of ARE in preserving normal cell functions.

5.2.5 Effect of progression towards senescence and sulforaphane on protein glycation, oxidation and nitration markers in MRC-5 fibroblasts *in vitro*.

Proteome and genome damage was assessed by quantitative screening of protein oxidation, nitration and glycation adducts, and deoxyguanosine glycation and oxidation adducts by stable isotopic dilution analysis LC-MS/MS. There were

no changes in cell protein content of glycation, oxidation and nitration adducts from passage 4 to passage 8. There were, however, increases in protein glycation, oxidation and nitration free adduct flux at passage 8 – decrease in flux of early glycation adduct FL, increases in flux of formation of AGEs (MG-H1, CML, 3DG-H and CMA) and oxidation adducts DT and GSA. This indicates that the in situ rates of protein glycation and oxidation in cells are increased in the later passage but this is within the capacity of the cell to remove these damaged proteins. This may nevertheless stress cell metabolism by decreasing the level of unmodified protein if there is not compensatory increase in expression to replace the proteolysed damage protein and strain cell metabolism for increased protein synthesis if the damaged protein is replaced. Previous studies with MRC-5 cells and BJ fibroblasts have found increased protein carbonyls by qualitative chromophoric derivatisation (Sitte et al., 1998; Sitte et al., 2000a; Sitte et al., 2000b.). Such methods are not robustly quantitative and often give higher response in assay blanks than test samples – reviewed in Thornalley and Rabbani (2014). Herein protein carbonyls were assayed directly and quantitatively as AASA and GSA. GSA was found to be the major protein carbonyl. The flux of GSA increased markedly in the later passage MRC-5 cells examined – consistent with previous findings of increased protein carbonyls being due to increased formation of GSA. Unlike previous findings, however, it is identified that the change in protein carbonyls in cell senescence is increased flux of formation rather than increased steady-state carbonyl residues in cell protein. This may change, however, in more advanced stages for senescence when cell proteolysis decline.

SFN changed the steady-state levels of damage to cell protein. It decreased dicarbonyl metabolite-derived AGEs, MG-H1, 3DG-H, CMA and glucosepane residues, and GSA residues in cell protein at passage 3. This may be due to increased expression of aldoketo reductases and antioxidant enzymes that metabolise dicarbonyls and oxidising metabolites. SFN decreased FL residue content of cell protein at passage 8 which may be due to the decreased glucose

uptake and metabolism found in SFN-treated cells. It also increased 3-NT residue content which may relate to increased NO availability through increased antioxidant activity and prevention of NO synthase inactivation. Importantly, SFN treatment also decreased flux of formation of FL, AGEs and oxidative damage adducts DT and GSA. This is probably related to enhanced protection against protein damage by increasing the metabolism of glycation and oxidizing agents. Flux of 3-NT was increased in late passage cells – again, as for the 3-NT residue increase with SFN, this likely reflects increased availability of NO with SFN treatment.

These findings indicate that SFN allows for counteracting the effects of senescence on damage caused by glycation of proteins. Indeed, SFN is thought to act through CR mimetics and decrease in caloric intake is a proven intervention that increases lifespan in rodents and nematodes (Pletcher et al., 2005; Walker et al., 2005; Wang et al., 2004 and Walford, 1982). The decrease in intracellular levels of protein glycation markers with SFN treatment in our study demonstrated this compound's ability to counteract glycation damage that would normally occur during the normal ageing process. Indeed, there have been few studies of quantitative changes in protein glycation in cell senescence but studies with anti-AGE antibodies suggested that protein AGE residue content increased during replicative senescence of WI-38 human embryonic fibroblasts (Ahmed et al., 2007). Moreover, in the BJ fibroblast model of proliferative and non-dividing cell senescence, protein carbonyls and lipofuscin fluorescence increased as cells entered senescence (Sitte et al., 2000). A similar effect was found in MRC-5 fibroblasts during proliferative senescence (Sitte et al., 1998). Therefore, by counteracting the effects seen in normal senescence (Sitte et al., 1998; Sitte et al., 2000; Ahmed et al., 2007), SFN successfully counteracts glycolytic damage to cell proteins.

5.2.6 Effect of progression towards senescence and sulforaphane on nucleotide glycation and oxidation in MRC-5 fibroblasts *in vitro*.

The concentration of the nucleotide damage markers MGdG, GdG and 8-OxodG in baseline and end of passage conditioned medium at passages 5 and 8 were determined in cultures of MRC-5 cells that had been incubated with and without 1 μ M SFN since passage 3 (when cPDL was 35.8). Incubation with SFN decreased the flux of formation of 8-OxodG but for nucleotide AGEs, GdG, MGdG and CEdG, these analytes were not detectable in fresh or end of passage conditioned medium. As demonstrated by Thornalley et al. (2010), increased 8-OxodG cellular content is correlated with increase DNA damage in tumour cell lines (Thornalley et al., 2010). Therefore, our results show that this decrease in 8-oxodG with SFN treatment indicate that this isothiocyanate counteracts nucleotide oxidation caused by cellular senescence in MRC-5 fibroblasts.

5.2.7 Effect of sulforaphane on dicarbonyl precursors of protein and nucleotide glycation in cultures of MRC-5 fibroblasts *in vitro*.

Dicarbonyl precursors of glycation, methylglyoxal (MG), 3-deoxyglucosone (3-DG) and glyoxal, were assessed by stable isotopic dilution analysis LC-MS/MS in cell culture media at baseline and at the end of the passage of MRC-5 cell cultures for passages 5, 8 and 11.

For glyoxal, the concentration of glyoxal was decreased at the end of passage with respect to baseline level at passages 8 (-37%, $P < 0.05$) and 11 (-52%, $P < 0.01$) for MRC-5 cells in control cultures but not for MRC-5 cells incubated with SFN. The concentration of glyoxal was decreased at the end of the passage with respect to baseline level in control cultures for all 3 passages combined: 171 ± 53 nM versus 105 ± 45 nM, $P < 0.05$ ($n = 9$). Combining measurement for passages 8 and 11 as “late passages”, the efflux of glyoxal was increased in control cultures in late passages with respect to passage 5 (4919 ± 1697 versus 1041 ± 413 pmol/ 10^6 cells, $P < 0.01$) but not in similar cultures treated with SFN. Glycation accounts for 0.1 to 0.2% of cellular arginine and lysine residues in the body (Thornalley et al., 2003). This physiological process causes damage to

proteins and results in the formation of glycated amino-acid residues (Xue et al., 2008a). These residues are formed by the spontaneous reaction between monosaccharide and proteins. Glycating agents are formed from the degradation of glycated proteins and lipid peroxidation and include dicarbonyls such as methylglyoxal, glyoxal and 3-deoxyglucosone (3-DG) (Thornalley et al., 2003) which act as precursors for advanced glycation end products (AGEs) directly linked with senescence progression. Therefore, our findings demonstrate that treatment with SFN in MRC-5 fibroblasts not only delays senescence but also confers protection against glycation damage through the decrease in glyoxal flux at the approach to senescence.

For MG, the concentration of MG was decreased at the end of passage with respect to baseline level at passage 5 (-32%, $P < 0.05$) and increased at the end of passage 11 with respect to baseline (+52%, $P < 0.05$) for MRC-5 cells incubated with SFN but was unchanged in MRC-5 cells in control cultures. The concentration of MG in medium of MRC-5 cells in cultures with SFN was increased at passage 8 with respect to passage 5, $P < 0.05$, but was unchanged in control cultures. Therefore, the efflux of MG from cells at passage termination (pmol per 10^6 cells) was deduced. The efflux of MG was increased in control cultures at passage 11 with respect to passage 5 and increased at passage 8 with respect to passage 5 in cultures with SFN. Combining measurement for passages 8 and 11 as “late passages”, the efflux of MG was increased in control cultures in late passages with respect to passage 5 (10297 ± 3614 versus 640 ± 230 pmol/ 10^6 cells, $P < 0.01$) and also in cultures treated with SFN (8163 ± 4964 versus 566 ± 79 pmol/ 10^6 cells, $P < 0.01$). In quantitative assessments of advanced glycation endproducts (AGEs) in physiological systems, glycation of proteins by the physiological metabolite MG produced levels of cellular and extracellular proteins modification approaching and sometimes exceeding that of glucose (Thornalley et al., 2003). Our findings, alongside results obtained by Thornalley et al. (2003) strengthen the argument that SFN successfully delays the increase damage of the dicarbonyl MG inside the cell proteins as seen by the approach of senescence.

For 3-DG, the concentration of 3-DG was increased at the end of passage with respect to baseline level at passage 5 (+48%, $P < 0.01$), at passage 8 (+215%, $P < 0.001$) and at passage 11 (+36%, $P < 0.05$) for control cultures of MRC-5 cells and increased at passage 8 (+198%, $P < 0.001$) for MRC-5 cells incubated with SFN. The concentration of 3-DG in cultures at the end of the passage was not changed significantly by addition of SFN for passages 5, 8 and 11. The concentration of 3-DG in baseline medium at passage 5 was higher than at passage 8 (268 ± 33 nM versus 163 ± 37 nM, $P < 0.05$) and lower than at passage 11 (268 ± 33 nM versus 383 ± 20 nM, $P < 0.01$). Therefore, the efflux of 3-DG from cells at passage termination (pmol per 10^6 cells) was deduced. The efflux of 3-DG was increased in control cultures at passages 8 and 11 with respect to passage 5 and also increased at passage 11 with respect to passage 8. The efflux of 3-DG was increased at passages 8 with respect to passage 5 in cultures with SFN. Combining measurement for passages 8 and 11 as “late passages”, the efflux of 3-DG was increased in control cultures in late passages with respect to passage 5 (22481 ± 10871 versus 2752 ± 907 pmol/ 10^6 cells, $P < 0.01$) but not in cultures treated with SFN. This is due to the fact that the decrease in 3-DG flux is countered by decreased metabolism by aldo-reductase (3-DG reductase activity) to 3-deoxyfructose and by aldehyde dehydrogenase to 2-keto-3-deoxyglucuronic acid (Baba et al., 2009; Collard et al., 2007).

5.2.8 Effect of progression towards senescence and sulforaphane on formation of N ϵ (γ -glutamyl)lysine (GEEK) in MRC-5 fibroblast cultures.

Increased expression of transglutaminase is implicated in fibroblast senescence (Kim et al., 2001; Dellorco et al., 1985) with expected increased formation of N ϵ (γ -glutamyl)lysine (GEEK). The culture media and intracellular protein concentration of GEEK in MRC-5 fibroblasts at passages 4 and 8 were determined in cultures of MRC-5 cells that had been incubated with and without 1 μ M SFN since passage 3 (when cPDL was 35.8). The concentration of GEEK in baseline medium at passage 4 and 8 was increased significantly at the end of

the passage in MRC-5 cells incubated with and without 1 μ M SFN ($P < 0.01$ and $P < 0.001$, respectively). Moreover, the flux of GEEK outside the cells was increased by 4 fold at passage 8 in both groups compared to passage 4, although there was no significant difference in efflux between treatment and control within the same passage. The concentration of GEEK at early passage 4 in the control culture and culture treated with 1 μ M SFN was 1.11 ± 0.61 mmol/mol(lys) and 0.91 ± 0.48 mmol/mol(lys) respectively. At passage 8, however, cellular protein concentration of GEEK in the control culture was significantly ($P < 0.05$) increased by 3-folds compared to control at passage 4. The concentration of GEEK in control at passage 8 was therefore 3.15 ± 0.71 mmol/mol(lys). Moreover, cellular protein concentration of GEEK in the 1 μ M SFN treatment group did not significantly fluctuate compared to control GEEK concentration at passage 4, but was 2-fold higher ($P < 0.05$) than GEEK concentration in the SFN-treated group at passage 4. However, there was a significant ($P < 0.05$) 1.5-fold decrease in cellular protein GEEK concentration at passage 8 in the 1 μ M SFN treated group when compared to the control. Indeed, at passage 8, cellular protein GEEK concentration was 1.74 ± 0.29 mmol/mol(lys) in the 1 μ M SFN treated group. These data indicate the following:

1. Transglutaminase-mediated crosslinking impose a significant increased covalent crosslinking on cell protein on the approach to senescence. This reflects a mean crosslink of ca. 2-6 % of proteins from passage 4 to 8 respectively.
2. The effect of SFN in decreasing GEEK residue content of cell protein rather than flux of formation of GEEK reflects SFN-induced increased clearance of crosslinked proteins which is likely protective for function.

GEEK residues and free adducts have not been hitherto robustly quantified. The method used herein is an adaptation of the published LC-MS/MS method (Schafer et al., 2005) which was improved in the host team by synthesis and use of stable isotopic GEEK for robust internal standardisation and by combining this with enzymatic hydrolysis and ultrafiltration methods to quantify GEEK residues and free adducts flux.

5.3 Characterization of the mechanism of decrease glucose metabolism by SFN and HESP action linked to delay of fibroblast senescence

5.3.1 Effect of the approach to senescence and treatment with sulforaphane and hesperetin on the consumption of glucose by MRC-5 and BJ fibroblasts in vitro

The concentration of glucose in cultures of MRC-5 fibroblasts at the beginning and end of passages 4, 8 and 12 was determined and the flux of glucose metabolized deduced. The consumption of glucose increased progressively from 2.59 ± 0.40 μmol per day per 10^6 cells at passage 4 to a maximum of 30.74 ± 2.20 μmol per day per 10^6 cells at passage 12. Incubation with 1 μM SFN from passage 3 decreased glucose consumption which was statistically significant at passages 10, 11 and 12 with glucose consumption decreased by 34%, 60% and 53% respectively ($P < 0.01$). Following observation of these results, treatment with 1 μM SFN of MRC-5 fibroblasts is thought to delay senescence through a caloric restriction mimetic effect. Caloric restriction mimetic (CRM) was a term first described by Lane and colleagues (1998) as a hypothetical class of drugs which imitates the anti-ageing effects associated with CR *in vivo* and which would act upon the same metabolic pathways without the need for a decrease in caloric intake. CRM have been proposed to regulate a vast number of pathways associated with energy metabolism (Lane *et al.*, 2007). Indeed, inhibitors of glycolysis have been shown to mimic metabolic and protective effects of CR (Guo *et al.*, 2001). Also, sirtuin regulators have been shown to delay the ageing process and extend lifespan in short-lived organisms (Guarente and Picard, 2005). Finally, insulin sensitisers have been explored as possible CRM due to the fact that insulin sensitivity has been shown to increase in animal CR studies (Kemnitz *et al.*, 1994; Kenyon *et al.*, 1993; Wolkow *et al.*, 2000; Clancy *et al.*, 2001). However, this theory has been disputed for the compound phenformin, a treatment for diabetes, due to the fact that *in vivo* treatment failed to show markers related to CR and lifespan (Lane *et al.*, 2007).

Culture media samples were available from a similar study of the approach of human BJ fibroblasts to senescence and delay by treatment with 1 μM SFN. The consumption of glucose increased progressively from 3.48 ± 0.09 μmol per day per 10^6 cells at passage 6 to a maximum of 14.80 ± 1.50 μmol per day per 10^6 cells at passage 19. Incubation with 1 μM SFN from passage 3 decreased glucose consumption by 30% at passage 19 ($P < 0.001$), although at earlier passage treatment with SFN had increased consumption of glucose. In the HESP study, the consumption of glucose increased progressively from 4.11 ± 0.24 μmol per day per 10^6 cells at passage 7 to a maximum of 38.41 ± 4.72 μmol per day per 10^6 cells at passage 9. Incubation with 5 μM hesperetin from passage 3 decreased glucose consumption which was statistically significant at passages 7 and 12 with glucose consumption decreased by 29% and 33% respectively ($P < 0.05$). These results therefore show that, like SFN, treatment with 5 μM HESP acts as a CRM activator by decreasing metabolism and glucose intake by MRC-5 fibroblast.

Finally, MRC-5 cell pellets (passage 4 and 10) content of GSH was determined by stable isotopic dilution analysis LC-MS/MS for SFN and control group and the cellular content of GSH increased ca. 3-fold in control cultures in passage 10 with respect to passage 4. Treatment with SFN did not change the cellular content of GSH at passage 4 but increased cellular content of GSH by 34% compared to control at passage 10. This higher cellular content of GSH in the SFN-treated group compared to control is in accordance with findings by Chen (2009) that increases in intracellular GSH prevents premature senescence and is supported by the findings that induction of WI38 cell senescence is initiated by a transient depletion of intracellular GSH and followed by a continuous increase in ROS formation. Along with our findings on decrease in L-lactate formation at the onset of senescence compared to control, this GSH increase has been linked similarly with decrease in the flux of formation of L-lactate in CR of ageing in mice models (Hargopan, Ramsey and Weindruch, 2003).

5.3.2 Characterization of the mechanism of decreased glucose metabolism by SFN and HESP action linked to delay of fibroblast senescence.

D-Lactate is the terminal product of MG metabolism by the glyoxalase system. It is weakly metabolized in human cells and is a measure of flux of MG formation. Increases in D-lactate levels have been associated with hyperglycaemia (Shinohara et al., 1998; Talasniemi et al., 2008, Thornalley et al., 2001). The concentration of D-lactate in the medium of cultures at baseline and end of passage were determined and the mean flux of formation of D-lactate deduced. The flux of D-lactate by MRC-5 fibroblasts was 0.31 ± 0.04 nmol per day per 10^6 cells at passage 4 of control cultures. This did not increase significantly at passage 8 but increased 11-fold at passage 12. At passage 11, SFN decreased the flux of formation of D-lactate by 28%. This CR restriction mimetic effect and decrease in the flux of formation of D-lactate is consistent with decreased formation of methylglyoxal as a consequence of decreased glycolysis. In a similar experiment with and without hesperetin the flux of formation of D-lactate was quantified in MRC-5 cell cultures at passages 7, 8 and 9. The flux of formation of D-lactate increased in control cultures at passage 9 with respect to the flux of formation of D-lactate at passage 7 and in HESP treated cultures at passages 8 and 9 with respect to the flux of formation of D-lactate at passage 7. However, HESP did not decrease the flux of formation of D-lactate significantly. This is in accordance with the fact that HESP has less ability to delay senescence by CR mimetics as shown in the glucose consumption results and senescence delay results in this study.

L-Lactate is a major metabolite of glucose metabolism and although it is formed and metabolized by MRC-5 cells *in vitro* there was a marked export from cells into the culture medium. In fresh culture medium used for passages 4, 8 and 12, the concentration of L-lactate was 0.31 – 0.93 mM which may be interpreted as background interference. At the end of the passages this has increased 3 – 4 fold. The flux of L-lactate export into the medium relates to cell number therefore the net increase of L-lactate in cell cultures during the passage was computed

from the difference in baseline and end of passage L-lactate concentrations and reported as nmol per day per 10^6 cells. In control cultures the apparent flux of L-lactate was not increased significantly at passage 8 with respect to passage 5. However, at passage 12 the apparent flux of L-lactate was increased ca. 11 fold with respect to passage 5. In cells treated with SFN the apparent flux of L-lactate was increased similarly excepting a 23% decrease in apparent flux of L-lactate at passage 12 compared to control cultures. This was reflected by a decrease in glycolytic activity as well as the flux of formation of D-lactate (% glucotriose) increase (** $p < 0.02$) in senescent MRC-5 fibroblasts treated with 1 μ M SFN compared to control.

5.3.3 Effect of sulforaphane on the cellular content of glycolytic intermediates

To investigate the effect of SFN on early-stage glycolysis in MRC-5 cells, the changes in the cellular concentrations of glycolytic intermediates were quantified. Key initial intermediates potentially regulated by SFN are G6P, F6P and PGA were quantified in MRC-5 cells with and without SFN. Short term incubation with SFN in high glucose concentration medium decreased the cellular content of G6P and concurrently increased the cellular content of PGA without change in the cellular content of F6P. The cellular contents of G6P, PGA and F6P were higher in control cells at passage 9 than at passage 5. Addition of SFN decreased F6P in passage 5 but was without effect on other glycolytic intermediates in passage 5 and passage 9. Although CR studies have consistently shown a beneficial effect towards extended life span in animals (Murphy and Partridge, 2008; Weindruch et al., 1986), the mechanism by which fluctuations of glucose metabolism acts on the Nrf2 system and senescence is still under scrutiny. Although the PPP is a well-established metabolic pathway, a direct regulator that activates the PPP during metabolic reprogramming has yet to be identified (Mitsuishi *et al.*, 2012). As shown by Bensaad et al. (2006), SFN has been shown to act as a CRM dietary bioactive through cellular contents of glycolytic intermediates with SFN-treatment. However, because glycolysis is

often facilitated in proliferating cells, alternative mechanisms that actively promote the PPP are expected to be involved. Also, as described by Singh *et al.* (2013), Nrf2 coordinates the regulation of key genes involved in various pathways of glucose metabolism, including the pentose phosphate pathway (PPP). Our study demonstrates the effects of SFN in delaying senescence by CR mimetics through the PPP by decreasing the cellular content of G6P and concurrently increasing the cellular content of PGA.

5.3.4. Characterization of glucose sensing by ChREBP/MondoA-Mlx transcription factors in response to SFN treatment in MRC-5 fibroblasts.

A transcription factor sensitive to the cellular content of G6P is carbohydrate response element binding protein or Mondo A in fibroblasts. When Mondo A is activated it binds G6P and translocates to the cell nucleus. To study the effect of SFN on cellular activation of Mondo A, MRC-5 cells were incubated with and without SFN with low and high glucose concentrations. MRC-5 cells were then fixed and immunocytofluorescence microscopy performed to study the subcellular location of Mondo A.

When MRC-5 cells were incubated overnight in low glucose concentration (0.2 mM) followed by 6 h with high glucose concentration (25 mM), immunostaining for Mondo A showed high intensity staining in the cell nucleus in control cultures which was suppressed by incubation with 1 μ M SFN. Following incubation in normal glucose concentration (5.5 mM) of MRC-5 cells, immunostaining for Mondo A showed no staining in the cell nucleus. However, high intensity staining was seen in the cell nucleus of cultures receiving subsequent treatment with high glucose concentration (25 mM) for 6h. which was then suppressed by incubation with 1 μ M SFN. When MRC-5 cells were incubated overnight in high glucose concentration (25 mM), immunostaining for Mondo A showed no staining in the cell nucleus in control cultures. Surprisingly, in the same cultures, when MRC-5 cells were incubated overnight in high glucose

concentration (25 mM) with addition of 1 μ M SFN, immunostaining for Mondo A showed slightly higher intensity staining in the cell nucleus.

Multicellular animals sense and control their glucose homeostasis at several levels. Systemic regulation by insulin and glucagon maintains levels of circulating glucose constant during fluctuating nutritional conditions. Upon feeding, elevated circulating glucose is taken up by muscle, liver and adipose tissue through the actions of insulin signaling, while starvation elevates glucagon levels to promote glycogenolysis and gluconeogenesis (Havua and Hietakangas 2012). The intracellular glucose is rapidly converted into glucose-6-phosphate and glucose-6-phosphate activates two paralogous basic helix-loop-helix-leucine zipper (bHLHZ) transcription factors (TFs) ChREBP and MondoA, which heterodimerize with their common binding partner Mlx. This bHLHZ complex resembles the evolutionarily related Myc–Max complex. As reviewed by Havua and Hietakangas (2012) ChREBP/Mondo–Mlx is known to mediate a majority of the glucose-induced transcriptional response by binding to target gene promoters containing so-called carbohydrate response elements (ChoREs).

The findings of this immunofluorescence study confirm findings by Billin and colleagues (2000), that regulation of ChREBP/MondoA–Mlx complexes involves shuttling between cytoplasm and nucleus. Moreover, treatment with SFN counteracted this translocation to the nucleus which is thought to be through CR mimetics activity of this bioactive compound. Moreover, translocation of Mondo A inside the nucleus as shown by immunostaining was more pronounced as a result of incubation with high glucose (25 mM) incubation which was also shown in the literature by the use of a glucose analog 2-deoxyglucose (2-DG) which was phosphorylated into 2-deoxyglucose-6-phosphate (2-DG6P), but which cannot be processed further, leading to 2-DG6P accumulation. In response to 2-DG treatment, MondoA–Mlx translocated into the nucleus and strongly transactivated target genes (Havua and Hietakangas, 2012) and furthermore, ChREBP was shown to be activated by fructose 2,6 bisphosphate in hepatocytes. Summary of the mechanism of activation of the Nrf2 system and delay of senescence by SFN in MRC-5 fibroblasts is shown in Figure 113.

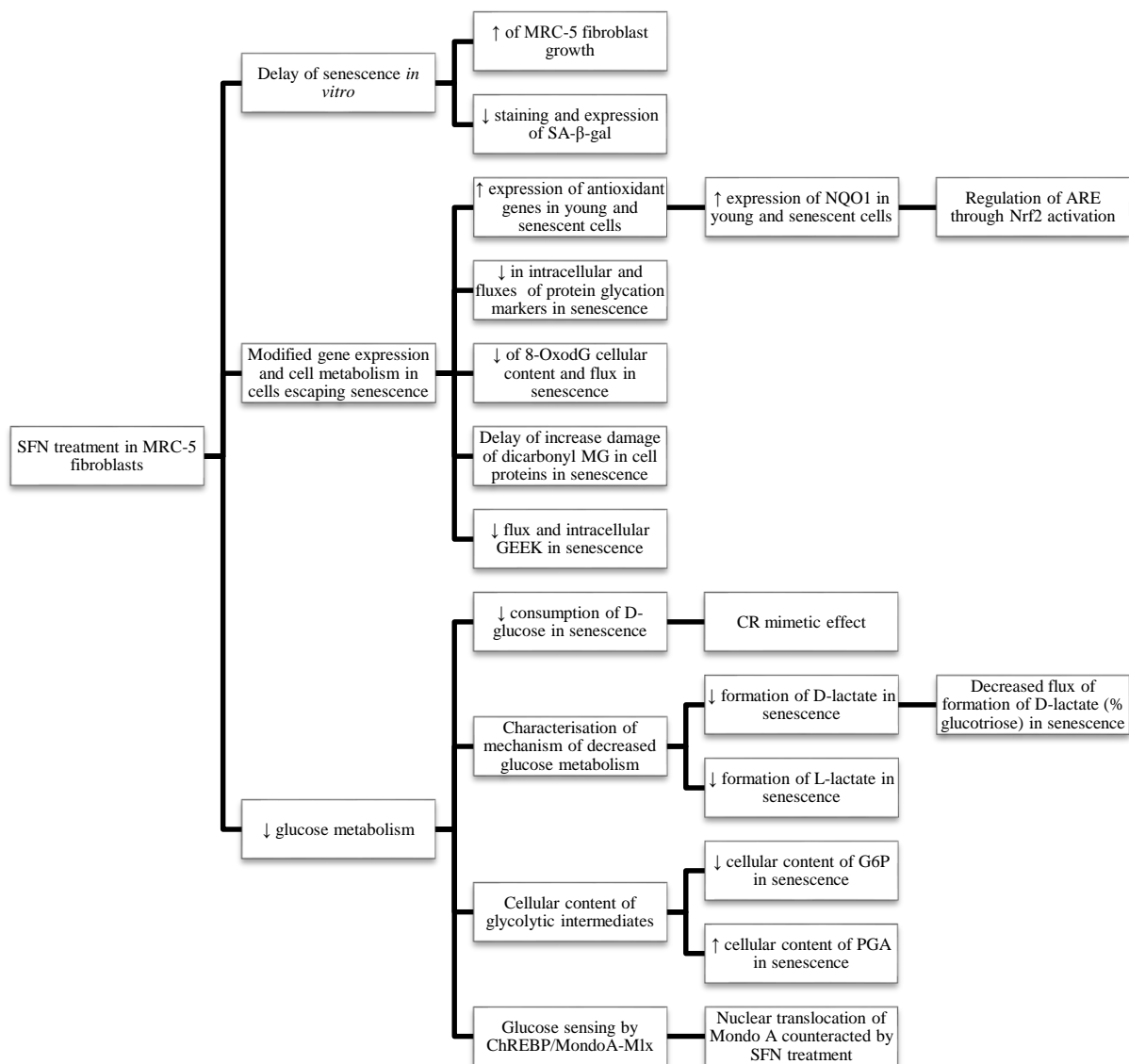


Figure 113. Summary of mechanism of activation of Nrf2 system and delay of senescence by SFN in MRC-5 fibroblasts.

6. Conclusion and Further work

6.1 Conclusion

This PhD project was comprised of three parts:

- i. To study the effects of SFN and HESP on MRC-5 cell senescence *in vitro*
- ii. To characterize gene expression and cell metabolism in cells escaping senescence by treatment with SFN and HESP
- iii. To characterize the mechanism of decrease glucose metabolism by SFN and HESP action linked to delay of fibroblast senescence

The effects of treatment of MRC-5 with the dietary bioactivators SFN and HESP was studied and shown to delay cellular senescence in these cells *in vitro*. Similar findings for SFN treatment of BJ cells were found previously by studies of the host team. SFN and HESP are compounds available in a diet rich in vegetables and fruit. The cell senescence model may translate to some aspects of human ageing – for example, immunosenescence and ageing of pre and post-mitotic cells. Therefore, this work may indicate routes to functional foods to support healthy ageing and reveal cell responses which may underlie the epidemiological evidence linking healthy ageing to a diet rich in fruits and vegetables.

SFN and HESP are thought to mediate health benefits by activation of transcription factor Nrf2 system which regulates the cellular expression of a battery of protective genes countering oxidative stress, environment toxic insults, lipid peroxidation, macromolecular damage, metabolic dysfunction and cell senescence (Rabbani and Thornalley, 2012b; Rabbani and Thornalley, 2014; Kapeta et al., 2010). Moreover, even in non-senescent young fibroblasts, SFN treatment had the ability to confer protection against oxidative damage by activating their transcription. Moreover, increased expression in NQO1 by SFN acts as a positive control for activation through the Nrf2 system (Jain and Jaiswal, 2007) and confirms its regulation of the ARE. Indeed, expression of anti-oxidant

genes were increased at early passage. These effects were replicated in young and senescent MRC-5 fibroblasts treated with and without 1 μ M SFN or 5 μ M HESP. Comparison of Nanostring and transcriptomic methods showed that Nanostring method has a better power of identification of changes in mRNA expression. ARE linked gene expression analysis from early to senescent MRC-5 findings confirmed gene expression decline related to approach to senescence, and also confirmed the involvement of ARE in preserving normal cell functions.

One aspect of Nrf2-regulated, ARE-linked gene expression is involvement in pathways of glucose metabolism, including the pentose phosphate pathway (PPP), therefore, G6PDH mRNA expression increase with treatment confirmed Nrf2 activation with SFN which may affect glucose metabolism in MRC-5 fibroblasts. The same effect was seen in the expression of the nutrient sensing thioredoxin interacting protein (TXNIP) which was increased by more than 2-fold. This finding has been demonstrated to link SFN supplementation to CR mimetics as TXNIP expression increases (Swindell, 2009). Importantly, Nrf2 activators through increasing expression of G6PDH may decrease G6P and thereby decrease activation of Mondo A and down-regulate expression of glycolytic and lipogenic genes,

Protection of the cellular proteome and genome was shown to be conferred by 1 μ M SFN treatment of MRC-5 cells. Decreased protein glycation and oxidation is part of the beneficial effects found in delay of cells senescence by SFN. A new finding was the effect of major quantitative covalent crosslink of cell protein by transglutaminases forming GEEK residues at up to 0.8% total lysine residues in cells approaching senescence. Suppression of the functional effects of this by enhancing clearance of crosslinked protein by SFN is likely a further contributory factor in the delay of cell senescence.

Caloric restriction mimetic mechanisms by treatment with 1 μ M SFN and 5 μ M HESP was shown due to the decrease in culture glucose consumption increase with senescence in these treatment groups and this CR restriction mimetic effect and decrease in the flux of formation of D- and L-lactate in the SFN-treated group was consistent with previous studies done in CR and ageing in

mice models (Hargopan, Ramsey and Weindruch, 2003). However, HESP did not decrease the flux of formation of D-lactate significantly. Moreover, in this study, SFN has been shown to act as a CRM dietary bioactive through cellular contents of glycolytic intermediates with SFN-treatment (Bensaad et al., 2006).

Finally, the mechanism by which SFN induces delay of senescence through CR has been shown to be due to the extraction of Mondo A from the cell nucleus to the cytoplasm.

6.2 Further Work

In this study, the delay of senescence of MRC-5 cells by SFN *in vitro* was discovered and the mechanism of action was investigated – discovered a major caloric restriction mimetic activity likely mediated through suppression of activation of MondoA, enhanced protection against protein and nucleotide damage and increased clearance of major crosslinked proteins. Further studies are required to build on this and secure the major aspects of this mechanism. Quantification of MondoA protein inside and outside the cell by Western Blotting was not performed and would provide essential corroborate evidence to confirm the MondoA down regulation hypothesis. Finally, in order to be of significance in the field of physiological ageing delay, experimental methods should be repeated *in vivo* in mouse models.

Appendix A. Isoforms Codeset design of genes of interest for Nanostring analysis: sulforaphane treatment in young MRC-5 fibroblasts *in vitro*

Gene	Probe NSID	Tot Isoforms	Isoforms Hit by Probe	# Hit
ACTB	NM_001101.2:1010	1	NM_001101	1
AKR1C1	NM_001353.5:1210	1	NM_001353	1
CAT	NM_001752.2:1130	1	NM_001752	1
CCL2	NM_002982.3:0	1	NM_002982	1
CDKN1A	NM_000389.2:1975	4	NM_000389;NM_078467;NM_001220778;NM_001220777	4
CDKN2A	NM_000077.3:975	4	NM_000077;NM_058197;NM_058195;NM_001195132	4
CLTC	NM_004859.2:290	1	NM_004859	1
CTSO	NM_001334.2:725	1	NM_001334	1
CXCL1	NM_001511.1:742	1	NM_001511	1
ELN	NM_000501.1:765	5	NM_000501;NM_001081755;NM_001081754;NM_001081753;NM_001081752	5
FASN	NM_004104.4:5387	1	NM_004104	1
FTH1	NM_002032.2:941	1	NM_002032	1
FYN	NM_002037.3:765	3	NM_002037;NM_153047;NM_153048	3
G6PD	NM_000402.2:1155	2	NM_000402;NM_001042351	2
GCLC	NM_001498.2:520	2	NM_001498;NM_001197115	2
GCLM	NM_002061.2:599	1	NM_002061	1
GLB1	NM_000404.2:955	3	NM_000404;NM_001079811;NM_001135602	3
GLO1	NM_006708.1:1240	1	NM_006708	1
GPX1	NM_000581.2:745	2	NM_000581;NM_201397	2
GSR	NM_000637.2:1525	4	NM_000637;NM_001195104;NM_001195103;NM_001195102	4
GSTP1	NM_000852.2:415	1	NM_000852	1
GUSB	NM_000181.1:1350	1	NM_000181	1
HMOX1	NM_002133.1:1430	1	NM_002133	1
ICAM1	NM_000201.1:1990	1	NM_000201	1

IL15	NM_172174.1:1685	3	NM_172174;NR_037840;NM_172175;NM_000585	4
IL1B	NM_000576.2:840	1	NM_000576	1
KEAP1	NM_012289.3:561	2	NM_012289;NM_203500	2
MAFG	NM_002359.2:3529	2	NM_002359;NM_032711	2
MMP13	NM_002427.2:951	1	NM_002427	1
MMP3	NM_002422.3:25	1	NM_002422	1
ABCC2	NM_000392.3:3150	1	NM_000392	1
NFE2L2	NM_006164.3:995	3	NM_006164;NM_001145413;NM_001145412	3
NFKB1	NM_003998.2:1675	2	NM_003998;NM_001165412	2
RELA	NM_021975.2:360	2	NM_021975;NM_001145138	2
NQO1	NM_000903.2:790	3	NM_000903;NM_001025434;NM_001025433	3
PFKFB4	NM_004567.2:400	1	NM_004567	1
PRDX1	NM_002574.2:632	4	NM_002574;NM_001202431;NM_181696;NM_181697	4
PSMA1	NM_148976.2:500	3	NM_148976;NM_001143937;NM_002786	3
PSMB5	NM_001130725.1:716	3	NM_001130725;NM_001144932;NM_002797	3
SERPINB2	NM_002575.1:305	2	NM_002575;NM_001143818	2
SERPINE1	NM_000602.2:2470	2	NM_000602;NM_001165413	2
SOD1	NM_000454.4:35	1	NM_000454	1
SOD2	NM_000636.2:640	3	NM_000636;NM_001024466;NM_001024465	3
SQSTM1	NM_001142298.1:1470	3	NM_001142298;NM_001142299;NM_003900	3
SREBF1	NM_001005291.1:1392	2	NM_001005291;NM_004176	2
TALDO1	NM_006755.1:262	1	NM_006755	1
TKT	NM_001064.2:1235	2	NM_001064;NM_001135055	2
TLR4	NM_138554.2:2570	3	NM_138554;NR_024169;NR_024168	3
TXN	NM_003329.2:55	1	NM_003329	1
TXNRD1	NM_001093771.1:1009	5	NM_001093771;NM_182729;NM_003330;NM_182743;NM_182742	5

Appendix B. Targets Codeset design of genes of interest for Nanostring analysis: sulforaphane treatment in young MRC-5 fibroblasts *in vitro*

Gene	Targ Regi on	Target Sequence
AKR1C1	1210 - 1310	AGAGGATGGCTCTATGCTGGTGA CTGGACACATCGCCTCTGGTTAAATCTCTCCTGCTTGGTGATTCAGCAAGCTAC AGCAAAGCCCATTGGCCAGAAA
GLO1	1240 - 1340	GGAAATGATATGGTACCCAGACACTGGGCTAGGCTGCAACTTTATCTCATTTAATACTCCCAGCTGTCATGTGAGAAA GAAAGCAGGCTAGGCATGTGAA
CAT	1130 - 1230	ATGCTTCAGGGCCGCCTTTTTGCCTATCCTGACACTCACCGCCATCGCCTGGGACCCAATTATCTTCATATACCTGTG AACTGTCCCTACCGTGTCTGAG
GCLC	520- 620	CTCAAGTGGGGCGATGAGGTGGAATACATGTTGGTATCTTTTGATCATGAAAATAAAAAAGTCCGGTTGGTCCTGTCT GGGGAGAAAGTTCTTGAAACTC
GCLM	599- 699	TCATCATCAACTAGAAGTGCAGTTGACATGGCCTGTTGAGTCTTGGAGTTGCACAGCTGGATTCTGTGATCATTGCTT CACCTCCTATTGAAGATGGAG
NQO1	790- 890	CCGAATTCAAATCCTGGAAGGATGGAAGAAACGCCTGGAGAATATTTGGGATGAGACACCACTGTATTTTGCTCCAAG CAGCCTCTTTGACCTAAACTTC
TXNRD1	1009 - 1109	AGTGATGATCTTTTCTCCTTGCCTTACTGCCCGGGTAAGACCCTGGTTGTTGGAGCATCCTATGTCGCTTTGGAGTGC GCTGGATTTCTTGCTGGTATTG
TXN	55- 155	CAGCCAAGATGGTGAAGCAGATCGAGAGCAAGACTGCTTTTCAGGAAGCCTTGGACGCTGCAGGTGATAAACTTGTA GTAGTTGACTTCTCAGCCACGTG
GSR	1525 - 1625	ATGCAGGGACTTGGGTGTGATGAAATGCTGCAGGGTTTTGCTGTTGCAGTGAAGATGGGAGCAACGAAGGCAGACTT TGACAACACAGTCGCCATTCACC
HMOX1	1430 - 1530	TGTTGTTTTTATAGCAGGGTTGGGGTGGTTTTTGGAGCCATGCGTGGGTGGGGAGGGAGGTGTTTAACGGCACTGTGG CCTTGGTCTAACTTTTGTGTGAA
SOD1	35- 135	GCCTATAAAGTAGTCGCGGAGACGGGGTGTGTTTTGCGTCGTAGTCTCCTGCAGCGTCTGGGGTTTTCCGTTGCAGT CCTCGGAACCAGGACCTCGGCCT

PRDX1	632-732	GACCCATGAACATTTCCTTTGGTATCAGACCCGAAGCGCACCATTGCTCAGGATTATGGGGTCTTAAAGGCTGATGAAG GCATCTCGTTCAGGGGCCTTTT
GPX1	745-845	GGTTTTCATCTATGAGGGTGTTCCTCTAAACCTACGAGGGAGGAACACCTGATCTTACAGAAAATACCACCTCGAGA TGGGTGCTGGTCCTGTTGATCC
FTH1	941-1041	GGTACCCAGGTGTTGTCTTTGAGGTCTTGGGATGAATCAGAAATCTATCCAGGCTATCTTCCAGATTCTTAAGTGCC GTTGTTCAAGTTCTAATCACACT
GSTP1	415-515	TTTTGAGACCCTGCTGTCCCAGAACCAGGGAGGCAAGACCTTCATTGTGGGAGACCAGATCTCCTTCGCTGACTACAA CCTGCTGGACTTGCTGCTGATC
Mrp2/UGT 1A1	3150-3250	CAGTGACTCTAAAATCTTCAATAGCACCGACTATCCAGCATCTCAGAGGGACATGAGAGTTGGAGTCTACGGAGCTCT GGGATTAGCCCAAGGTATATTT
TALDO1	262-362	GCTGGGCGGGTCACAAGAGGACCAGATTA AAAATGCTATTGATAAACTTTTTGTGTTGTTTGGAGCAGAAATACTAAAG AAGATTCCGGGCCGAGTATCC
TKT	1235-1335	TGTGCCACCCGCAACAGGACGGTGCCCTTCTGCAGCACTTTTGCAGCCTTCTTACGCGGGCCTTTGACCAGATTCTG CATGGCCGCCATCTCCGAGAGCA
G6PD	1155-1255	ACAACATCGCCTGCGTTATCCTCACCTTCAAGGAGCCCTTTGGCACTGAGGGTTCGCGGGGGCTATTTTCGATGAATTTG GGATCATCCGGGACGTGATGCA
SREBF1	1392-1492	TTCGCTTTCTGCAACACAGCAACCAGAACTCAAGCAGGAGAACCTAAGTCTGCGCACTGCTGTCCACAAAAGCAAAT CTCTGAAGGATCTGGTGTCTGGC
FASN	5387-5487	GAGGTGCTTGGCTACGCACGGTCGCTTCTGGA AATTGGCAAATTCGACCTTTCTCAGAACCACCCGCTCGGCATGG CTATCTTCTGAAGAACGTGACA
PFKFB4	400-500	TGATGCCACAAACACCACCCGAGAACGGAGAGCGACCATCTTTAATTTTGGAGAACAGAATGGCTACAAGACCTTTTT TGTCGAGTCCATCTGTGTGGAT
NFE2L2	995-1095	TCCCGGTCACATCGAGAGCCCAGTCTTCATTGCTACTAATCAGGCTCAGTCACCTGAACTTCTGTTGCTCAGGTAGC CCCTGTTGATTTAGACGGTATG
KEAP1	561-661	CTCATTGAATTCGCTACACGGCCTCCATCTCCATGGGCGAGAAGTGTGTCCTCCACGTCATGAACGGTGCTGTCATG TACCAGATCGACAGCGTTGTCC
MAFG	3529-3629	CTTCCCCTGGATTTCTGACATAGATGGTGTGTTTCATGTGCAGGTGTGAGTGTGCTGTCTTCTGATCTCTGTTGATCC CGCTTTCCTACTGAGAGGGTG
FYN	765-865	GTCTTTGGAGGTGTGAACCTTCGTCTCATAACGGGACCTTGCCTACGAGAGGAGGAACAGGAGTGACACTCTTTGT GGCCCTTTATGACTATGAAGCAC
PSMA1	500-600	GGTTGCATTGAAAAGGGCGCAATCAGAGCTTGCAGCTCATCAGAAAAAATCTCCATGTTGACAACCATATTGGTATC TCAATTGCGGGGCTTACTGCT

PSMB5	716-816	CAGCTGCTTGTGTTTCTTGGGGTGA CTGTCATTGGTAATACGGACACAGT GACCCATCCTCCATCCTATTTATAGT GGAAGGGCCTTCAATTGTATCAGT
SQSTM1	1470-1570	TCATAGTTGTGTTAAGCTTGCGTAGA AATTGCAGGTCTCTGTACGGGCCAGT TTTCTCTGCCTTCTTCCAGGATCAG GGGTTAGGGTGCAAGAAGCCATTTA
CCL2	0-100	GAGGAACCGAGAGGCTGAGACTAACCC CAGAAACATCCAATTCTCAAAGCTCG CACTCTCGCCTCCAGCATGAAAGTCT CTGCCGCCCTTCTGTGC
CXCL1	742-842	TATGTTAATATTTCTGAGGAGCCTGCA ACATGCCAGCCACTGTGATAGAGGCT GGCGGATCCAAGCAAATGGCCAATG AGATCATTGTGAAGGCAGGGGA
IL15	1685-1785	AGGGTGATAGTCAAATTATGTATTGGT GGGGCTGGGTACCAATGCTGCAGGT CAACAGCTATGCTGGTAGGCTCCTG CCAGTGTGGAACCACTGACTACT
IL1B	840-940	GGGACCAAAGGCGGCCAGGATATAACT GACTTCACCATGCAATTTGTGTCTT CCTAAAGAGAGCTGTACCCAGAGAGT CCTGTGCTGAATGTGGACTCAA
TLR4	2570-2670	ACTCAGAAAAGCCCTGCTGGATGGTAA ATCATGGAATCCAGAAGGAACAGTGG GGTACAGGATGCAATTGGCAGGAAG CAACATCTATCTGAAGAGGAAAA
NFKB3	360-460	GATGGCTTCTATGAGGCTGAGCTCTG CCCCGACCGCTGCATCCACAGTTTCC AGAACCTGGGAATCCAGTGTGTGAA GAAGCGGGACCTGGAGCAGGCTA
NFKB1	1675-1775	AGGGTATAGCTTCCCACACTATGGATT TTCCTACTTATGGTGGGATTACTTTCC ATCCTGGAACTACTAAATCTAATGCT GGGATGAAGCATGGAACCATG
ICAM1	1990-2090	GAAATACTGAAACTTGCTGCCTATTGG GTATGCTGAGGCCACAGACTTACAGA AGAAGTGGCCCTCCATAGACATGT GTAGCATCAAAACACAAAGGCC
MMP3	25-125	AGGCATAGAGACAACATAGAGCTAAGT AAAGCCAGTGGAATGAAGAGTCTTCC AATCCTACTGTTGCTGTGCGTGGC AGTTTGCTCAGCCTATCCATTG
MMP13	951-1051	CTGGCGCCTGCATCCTCAGCAGGTTG ATGCGGAGCTGTTTTAACGAAATCAT TTTTGGCCAGAACTTCCCAACCGTAT TGATGCTGCATATGAGCACCCCT
SOD2	640-740	GCTTGTCCAAATCAGGATCCACTGCA AGGAACAACAGGCCTTATTCCACTG CTGGGGATTGATGTGTGGGAGCACGC TTACTACCTTCAGTATAAAAATG
ELN	765-865	GCAGCAGCGGCAGCTAAAGCAGCAGC AAAGTTTCGGTGCTGGAGCAGCCGG AGTCCTCCCTGGTGTGGAGGGGCT GGTGTTCCTGGCGTGCCTGGGGCAA
CTSO	725-825	ACCAAGAAGATGAAATGGCAAAGCACT TCTTACCTTTGGCCCTTTGGTAGTCA TAGTAGATGCAGTGAGCTGGCAAG ATTATCTGGGAGGCATTATACA
SERPINE1	2470-2570	TGTGTTCAATAGATTTAGGAGCAGAA ATGCAAGGGGCTGCATGACCTACCAG GACAGAACTTTCCCAATTACAGGGT GACTCACAGCCGCATTGGTGAC

SERPINB 2	305- 405	CTGTGGGTTTCATGCAGCAGATCCAGAAGGGTAGTTATCCTGATGCGATTTTGCAGGCACAAGCTGCAGATAAAATCCA TTCATCCTTCCGCTCTCTCAGC
GLB1	955- 1055	CTCACTCCACAATCAAGACCGAAGCAGTGGCTTCCCTCTATGATATACTTGCCCGTGGGGCGAGTGTGAACTTGT ACATGTTTATAGGTGGGACCAA
CDKN2A	975- 1075	AAGCGCACATTCATGTGGGCATTTCTTGCGAGCCTCGCAGCCTCCGGAAGCTGTGCGACTTCATGACAAGCATTITGTG AACTAGGGAAGCTCAGGGGGGT
CDKN1A	1975 - 2075	CATGTGTCCTGGTTCCCGTTTCTCCACCTAGACTGTAAACCTCTCGAGGGCAGGGACCACACCCTGTACTGTTCTGTG TCTTTCACAGCTCCTCCCACAA
ACTB	1010 - 1110	TGCAGAAGGAGATCACTGCCCTGGCACCCAGCACAATGAAGATCAAGATCATTGCTCCTCCTGAGCGCAAGTACTCC GTGTGGATCGGCGGCTCCATCCT
CLTC	290- 390	GGGTATCAACCCAGCAAACATTGGCTTCACTACCCTGACTATGGAGTCTGACAAATTCATCTGCATTAGAGAAAAAGTA GGAGAGCAGGCCAGGTGGTA
GUSB	1350 - 1450	CGGTCGTGATGTGGTCTGTGGCCAACGAGCCTGCGTCCCACCTAGAAATCTGCTGGCTACTACTTGAAGATGGTGATC GCTCACACCAAATCCTTGGACCC

Appendix C. Isoforms Codeset design of genes of interest for Nanostring analysis: early and late passage expression analysis in response to sulforaphane and hesperetin

Gene	Probe NSID	Tot Isoforms	Isoforms Hit by Probe	# Hit
ABCC2	NM_000392.3:3150	1	NM_000392	1
ACTB	NM_001101.2:1010	1	NM_001101	1
AKR1C1	NM_001353.5:1210	1	NM_001353	1
CAT	NM_001752.2:1130	1	NM_001752	1
CCL2	NM_002982.3:0	1	NM_002982	1
CDKN1A	NM_000389.2:1975	4	NM_000389;NM_078467;NM_001220778;NM_01220777	4
CLTC	NM_004859.2:290	1	NM_004859	1
COL1A1	NM_000088.3:5210	1	NM_000088	1
ELN	NM_001081754.1:2666	13	NM_001081754;NM_000501;NM_001278918;NM_001278917;NM_001278916;NM_001278915;NM_001278914;NM_001278913;NM_001278912;NM_001081755;NM_001081753;NM_001081752;NM_001278939	13
FASN	NM_004104.4:5387	1	NM_004104	1
FTH1	NM_002032.2:392	1	NM_002032	1
G6PD	NM_000402.2:1155	2	NM_000402;NM_001042351	2
GCLC	NM_001498.2:520	2	NM_001498;NM_001197115	2
GCLM	NM_002061.2:599	1	NM_002061	1
GLB1	NM_000404.2:955	3	NM_000404;NM_001079811;NM_001135602	3
GLO1	NM_006708.1:1240	1	NM_006708	1
GPX1	NM_000581.2:745	2	NM_000581;NM_201397	2
GSR	NM_000637.2:1525	4	NM_000637;NM_001195104;NM_001195103;NM_001195102	4

GSTP1	NM_000852.2:415	1	NM_000852	1
GUSB	NM_000181.1:1350	1	NM_000181	1
HIF1A	NM_001530.2:1985	3	NM_001530;NM_001243084;NM_181054	3
HK1	NM_000188.2:3355	5	NM_000188;NM_033497;NM_033498;NM_033500;NM_033496	5
HMOX1	NM_002133.1:1430	1	NM_002133	1
ICAM1	NM_000201.2:2253	1	NM_000201	1
KEAP1	NM_012289.3:561	2	NM_012289;NM_203500	2
MAFG	NM_002359.2:3529	2	NM_002359;NM_032711	2
MLX	NM_170607.2:565	3	NM_170607;NM_198205;NM_198204	3
MLXIP	NM_014938.3:945	1	NM_014938	1
MMP1	NM_002421.2:700	2	NM_002421;NM_001145938	2
MMP13	NM_002427.2:951	1	NM_002427	1
MMP3	NM_002422.3:25	1	NM_002422	1
NFE2L2	NM_006164.3:995	3	NM_006164;NM_001145413;NM_001145412	3
NFKB1	NM_003998.2:1675	2	NM_003998;NM_001165412	2
NQO1	NM_000903.2:790	3	NM_000903;NM_001025434;NM_001025433	3
PFKFB2	NM_001018053.1:445	2	NM_001018053;NM_006212	2
PRDX1	NM_002574.2:632	4	NM_002574;NM_001202431;NM_181696;NM_181697	4
PSMA1	NM_148976.2:500	3	NM_148976;NM_001143937;NM_002786	3
PSMB5	NM_001130725.1:716	3	NM_001130725;NM_001144932;NM_002797	3
RELA	NM_021975.2:360	4	NM_021975;NM_001145138;NM_001243985;NM_001243984	4
SERPINB2	NM_002575.1:305	2	NM_002575;NM_001143818	2
SOD1	NM_000454.4:35	1	NM_000454	1
SOD2	NM_000636.2:640	3	NM_000636;NM_001024466;NM_001024465	3
SQSTM1	NM_003900.3:1445	3	NM_003900;NM_001142299;NM_001142298	3
SREBF1	NM_001005291.1:1392	2	NM_001005291;NM_004176	2

TALDO1	NM_006755.1:262	1	NM_006755	1
TKT	NM_001064.2:1235	4	NM_001064;NR_047580;NM_001135055;NM_01258028	4
TLR4	NM_138554.2:2570	3	NM_138554;NM_138557;NM_003266	3
TXN	NM_003329.2:55	2	NM_003329;NM_001244938	2
TXNIP	NM_006472.1:255	1	NM_006472	1
TXNRD1	NM_001093771.1:1009	7	NM_001093771;NM_001261446;NM_001261445;NM_003330;NM_182743;NM_182729;NM_182742	7

Appendix D. Targets Codeset design of genes of interest for Nanostring analysis: early and late passage expression analysis in response to sulforaphane and hesperetin

Gene	Targ Regi on	Target Sequence
Mrp2/UGT 1A1	3151	CAGTGACTCTAAAATCTTCAATAGCACCGACTATCCAGCATCTCAGAGGGACATGAGAGTTGGAGTCTACGGAGCTCT GGGATTAGCCCAAGGTATATTT
	3250	
ACTB	1011	TGCAGAAGGAGATCACTGCCCTGGCACCCAGCACAAATGAAGATCAAGATCATTGCTCCTCCTGAGCGCAAGTACTCC GTGTGGATCGGCGGCTCCATCCT
	1110	
AKR1C1	1211	AGAGGATGGCTCTATGCTGGTGACTGGACACATCGCCTCTGGTTAAATCTCTCCTGCTTGGTGATTTTCAGCAAGCTAC AGCAAAGCCCATTGGCCAGAAA
	1310	
CAT	1131	ATGCTTCAGGGCCGCCTTTTTGCCTATCCTGACACTCACCGCCATCGCCTGGGACCCAATTATCTTCATATACCTGTG AACTGTCCCTACCGTGCTCGAG
	1230	
CCL2	1-	GAGGAACCGAGAGGCTGAGACTAACCAGAAACATCCAATTCTCAAAGCTCGCACTCTCGCCTCCAGCATGA AAGTCTCTGCCGCCCTTCTGTGC
	100	
CDKN1A	1976	CATGTGTCCTGGTTCCCGTTTCTCCACCTAGACTGTAAACCTCTCGAGGGCAGGGACCACACCCTGTACTGTTCTGTG TCTTTCACAGCTCCTCCCACAA
	2075	
CLTC	291-	GGGTATCAACCCAGCAAACATTGGCTTCAGTACCCTGACTATGGAGTCTGACAAATTCATCTGCATTAGAGAAAAAGT AGGAGAGCAGGCCAGGTGGTA
	390	
COL1A1	5211	CAGAAACATCGGATTTGGGGAACGCGTGTCAATCCCTTGTGCCGCAGGGCTGGGCGGGAGAGACTGTTCTGTTCCCTT GTGTAAGTGTGTTGCTGAAAGAC
	5310	
ELN	2667	CCACCGTTGGCTGCCATCCAGTTGGTACCCAAGCACCTGAAGCCTCAAAGCTGGATTCGCTCTAGCATCCCTCCTCT CCTGGGTCCACTTGGCCGTCTCC
	2766	

	5388	
	-	GAGGTGCTTGGCTACGCACGGTCGCTTCCTGGAAATTGGCAAATTCGACCTTTCTCAGAACCACCCGCTCGGCATGG
FASN	5487	CTATCTTCCTGAAGAACGTGACA
	393-	CCAAATACTTTCTTCACCAATCTCATGAGGAGAGGGAAACATGCTGAGAACTGATGAAGCTGCAGAACCAACGAGGTG
FTH1	492	GCCGAATCTTCCTTCAGGATAT
	1156	
	-	ACAACATCGCCTGCGTTATCCTCACCTTCAAGGAGCCCTTTGGCACTGAGGGTCGCGGGGGCTATTTTCGATGAATTT
G6PD	1255	GGGATCATCCGGGACGTGATGCA
	521-	CTCAAGTGGGGCGATGAGGTGGAATACATGTTGGTATCTTTTGATCATGAAAATAAAAAAGTCCGGTTGGTCCTGTCT
GCLC	620	GGGGAGAAAGTTCTTGAAACTC
	600-	TCATCATCAACTAGAAGTGCAGTTGACATGGCCTGTTGAGTTCCTGGAGTTGCACAGCTGGATTCTGTGATCATTGCT
GCLM	699	TCACCTCCTATTGAAGATGGAG
	956-	CTCACTCCACAATCAAGACCGAAGCAGTGGCTTCCTCCCTCTATGATATACTTGCCCGTGGGGCGAGTGTGAACTTGT
GLB1	1055	ACATGTTTATAGGTGGGACCAA
	1241	
	-	GGAAATGATATGGTACCCAGACACTGGGCTAGGCTGCAACTTTATCTCATTTAATACTCCCAGCTGTCATGTGAGAAA
GLO1	1340	GAAAGCAGGCTAGGCATGTGAA
	746-	GGTTTTCATCTATGAGGGTGTTCCTCTAAACCTACGAGGGAGGAACACCTGATCTTACAGAAAATACCACCTCGAGA
GPX1	845	TGGGTGCTGGTCCTGTTGATCC
	1526	
	-	ATGCAGGGACTTGGGTGTGATGAAATGCTGCAGGGTTTTGCTGTTGCAGTGAAGATGGGAGCAACGAAGGCAGACTT
GSR	1625	TGACAACACAGTCGCCATTCAAC
	416-	TTTTGAGACCCTGCTGTCCCAGAACCAGGGAGGCAAGACCTTCATTGTGGGAGACCAGATCTCCTTCGCTGACTACA
GSTP1	515	ACCTGCTGGACTTGCTGCTGATC
	1351	
	-	CGGTCGTGATGTGGTCTGTGGCCAACGAGCCTGCGTCCCACCTAGAATCTGCTGGCTACTACTTGAAGATGGTGATC
GUSB	1450	GCTCACACCAAATCCTTGGACCC
	1986	
	-	ATGGATGATGACTTCCAGTTACGTTCCCTTCGATCAGTTGTCACCATTAGAAAGCAGTTCCGCAAGCCCTGAAAGCGCA
HIF1A	2085	AGTCCTCAAAGCACAGTTACAG
	3356	
	-	CTGTGGCCTGGCATCGCATCGTGGTGTGTCAATGCCACAAAATCGTGTGTCCGTGGAACCAGTCCTAGCCGCGTGTG
HK1	3455	ACAGTCTTGCATTCTGTTTGTCT

	1431	
HMOX1	- 1530	TGTTGTTTTTATAGCAGGGTTGGGGTGGTTTTTGGAGCCATGCGTGGGTGGGGAGGGAGGTGTTTAAACGGCACTGTGG CCTTGGTCTAACTTTTGTGTGAA
	2254	
ICAM1	- 2353	AAATACTGAAACTTGCTGCCTATTGGGTATGCTGAGGCCCCACAGACTTACAGAAGAAGTGGCCCTCCATAGACATGT GTAGCATCAAACACAAAGGCC
KEAP1	562- 661	CTCATTGAATTCGCCTACACGGCCTCCATCTCCATGGGCGAGAAGTGTGTCCTCCACGTCATGAACGGTGCTGTCAT GTACCAGATCGACAGCGTTGTCC
	3530	
MAFG	- 3629	CTTCCCCTGGATTCCTGACATAGATGGTGTGTTTCATGTGCAGGTGTGAGTGTGCTGTCCTTCTGATCTCTGTTGATC CCGCTTTCCTACTGAGAGGGTG
MLX	566- 665	CTCCCAAAGCTCAGCAAAGCCATCGTTCTACAAAAGACCATTGACTACATTGAGTTTTTGCACAAGGAGAAGAAAA GCAGGAGGAGGAGGTGTCCACG
MLXIP	946- 1045	CTGATTCCTTTGCAGCCTAACCTGGACTTCATGGACACCTTTGAGCCTTTCCAGGACCTCTTCTCTTAGCCGCTCC ATTTTTGGCTCCATGCTACCTG
MMP1	701- 800	CAACTTACATCGTGTGCGGCTCATGAACTCGGCCATTCTCTTGGACTCTCCATTCTACTGATATCGGGGCTTTGAT GTACCCTAGCTACACCTTCAGT
MMP13	952- 1051	CTGGCGCCTGCATCCTCAGCAGTTGATGCGGAGCTGTTTTAACGAAATCATTTTGGCCAGAACTTCCCAACCGTAT TGATGCTGCATATGAGCACCT
MMP3	26- 125	AGGCATAGAGACAACATAGAGCTAAGTAAAGCCAGTGGAATGAAGAGTCTTCCAATCCTACTGTTGCTGTGCGTGGC AGTTTGCTCAGCCTATCCATTG
NFE2L2	996- 1095	TCCCGGTACATCGAGAGCCCAGTCTTCATTGCTACTAATCAGGCTCAGTCACCTGAAACTTCTGTTGCTCAGGTAGC CCCTGTTGATTTAGACGGTATG
	1676	
NFKB1	- 1775	AGGGTATAGCTTCCCACACTATGGATTCCTACTTATGGTGGGATTACTTTCCATCCTGGAACTACTAAATCTAATGCT GGGATGAAGCATGGAACCATG
NQO1	791- 890	CCGAATTCAAATCCTGGAAGGATGGAAGAAACGCCTGGAGAATATTTGGGATGAGACACCACTGTATTTTGTCCAAG CAGCCTCTTTGACCTAACTTC
PFKFB2	446- 545	GTTAAGGCGTATCTCACTGAGGAGAATGGTCAGATTGCGGTGTTTGTATGCCACCAATACAACCCGGGAGAGGAGGGA CATGATTTTGAACCTTTGCTGAAC
PRDX1	633- 732	GACCATGAACATTCCTTTGGTATCAGACCCGAAGCGCACCATTGCTCAGGATTATGGGGTCTTAAAGGCTGATGAAG GCATCTCGTTCAGGGGCCTTTT
PSMA1	501-	GGTTGCATTGAAAAGGGCGCAATCAGAGCTTGCAGCTCATCAGAAAAAATTCTCCATGTTGACAACCATATTGGTAT

	600	CTCAATTGCGGGGCTTACTGCT
PSMB5	717-816	CAGCTGCTTGTGTTTTCTTGGGGTACTGTCATTGGTAATACGGACACAGTGACCCATCCTCCATCCTATTTATAGTGG AAGGGCCTTCAATTGTATCAGT
NFKB3	361-460	GATGGCTTCTATGAGGCTGAGCTCTGCCCGGACCGCTGCATCCACAGTTTCCAGAACCTGGGAATCCAGTGTGTGAA GAAGCGGGACCTGGAGCAGGCTA
SERPIN2	306-405	CTGTGGGTTTCATGCAGCAGATCCAGAAGGGTAGTTATCCTGATGCGATTTTGCAGGCACAAGCTGCAGATAAAATCCA TTCATCCTTCCGCTCTCTCAGC
SOD1	36-135	GCCTATAAAGTAGTCGCGGAGACGGGGTGCTGGTTTGCCTCGTAGTCTCCTGCAGCGTCTGGGGTTTCCGTTGCAGT CCTCGGAACCAGGACCTCGGCGT
SOD2	641-740	GCTTGTCCAAATCAGGATCCACTGCAAGGAACAACAGGCCTTATTCCACTGCTGGGGATTGATGTGTGGGAGCACGC TACTACCTTCAGTATAAAAATG
SQSTM1	1446-1545	GGGCCAGTTTCTCTGCCTTCTTCCAGGATCAGGGGTTAGGGTGCAAGAAGCCATTTAGGGCAGCAAAACAAGTGACA TGAAGGGAGGGTCCCTGTGTGTG
SREBF1	1393-1492	TTCGCTTTCTGCAACACAGCAACCAGAACTCAAGCAGGAGAACCTAAGTCTGCGCACTGCTGTCCACAAAAGCAAAT CTCTGAAGGATCTGGTGTCTGGC
TALDO1	263-362	GCTGGGCGGGTCAACAAGAGGACCAGATTAATAATGCTATTGATAAACTTTTTGTGTTGTTTGGAGCAGAAATACTAAA GAAGATTCCGGGCCGAGTATCC
TKT	1236-1335	TGTGCCACCCGCAACAGGACGGTGCCCTTCTGCAGCACTTTTGCAGCCTTCTTACGCGGGCCTTTGACCAGATTCCG CATGGCCGCCATCTCCGAGAGCA
TLR4	2571-2670	ACTCAGAAAAGCCCTGCTGGATGGTAAATCATGGAATCCAGAAGGAACAGTGGGTACAGGATGCAATTGGCAGGAAG CAACATCTATCTGAAGAGGAAAA
TXN	56-155	CAGCCAAGATGGTGAAGCAGATCGAGAGCAAGACTGCTTTTTCAGGAAGCCTTGGACGCTGCAGGTGATAAACTTGTA GTAGTTGACTTCTCAGCCACGTG
TXNIP	256-355	TGGTCTTTAACGACCCTGAAAAGGTGTACGGCAGTGCCGAGAGGGTGGCTGGCCGGGTGATAGTGGAGGTGTGTGA AGTTACTCGTGTCAAAGCCGTTAG
TXNRD1	1010-1109	AGTGATGATCTTTTCTCCTTGCCCTTACTGCCCGGGTAAGACCCTGGTTGTTGGAGCATCCTATGTCGCTTTGGAGTGC GCTGGATTTCTTGCTGGTATTG

Appendix E. Significant changes in microarray gene expression between controls at passage 3 and controls at passage 11 after Bonferroni factor of 20773 was applied (P<0.05)

Gene ID	Significance with BF correction of 20773	Expression
C11orf70	1.326E-08	3.873
CXCL2	1.945E-08	-3.042
LOC644727	1.990E-08	-4.504
MOB4	2.398E-08	1.810
COL4A3BP	2.690E-08	0.808
LOC100499177	3.265E-08	-1.763
ZMAT2	3.835E-08	1.089
PDE4DIP	6.129E-08	-1.856
PRO2852	7.802E-08	-5.223
SCARNA13	9.806E-08	-2.984
HLA-E	1.014E-07	1.248
DNAJC6	1.063E-07	6.408
ABTB2	1.160E-07	0.989
BANK1	1.211E-07	3.530
CPPED1	1.405E-07	3.103
CCDC144A	1.457E-07	-3.928
COLEC11	1.556E-07	-1.782
CCRL1	1.667E-07	5.636
CCDC144A	1.678E-07	-4.259
HSD11B1L	1.738E-07	0.754
LRRC69	2.236E-07	2.971
HIST2H2AC	3.036E-07	-2.363
APBB1IP	3.342E-07	5.911
SNORD12C	3.411E-07	-6.019
GMFG	3.484E-07	2.075
UHMK1	3.547E-07	1.499
DNAJC19	3.887E-07	0.815
SLC14A1	4.280E-07	2.571
MTRF1	4.325E-07	-1.240
OXR1	4.334E-07	-1.473
SNORD114-3	4.419E-07	-3.536
MMP3	4.622E-07	3.768
PPM1N	4.927E-07	-2.089
LOC400499	5.310E-07	-1.547

RGS16	5.439E-07	3.234
TAX1BP1	5.536E-07	0.763
TRIM63	5.764E-07	5.257
LOC400550	5.784E-07	1.039
PPP1R3G	6.246E-07	2.781
TMEM165	6.733E-07	0.797
TRIM45	6.780E-07	-1.942
BCOR	6.809E-07	-2.952
COL23A1	6.865E-07	-2.410
MUC1	7.121E-07	1.060
SNORD114-26	7.494E-07	-3.226
FOSB	7.602E-07	-3.919
KCTD12	7.644E-07	1.575
NDST2	7.842E-07	1.232
GPC4	7.866E-07	1.598
MANBAL	7.913E-07	1.454
AMPD3	7.975E-07	-2.095
STYK1	8.146E-07	2.393
ATCAY	9.127E-07	5.906
LOC731275	9.143E-07	-2.289
ABCC3	9.385E-07	-1.803
LOC401320	9.615E-07	-3.689
LYPD5	9.626E-07	4.434
TMEM176A	9.838E-07	4.391
FBXL17	1.004E-06	-3.316
PRPF39	1.015E-06	-1.875
LOC645752	1.017E-06	-3.422
D4S234E	1.042E-06	2.331
HIST1H4A	1.051E-06	-3.158
ADHFE1	1.057E-06	-2.916
FLJ41170	1.068E-06	-4.372
XLOC_12_001134	1.072E-06	-2.417
NPY	1.074E-06	6.502
ND1	1.075E-06	-1.857
LOC440149	1.125E-06	1.861
LYNX1	1.147E-06	0.850
NKTR	1.164E-06	-2.329
ABCC10	1.256E-06	-2.888
XLOC_003406	1.294E-06	-1.788
GOLGA6L9	1.330E-06	-2.410
NAMPT	1.353E-06	-6.265
DAAM2	1.371E-06	1.946
FOXL2	1.391E-06	5.013
LOC400464	1.437E-06	-3.514

CASKIN2	1.468E-06	-4.393
TBC1D3G	1.470E-06	-2.861
INA	1.477E-06	2.182
PDP2	1.508E-06	1.343
ACAD10	1.516E-06	-0.639
XLOC_012991	1.573E-06	-3.685
SMA4	1.579E-06	-4.063
SYPL2	1.637E-06	2.921
ZNF169	1.666E-06	-1.954
FBXL19-AS1	1.688E-06	-2.960
SORT1	1.698E-06	1.685
SNORD114-17	1.703E-06	-3.510
SAP25	1.736E-06	-3.412
MALAT1	1.739E-06	-3.784
SEPP1	1.771E-06	3.632
CTBS	1.785E-06	1.041
LAT	1.789E-06	-1.954
MATN3	1.792E-06	1.965
RNU6ATAC	1.810E-06	-5.818
UFD1L	1.813E-06	1.251
SLC25A16	1.826E-06	-3.112
PDK2	1.836E-06	1.730
Q8RQM5	1.866E-06	-2.145
FLJ44342	1.866E-06	-3.414
RCAN3	1.867E-06	1.435
SHC4	1.922E-06	1.947
FLJ45248	1.929E-06	-1.719
PSG1	1.935E-06	1.955
L2HGDH	2.036E-06	-2.435
LOC401357	2.039E-06	-2.418
NR5A2	2.050E-06	6.826
XLOC_003526	2.070E-06	-4.758
LOC100130587	2.078E-06	-5.856
RPL23AP32	2.083E-06	-4.432
XLOC_003526	2.101E-06	-5.374
TMEM47	2.118E-06	2.687
PDE11A	2.128E-06	5.175
CTSL1	2.136E-06	-3.463
HSD17B6	2.140E-06	4.681
TMX2	2.176E-06	0.660
ZNF525	2.190E-06	0.652
ANKRD36	2.228E-06	-4.618
SLC9A7P1	2.243E-06	1.765
CISH	2.243E-06	-5.363

FAM22G	2.263E-06	-2.473
LOC400550	2.263E-06	-0.890
XLOC_000390	2.296E-06	-4.266
PSG9	2.303E-06	1.680
RAI1	2.311E-06	-0.288
DAP	2.322E-06	2.487
MAP7D3	2.375E-06	1.661
C7orf30	2.382E-06	1.330
MIAT	2.393E-06	-5.711

Appendix F. Significant changes in microarray gene expression between SFN treatment at passage 11 and control at passage 3 after Bonferroni factor of 20773 was applied (P<0.05)

Gene ID	Significance with BF correction of 20773	Expression
FAM46C	4.842E-11	1.645
FAM63A	3.662E-10	1.669
DIXDC1	9.153E-10	2.502
FAM134A	1.159E-09	1.434
FOSB	4.031E-09	-3.437
KIAA1826	1.935E-08	1.233
NR5A2	2.379E-08	6.621
DUSP11	2.664E-08	2.858
SNORD99	2.724E-08	-4.627
MYO15B	2.949E-08	-1.737
HLA-DMB	3.606E-08	5.228
SNORD113-3	3.925E-08	-2.784
MOB4	3.939E-08	1.922
XLOC_12_002033	3.959E-08	-3.401
FNBP4	4.649E-08	-1.462
USP39	6.608E-08	0.898
TPD52L2	6.789E-08	1.538
INPP5F	6.914E-08	1.869
XLOC_003853	7.365E-08	1.000
D4S234E	7.372E-08	2.701
XLOC_12_012319	7.527E-08	3.512
SLC46A1	8.204E-08	1.697
SULF1	8.599E-08	4.352
MPP2	1.004E-07	4.429
ERLEC1	1.034E-07	1.654
KRTAP10-1	1.065E-07	-1.036
FAM3C	1.072E-07	1.605
TBC1D10B	1.210E-07	0.989
DUSP5	1.309E-07	-2.178
LOC100507319	1.381E-07	1.397
TCP1	1.421E-07	0.981
FLJ45445	1.450E-07	-1.452
PCTP	1.468E-07	1.174
MRPL37	1.481E-07	1.066
FRAT1	1.485E-07	2.007
ANKRD43	1.501E-07	4.586

AP1B1	1.571E-07	2.003
ATCAY	1.577E-07	6.412
SSX2IP	1.618E-07	1.295
REXO1L1	1.711E-07	-3.236
FZD4	1.731E-07	2.420
ACTG1	1.740E-07	1.101
LOC100133050	1.758E-07	-2.800
RCAN1	1.769E-07	1.626
PLOD1	1.776E-07	1.256
C6orf97	1.779E-07	2.748
DACT1	1.825E-07	2.610
KCNQ1OT1	1.838E-07	-2.595
ARSJ	1.874E-07	0.819
SERPINE2	1.892E-07	1.697
NUP93	1.898E-07	1.231
DNAJC6	1.961E-07	6.644
POLR2E	1.972E-07	1.279
EDIL3	2.007E-07	2.311
XLOC_012645	2.040E-07	4.841
ITPR1	2.178E-07	2.091
LOC440028	2.188E-07	1.817
SLC35E4	2.204E-07	-2.310
TPRG1L	2.269E-07	2.770
MICB	2.298E-07	2.555
VAMP3	2.318E-07	0.706
HINT3	2.362E-07	1.536
TRAPPC4	2.385E-07	1.055
PCSK6	2.501E-07	6.376
INO80C	2.556E-07	1.440
LOC645638	2.570E-07	2.286
LYPD5	2.638E-07	4.996
MPP2	2.775E-07	4.099
NPIP	2.775E-07	-2.451
MOB1A	2.819E-07	1.966
THAP10	2.833E-07	1.679
C19orf18	2.993E-07	-1.018
ZNF219	3.008E-07	1.591
YIPF6	3.154E-07	1.143
ASTN2	3.154E-07	2.175
LOC100506175	3.199E-07	2.675
ANGPT2	3.212E-07	3.710
PRKD3	3.337E-07	1.188
CAMK2D	3.511E-07	-2.191
ANKRD29	3.619E-07	4.024

C11orf70	3.636E-07	3.633
TOPBP1	3.688E-07	-0.491
RAD9A	3.698E-07	-1.669
GK	3.716E-07	-4.544
MMP3	3.783E-07	4.208
LOC400499	3.860E-07	-2.174
SRRT	3.987E-07	-0.561
MED20	4.006E-07	0.735
C9orf30	4.165E-07	-0.834
POTEE	4.224E-07	1.237
WRB	4.282E-07	2.388
TGFB2	4.568E-07	2.193
HIF1A	4.611E-07	1.086
SRI	4.685E-07	1.423
FOXL2	4.690E-07	5.220
IER3IP1	4.728E-07	1.000
APBB1IP	5.041E-07	6.804
NDN	5.164E-07	3.398
TARBP1	5.191E-07	-2.114
MAP3K8	5.309E-07	-3.990
PDE11A	5.342E-07	5.742
RNASET2	5.581E-07	1.276
SSBP3	5.584E-07	1.069
XLOC_12_006399	5.718E-07	-4.501
ADAMTS5	5.863E-07	4.331
C5orf62	5.953E-07	2.231
CMKLR1	6.077E-07	4.518
TOMM20	6.123E-07	1.267
ZNF526	6.144E-07	-2.635
SSX2IP	6.194E-07	3.923
SYPL2	6.217E-07	2.676
ARMC4	6.228E-07	0.922
CCRL1	6.266E-07	5.807
MCART1	6.301E-07	0.705
TEK	6.314E-07	1.855
PTGDS	6.543E-07	-4.817
ACAA2	6.543E-07	2.498
LOC729040	6.576E-07	-2.220
LCE2C	6.655E-07	2.971
FAM60A	6.703E-07	1.051
RGS16	6.748E-07	3.644
TXNIP	6.785E-07	6.814
PPAPDC3	6.827E-07	4.083
TMCO7	6.839E-07	1.584

STARD13	6.933E-07	-3.174
SLC35E1	6.974E-07	1.015
EIF4E2	7.031E-07	1.314
MR1	7.034E-07	1.610
MAEA	7.637E-07	1.131
PSMB9	7.644E-07	1.269
LOC100507150	7.648E-07	4.448
MB21D1	7.843E-07	-1.878
RCAN2	7.900E-07	3.015
VAMP4	8.004E-07	0.958
GPRASP1	8.270E-07	-2.094
GALNT1	8.272E-07	1.445
ZYG11B	8.296E-07	1.759
IQCE	8.430E-07	1.858
TSPYL5	8.472E-07	3.541
TMEM176B	8.574E-07	3.933
FKBP1B	8.607E-07	1.734
CENPBD1	8.640E-07	1.278
FLJ32255	8.818E-07	1.559
GLS	9.062E-07	1.413
SYNGR2	9.071E-07	1.424
USP22	9.331E-07	1.437
PDE1C	9.475E-07	2.840
INHBB	9.668E-07	4.277
AGAP11	9.843E-07	-3.313
LIMCH1	9.855E-07	5.947
C4orf3	9.867E-07	1.836
TGFBRAP1	1.022E-06	1.228
C11orf63	1.044E-06	2.624
LOC729737	1.057E-06	-2.978
FBXL3	1.066E-06	1.590
SEMA4F	1.070E-06	1.131
FBXL8	1.080E-06	0.493
SHC4	1.080E-06	2.327
ZNF799	1.081E-06	-2.354
AASS	1.083E-06	-1.975
ST8SIA5	1.097E-06	3.506
MAP3K8	1.104E-06	-4.493
CYB561D1	1.120E-06	2.178
NSF	1.124E-06	1.658
SLC2A3	1.132E-06	-2.833
LOC440149	1.133E-06	1.740
LOC145474	1.133E-06	-3.571
LOC100506528	1.135E-06	-0.927

PDCD10	1.138E-06	1.343
ANKRD1	1.141E-06	3.727
LOC644727	1.156E-06	-4.274
ARMCX4	1.169E-06	-3.202
TMEM45A	1.207E-06	1.978
RN7SL1	1.209E-06	-2.302
LRRC57	1.239E-06	1.578
SEC23B	1.243E-06	1.647
XLOC_000527	1.264E-06	0.381
CSNK1G1	1.282E-06	1.579
KLHL5	1.291E-06	1.677
HSD17B6	1.299E-06	5.425
NUDT4	1.304E-06	1.332
HNRNPU-AS1	1.327E-06	-4.628
YME1L1	1.330E-06	0.728
SUN1	1.333E-06	-0.857
LOC100507904	1.334E-06	-2.385
FTO	1.354E-06	-5.895
MSH5	1.363E-06	-3.361
SNORA70F	1.367E-06	-3.417
ZNF337	1.396E-06	-2.428
ITPRIPL2	1.416E-06	1.574
CPPED1	1.428E-06	3.506
XLOC_12_000649	1.434E-06	1.283
ATP9A	1.434E-06	1.817
CALCOCO2	1.446E-06	2.083
PMP22	1.462E-06	-3.304
SNORA9	1.486E-06	-0.813
C12orf53	1.517E-06	1.458
PGM2L1	1.525E-06	3.628
ARHGEF3	1.535E-06	2.352
AGMAT	1.553E-06	4.543
GNPTAB	1.574E-06	-2.516
C14orf129	1.594E-06	1.975
ZNF174	1.595E-06	1.482
NISCH	1.621E-06	-1.617
LOC645638	1.635E-06	1.853
SELT	1.636E-06	1.950
CTNND2	1.637E-06	5.448
C3orf72	1.641E-06	3.594
CAPN1	1.656E-06	1.475
HIGD1A	1.661E-06	1.866
TMEM167B	1.665E-06	2.186
MGAT3	1.668E-06	6.218

PCDHB2	1.677E-06	2.190
KPNA3	1.681E-06	1.447
FGFR1OP2	1.697E-06	-4.162
LOC100506778	1.698E-06	-1.147
LPIN1	1.734E-06	-1.424
GLRX2	1.747E-06	1.137
LARS	1.752E-06	-1.257
PCSK6	1.758E-06	4.589
EIF1AY	1.770E-06	1.434
MXRA7	1.776E-06	1.965
MANBAL	1.794E-06	1.497
STYK1	1.805E-06	2.827
KCND2	1.808E-06	4.165
C11orf87	1.836E-06	3.571
TMEM176A	1.841E-06	4.236
TSPAN31	1.843E-06	1.474
LOC100302640	1.860E-06	1.808
ARRDC4	1.871E-06	3.066
WFDC1	1.888E-06	3.932
RGS17	1.903E-06	-3.368
PSG2	1.922E-06	1.193
NFASC	1.924E-06	2.372
XLOC_12_002767	1.940E-06	2.051
COPZ2	1.965E-06	1.282
ABCA11P	1.992E-06	0.462
C6orf97	2.024E-06	4.086
IGF2	2.037E-06	3.130
MED7	2.043E-06	1.003
PRRX2	2.077E-06	3.357
RPL7	2.126E-06	0.360
PMPCA	2.126E-06	0.895
RAP1A	2.134E-06	1.416
LOC729603	2.140E-06	-1.814
DHRS4L1	2.151E-06	-5.252
KIAA0754	2.151E-06	-3.975
CCK	2.163E-06	3.064
TERF2	2.170E-06	1.796
C11orf58	2.174E-06	1.072
UBE2G2	2.206E-06	-0.552
SNORD114-17	2.207E-06	-3.156
THBS1	2.207E-06	2.211
XLOC_009474	2.208E-06	-1.177
RFTN1	2.223E-06	1.299
SNORA77	2.224E-06	-2.559

LOC100506123	2.228E-06	-3.136
SEPP1	2.237E-06	3.413
LRRC10	2.243E-06	-4.038
NRK	2.246E-06	4.933
FRMD4A	2.292E-06	-5.024
FAM50B	2.299E-06	1.382
XAGE-4	2.300E-06	-6.565
MRAS	2.314E-06	2.357
XLOC_009895	2.323E-06	-3.088
FLJ40606	2.324E-06	-3.177
MCTP2	2.338E-06	6.004
VAMP3	2.351E-06	0.915
XLOC_006416	2.369E-06	-2.801
SLC10A3	2.375E-06	1.985
POC1B	2.378E-06	1.088
CXCR7	2.389E-06	6.086
PMEPA1	2.393E-06	2.752
KIAA0528	2.396E-06	-1.287

Bibliography

- ABBOTT, A. 2004. Ageing: growing old gracefully. *Nature*, 428, 116-118.
- ABRAHAM, D., INCE, T., MUIR, H. & OLSEN, I. 1989. Fibroblast matrix and surface components that mediate cell-to-cell interaction with lymphocytes. *J Invest Dermatol*, 93, 335-340.
- AGARWAL, B. & BAUR, J. A. 2011. Resveratrol and life extension. *Annals of the New York Academy of Sciences*, 1215, 138-143.
- AHMED, A. & TOLLEFSBOL, T. 2001. Telomeres and telomerase: basic science implications for aging. *J Am Geriatr Soc*, 49, 1105-1109.
- AHMED, N., ARGIROV, O. K., MINHAS, H. S., CORDEIRO, C. A. & THORNALLEY, P. J. 2002. Assay of advanced glycation endproducts (AGEs): surveying AGEs by chromatographic assay with derivatization by 6-aminoquinolyl-N-hydroxysuccinimidyl-carbamate and application to Nepsilon-carboxymethyl-lysine- and Nepsilon-(1-carboxyethyl)lysine-modified albumin. *Biochem J*, 364, 1-14.
- AMEER, B., WEINTRAUB, R. A., JOHNSON, J. V., YOST, R. A. & ROUSEFF, R. L. 1996. Flavanone absorption after naringin, hesperidin, and citrus administration. *Clin. Pharmacol. Ther*, 60, 34-40.
- AN, J.H., VRANAS, K., LUCKE, M., INOUE, H., HISAMOTO, N., MATSUMOTO, K., BLACKWELL, T.K. 2005. Regulation of the *Caenorhabditis elegans* oxidative stress defense protein SKN-1 by glycogen synthase kinase-3. *Proc. Natl. Acad. Sci. USA*, 102, 16275-16280.
- ANDERSON, R. M. & WEINDRUCH, R. 2007. Metabolic reprogramming in dietary restriction. *Interdiscip Top Gerontol*, 35, 18-38.
- ANISIMOV, V. N. 2003. The relationship between aging and carcinogenesis: a critical appraisal. *Crit Rev Oncol Hematol*, 45, 277-304.
- APOPA, P. L., HE, X. & MA, Q. 2008. Phosphorylation of Nrf2 in the transcription activation domain by casein kinase 2 (CK2) is critical for the nuclear translocation and transcription activation function of Nrf2 in IMR-32 neuroblastoma cells. *J Biochem Mol Toxicol*, 22, 63-76.
- ARAMAYO, R., SHERMAN, M. B., BROWNLESS, K., LURZ, R., OKOROKOV, A. L. & ORLOVA, E. V. 2011. Quaternary structure of the specific p53-DNA complex reveals the mechanism of p53 mutant dominance. *Nucleic acids research*, 39, 8960-8971.
- ARGYROPOULOS, C., WANG, K., MCCLARTY, S., HUANG, D., BERNARDO, J., ELLIS, D., ORCHARD, T., GALAS, D., and JOHNSON, J. 2013. Urinary microRNA profiling in the nephropathy of type 1 diabetes. *PloS one*, 8, e54662.

- ATADJA, P., WONG, H., GARKAVTSEV, I., VEILLETTE, C. & RIABOWOL, K. 1995. Increased activity of p53 in senescing fibroblasts. *Proc Natl Acad Sci U S A*, 92, 8348-8352.
- BABA, A. H., & MITRA, S. 2009. Testing for transistor aging. VLSI Test Symposium, *VTS'09. 27th IEEE*, 215-220.
- BADADANI, M. 2012. Autophagy mechanism, regulation, functions, and disorders. *ISRN Cell Biology*, 12, 552-571.
- BALABAN, R. S., NEMOTO, S. & FINKEL, T. 2005. Mitochondria, oxidants, and aging. *Cell*, 120, 483-495.
- BARKER, G. & SMART, K. 1996. Morphological Changes Associated with the Cellular Aging of a Brewing Yeast Strain. . *Journal of American Society of Brewing Chemistry*, 54, 121-126.
- BARNETT, Y. A. & BARNETT, C. R. 2000. *Aging methods and protocols*, Springer.
- BASS, T. M., WEINKOVE, D., HOUTHOOFD, K., GEMS, D., & PARTRIDGE, L. 2007. Effects of resveratrol on lifespan in drosophila melanogaster and caenorhabditis elegans. *Mechanisms of Ageing & Development*, 128, 546-552.
- BAUR, J.A. & SINCLAIR, D.A. 2006. Therapeutic potential of resveratrol: the in vivo evidence. *Nat Rev Drug Discov*, 5, 493-506.
- BECKMAN, K. B. & AMES, B. N. 1998. The free radical theory of aging matures. *Physiol Rev*, 78, 547-581.
- BEN-DOR, A., STEINER, M., GHEBER, L., DANILENKO, M., DUBI, N., LINNEWIEL, K., ZICK, A., SHARONI, Y. & LEVY, J. 2005. Carotenoids activate the antioxidant response element transcription system. *Mol Cancer Ther*, 4, 177-186.
- BEN-PORATH, I. & WEINBERG, R. A. 2005. The signals and pathways activating cellular senescence. *Int J Biochem Cell Biol*, 37, 961-976.
- BENSAAD, K., TSURUTA, A., SELAK, M.A., VIDAL, M.N., NAKANO, K., BARTRONS, R., GOTTLIEB, E., VOUSDEN, K.H. 2006. TIGAR, a p53-inducible regulator of glycolysis and apoptosis, *Cell.*, 126, 107-120.
- BERG, B. N. & SIMMS, H. S. 1960. Nutrition and longevity in the rat. II. Longevity and onset of disease with different levels of food intake. *J Nutr*, 71, 255-263.
- BERTRAND, H.A., LYND, F.T., MASORO, E.J., YU, B.P. 1980. Changes in adipose mass and cellularity through the adult life of rats fed ad libitum or a life-prolonging restricted diet. *J. Gerontol.*, 35, 827-835.

- BILLIN, A. N., A. L. EILERS, K. L. COULTER, J. S. LOGAN, AND D. E. AYER. 2000. MondoA, a novel basic helix-loop-helix-leucine zipper transcriptional activator that constitutes a positive branch of a max-like network. *Mol. Cell. Biol.*, 20, 8845-8854.
- BINET, R., YTHIER, D., ROBLES, A. I., COLLADO, M., LARRIEU, D., FONTI, C., BRAMBILLA, E., BRAMBILLA, C., SERRANO, M., HARRIS, C. C. & PEDEUX, R. 2009. WNT16B is a new marker of cellular senescence that regulates p53 activity and the phosphoinositide 3-kinase/AKT pathway. *Cancer Res*, 69, 9183-9191.
- BISHOP, N. A. & GUARENTE, L. 2007. Two neurons mediate diet-restriction-induced longevity in *C. elegans*. *Nature*, 447, 545-549.
- BJELAKOVIC, G., NIKOLOVA, D., GLUUD, L. L., SIMONETTI, R. G. & GLUUD, C. 2007. Mortality in randomized trials of antioxidant supplements for primary and secondary prevention: systematic review and meta-analysis. *JAMA*, 297, 842-857.
- BLUHER M, KAHN BB, KAHN CR. 2003. Extended longevity in mice lacking the insulin receptor in adipose tissue. *Science*, 299, 572-574.
- BODNAR, A. G., OUELLETTE, M., FROLKIS, M., HOLT, S. E., CHIU, C. P., MORIN, G. B., HARLEY, C. B., SHAY, J. W., LICHTSTEINER, S. & WRIGHT, W. E. 1998. Extension of life-span by introduction of telomerase into normal human cells. *Science*, 279, 349-352.
- BOOKCHIN, R. M. & GALLOP, P. M. 1968. Structure of hemoglobin A1c: nature of the N-terminal beta chain blocking group. *Biochem Biophys Res Commun*, 32, 86-93.
- BRADFORD, M. M. 1976. A rapid and sensitive method for the quantitation of microgram quantities of protein utilizing the principle of protein-dye binding. *Analytical Biochemistry*, 72, 248-254.
- BRANDES, D., MURPHY, D. G., ANTON, E. B. & BARNARD, S. 1972. Ultrastructural and cytochemical changes in cultured human lung cells. *J Ultrastruct Res*, 39, 465-483.
- BREITMAN, T. R., COLLINS, S. J. & KEENE, B. R. 1980. Replacement of serum by insulin and transferrin supports growth and differentiation of the human promyelocytic cell line, HL-60. *Exp Cell Res*, 126, 494-8.
- BROGIOLO, W., STOCKER, H., IKEYA, T., RINTELEN, F., FERNANDEZ, R. & HAFEN, E. 2001. An evolutionarily conserved function of the *Drosophila* insulin receptor and insulin-like peptides in growth control. *Curr Biol*, 11, 213-221.
- BROWN-BORG, H. M. & RAKOCZY, S. G. 2005. Glutathione metabolism in long-living Ames dwarf mice. *Exp Gerontol*, 40, 115-120.

- BUCHHOLZ, A., TAKORS, R., WANDREY, C. 2001. Quantitation of intracellular metabolites in *Escherichia coli* K12 using liquid chromatographic-electrospray ionization tandem mass spectrometric techniques. *Anal Biochem*, 295, 129-137.
- CALABRESE, V., CORNELIUS, C., DINKOVA-KOSTOVA, A. T. & CALABRESE, E. J. 2009. Vitagenes, cellular stress response, and acetylcarnitine: relevance to hormesis. *Biofactors*, 35, 146-160.
- CAMPISI, J. 2005. Senescent cells, tumor suppression, and organismal aging: good citizens, bad neighbors. *Cell*, 120, 513-522.
- CARREL, A. & EBELING, A. H. 1921. Age and multiplication of fibroblasts. *The Journal of experimental medicine*, 34, 599-623.
- CARROLL, M.J., GROMOVA, A.V., MILLER, K.R., TANG, H., WANG, X.S., TRIPATHY, A., SINGLETON, S.F., COLLINS, E.J., LEE, A.L. 2011. Direct detection of structurally resolved dynamics in a multiconformation receptor-ligand complex. *Journal of the American Chemical Society*, 133, 6422-6428.
- CASTELLANI, R. J., HONDA, K., ZHU, X., CASH, A. D., NUNOMURA, A., PERRY, G. & SMITH, M. A. 2004. Contribution of redox-active iron and copper to oxidative damage in Alzheimer disease. *Ageing Res Rev*, 3, 319-326.
- CEFALU, W. T., WAGNER, J. D., WANG, Z. Q., BELL-FARROW, A. D., COLLINS, J., HASKELL, D., BECHTOLD, R., AND MORGAN, T. 1997. A study of caloric restriction and cardiovascular aging in cynomolgus monkeys (*Macaca fascicularis*): A potential model for aging research. *J. Gerontol*, 52, B10-19.
- CHANCE, B., SIES, H. & BOVERIS, A. 1979. Hydroperoxide metabolism in mammalian organs. *Physiol Rev*, 59, 527-605.
- CHANG, H.Y., CHI, J.-T., DUDOIT, S., BONDRE, C., VAN DE RIJN, M., BOTSTEIN, D. et al. 2002. Diversity, topographic differentiation, and positional memory in human fibroblasts. *Proc Natl Acad Sci USA*, 99, 12877-12882.
- CHEN, C. T., CHEN, W. J., LIU, C. Z., CHANG, L. Y., & CHEN, Y. C. 2009. Glutathione-bound gold nanoclusters for selective-binding and detection of glutathione S-transferase-fusion proteins from cell lysates. *Chem. Commun.*, 48, 7515-7517.
- CHEN, C., PUNG, D., LEONG, V., HEBBAR, V., SHEN, G., NAIR, S., LI, W. & KONG, A. N. 2004. Induction of detoxifying enzymes by garlic organosulfur compounds through transcription factor Nrf2: effect of chemical structure and stress signals. *Free Radic Biol Med*, 37, 1578-1590.

- CHENG, L. Q., NA, J. R., BANG, M. H., KIM, M. K., & YANG, D. C. 2008. Conversion of major ginsenoside Rb1 to 20 -ginsenoside Rg3 by *Microbacterium* sp. GS514. *Phytochemistry*, 69, 218-224.
- CHONDROGIANNI, N., KAPETA, S., CHINOI, I., VASSILATOU, K., PAPASSIDERI, I., & GONOS, E. S. 2010. Anti-ageing and rejuvenating effects of quercetin. *Experimental gerontology*, 45, 763-771.
- CHUAIRE-NOACK, L., SÁNCHEZ-CORREDOR, M. C. & RAMÍREZ-CLAVIJO, S. R. 2010. The dual role of senescence in tumorigenesis. *Int. J. Morphol*, 28, 37-50.
- CHULAROJMONTRI, L., GERDPRASERT, O., WATTANAPITAYAKUL, S. K. 2013. Pummelo protects doxorubicin-induced cardiac cell death by reducing oxidative stress, modifying glutathione transferase expression, and preventing cellular senescence. *Evidence-Based Complementary and Alternative Medicine*. 43, 103-112.
- CHUNG, J.H., MANGANIELLO, V., DYCK, J.R.B. 2009. Resveratrol as a caloric restriction mimetic: therapeutic implications. *Trends in Cell Biology*, 22, 546-555.
- CLANCY, D.J., GEMS, D., HARSHMAN, L.G., OLDHAM, S., STOCKER, H., HAFEN, E., LEEVERS, S.J., PARTRIDGE, L. 2001. Extension of lifespan by loss of CHICO, a *Drosophila* insulin receptor substrate protein. *Science*, 292, 104-106.
- CLARKE, J.D., DASHWOOK, R.H., HO, E. 2008. Multi-targeted prevention of cancer by sulforaphane. *Cancer letters*, 269, 291-304.
- CLELLAND, J. D. & THORNALLEY, P. J. 1990. Synthesis of ¹⁴C-labelled methylglyoxal and S-D-lactoylglutathione. *Journal of Labelled Compounds and Radiopharmaceuticals*, 28, 1455-1464.
- COLLARD, H. R., ANSTROM, K. J., SCHWARZ, M. I., & ZISMAN, D. A. 2007. Sildenafil improves walk distance in idiopathic pulmonary fibrosis. *CHEST Journal*, 131, 897-899.
- COLLINS, A. R., LYON, C. J., XIA, X., LIU, J. Z., TANGIRALA, R. K., YIN, F., BOYADJIAN, R., BIKINEYEVA, A., PRATICO, D., HARRISON, D. G. & HSUEH, W. A. 2009. Age-accelerated atherosclerosis correlates with failure to upregulate antioxidant genes. *Circ Res*, 104, 42-54.
- COLMAN, R.J., KEMNITZ, J.W., LANE, M.A., ABBOTT, D.H., BINKLEY, N. 1999. Skeletal effects of aging and menopausal status in female rhesus macaques. *J Clin Endocrinol Metab*, 84, 4144–4148.
- COOKE, M. S., OLINSKI, R. & LOFT, S. 2008. Measurement and meaning of oxidatively modified DNA lesions in urine. *Cancer Epidemiol Biomarkers Prev*, 17, 3-14.

- COSME-BLANCO, W., SHEN, M. F., LAZAR, A. J., PATHAK, S., LOZANO, G., MULTANI, A. S. & CHANG, S. 2007. Telomere dysfunction suppresses spontaneous tumorigenesis in vivo by initiating p53-dependent cellular senescence. *EMBO reports*, 8, 497-503.
- CRISTOFALO, V. J. & PIGNOLO, R. J. 1993. Replicative senescence of human fibroblast-like cells in culture. *Physiol Rev*, 73, 617-638.
- CRISTOFALO, V. J., ALLEN, R. G., PIGNOLO, R. J., MARTIN, B. G. & BECK, J. C. 1998. Relationship between donor age and the replicative lifespan of human cells in culture: a reevaluation. *Proc Natl Acad Sci U S A*, 95, 10614-10629.
- CRISTOFALO, V. J., BECK, J. & ALLEN, R. G. 2003. Commentary: Cell Senescence: An Evaluation of Replicative Senescence in Culture as a Model for Cell Aging In Situ. *The Journals of Gerontology Series A: Biological Sciences and Medical Sciences*, 58, B776-B779.
- CRISTOFALO, V. J., LORENZINI, A., ALLEN, R. G., TORRES, C. & TRESINI, M. 2004. Replicative senescence: a critical review. *Mech Ageing Dev*, 125, 827-848.
- CULLINAN, S. B., GORDAN, J. D., JIN, J., HARPER, J. W. & DIEHL, J. A. 2004. The Keap1-BTB protein is an adaptor that bridges Nrf2 to a Cul3-based E3 ligase: oxidative stress sensing by a Cul3-Keap1 ligase. *Mol Cell Biol*, 24, 8477-8486.
- D'ADDA DI FAGAGNA, F., REAPER, P. M., CLAY-FARRACE, L., FIEGLER, H., CARR, P., VON ZGLINICKI, T., SARETZKI, G., CARTER, N. P. & JACKSON, S. P. 2003. A DNA damage checkpoint response in telomere-initiated senescence. *Nature*, 426, 194-198.
- DANG, W., STEFFEN, K. K., PERRY, R., DORSEY, J. A., JOHNSON, F. B., SHILATIFARD, A., KAEBERLEIN, M., KENNEDY, B. K. & BERGER, S. L. 2009. Histone H4 lysine 16 acetylation regulates cellular lifespan. *Nature*, 459, 802-807.
- DAS, D. K., & MAULIK, N. 2006. Resveratrol in cardioprotection: a therapeutic promise of alternative medicine. *Molecular interventions*, 6, 36-39.
- DAZERT, E., HALL, M.N. 2011. mTOR signaling in disease. *Curr Opin Cell Biol*, 3, 112-124.
- DE MAGALHAES, J. P. & CHURCH, G. M. 2005. Genomes optimize reproduction: aging as a consequence of the developmental program. *Physiology (Bethesda)*, 20, 252-259.
- DE MAGALHAES, J. P. 2004. From cells to ageing: a review of models and mechanisms of cellular senescence and their impact on human ageing. *Exp Cell Res*, 300, 1-10.

- DE MAGALHES, J.P., CHAINIAUX, F., REMACLE, J., TOUSSAINT, O. 2002. Stress-induced premature senescence in BJ and hTERT-BJ1 human foreskin fibroblasts. *FEBS Letters*, 523, 157-162.
- DEBACQ-CHAINIAUX, F., ERUSALIMSKY, J. D., CAMPISI, J. & TOUSSAINT, O. 2009. Protocols to detect senescence-associated beta-galactosidase (SA-beta-gal) activity, a biomarker of senescent cells in culture and in vivo. *Nat Protoc*, 4, 1798-1806.
- DECHAUD, H., RAVARD, C., CLAUSTRAT, F., BRAC DE LA PERRIERE, A., PUGEAT, M. 1999. Xenoestrogen interaction with human sex hormone-binding globulin (hSHBG). *Steroids*, 64, 328-334.
- DELLORCO, R.T., ANDERSON, L.E., CONWAY, E., BIRCKBICHLER, P.J. 1985. Variable transglutaminase activity in human-diploid fibroblasts during in vitro senescence. *Cell Biology International Reports*, 9, 945-956.
- DELPierre, G., RIDER, M. H., COLLARD, F., STROOBANT, V., VANSTAPEL, F., SANTOS, H. & VAN SCHAFTINGEN, E. 2000. Identification, cloning, and heterologous expression of a mammalian fructosamine-3-kinase. *Diabetes*, 49, 1627-1634.
- DEMROW, H. S., SLANE, P. R., FOLTS, J. D. 1995. Administration of wine and grape juice inhibits in vivo platelet activity and thrombosis in stenosed canine coronary arteries. *Circulation*, 91, 1182-1188.
- DIMRI, G. P., LEE, X., BASILE, G., ACOSTA, M., SCOTT, G., ROSKELLEY, C., MEDRANO, E. E., LINSKENS, M., RUBELJ, I., PEREIRA-SMITH, O. & ET AL. 1995. A biomarker that identifies senescent human cells in culture and in aging skin in vivo. *Proc Natl Acad Sci U S A*, 92, 9363-9367.
- DINKOVA-KOSTOVA, A. T., LIBY, K. T., STEPHENSON, K. K., HOLTZCLAW, W. D., GAO, X., SUH, N., WILLIAMS, C., RISINGSONG, R., HONDA, T., GRIBBLE, G. W., SPORN, M. B. & TALALAY, P. 2005. Extremely potent triterpenoid inducers of the phase 2 response: correlations of protection against oxidant and inflammatory stress. *Proc Natl Acad Sci U S A*, 102, 4584-4589.
- DU, X., STOCKLAUSER-FARBER, K. & ROSEN, P. 1999. Generation of reactive oxygen intermediates, activation of NF-kappaB, and induction of apoptosis in human endothelial cells by glucose: role of nitric oxide synthase? *Free Radic Biol Med*, 27, 752-763.
- EILERS, A. L., SUNDWALL, E., LIN, M., SULLIVAN, A. A., AYER, D. E. 2002. A novel heterodimerization domain, CRM1, and 14-3-3 control subcellular localization of the MondoA-Mlx heterocomplex. *Molec. Cell Biol*, 22, 8514-8526.

- ERLUND, I. 2004. Review of the flavonoids quercetin, hesperetin, and naringenin. Dietary sources, bioactivities, bioavailability, and epidemiology. *Nutrition Research*, 24 , 851-874.
- ERLUND, I., MERIRINNE, E., ALFTHAN, G., ARO, A. 2001. Plasma Kinetics and Urinary Excretion of the Flavanones Naringenin and Hesperetin in Humans after Ingestion of Orange Juice and Grapefruit Juice. *The Journal of Nutrition*, 131, 235-241.
- ERLUND, I., SILASTE, M.L., ALFTHAN, G., RANTALA, M., KESANIEMI Y, A., ARO, A. 2002. Plasma concentrations of the flavonoids hesperetin, naringenin and quercetin in human subjects following their habitual diets, and diets high or low in fruit and vegetables. *European Journal of Clinical Nutrition* , 56, 891-898.
- FABRIZIO, P. & LONGO, V. D. 2003. The chronological life span of *Saccharomyces cerevisiae*. *Aging Cell*, 2, 73-81.
- FAHEY, J.W., ZHANG, Y. AND TALALAY, P. 1997. Broccoli sprouts: An exceptionally rich source of inducers of enzymes that protect against chemical carcinogens. *Proc. Nat. Acad. Sci. USA*, 94, 10367-10372.
- FAHEY, J. W., ZALCMANN, A. T. & TALALAY, P. 2001. The chemical diversity and distribution of glucosinolates and isothiocyanates among plants. *Phytochemistry*, 56, 5-51.
- FARAGHER, R. G., BURTON, D. G., MAJECHA, P., FONG, N. S., DAVIS, T., SHEERIN, A. & OSTLER, E. L. 2011. Resveratrol, but not dihydroresveratrol, induces premature senescence in primary human fibroblasts. *Age (Dordr)*, 33, 555-564.
- FINCH, C. E. 2010. Evolution of the human lifespan and diseases of aging: Roles of infection, inflammation, and nutrition. *Proceedings of the National Academy of Sciences*, 107, 1718-1724.
- FINKEL, T. & HOLBROOK, N. J. 2000. Oxidants, oxidative stress and the biology of ageing. *Nature*, 408, 239-247.
- FINKEL, T. 1998. Oxygen radicals and signaling. *Curr Opin Cell Biol*, 10, 248-53.
- FINOT, P.-A., MOTTU, F., BUJARD, E. & MAURON, J. 1978. *N-Substituted lysines as sources of lysine in nutrition. Nutritional Improvement of Food and Feed Proteins*. Springer.
- FONTANA, L., PARTRIDGE, L. & LONGO, V. D. 2010. Extending healthy life span--from yeast to humans. *Science*, 328, 321-326.
- FOREMAN, K. E. & TANG, J. 2003. Molecular mechanisms of replicative senescence in endothelial cells. *Exp Gerontol*, 38, 1251-1257.

- FOYER, C., FARAGHER, R. & THORNALLEY, P. 2009. *Redox metabolism and longevity relationships in animals and plants*, Garland Science.
- FRIEDMAN, D. B. & JOHNSON, T. E. 1988. A mutation in the age-1 gene in *Caenorhabditis elegans* lengthens life and reduces hermaphrodite fertility. *Genetics*, 118, 75-86.
- FUJITA, K., MONDAL, A. M., HORIKAWA, I., NGUYEN, G. H., KUMAMOTO, K., SOHN, J. J., BOWMAN, E. D., MATHE, E. A., SCHETTER, A. J. & PINE, S. R. 2009. p53 isoforms $\Delta 133p53$ and p53 β are endogenous regulators of replicative cellular senescence. *Nature cell biology*, 11, 1135-1142.
- FULLOP, T., LARBI, A., WITKOWSKI, J. M., MCELHANEY, J., LOEB, M., MITNITSKI, A. & PAWELEC, G. 2010. Aging, frailty and age-related diseases. *Biogerontology*, 11, 547-563.
- FUNK, W. D., WANG, C. K., SHELTON, D. N., HARLEY, C. B., PAGON, G. D. & HOEFFLER, W. K. 2000. Telomerase expression restores dermal integrity to in vitro-aged fibroblasts in a reconstituted skin model. *Exp Cell Res*, 258, 270-278.
- FURUMOTO, K., INOUE, E., NAGAO, N., HIYAMA, E., MIWA, N. 1998. Age-dependent telomere shortening is slowed down by enrichment of intracellular vitamin C via suppression of oxidative stress. *Life Sci.*, 63, 935-948.
- FUSCO, D., COLLOCA, G., LO MONACO, M. R. & CESARI, M. 2007. Effects of antioxidant supplementation on the aging process. *Clin Interv Aging*, 2, 377-387.
- GAMERDINGER, M., HAJIEVA, P., KAYA, A. M., WOLFRUM, U., HARTL, F. U. & BEHL, C. 2009. Protein quality control during aging involves recruitment of the macroautophagy pathway by BAG3. *Embo j*, 28, 889-901.
- GAO, L., WANG, J., SEKHAR, K. R., YIN, H., YARED, N. F., SCHNEIDER, S. N., SASI, S., DALTON, T. P., ANDERSON, M. E., CHAN, J. Y., MORROW, J. D. & FREEMAN, M. L. 2007. Novel n-3 fatty acid oxidation products activate Nrf2 by destabilizing the association between Keap1 and Cullin3. *J Biol Chem*, 282, 2529-2537.
- GARROW, J. S. 1974. Energy balance and obesity in man, *North-Holland Publishing Company*.
- GARTHWAITE, S.M., CHENG, H., BRYAN, J.E., CRAIG, B.W., HOLLOSZY, J.O., 1986. Ageing, exercise, and food restriction. Effects on body composition. *Mech. Ageing Dev*, 36, 187-196.
- GEISS, G.K., BUMGARNER, R.E., BIRDITT, B., DAHL, T., DOWIDAR, N., DUNAWAY, D.L., FELL, H.P, FERREE, S., GEORGE, R.D., GROGAN,

- T. 2008. Direct multiplexed measurement of gene expression with color-coded probe pairs. *Nat Biotechnol*, 26, 317–325.
- GERBITZ, K. D., GEMPEL, K. and BRDICZKA, D. 1996. Mitochondria and diabetes. Genetic, biochemical, and clinical implications of the cellular energy circuit. *Diabetes*, 45, 113-126.
- GEWIRTZ, D. A., HOLT, S. E. & ELMORE, L. W. 2008. Accelerated senescence: an emerging role in tumor cell response to chemotherapy and radiation. *Biochem Pharmacol*, 76, 947-957.
- GIACCO, F., DU, X., D'AGATI, V. D., MILNE, R., SUI, G., GEOFFRION, M. & BROWNLEE, M. 2014. Knockdown of glyoxalase 1 mimics diabetic nephropathy in nondiabetic mice. *Diabetes*, 63, 291-299.
- GIOVANNELLI, L., PITOZZI, V., JACOMELLI, M., MULINACCI, N., LAURENZANA, A., DOLARA, P. & MOCALI, A. 2011. Protective effects of resveratrol against senescence-associated changes in cultured human fibroblasts. *J Gerontol A Biol Sci Med Sci*, 66, 9-18.
- GLASEL, J. A. 1995. Validity of nucleic acid purities monitored by 260nm/280nm absorbance ratios. *Biotechniques*, 18, 62-3.
- GOMPERTZ, B. 1825. On the nature of the function expressive of the law of human mortality, and on a new mode of determining the value of life contingencies. *Royal Society of London Philosophical Transactions Series I*, 115, 513-583.
- GREENBERG, S. B., GROVE, G. L. & CRISTOFALO, V. J. 1977. Cell size in aging monolayer cultures. *In Vitro*, 13, 297-300.
- GUO, Z., LEE, J., LANE, M. 2001. Iodoacetate protects hippocampal neurons against excitotoxic and oxidative injury: involvement of heat-shock proteins and Bcl-2. *Journal of Neurochemistry*, 79, 361-370.
- HAGOPIAN, K., RAMSEY, J. J., & WEINDRUCH, R. 2003. Caloric restriction increases gluconeogenic and transaminase enzyme activities in mouse liver. *Experimental gerontology*, 38(3), 267-278.
- HALDANE, J. B. S. 1941. *New paths in genetics*. New Paths in Genetics.
- HALICKA, H. D., ZHAO, H., LI, J., TRAGANOS, F., STUDZINSKI, G. P., & DARZYNKIEWICZ, Z. 2012. Attenuation of constitutive DNA damage signaling by 1, 25-dihydroxyvitamin D3. *Aging (Albany NY)*, 4, 270-278.
- HARLEY, C. B., FUTCHER, A. B. & GREIDER, C. W. 1990. Telomeres shorten during ageing of human fibroblasts. *Nature*, 345, 458-460.
- HARMAN, D. 1956. Aging: a theory based on free radical and radiation chemistry. *J Gerontol*, 11, 298-300.

- HARMAN, D. 1994. Aging: prospects for further increases in the functional life span. *Age*, 17, 119-146.
- HARMAN, D. 2010. The free radical theory of aging. *Antioxidants and Redox Signaling*, 5, 557-561.
- HARRISON, D. E., ARCHER, J. R. & ASTLE, C. M. 1984. Effects of food restriction on aging: separation of food intake and adiposity. *Proc. Natl. Acad. Sci. USA*, 81, 1835-1838.
- HAVULA, E., & HIETAKANGAS, V. 2012. Glucose sensing by ChREBP/MondoA-Mlx transcription factors. *Seminars in cell & developmental biology*, 23, 640-647.
- HAYASHI R, H., TAGUCHI K, I., UESUGI K, I., DUNCAN, T., TSUJIKAWA, M., NAKAZAWA, T., YAMAMOTO, M., NISHIDA, K. 2013. The role of the Nrf2-mediated defense system in corneal epithelial wound healing. *Free Radical Biology and Medicine*, 61, 333-342.
- HAYASHI, R., HIMORI, N., TAGUCHI, K., ISHIKAWA, Y., UESUGI, K., ITO, M., DUNCAN, T., TSUJIKAWA, M., NAKAZAWA, T., YAMAMOTO, M. & NISHIDA, K. 2013. The role of the Nrf2-mediated defense system in corneal epithelial wound healing. *Free Radic Biol Med*, 61c, 333-342.
- HAYFLICK, L. & MOORHEAD, P. S. 1961. The serial cultivation of human diploid cell strains. *Experimental cell research*, 25, 585-621.
- HAYFLICK, L. 1965. THE LIMITED IN VITRO LIFETIME OF HUMAN DIPLOID CELL STRAINS. *Exp Cell Res*, 37, 614-636.
- HERBIG, U., FERREIRA, M., CONDEL, L., CAREY, D. & SEDIVY, J. M. 2006. Cellular senescence in aging primates. *Science*, 311, 1257.
- HERR, I. & BUCHLER, M. W. 2010. Dietary constituents of broccoli and other cruciferous vegetables: implications for prevention and therapy of cancer. *Cancer Treat Rev*, 36, 377-383.
- HINTZE, K. J. & NABOR, D. 2008. Effects Sulforaphane on IMR-90 Phase II Enzyme Induction and Cell Senescence. *The FASEB Journal*, 22, 700-729.
- HOLBROOK, K. A., & BYERS, P. H. 1989. Skin is a window on heritable disorders of connective tissue. *American journal of medical genetics*, 34, 105-121.
- HOLEHAN, A. M., and B. J. MERRY. 1986. The experimental manipulation of aging by diet. *Biol. Rev. Camb. Philos. Soc*, 61, 329-368.
- HOLLIDAY, R. & TARRANT, G. M. 1972. Altered enzymes in ageing human fibroblasts. *Nature*, 238, 26-30.

- HOWITZ, K.T., BITTERMAN, K.J., COHEN, H.Y., LAMMING, D.W., LAVU, S., WOOD, J.G., ZIPKIN, R.E., CHUNG, P., KISIELEWSKI, A., ZHANG, L.-L. et al. 2003. Small molecule activator of sirtuins extend *Saccharomyces cerevisiae* lifespan. *Nature*, 425, 191–196.
- HUGES, K. A. & REYNOLDS, R. M. 2005. Evolutionary and mechanistic theories of ageing. *Annu Rev Entomol*, 50, 421-445.
- HUGHES, S. E., EVASON, K., XIONG, C. & KORNFELD, K. 2007. Genetic and pharmacological factors that influence reproductive aging in nematodes. *PLoS genetics*, 3, e25.
- HUOT, T.J., ROWE, J., HARLAND, M., DRAYTON, S., BROOKES, S., GOOPTU, C., PURKIS, P., FRIED, M., BATAILLE, V., HARA, E. 2002. Biallelic mutations in p16(INK4a) confer resistance to Ras- and Ets-induced senescence in human diploid fibroblasts. *Mol. Cell. Biol.* 22 , 8135–8143.
- HURSTING, S. D., LAVIGNE, J. A., BERRIGAN, D., PERKINS, S. N. & BARRETT, J. C. 2003. Calorie restriction, aging, and cancer prevention: mechanisms of action and applicability to humans. *Annu Rev Med*, 54, 131-152.
- HUTTER, E., RENNER, K., PFISTER, G., STOCKL, P., JANSEN-DURR, P. & GNAIGER, E. 2004. Senescence-associated changes in respiration and oxidative phosphorylation in primary human fibroblasts. *Biochem J*, 380, 919-928.
- INSTITUTE-FOR-HEALTH-METRICS-AND-EVALUATION. 2013. *The Global Burden of Disease: Generating Evidence, Guiding Policy*. Seattle, USA.
- ISHII, T., ITOH, K., RUIZ, E., LEAKE, D. S., UNOKI, H., YAMAMOTO, M. & MANN, G. E. 2004. Role of Nrf2 in the regulation of CD36 and stress protein expression in murine macrophages: activation by oxidatively modified LDL and 4-hydroxynonenal. *Circ Res*, 94, 609-616.
- ISOBE, K. & NISHISE, H. 1994. Enzymatic production of glyoxal from ethylene glycol using alcohol oxidase from methanol yeast. *Biosci.Biotech.Biochem*, 58, 170-173.
- JACOBS, J. P., JONES, C. M. & BAILLE, J. P. 1970. Characteristics of a human diploid cell designated MRC-5. *Nature*, 227, 168-170.
- JAIN, A. K. and JAISWAL, A. K. 2007. GSK-3beta acts upstream of Fyn kinase in regulation of nuclear export and degradation of NF-E2 related factor 2. *J. Biol. Chem.* 282, 16502-16510.
- JAIN, A. K., BLOOM, D. A. & JAISWAL, A. K. 2005. Nuclear import and export signals in control of Nrf2. *J Biol Chem*, 280, 29158-68.
- JASPER, H.2008. SKNy worms and long life. *Cell*, 132, 915-916.

- JEONG, W. S., KEUM, Y. S., CHEN, C., JAIN, M. R., SHEN, G., KIM, J. H., LI, W. & KONG, A. N. 2005. Differential expression and stability of endogenous nuclear factor E2-related factor 2 (Nrf2) by natural chemopreventive compounds in HepG2 human hepatoma cells. *J Biochem Mol Biol*, 38, 167-176.
- JEYAPALAN, J. C., FERREIRA, M., SEDIVY, J. M. & HERBIG, U. 2007. Accumulation of senescent cells in mitotic tissue of aging primates. *Mech Ageing Dev*, 128, 36-44.
- JIANG, H., JU, Z. & RUDOLPH, K. 2007. Telomere shortening and ageing. *Zeitschrift für Gerontologie und Geriatrie*, 40, 314-324.
- JOHNSON, T. E. & WOOD, W. B. 1982. Genetic analysis of life-span in *Caenorhabditis elegans*. *Proc Natl Acad Sci U S A*, 79, 6603-6607.
- JOSHIPURA, K.J., ASCHERIO, A., MANSON, J.E. 1999. Fruit and vegetable intake in relation to risk of ischemic stroke. *JAMA*, 282, 1233-1239.
- JUNG, K-A., KWAK, M-K. 2010. The Nrf2 System as a Potential Target for the Development of Indirect Antioxidants. *Molecules*, 15, 7266-7291.
- JUNG, T., HOHN, A., CATALGOL, B. & GRUNE, T. 2009. Age-related differences in oxidative protein-damage in young and senescent fibroblasts. *Arch Biochem Biophys*, 483, 127-135.
- KAEBERLEIN, M., MCVEY, M., GUARENTE, L. 1999. The SIR2/3/4 complex and SIR2 alone promote longevity in *Saccharomyces cerevisiae* by two different mechanisms. *Genes Dev.*, 13, 2570-2580.
- KALETSKY, R. & MURPHY, C. T. 2010. The role of insulin/IGF-like signaling in *C. elegans* longevity and aging. *Dis Model Mech*, 3, 415-9.
- KALLIFATIDIS, G., RAUSCH, V., BAUMANN, B. 2009. Sulforaphane targets pancreatic tumour-initiating cells by NF-kappaB-induced anti-apoptotic signalling. *Gut*, 58, 949-963.
- KANO, J. & ISHIKAWA, F. 2003. Composition and conservation of the telomeric complex. *Cell Mol Life Sci*, 60, 2295-2302.
- KAPETA, S., CHONDROGIANNI, N. & GONOS, E. S. 2010. Nuclear erythroid factor 2-mediated proteasome activation delays senescence in human fibroblasts. *J Biol Chem*, 285, 8171-8184.
- KASHINO, G., KODAMA, S., NAKAYAMA, Y., SUZUKI, K., FUKASE, K., GOTO, M., & WATANABE, M. 2003. Relief of oxidative stress by ascorbic acid delays cellular senescence of normal human and Werner syndrome fibroblast cells. *Free Radical Biology and Medicine*, 35, 438-443.
- KAWAGUCHI, T., TAKENOSHITA, M., KABASHIMA, T., UYEDA, K. 2001. Glucose and cAMP regulate the L-type pyruvate kinase gene by

phosphorylation/dephosphorylation of the carbohydrate response element binding protein . *Proc Natl Acad Sci*, 98, 13710-13715.

- KAWAII, S., TOMONO, Y., KATASE, E., OGAWA, K. & YANO, M. 1999. Quantitation of flavonoid constituents in Citrus fruits. *J. Agric. Food Chem.*, 47, 3565-3571.
- KEMNITZ, J. W., ROECKER, E. B., WEINDRUCH, R., ELSON, D. F., BAUM, S. T. & BERGMAN, R. N. 1994. Dietary restriction increases insulin sensitivity and lowers blood glucose in rhesus monkeys. *Am J Physiol*, 266, E540-547.
- KENNEDY, B. K., AUSTRIACO, N. R., JR. & GUARENTE, L. 1994. Daughter cells of *Saccharomyces cerevisiae* from old mothers display a reduced life span. *J Cell Biol*, 127, 1985-1993.
- KENYON, C. J. 2010. The genetics of ageing. *Nature*, 464, 504-512.
- KENYON, C., CHANG, J., GENSCHE, E., RUDNER, A. & TABTIANG, R. 1993. A *C. elegans* mutant that lives twice as long as wild type. *Nature*, 366, 461-464.
- KERNS, M., DEPIANTO, D., YAMAMOTO, M., COULOMBE, P.A. 2010. Differential Modulation of Keratin Expression by Sulforaphane Occurs via Nrf2-dependent and -independent Pathways in Skin Epithelia. *Molecular Biology of the Cell* , 21, 4068-4075.
- KIM SH, S. H., KAMINKER, P. & CAMPISI, J. 2002. Telomeres, aging and cancer: in search of a happy ending. *Oncogene*, 21, 503-511.
- KIM, J.H., CHOY, H.E., NAM, K.H., PARK, S.C. 2001. Transglutaminase-Mediated Crosslinking of Specific Core Histone Subunits and Cellular Senescence. *Annals of the New York Academy of Sciences* , 928, 65-70.
- KIMURA, K. D., TISSENBAUM, H. A., LIU, Y. & RUVKUN, G. 1997. *daf-2*, an insulin receptor-like gene that regulates longevity and diapause in *Caenorhabditis elegans*. *Science*, 277, 942-946.
- KIRKWOOD, T. B. 2002. Evolution of ageing. *Mech Ageing Dev*, 123, 737-745.
- KIRKWOOD, T. B. 2005. Understanding the odd science of aging. *Cell*, 120, 437-447.
- KIRKWOOD, T.B. 1977. Evolution of ageing. *Nature*, 270, 301-304.
- KNEKT, P., JARVINEN, R., REUNANEN, A., MAATELA, J. 1996. Flavonoid intake and coronary mortality in Finland: a cohort study. *Br Med J*, 312 , 478-481.
- KOBAYASHI, A., KANG, M. I., WATAI, Y., TONG, K. I., SHIBATA, T., UCHIDA, K. & YAMAMOTO, M. 2006. Oxidative and electrophilic

stresses activate Nrf2 through inhibition of ubiquitination activity of Keap1. *Mol Cell Biol*, 26, 221-229.

- KOPEC, A.K., THOMPSON, C.M., KIM, S., FORGACS, A.L., ZACHAREWSKI, T.R. 2012. Comparative toxicogenomic analysis of oral Cr(VI) exposure effects in rat and mouse small intestinal epithelia. *Toxicol Appl Pharmacol*, 262, 124–138.
- KOSOWER, N. S., KOSOWER, E. M., WERTHEIM, B. & CORREA, W. S. 1969. Diamide, a new reagent for the intracellular oxidation of glutathione to the disulfide. *Biochem Biophys Res Commun*, 37, 593-6.
- KUILMAN, T. & PEEPER, D. S. 2009. Senescence-messaging secretome: SMS-ing cellular stress. *Nat Rev Cancer*, 9, 81-94.
- KUILMAN, T., MICHALOGLOU, C., MOOI, W. J. & PEEPER, D. S. 2010. The essence of senescence. *Genes Dev*, 24, 2463-2479.
- KUROWSKA, E.M., SPENCE, J.D., JORDAN, J., WETMORE, S., FREEMAN, D.J., PICHÉ, L.A., SERRATORE, P. 2000. HDL cholesterol-raising effect of orange juice in subjects with hypercholesterolemia. *The American Journal of Clinical Nutrition*, 72, 1095-1100.
- KURZ, D., DECARY, S., HONG, Y. AND ERUSALIMSKY, J.D. 2000. Senescence-associated β -galactosidase reflects an increase in lysosomal mass during replicative ageing of human endothelial cells. *Journal of Cell Science*, 113, 3613-3622.
- LAGOUGE, M., ARGMANN, C., GERHART-HINES, Z., MEZIANE, H., LERIN, C., DAUSSIN, F., MESSADEQ, N., MILNE, J., LAMBERT, P., ELLIOTT, P. 2006. Resveratrol improves mitochondrial function and protects against metabolic disease by activating SIRT1 and PGC-1 α . *Cell*, 22, 13-21.
- LAM, P. Y., YIN, F., HAMILTON, R. T., BOVERIS, A. & CADENAS, E. 2009. Elevated neuronal nitric oxide synthase expression during ageing and mitochondrial energy production. *Free Radic Res*, 43, 431-439.
- LAMBERT, A.J., BRAND, M.D., BUCKINGHAM, J.A., ESTEVES, T.C., GREEN, K., MURPHY, M.P., PAKAY, J.L., TALBOT, D.A., and ECHTAY, K.S. 1999. Mitochondrial superoxide and aging: uncoupling-protein activity and superoxide production. *Biochemical Society Symposia*, 71, 203-214.
- LAMPE, J. W. 2009. Sulforaphane: from chemoprevention to pancreatic cancer treatment? *Gut*, 58, 900-902.
- LANE, M. A. 1998. Calorie restriction in nonhuman primates: Implications for age related disease risk. *J. Anti-Aging Med.* 1, 315–325.
- LANE, M. A., BAER, D. J., RUMPLER, W. V., WEINDRUCH, R., INGRAM, D. K., TILMONT, E. M., CUTLER, R. G. & ROTH, G. S. 1996. Calorie

- restriction lowers body temperature in rhesus monkeys, consistent with a postulated anti-aging mechanism in rodents. *Proceedings of the National Academy of Sciences*, 93, 4159-4164.
- LANE, M. A. 1995. Aging and food restriction alters some indices of bone metabolism in male rhesus monkeys (*Macaca mulatta*). *J. Nutr.* 125, 1600–1610.
- LANE, M.A., ROTH, G.S. & INGRAM, D.K., 2007. Caloric restriction mimetics: a novel approach for biogerontology. *Methods In Molecular Biology*, 371, p.143-149.
- LASSEGUE, B. & CLEMPUS, R. E. 2003. Vascular NAD(P)H oxidases: specific features, expression, and regulation. *Am J Physiol Regul Integr Comp Physiol*, 285, R277-297.
- LAU, A., TIAN, W., WHITMAN, S. A. & ZHANG, D. D. 2013. The predicted molecular weight of Nrf2: it is what it is not. *Antioxid Redox Signal*, 18, 91-93.
- LAWLESS, C., WANG, C., JURK, D., MERZ, A., ZGLINICKI, T.V. 2010. Quantitative assessment of markers for cell senescence. *Experimental Gerontology*, 45, 772-778.
- LE MARCHAND, L., MURPHY, S. P., HANKIN, J. H., WILKENS, L. R., & KOLONEL, L. N. 2000. Intake of flavonoids and lung cancer. *Journal of the National Cancer Institute*, 92, 154-160.
- LEE, B.Y., HAN JA, I.M., MORRONE, A., JOHUNG, K. 2006. Senescence-associated β -galactosidase is lysosomal β -galactosidase. *Aging Cell*, 5, 187-195.
- LEE, J. O., RUSSO, A. A. & PAVLETICH, N. P. 1998. Structure of the retinoblastoma tumour-suppressor pocket domain bound to a peptide from HPV E7. *Nature*, 391, 859-865.
- LEE, S. H., PARK, Y. B., BAE, K. H., BOK, H., KWON, Y. K., LEE, E. S., & CHOI, M. S. 1999. Cholesterol-lowering activity of naringenin via inhibition of 3-hydroxy-3-methylglutaryl coenzyme A reductase and acyl coenzyme A: cholesterol acyltransferase in rats. *Annals of nutrition and metabolism*, 43, 173-180.
- LEWIS, S., GOLDSPINK, D., PHILLIPS, J., MERRY, B., HOLEHAN, A. 1985. The effects of aging and chronic dietary restriction on whole body growth and protein turnover in the rat. *Exp. Gerontol.*, 20, 253–260.
- LI, G., LIAO, Y., WANG, X., SHENG, S. & YIN, D. 2006a. In situ estimation of the entire color and spectra of age pigment-like materials: application of a front-surface 3D-fluorescence technique. *Exp Gerontol*, 41, 328-336.

- LI, H.L. et al. 2013. Curcumin prevents and reverses murine cardiac hypertrophy. *J. Clin. Invest.*, 118, 879–893.
- LI, M. V., CHANG, B., IMAMURA, M., POUNGVARIN, N. & CHAN, L. 2006b. Glucose-dependent transcriptional regulation by an evolutionarily conserved glucose-sensing module. *Diabetes*, 55, 1179-1189.
- LI, Y., HUANG, T.T., CARLSON, E.J., MELOV, S., URSELL, P.C. et al. 1995. Dilated cardiomyopathy and neonatal lethality in mutant mice lacking manganese superoxide dismutase. *Nat. Genet.*, 11, 376–381.
- LIM, S.S., VOS, T., FLAXMAN, A.D., DANAEI, G., SHIBUYA, K., ADAIR-ROHANI, H., ALMAZROA, M.A., AMANN, M., ANDERSON, H.R., ANDREWS, K.G., ARYEE, M., ATKINSON, C., BACCHUS, L.J., BAHALIM, A.N., BALAKRISHNAN, K., BALMES, J., BARKER-COLLO, S., BAXTER, A., BELL, M.L., BLORE, J.D., BLYTH, F., BONNER, C., BORGES, G., BOURNE, R., BOUSSINESQ, M., BRAUER, M., BROOKS, P., BRUCE, N.G., BRUNEKREEF, B., BRYAN-HANCOCK, C., BUCELLO, C., BUCHBINDER, R., BULL, F., BURNETT, R.T., BYERS, T.E., et al. 2010. A comparative risk assessment of burden of disease and injury attributable to 67 risk factors and risk factor clusters in 21 regions, 1990–2010: a systematic analysis for the Global Burden of Disease Study 2010. *The Lancet*, 380, 2224-2260.
- LIPETZ, J. & CRISTOFALO, V. J. 1972. Ultrastructural changes accompanying the aging of human diploid cells in culture. *J Ultrastruct Res*, 39, 43-56.
- LO, S. C. & HANNINK, M. 2008. PGAM5 tethers a ternary complex containing Keap1 and Nrf2 to mitochondria. *Exp Cell Res*, 314, 1789-1803.
- LO, S.C., HANNINK, M. 2006. PGAM5, a Bcl-XL-interacting protein, is a novel substrate for the redox-regulated Keap1-dependent ubiquitin ligase complex. *J. Biol. Chem.*, 281, 37893–37903.
- LÓPEZ-OTÍN, C., BLASCO, M. A., PARTRIDGE, L., SERRANO, M. & KROEMER, G. 2013. The hallmarks of aging. *Cell*, 153, 1194-1217.
- LORENZ, M., SARETZKI, G., SITTE, N., METZKOW, S., VON ZGLINICKI, T. 2001. BJ fibroblasts display high antioxidant capacity and slow telomere shortening independent of hTERT transfection. *Free Radical Biology and Medicine*, 31, 824-831.
- LOWE, S. W., CEPERO, E. & EVAN, G. 2004. Intrinsic tumour suppression. *Nature*, 432, 307-315.
- LU, T. & FINKEL, T. 2008. Free radicals and senescence. *Exp Cell Res*, 314, 1918-1922.
- LY, D. H., LOCKHART, D. J., LERNER, R. A. & SCHULTZ, P. G. 2000. Mitotic misregulation and human aging. *Science*, 287, 2486-2492.

- MA, L., SHAM, Y.Y., WALTERS, K.J. & TOWLE, H.C. 2007. A critical role for the loop region of the basic helix–loop–helix/leucine zipper protein Mlx in DNA binding and glucose-regulated transcription. *Nucleic Acids Research*, 35, 35–44.
- MADSON, M. A. & FEATHER, M. S. 1981. An improved preparation of 3-deoxy-D-erythro-hexos-2-ulose via the bis(benzoylhydrazone) and some related constitutional studies. *Carbohydrate Research*, 94, 183-191.
- MAIESE, K., LI, F., CHONG, Z. Z. & SHANG, Y. C. 2008. The Wnt signaling pathway: aging gracefully as a protectionist? *Pharmacol Ther*, 118, 58-81.
- MAIR, W., GOYMER, P., PLETCHER, S. D. & PARTRIDGE, L. 2003. Demography of dietary restriction and death in *Drosophila*. *Science*, 301, 1731-1733.
- MAKPOL, S., DURANI, L. W., CHUA, K. H., YUSOF, M., ANUM, Y., NGAH, W., & ZURINAH, W. 2011. Tocotrienol-rich fraction prevents cell cycle arrest and elongates telomere length in senescent human diploid fibroblasts. *BioMed Research International*, 4, 221-234.
- MALHOTRA, D., PORTALES-CASAMAR, E., SINGH, A., SRIVASTAVA, S., ARENILLAS, D., HAPPEL, C., SHYR, C., WAKABAYASHI, N., KENSLER, T. W., WASSERMAN, W. W. & BISWAL, S. 2010. Global mapping of binding sites for Nrf2 identifies novel targets in cell survival response through ChIP-Seq profiling and network analysis. *Nucleic Acids Res*, 38, 5718-5734.
- MANN, G. E., ROWLANDS, D. J., LI, F. Y., DE WINTER, P. & SIOW, R. C. 2007. Activation of endothelial nitric oxide synthase by dietary isoflavones: role of NO in Nrf2-mediated antioxidant gene expression. *Cardiovascular research*, 75, 261-274.
- MARTIN, G. M., SPRAGUE, C. A. & EPSTEIN, C. J. 1970. Replicative life-span of cultivated human cells. Effects of donor's age, tissue, and genotype. *Lab Invest*, 23, 86-92.
- MARTIN, J. E. & SHEAFF, M. T. 2007. The pathology of ageing: concepts and mechanisms. *J Pathol*, 211, 111-113.
- MASORO, E. J. 2005. Overview of caloric restriction and ageing. *Mechanisms of ageing and development*, 126, 913-922.
- MASORO, E. J. 2006. Cell Senescence: Brilliant Insight or Foolish Notion? *The Gerontologist*, 46, 297-300.
- MATLASHEWSKI, G., LAMB, P., PIM, D., PEACOCK, J., CRAWFORD, L. & BENCHIMOL, S. 1984. Isolation and characterization of a human p53 cDNA clone: expression of the human p53 gene. *Embo j*, 3, 3257-3262.

- MCCAY, C. M., CROWELL, M. F. & MAYNARD, L. A. 1989. The effect of retarded growth upon the length of life span and upon the ultimate body size. 1935. *Nutrition*, 5, 155-171; discussion 172.
- MCFARLAND, G. A., & HOLLIDAY, R. 1999. Further evidence for the rejuvenating effects of the dipeptide L-carnosine on cultured human diploid fibroblasts. *Experimental gerontology*, 34, 35-45.
- MCLELLAN, A. C., PHILLIPS, S. A. & THORNALLEY, P. J. 1992. Fluorimetric assay of D-lactate. *Anal Biochem*, 206, 12-6.
- MICHISHITA, E., GARCES, G., BARRETT, J.C. AND HORIKAWA, I. 2006. Upregulation of the KIAA1199 gene is associated with cellular mortality. *Cancer Letters*, 239(1), 71-77.
- MINAMINO, T., MIYAUCHI, H., YOSHIDA, T., ISHIDA, Y., YOSHIDA, H. & KOMURO, I. 2002. Endothelial cell senescence in human atherosclerosis: role of telomere in endothelial dysfunction. *Circulation*, 105, 1541-1544.
- MISKIN, R. & MASOS, T. 1997. Transgenic mice overexpressing urokinase-type plasminogen activator in the brain exhibit reduced food consumption, body weight and size, and increased longevity. *J Gerontol A Biol Sci Med Sci*, 52, B118-124.
- MITSUISHI, Y., TAGUCHI, K., KAWATANI, Y., SHIBATA, T., NUKIWA, T., ABURATANI, H., YAMAMOTO, M. & MOTOHASHI, H. 2012. Nrf2 redirects glucose and glutamine into anabolic pathways in metabolic reprogramming. *Cancer Cell*, 22, 66-79.
- MORALES, C.P., HOLT, S.E., OUELLETTE, M., KAUR, K.J., YAN, Y., WILSON, K.S., WHITE, M.A., WRIGHT, W.E., SHAY, J.W. 1999. Absence of cancer-associated changes in human fibroblasts immortalized with telomerase. *Nature Genetics*, 21, 115-118.
- MORCOS, M., DU, X., PFISTERER, F., HUTTER, H., SAYED, A. A., THORNALLEY, P., AHMED, N., BAYNES, J., THORPE, S., KUKUDOV, G., SCHLOTTERER, A., BOZORGMEHR, F., EL BAKI, R. A., STERN, D., MOEHRLEN, F., IBRAHIM, Y., OIKONOMOU, D., HAMANN, A., BECKER, C., ZEIER, M., SCHWENGER, V., MIFTARI, N., HUMPERT, P., HAMMES, H. P., BUECHLER, M., BIERHAUS, A., BROWNLEE, M. & NAWROTH, P. P. 2008. Glyoxalase-1 prevents mitochondrial protein modification and enhances lifespan in *Caenorhabditis elegans*. *Aging Cell*, 7, 260-269.
- MURPHY, M. 2009. How mitochondria produce reactive oxygen species. *Biochem. J*, 417, 1-13.
- MURPHY, M. P. & PARTRIDGE, L. 2008. Toward a control theory analysis of aging. *Annu Rev Biochem*, 77, 777-798.

- N. M. BORRADAILE, K. K. CARROLL, AND E. M. KUROWSKA, 1999. Regulation of HepG2 cell apolipoprotein B metabolism by the citrus flavanones hesperetin and naringenin, *Lipids*, 34, 591–598.
- NA, H. K., & SURH, Y. J. 2000. Modulation of Nrf2-mediated antioxidant and detoxifying enzyme induction by the green tea polyphenol EGCG. *Food and Chemical Toxicology*, 46, 1271-1278.
- NA, R., STENDER, I. M., MA, L. & WULF, H. C. 2000. Autofluorescence spectrum of skin: component bands and body site variations. *Skin Res Technol*, 6, 112-117.
- NAKAMURA, A., CHIANG, Y.J., HATHCOCK, K., HORIKAWA, I., SEDELNIKOVA, O., HODES, R., BONNER, W. 2008. Both telomeric and non-telomeric DNA damage are determinants of mammalian cellular senescence. *Epigenetics & Chromatin*, 1, 6-10.
- NASKALSKI, J. W., MARCINKIEWICZ, J. & DROZDZ, R. 2002. Myeloperoxidase-mediated protein oxidation: its possible biological functions. *Clin Chem Lab Med*, 40, 463-468.
- NEGRE-SALVAYRE, A., AUGÉ, N., AYALA, V., BASAGA, H., BOADA, J., BRENKE, R., CHAPPLE, S., COHEN, G., FEHER, J., GRUNE, T., LENGYEL, G., MANN, G. E., PAMPLONA, R., POLI, G., PORTEROTIN, M., RIAHI, Y., SALVAYRE, R., SASSON, S., SERRANO, J., SHAMNI, O., SIEMS, W., SIOW, R. C., WISWEDEL, I., ZARKOVIC, K. & ZARKOVIC, N. 2010. Pathological aspects of lipid peroxidation. *Free Radic Res*, 44, 1125-1171.
- NIKI, E., NOGUCHI, N., TSUCHIHASHI, H. & GOTOH, N. 1995. Interaction among vitamin C, vitamin E, and beta-carotene. *Am J Clin Nutr*, 62, 1322s-1326s.
- NORWOOD, T. H. & PENDERGRASS, W. R. 1992. The cultured diploid fibroblast as a model for the study of cellular aging. *Critical Reviews in Oral Biology & Medicine*, 3, 353-370.
- NUSSE, R. 2005. Wnt signaling in disease and in development. *Cell Res*, 15, 28-32.
- O'DONOVAN, V. & TULLY, O. 1996. Lipofuscin (age pigment) as an index of crustacean age: correlation with age, temperature and body size in cultured juvenile "Homarus gammarus" L. *Journal of Experimental Marine Biology and Ecology*, 207, 1-14.
- OKAWA, H., MOTOHASHI, H., KOBAYASHI, A., ABURATANI, H., KENSLER, T. W. & YAMAMOTO, M. 2006. Hepatocyte-specific deletion of the keap1 gene activates Nrf2 and confers potent resistance against acute drug toxicity. *Biochem Biophys Res Commun*, 339, 79-88.
- ORR, W. C., RADYUK, S. N., PRABHUDESAI, L., TOROSER, D., BENES, J. J., LUCHAK, J. M., MOCKETT, R. J., REBRIN, I., HUBBARD, J. G. &

- SOHAL, R. S. 2005. Overexpression of glutamate-cysteine ligase extends life span in *Drosophila melanogaster*. *J Biol Chem*, 280, 37331-37338.
- PARTRIDGE, L. & GEMS, D. 2002. Mechanisms of ageing: public or private? *Nat Rev Genet*, 3, 165-175.
- PARTRIDGE, L., & GEMS, D. 2005. Beyond the evolutionary theory of ageing, from functional genomics to evogero. *Trends in ecology & evolution*, 21, 334-340.
- PASSTOORS, W.M., BEEKMAN, M., DEELEN, J., VAN DER BREGGEN, R., MAIER, A.B., GUIGAS, B., DERHOVANESSIAN, E., VAN HEEMST, D. 2013. Gene expression analysis of mTOR pathway: association with human longevity. *Aging Cell*, 12, 24–31.
- PEARL, R. 1928. *The rate of living*, University Press.
- PEARSON, K. J., LEWIS, K. N., PRICE, N. L., CHANG, J. W., PEREZ, E., CASCAJO, M. V., TAMASHIRO, K. L., POOSALA, S., CSISZAR, A., UNGVARI, Z., KENSLER, T. W., YAMAMOTO, M., EGAN, J. M., LONGO, D. L., INGRAM, D. K., NAVAS, P. & DE CABO, R. 2008. Nrf2 mediates cancer protection but not longevity induced by caloric restriction. *Proc Natl Acad Sci U S A*, 105, 2325-2330.
- PELTZ, L., GOMEZ, J., MARQUEZ, M., ALENCASTRO, F., ATASHPANJEH, N., QUANG, T., BACH, T. and ZHAO, Y. 2012. Resveratrol exerts dosage and duration dependent effect on human mesenchymal stem cell development. *PLoS One* , 7, e37162.
- PETERS JR, T. 1995. *All about albumin: biochemistry, genetics, and medical applications*, Academic press.
- PETERSON, C.W., STOLTZMAN, C.A., SIGHINOLFI, M.P., HAN, K.S., AYER, D.E. 2010. Glucose controls nuclear accumulation, promoter binding, and transcriptional activity of the MondoA-Mlx heterodimer. *Mol Cell Biol* , 30, 2887–2895.
- PI, J., BAI, Y., REECE, J. M., WILLIAMS, J., LIU, D., FREEMAN, M. L., FAHL, W. E., SHUGAR, D., LIU, J., QU, W., COLLINS, S. & WAALKES, M. P. 2007. Molecular mechanism of human Nrf2 activation and degradation: role of sequential phosphorylation by protein kinase CK2. *Free Radic Biol Med*, 42, 1797-1806.
- PIERCE, S. B., COSTA, M., WISOTZKEY, R., DEVADHAR, S., HOMBURGER, S. A., BUCHMAN, A. R., FERGUSON, K. C., HELLER, J., PLATT, D. M., PASQUINELLI, A. A., LIU, L. X., DOBERSTEIN, S. K. & RUVKUN, G. 2001. Regulation of DAF-2 receptor signaling by human insulin and ins-1, a member of the unusually large and diverse *C. elegans* insulin gene family. *Genes Dev*, 15, 672-686.
- PIGNOLO, R.J., MASORO, E.J., NICHOLS, W.W., BRADT, C.I., CRISTOFALO, V.J. 1992. Skin fibroblasts from aged Fischer 344 rats

undergo similar changes in replicative life span but not immortalization with caloric restriction of donors. *Exp. Cell Res.*, 201, 16–22.

- PIROLA, L., & FRÖJDÖ, S. 2008. Resveratrol: one molecule, many targets. *IUBMB life*, 60, 323-332.
- PITTOZZI, V., MOCALI, A., LAURENZANA, A., GIANNONI, E., CIFOLA, I., BATTAGLIA, C., CHIARUGI, P., DOLARA, P. & GIOVANNELLI, L. 2013. Chronic resveratrol treatment ameliorates cell adhesion and mitigates the inflammatory phenotype in senescent human fibroblasts. *J Gerontol A Biol Sci Med Sci*, 68, 371-381.
- PLETCHER, S.D., KHAZAELI, A.A., CURTSINGER, J.W. 2000. Why do life spans differ? Partitioning mean longevity differences in terms of age-specific mortality parameters. *J. Gerontol. A Biol. Sci. Med. Sci.*, 55, B381–B389.
- POLLACK, R.M., CRANDALL, J.P. 2013. Resveratrol: Therapeutic Potential for Improving Cardiometabolic Health. *American Journal of Hypertension* , 26, 1260-1268.
- POWELL, C. D., QUAIN, D. E. & SMART, K. A. 2003. The impact of brewing yeast cell age on fermentation performance, attenuation and flocculation. *FEMS Yeast Res*, 3, 149-157.
- PRICE, J. S., WATERS, J. G., DARRAH, C., PENNINGTON, C., EDWARDS, D. R., DONELL, S. T. & CLARK, I. M. 2002. The role of chondrocyte senescence in osteoarthritis. *Aging Cell*, 1, 57-65.
- RABBANI, N. & THORNALLEY, P. J. 2012a. Glycation research in amino acids: a place to call home. *Amino Acids*, 42, 1087-1096.
- RABBANI, N. & THORNALLEY, P. J. 2012b. Methylglyoxal, glyoxalase 1 and the dicarbonyl proteome. *Amino Acids*, 42, 1133-1142.
- RABBANI, N. & THORNALLEY, P. J. 2014. Dicarbonyl proteome and genome damage in metabolic and vascular disease. *Biochem Soc Trans*, 42, 425-432.
- RABBANI, N., SHAHEEN, F., ANWAR, A., MASANIA, J. & THORNALLEY, P. J. 2014. Assay of methylglyoxal-derived protein and nucleotide AGEs. *Biochem Soc Trans*, 42, 511-7.
- RAI, P., ONDER, T.T., YOUNG, J.J., MCFALINE, J.L., PANG, B., DEDON, P.C., WEINBERG, R.A. 2009. Continuous elimination of oxidized nucleotides is necessary to prevent rapid onset of cellular senescence. *Proceedings of the National Academy of Sciences* , 106, 169-174.
- RAMSEY, J.J., JOHNSON, D.E., HOSSNER, K.L., JOHNSON, K.A. 1996. Metabolic rate, organ mass and mitochondrial proton leak variations in lean and obese rats. *Comp Biochem Physiol B Biochem Mol Biol.*, 113, 461–466.

- ROBERT, L. & LABAT-ROBERT, J. 2000. Aging of connective tissues: from genetic to epigenetic mechanisms. *Biogerontology*, 1, 123-131.
- ROBERT, L., JACOB, M. P. & LABAT-ROBERT, J. 1992. Cell-matrix interactions in the genesis of arteriosclerosis and atheroma. Effect of aging. *Ann NY Acad Sci*, 673, 331-341.
- RONINSON, I. B. 2003. Tumor cell senescence in cancer treatment. *Cancer Res*, 63, 2705-2715.
- RUBIOLO, J. A., MITHIEUX, G. & VEGA, F. V. 2008. Resveratrol protects primary rat hepatocytes against oxidative stress damage: activation of the Nrf2 transcription factor and augmented activities of antioxidant enzymes. *Eur J Pharmacol*, 591, 66-72.
- RUSHMORE, T. H., MORTON, M. R. & PICKETT, C. B. 1991. The antioxidant responsive element. Activation by oxidative stress and identification of the DNA consensus sequence required for functional activity. *J Biol Chem*, 266, 11632-11639.
- SALAMA, R., SADAIE, M., HOARE, M. & NARITA, M. 2014. Cellular senescence and its effector programs. *Genes & development*, 28, 99-114.
- SANS, C.L., SATTERWHITE, D.J., STOLTZMAN, C.A., BREEN, K.T., and AYER, D.E. 2006. MondoA-Mlx heterodimers are candidate sensors of cellular energy status: mitochondrial localization and direct regulation of glycolysis. *Mol Cell Biol*, 26, 4863 - 4871.
- SCHAFER, C., SCHOTT, M., BRANDL, F., NEIDHART, S., CARLE, R. 2005. Identification and Quantification of ϵ -(γ -Glutamyl)lysine in Digests of Enzymatically Cross-Linked Leguminous Proteins by High-Performance Liquid Chromatography–Electrospray Ionization Mass Spectrometry (HPLC-ESI-MS). *Journal of Agricultural and Food Chemistry*, 53, 2830-2837.
- SCHILDER, Y. D., HEISS, E. H., SCHACHNER, D., ZIEGLER, J., REZNICEK, G., SORESCU, D., & DIRSCH, V. M. 2009. NADPH oxidases 1 and 4 mediate cellular senescence induced by resveratrol in human endothelial cells. *Free Radical Biology and Medicine*, 46, 1598-1606.
- SCHRINER, S. E., LINFORD, N. J., MARTIN, G. M., TREUTING, P., OGBURN, C. E., EMOND, M., COSKUN, P. E., LADIGES, W., WOLF, N., VAN REMMEN, H., WALLACE, D. C. & RABINOVITCH, P. S. 2005. Extension of murine life span by overexpression of catalase targeted to mitochondria. *Science*, 308, 1909-1911.
- SEJERSEN, H. & RATTAN, S. I. 2009. Dicarbonyl-induced accelerated aging in vitro in human skin fibroblasts. *Biogerontology*, 10, 203-211.
- SELL, D.R., BIEMEL, K.M., REIHL, O., LEDERER, M.O., STRAUCH, C.M. AND MONNIER, V.M. 2005. Glucosepane is a major protein cross-link

- of the senescent human extracellular matrix: relationship with diabetes. *The Journal of Biological Chemistry*, 280, 12810-12815.
- SELMAN, C., TULLET, J., WIESER, D., IRVINE, E., LINGARD, S.J., CHOUDHURY, A.I., CLARET, M. 2009. Ribosomal protein S6 kinase 1 signaling regulates mammalian life span. *Science*, 326, 140-144.
- SERRA, V., VON ZGLINICKI, T., LORENZ, M., SARETZKI, G. 2003. Extracellular superoxide dismutase is a major antioxidant in human fibroblasts and slow telomere shortening. *J Biol Chem*, 278, 6824-6830.
- SHAPIRO, R.L., HATHEWAY, C., SWERDLOW, D.L. 1998. Botulism in the United States: a clinical and epidemiologic review. *Annals of Internal Medicine*, 129, 221 - 228.
- SHAY, J. W. & WRIGHT, W. E. 2000. Hayflick, his limit, and cellular ageing. *Nat Rev Mol Cell Biol*, 1, 72-76.
- SHELTON, D.N., CHANG, E., WHITTIER, P.S., CHOI, D., FUNK, W.D. 1999. Microarray analysis of replicative senescence. *Current Biology*, 9, 939-945.
- SHIN, Y. W., BOK, S. H., JEONG, T. S., BAE, K. H., JEOUNG, N. H., CHOI, M. S., LEE, S. H. and PARK, Y. B. 1999. Hypocholesterolemic effect of naringin associated with hepatic cholesterol regulating enzyme changes in rats. *Int. J. Vitamin Nutr. Res*, 69, 341-347.
- SHINICHI, S., YU, S., HALLOWS, W.C., XU, J., VANN, J.M., LEEUWENBURGH, C., TANOKURA, M., DENU, J.M. and PROLLA, T.A. 2010. Sirt3 mediates reduction of oxidative damage and prevention of age-related hearing loss under caloric restriction. *Cell*, 143, 802-812.
- SHINOHAR, A. M., THORNALLEY, P. J., GIARDINO, I., BEISSWENGER, P., THORPE, S. R., ONORATO, J., et al. 1998. Overexpression of glyoxalase-I in bovine endothelial cells inhibits intracellular advanced glycation endproduct formation and prevents hyperglycemia-induced increases in macromolecular endocytosis. *J. Clin. Invest.*, 101, 1142-1147.
- SIES, H. 1993. Strategies of antioxidant defense. *Eur J Biochem*, 215, 213-219.
- SIMONS, M. J., KOCH, W. & VERHULST, S. 2013. Dietary restriction of rodents decreases aging rate without affecting initial mortality rate -- a meta-analysis. *Aging Cell*, 12, 410-414.
- SINCLAIR, D., MILLS, K. & GUARENTE, L. 1998. Aging in *Saccharomyces cerevisiae*. *Annu Rev Microbiol*, 52, 533-560.
- SINGH, A., BODAS, M., WAKABAYASHI, N., BUNZ, F., BISWAL, S. 2013. Gain of Nrf2 function in non-small-cell lung cancer cells confers radioresistance. *Antioxid Redox Signal*, 13, 1627-1637.

- SITTE, N., MERKER, K., GRUNE, T. 1998. Proteasome-dependent degradation of oxidized proteins in MRC-5 fibroblasts. *FEBS Letters*, 440, 399-402.
- SITTE, N., MERKER, K., VON ZGLINICKI, T., DAVIES, K.J.A., GRUNE, T. 2000b. Protein oxidation and degradation during cellular senescence of human BJ fibroblasts: part II--aging of non-dividing cells. *FASEB Journal*, 14, 2503-2510.
- SITTE, N., MERKER, K., VON ZGLINICKI, T., GRUNE, T., DAVIES, K.J.A. 2000a. Protein oxidation and degradation during cellular senescence of human BJ fibroblasts: part I--effects of proliferative senescence. *The FASEB Journal*, 14, 2495-2502.
- SKYTTHE, A., PEDERSEN, N. L., KAPRIO, J., STAZI, M. A., HJELMBORG, J. V., IACHINE, I., VAUPEL, J. W. & CHRISTENSEN, K. 2003. Longevity studies in GenomEUtwin. *Twin Res*, 6, 448-454.
- SO, F.V., GUTHRIE, N., CHAMBERS, A.F., MOUSSA, M., CARROLL, K.K. 1996. Inhibition of human breast cancer cell proliferation and delay of mammary tumorigenesis by flavonoids and citrus juices. *Nutr. Cancer*, 26, 167-181.
- SOHAL, R. S. 1981. *Age pigments*, Elsevier/North-Holland Biomedical Press Amsterdam.
- SOTI, C. & CSERMELY, P. 2003. Aging and molecular chaperones. *Exp Gerontol*, 38, 1037-1040.
- SPEAKMAN, J.R., TALBOT, D.A., SELMAN, C., SNART, S., MCLAREN, J.S., REDMAN, P., KROL, E., JACKSON, D.M., JOHNSON, M.S., and BRAND, M.D. 2004. Uncoupled and surviving: individual mice with high metabolism have greater mitochondrial uncoupling and live longer. *Aging cell*, 3, 87-95.
- STEIN, G. H., BEESON, M. & GORDON, L. 1990. Failure to phosphorylate the retinoblastoma gene product in senescent human fibroblasts. *Science*, 249, 666-669.
- STEINKRAUS, K. A., KAEBERLEIN, M. & KENNEDY, B. K. 2008. Replicative aging in yeast: the means to the end. *Annu Rev Cell Dev Biol*, 24, 29-54.
- STOLTZMAN, C.A., PETERSON, C.W., BREEN, K.T., MUOIO, D.M., BILLIN, A.N., AYER, D.E. 2008. Glucose sensing by MondoA:MLx complexes: a role for hexokinases and direct regulation of thioredoxin-interacting protein expression. *Proceedings of the National Academy of Sciences of the United States of America.*, 105, 6912-6917.
- STRACHAN, T. & READ, A. P. 1999. *Human Molecular Genetics*. New York: Wiley-Liss

- STROBER, W. 2001. Trypan blue exclusion test of cell viability. *Curr Protoc Immunol*, Appendix 3, Appendix 3B.
- SURH, Y.J., KUNDU, J.K., NA, H.K., 2008. Nrf2 as a master redox switch in turning on the cellular signaling involved in the induction of cytoprotective genes by some chemopreventive phytochemicals. *Planta Med.* 74, 1526–1539.
- SUZUKI, M., WILLCOX, D. C., ROSENBAUM, M. W. & WILLCOX, B. J. 2010. Oxidative stress and longevity in okinawa: an investigation of blood lipid peroxidation and tocopherol in okinawan centenarians. *Curr Gerontol Geriatr Res*, 5, 380-460.
- SWINDELL, W. R. 2009. Genes and gene expression modules associated with caloric restriction and aging in the laboratory mouse. *BMC genomics*, 10, 585-589.
- SYKIOTIS, G. P. & BOHMANN, D. 2008. Keap1/Nrf2 signaling regulates oxidative stress tolerance and lifespan in *Drosophila*. *Dev Cell*, 14, 76-85.
- TAGUCHI, K., MOTOHASHI, H. & YAMAMOTO, M. 2011. Molecular mechanisms of the Keap1-Nrf2 pathway in stress response and cancer evolution. *Genes Cells*, 16, 123-140.
- TALASNIEMI, J.P., PENNANEN, S., SAVOLAINEN, H., NISKANEN, L., LIESIVUORI, J. 2008. Analytical investigation: assay of D-lactate in diabetic plasma and urine. *Clin Biochem.*, 41, 1099–1103.
- TANIGAWA, S., FUJII, M. & HOU, D. X. 2007. Action of Nrf2 and Keap1 in ARE-mediated NQO1 expression by quercetin. *Free Radic Biol Med*, 42, 1690-1703.
- TATAR, M., BARTKE, A. & ANTEBI, A. 2003. The endocrine regulation of aging by insulin-like signals. *Science*, 299, 1346-1351.
- TESTA, F., BIASI, G., POLI, E. 2014. Chiarpotto Calorie restriction and dietary restriction mimetics: a strategy for improving healthy aging and longevity. *Curr. Pharm. Des.*, 20, 1–28.
- THEODORE, M., KAWAI, Y., YANG, J., KLESHCHENKO, Y., REDDY, S. P., VILLALTA, F. & ARINZE, I. J. 2008. Multiple nuclear localization signals function in the nuclear import of the transcription factor Nrf2. *J Biol Chem*, 283, 8984-8994.
- THIMMULAPPA, R. K., MAI, K. H., SRISUMA, S., KENSLER, T. W., YAMAMOTO, M. & BISWAL, S. 2002. Identification of Nrf2-regulated genes induced by the chemopreventive agent sulforaphane by oligonucleotide microarray. *Cancer Res*, 62, 5196-5203.
- THORNALLEY, P. J. & RABBANI, N. 2014. Detection of oxidized and glycated proteins in clinical samples using mass spectrometry--a user's perspective. *Biochim Biophys Acta*, 1840, 818-829.

- THORNALLEY, P. J. 1993. The glyoxalase system in health and disease. *Mol Aspects Med*, 14, 287-371.
- THORNALLEY, P. J., BATTAH, S., AHMED, N., KARACHALIAS, N., AGALOU, S., BABAEI-JADIDI, R. & DAWNAY, A. 2003. Quantitative screening of advanced glycation endproducts in cellular and extracellular proteins by tandem mass spectrometry. *Biochem J*, 375, 581-592.
- THORNALLEY, P. J., WARIS, S., FLEMING, T., SANTARIUS, T., LARKIN, S. J., WINKLHOFFER-ROOB, B. M., STRATTON, M. R. & RABBANI, N. 2010. Imidazopurinones are markers of physiological genomic damage linked to DNA instability and glyoxalase 1-associated tumour multidrug resistance. *Nucleic Acids Res*, 38, 5432-5442.
- TIMMERS, S., KONINGS, E., BILET, L., HOUTKOOP, E.R., RIEKELT, H., VAN DE WEIJER, T., GOOSSENS, G.I., JS, H., HOEKS, J., VAN DER KRIEKEN, S., RYU, D., KERSTEN, S., MOONEN-KORNIPS, E., HESSELINK MATTHIJS, K., KUNZ, I., SCHRAUWEN-HINDERLING, V.B., BLAAK, E.E., AUWERX, J., SCHRAUWEN, P. 2011. Calorie Restriction-like Effects of 30 Days of Resveratrol Supplementation on Energy Metabolism and Metabolic Profile in Obese Humans. *Cell Metabolism* , 14, 612-622.
- TREIBER, N., MAITY, P., SINGH, K., KOHN, M., KEIST, A.F., FERCHIU, F., SANTE, L. et al. 2011. Accelerated aging phenotype in mice with conditional deficiency for mitochondrial superoxide dismutase in the connective tissue. *Aging cell*, 10, 239-254.
- TULLET, J.M., HERTWECK M, A.N., BAKER, J., HWANG, J.Y., LIU, S., OLIVEIRA, R.P., BAUMEISTER, R., BLACKWELL, T.K. 2008. Direct inhibition of the longevity-promoting factor SKN-1 by insulin-like signaling in *C. elegans*. *Cell*, 132, 1025–1038.
- UEHARA, T., MINOWA, Y., MORIKAWA, Y., KONDO, C., MARUYAMA, T., KATO, I., NAKATSU, N., IGARASHI, Y., ONO, A., HAYASHI, H. 2011. Prediction model of potential hepatocarcinogenicity of rat hepatocarcinogens using a large-scale toxicogenomics database. *Toxicol Appl Pharmacol*, 255, 297–306.
- VALENZANO, D. R., TERZIBASI, E., GENADE, T., CATTANEO, A., DOMENICI, L. & CELLERINO, A. 2006. Resveratrol prolongs lifespan and retards the onset of age-related markers in a short-lived vertebrate. *Curr Biol*, 16, 296-300.
- VAN ACKER, F. A., SCHOUTEN, O., HAENEN, G. R., VAN DER VIJGH, W. J., & BAST, A. 2000. Flavonoids can replace α -tocopherol as an antioxidant. *FEBS letters*, 473, 145-148.
- VAN HUMMELEN, P., SASAKI, J. 2010. State-of-the-art genomics approaches in toxicology. *Mutat Res*, 705, 165–171.

- VAN REMMEN, H., IKENO, Y., HAMILTON, M., PAHLAVANI, M., WOLF, N., THORPE, S.R., ALDERSON, N.L. et al. 2003. Life-long reduction in MnSOD activity results in increased DNA damage and higher incidence of cancer but does not accelerate aging. *Physiological genomics*, 16, 29-37.
- VEIGA DA-CUNHA, M., JACQUEMIN, P., DELPIERRE, G., GODFRAIND, C., THEATE, I., VERTOMMEN, D., CLOTMAN, F., LEMAIGRE, F., DEVUYST, O. & VAN SCHAFTINGEN, E. 2006. Increased protein glycation in fructosamine 3-kinase-deficient mice. *Biochem J*, 399, 257-264.
- WALKER, G., HOUTHOOFD, K., VANFLETEREN, J. R. & GEMS, D. 2005. Dietary restriction in *C. elegans*: from rate-of-living effects to nutrient sensing pathways. *Mech Ageing Dev*, 126, 929-937.
- WATSON, J. D. 1972. Origin of concatemeric T7 DNA. *Nat New Biol*, 239, 197-201.
- WEINDRUCH, R., & WALFORD, R. L. 1982. Dietary restriction in mice beginning at 1 year of age: effect on life-span and spontaneous cancer incidence. *Science*, 215, 1415-1418.
- WEINDRUCH, R., KAYO, T., LEE, C. K. & PROLLA, T. A. 2002. Gene expression profiling of aging using DNA microarrays. *Mech Ageing Dev*, 123, 177-193.
- WEINDRUCH, R., WALFORD, R. L., FLIGIEL, S. & GUTHRIE, D. 1986. The retardation of aging in mice by dietary restriction: longevity, cancer, immunity and lifetime energy intake. *J Nutr*, 116, 641-654.
- WEINERT, B. T. & TIMIRAS, P. S. 2003. Invited review: theories of aging. *Journal of Applied Physiology*, 95, 1706-1716.
- WEINKOVE, D. & LEEVERS, S. J. 2000. The genetic control of organ growth: insights from *Drosophila*. *Curr Opin Genet Dev*, 10, 75-80.
- WILLCOX, B. J., WILLCOX, D. C., TODORIKI, H., FUJIYOSHI, A., YANO, K., HE, Q., CURB, J. D. & SUZUKI, M. 2007. Caloric restriction, the traditional Okinawan diet, and healthy aging: the diet of the world's longest-lived people and its potential impact on morbidity and life span. *Ann N Y Acad Sci*, 1114, 434-455.
- WOLKOW, C.A., KIMURA, K.D., LEE, G. 2000. Ruvkun Regulation of *C. elegans* life span by insulin-like signaling in the nervous system. *Science*, 290, 147-150.
- WOOD, J. G., ROGINA, B., LAVU, S., HOWITZ, K., HELFAND, S. L., TATAR, M., & SINCLAIR, D. 2004. Sirtuin activators mimic caloric restriction and delay ageing in metazoans. *Nature*, 430, 686-689.

- WRIGHT, W. E. & SHAY, J. W. 2000. Telomere dynamics in cancer progression and prevention: fundamental differences in human and mouse telomere biology. *Nat Med*, 6, 849-851.
- WU, Z., LIU, S. Q. & HUANG, D. 2013. Dietary restriction depends on nutrient composition to extend chronological lifespan in budding yeast *Saccharomyces cerevisiae*. *PLoS one*, 8, e64448.
- WULLSCHLEGER, S., LOEWITH, R., & HALL, M. N. 2006. TOR signaling in growth and metabolism. *Cell*, 124, 471-484.
- XIAO, B., SPENCER, J., CLEMENTS, A., ALI-KHAN, N., MITTNACHT, S., BROCCO, C., BURGHAMMER, M., PERRAKIS, A., MARMORSTEIN, R. & GAMBLIN, S. J. 2003. Crystal structure of the retinoblastoma tumor suppressor protein bound to E2F and the molecular basis of its regulation. *Proc Natl Acad Sci U S A*, 100, 2363-2368.
- XUE, M., ANTONYSUNIL, A., RABBANI, N., THORNALLEY, P., FOYER, C., FARAGHAR, R. & THORNALLEY, P. 2008a. *Protein damage by glycation, oxidation and nitration in the ageing process. Advances in quantitation of protein damage and the emerging importance of decline in enzymatic defences as the ageing phenotype develops*. Redox metabolism and longevity relationships in animals and plants. Garland Science, London, 227-265.
- XUE, M., MOMIJI, H., RABBANI, N., BARKER, G. & RAND, D. 2012a. Control of ARE-linked gene expression by cytoplasm-nucleus translocational oscillations of Nrf2. *Free Radical Biology and Medicine*, 53, S37.
- XUE, M., QIAN, Q., ADAIKALAKOTESWARI, A., RABBANI, N., BABAEI-JADIDI, R. & THORNALLEY, P. J. 2008b. Activation of NF-E2-related factor-2 reverses biochemical dysfunction of endothelial cells induced by hyperglycemia linked to vascular disease. *Diabetes*, 57, 2809-2817.
- XUE, M., RABBANI, N., MOMIJI, H., IMBASI, P., ANWAR, M. M., KITTERINGHAM, N., PARK, B. K., SOUMA, T., MORIGUCHI, T., YAMAMOTO, M. & THORNALLEY, P. J. 2012. Transcriptional control of glyoxalase 1 by Nrf2 provides a stress-responsive defence against dicarbonyl glycation. *Biochem J*, 443, 213-222.
- XUE, P., HOU, Y., CHEN, Y., YANG, B., FU, J., ZHENG, H., YARBOROUGH, K., WOODS, C. G., LIU, D., YAMAMOTO, M., ZHANG, Q., ANDERSEN, M. E. & PI, J. 2013. Adipose deficiency of Nrf2 in ob/ob mice results in severe metabolic syndrome. *Diabetes*, 62, 845-854.
- YAMAMOTO, M., KO, L.J., LEONARD, M.W., BEUG, H., ORKIN, S.H. & ENGEL, J.D. 1990. Activity and tissue-specific transcription factor NF-E1 multi-gene family. *Genes Dev.*, 4, 1650-1665.

- YAO, C.Q., PROKOPEC, S.D., WATSON, J.D., PANG, R., P'NG, C., CHONG, L.C., HARDING, N.J., POHJANVIRTA, R., OKEY, A.B., BOUTROS, P.C. 2012. Inter-strain heterogeneity in rat hepatic transcriptomic responses to 2,3,7,8-tetrachlorodibenzo-p-dioxin (TCDD). *Toxicol Appl Pharmacol*, 260, 135–145.
- YATES, M.S., TRAN, Q.T., DOLAN, P.M., OSBURN, W.O., SHIN, S., MCCULLOCH, C.C., SILKWORTH, J.B., TAGUCHI, K., YAMAMOTO, M., WILLIAMS, C.R., LIBY, K.T., SPORN, M.B., SUTTER, T.R., KENSLER, T.W. 2009. Genetic versus chemoprotective activation of Nrf2 signaling: overlapping yet distinct gene expression profiles between Keap1 knockout and triterpenoid-treated mice. *Carcinogenesis*, 30, 1024–1031.
- YE, Y., LI, J., YUAN, Z. 2013. Effect of Antioxidant Vitamin Supplementation on Cardiovascular Outcomes: A Meta-Analysis of Randomized Controlled Trials. *PLoS ONE*, 8:e56803.
- YU, B. P. 1996. Aging and oxidative stress: modulation by dietary restriction. *Free Radic Biol Med*, 21, 651-668.
- YU, B. P., MASORO, E. J., & MCMAHAN, C. A. 1982. Nutritional influences on aging of Fischer 344 rats: I. Physical, metabolic, and longevity characteristics. *Journal of gerontology*, 40, 657-670.
- ZAINAL, T.A., OBERLEY, T.D., ALLISON, D.B., SZWEDA, L.I., WEINDRUCH, R. 2000. Caloric restriction of rhesus monkeys lowers oxidative damage in skeletal muscle. *FASEB J*, 14, 1825–1836.
- ZALATNAI, A. 2006. Molecular aspects of stromal-parenchymal interactions in malignant neoplasms. *Curr Mol Med*, 6, 685-693.
- ZHANG, J., DAY, I.N., BYRNE, C.D. 2002. A novel medium throughput quantitative competitive PCR technology to simultaneously measure mRNA levels from multiple genes. *Nucleic Acids Res*, 30, 303-309.